



LEIBNIZ INSTITUTE FOR
BAL TIC SEA RESEARCH
WARNEMÜNDE

Universität
Rostock



Traditio et Innovatio

Spatial and Temporal Variability in the Northeast Atlantic Subtropical Gyre and Implications for the Biogeochemistry of the Region

Cumulative Dissertation

to obtain the academic degree
Doctor rerum naturalium (Dr. rer. nat.)
of the Faculty of Mathematics and Natural Sciences
at the University of Rostock

submitted by

Helena Cristina Vieira Frazão

born on 13.12.1992 in Leiria, Portugal

Rostock, 2022

The work in this thesis was carried out between September 2018 and April 2022 under the supervision of Prof. Dr. Joanna J. Waniek in the working group “Bio-physical interactions” within the Marine Chemistry department at the Leibniz Institute for Baltic Sea Research Warnemünde, Germany.

Gutachter:

Prof. Dr. habil. Joanna J. Waniek, Leibniz-Institut für Ostseeforschung Warnemünde
PD Dr. Birgit Gaye, Universität Hamburg, Institut für Geologie

Jahr der Einreichung: 12.April.2022

Jahr der Verteidigung: 1.July.2022

Eidesstattliche Erklärung

Ich versichere hiermit an Eides statt, dass ich die vorliegende Arbeit selbstständig angefertigt und ohne fremde Hilfe verfasst habe, keine außer den von mir angegebenen Hilfsmitteln und Quellen dazu verwendet habe und die den benutzten Werken inhaltlich und wörtlich entnommenen Stellen als solche kenntlich gemacht habe.

Helena Cristina Vieira Frazão

Contents

Abstract	iii
Zusammenfassung	v
1 Introduction	1
1.1 The role of the North Atlantic Ocean in climate	1
1.2 The North Atlantic Subtropical Gyre	3
1.3 The Azores Front-Current system	5
2 Aims	9
3 Methodological Approach	11
3.1 Datasets	11
3.1.1 Temperature and currents from the Kiel 276 mooring	11
3.1.2 CTD profiles and Argo floats	11
3.1.3 Objective analyses data	13
3.1.4 Reanalysis data	13
3.2 Climate Indexes	14
3.2.1 North Atlantic Oscillation	14
3.2.2 Atlantic Multidecadal Oscillation	14
3.3 Validation and quality control	14
3.3.1 Temperature and currents time-series from the Kiel 276 mooring . .	14
3.3.2 Quality control and monthly objective analyses fields from the in situ data	15
3.3.3 Azores Current, Gulf Stream, Azores Front and Ocean Heat Content	16
3.3.4 Vertical distribution of Chl <i>a</i> and CO ₂ uptake estimates	16
4 Results and Discussion	19
4.1 Long-term variability of the Azores Front-Current system	19
4.2 Mediterranean Water Outflow in the Northeast Atlantic	25
4.3 Deeper Northeast Atlantic	28
4.4 Carbon uptake in the North Atlantic Subtropical Gyre	31

5 Summary and Outlook	37
References	40
Contributions to the manuscripts	62
Publication I: The forgotten Azores Current: a long-term perspective	63
Publication II: Mediterranean Water Properties at the Eastern Limit of the North Atlantic Subtropical Gyre Since 1981	85
Publication III: 30 years of temporal variability of temperature and currents below the main thermocline between 1980–2009 in the subtropical Northeast Atlantic (Kiel 276, 33°N, 22°W)	106
List of Figures	124
List of Abbreviations	127
Curriculum Vitae	128
Acknowledgments	132

Abstract

Ocean circulation plays a vital role in our climate system, redistributing heat and salt through the different ocean basins, moderating the Earth's climate as we know it. Moreover, ocean circulation also redistributes nutrients, carbon, and other elements, sustaining the biological production in the ocean, leading to further uptake of atmospheric carbon dioxide, transporting it into the deep ocean interior, where it rests in the deep sediments of the seafloor. Density-driven changes together with external forcing of natural and anthropogenic origin drive most of the observed changes in ocean circulation on a wide range of temporal and spatial scales. Nevertheless, the variability and trends of the ocean's processes are not always linear and uniformly distributed in space and time. Thus, understanding the spatial and temporal variability of the ocean's processes is of crucial importance to better perceive and foresee the repercussions on Earth's climate, ocean circulation, and properties changes, as well as on biogeochemical cycles.

In this thesis, the long-term variability of the water column properties and currents are assessed on a multi-decadal timescale in the Northeast Atlantic Subtropical Gyre. This region is of particular interest due to the influence of the Azores Current at the surface, the main feature of recirculation in the eastern Atlantic; the associated Azores Front, which separates two distinct biogeochemical regimes; and by the presence of the Mediterranean Outflow Water at intermediate depths, a source of heat and salt for the North Atlantic basin.

In the Northeast Atlantic, the Azores Current velocity in the upper 1000 m, significantly declined by 24% in the 1960s and the 1970s. It is suggested that the recent weakening of the Atlantic Meridional Overturning Circulation, together with the Gulf Stream that started in the 1960s, caused a decline of the Azores Current that is delayed by about two years. Concurrently, the Azores Front, the northern border of the Azores Current, has been gradually migrating poleward at a rate of 12 m day^{-1} since the 1970s. Furthermore, the position of the Azores Front was shown to be strongly correlated with the Ocean Heat Content in the upper 400 m and the Atlantic Multidecadal Oscillation. Thus, the expansion of subtropical mode waters may be forcing the Azores Front to migrate poleward.

The variability of the Mediterranean Water Outflow in the Northeast Atlantic was evaluated on two sites – along its western branch and at the Kiel 276 site. Along the western branch, the Mediterranean Water Outflow cooled and freshened between the 1980s and

2018, alternated by periods of warming and salinification. The variability in the properties of the Mediterranean Water Outflow is connected with the predominant North Atlantic Oscillation phase, which leads the changes in the water properties at the core of the Mediterranean Outflow Water by 7-8 years. On the other hand, the dissolved oxygen concentration in the Mediterranean Outflow Water core does not correlate with the NAO.

At Kiel 276 site, the temperature increased by $0.03 \pm 0.01 \text{ }^\circ\text{C year}^{-1}$ at 1000 m and $0.02 \pm 0.02 \text{ }^\circ\text{C year}^{-1}$ at 1600 m between 1980 and 2009, accompanied by an intensification of the currents down to 5000 m. Consequently, the mean kinetic energy increased in the entire water column. On the other hand, the fluctuating part of the kinetic energy only increased down to 1000 m, possibly due to the rise in the number of Mediterranean Water lenses that crossed the Kiel 276 mooring site. Interestingly, the integral time scales, for both velocity components and temperature are of the order of 30 days, and they do not differ between the upper and deeper water column, indicating that mesoscale events prevail in the entire water column.

The reported changes in the circulation and water properties in the Northeast Atlantic impacted the biogeochemistry of the region. The integrated nitrate concentration in the upper 300 m decreased since the 1970s in the North Atlantic Subtropical Gyre, concurrently with rapid warming of the water column. The warming of the upper water column might lead to an increased stratification, hampering the vertical supply of nutrients into the euphotic layer, thus reducing the concentration of Chlorophyll *a* (Chl *a*). The integrated Chl *a* concentration in the upper 300 m has been declining since the beginning of the 20th century, and a reduction of 617 Mt in the carbon uptake was determined between 1871 and 2010 for the entire subtropical North Atlantic.

Zusammenfassung

Die Ozeanzirkulation spielt eine wichtige Rolle in unserem Klimasystem, indem sie Wärme und Salz in den verschiedenen Ozeanbecken umverteilt und so das Klima der Erde, wie wir es kennen, mäßigt. Darüber hinaus werden durch die Ozeanzirkulation auch Nährstoffe, Kohlenstoff und andere Elemente umverteilt, wodurch die biologische Produktion im Ozean aufrechterhalten wird. Dies führt zur Aufnahme von atmosphärischem Kohlendioxid, welches in das Innere des Ozeans transportiert wird, wo es in den tiefen Sedimenten des Meeresbodens eingelagert wird. Die am häufigsten beobachteten Veränderungen der Ozeanzirkulation sind dichtebedingte Veränderungen, die mit externen (natürlichen und anthropogenen) Antrieben zusammenhängen und auf verschiedenen zeitlichen und räumlichen Skalen stattfinden. Die Variabilität und die Trends der ozeanischen Prozesse sind jedoch nicht immer linear und sie verteilen sich ungleichmäßig in Raum und Zeit. Daher ist das Verständnis der räumlich-zeitlichen Variabilität der Ozeanprozesse von größter Bedeutung, um die Auswirkungen auf das Erdklima, die Ozeanzirkulation und die Veränderungen der Meeresseigenschaften sowie die biogeochemischen Kreisläufe besser erkennen und vorhersagen zu können.

In dieser Arbeit werden die langfristige Variabilität der Wassereigenschaften in der gesamten Wassersäule und die Strömungseigenschaften im subtropischen Wirbel des Nordostatlantiks auf einer multidekadischen Zeitskala betrachtet. Diese Region ist von besonderem Interesse wegen des Einflusses des Azorenstromes, der wichtigsten Zirkulationsströmung im Ostatlantik, an der Oberfläche des subtropischen Wirbels. Der Azorenstrom bestimmt auch die Lage der mit ihm verbundenen Azorenfront, die zwei unterschiedliche biogeochemische Regime voneinander trennt. Darüber hinaus stellt der Mittelmeerwasser- ausstrom in mittleren Tiefen eine Wärme- und Salzquelle für den Nordatlantik dar, der die Region des subtropischen Wirbels beeinflusst.

Die Geschwindigkeit des Azorenstromes in den oberen 1000 m hat in den 1960er und 1970er Jahren um 24 % abgenommen. Es konnte zeigen, dass die Abschwächung der Atlantischen Umwälzbewegung und des Golfstromes seit den 1960er Jahren zu einem um etwa zwei Jahre verzögert auftretenden Rückgang des Azorenstromes geführt hat. Gleichzeitig bewegt sich die Azorenfront, die nördliche Grenze des Azorenstromes, seit den 1970er Jahren mit einer Geschwindigkeit von 12 m pro Tag polwärts. Die Position der Azorenfront ist stark mit dem Wärmehalt des Ozeans in den oberen 400 m und der Atlantischen

Multidekadischen Oszillation korreliert. Somit ist es möglich, dass die Ausdehnung der subtropischen Gewässer die Azorenfront polwärts drängt.

Die Variabilität des Mittelmeerwasserausstromes im Nordostatlantik wurde von mir entlang seiner westlichen Ausbreitungsregion und an der Verankerungsposition der Kiel 276 untersucht. In der westlichen Ausbreitungsregion kühlte sich der Mittelmeerwasserausstrom zwischen 1981 und 2018 ab und wurde gleichzeitig salzärmer, wobei diese Abkühlung von kurzen Perioden der Erwärmung und Versalzung unterbrochen wurde. Diese Variabilität hängt mit der Phase der Nordatlantischen Oszillation zusammen, die den Veränderungen der Wassereigenschaften im Kern des Mittelmeerausstromes um 7-8 Jahre vorausseilt. Die Sauerstoffkonzentration im Kern des Mittelmeerwasserausstromes zeigt jedoch keine Korrelation mit der Nordatlantischen Oszillation.

An der Verankerungsstation Kiel 276 stieg die Temperatur zwischen 1980 und 2009 in 1000 m Tiefe um $0.03 \pm 0.01 \text{ } ^\circ\text{C Jahr}^{-1}$ und in 1600 m Tiefe um $0.02 \pm 0.02 \text{ } ^\circ\text{C Jahr}^{-1}$ an, begleitet von einer Intensivierung der Strömungen bis in 5000 m Tiefe. Folglich nahm die mittlere kinetische Energie in der gesamten Wassersäule zu, wobei der fluktuierende Anteil der kinetischen Energie nur im Bereich bis 1000 m Tiefe anstieg. Dies ist möglicherweise auf die Zunahme der Anzahl der Mittelmeerwasserwirbel zurückzuführen, die die Verankerungsposition der Station Kiel 276 passierten. Interessanterweise liegen die integralen Zeitskalen sowohl für die Geschwindigkeitskomponenten als auch für die Temperatur in der Größenordnung von 30 Tagen. Sie unterscheiden sich nicht zwischen der oberen und der tieferen Wassersäule, was darauf hindeutet, dass in der gesamten Wassersäule mesoskalige Ereignisse vorherrschen.

Die berichteten Veränderungen der Zirkulation und der Wassereigenschaften im Nordostatlantik wirkten sich auf die Biogeochemie der Region aus. Die integrierte Nitratkonzentration in den oberen 300 m nahm seit den 1970er Jahren im Subtropischen Wirbel des Nordatlantiks ab, parallel zu einer schnellen Erwärmung der Wassersäule. Die Erwärmung der oberen Wassersäule könnte zu einer verstärkten Schichtung führen, welche die vertikale Zufuhr von Nährstoffen in die euphotische Zone behindert und damit die Chl *a*-Konzentration verringert. Die integrierte Chl *a*-Konzentration in den oberen 300 m ist seit Beginn des 20. Jahrhunderts rückläufig, und für den gesamten subtropischen Nordatlantik wurde eine Verringerung der Kohlenstoffaufnahme um -617 Mio. Tonnen zwischen 1871 und 2010 festgestellt.

1. Introduction

1.1. The role of the North Atlantic Ocean in climate

The North Atlantic (NA) Ocean plays an essential role in climate regulation, as it is a crucial part of the thermohaline circulation. Although its modest size, only 11.5% of the world ocean area (Eakins & Sharman, 2010), the North Atlantic contributes to a large extent to the transport of heat from the tropics into the polar region in the upper water column. At the same time, it carries cold, dense polar water southward through the Atlantic Ocean in the deepest part, redistributing this cold water to the other ocean basins (Lozier, 2012). The Atlantic branch of the thermohaline circulation is known as the Atlantic Meridional Overturning Circulation (AMOC). Johns et al. (2011) estimated that the Meridional Overturning Circulation (MOC)¹ in the subtropical North Atlantic at 26°N accounts for 70% of the ocean’s global net poleward heat flux and 25% of the total heat flux.

It was a great shock to the scientific community when Bryden et al. (2005) estimated an AMOC decline of about 30% relative to its 1957 state. Since then, intensive efforts have been made to monitor and study the variability of the heat transport in the North Atlantic basin. Most notably the RAPID-MOCA array at 26.5°N since 2004 (Cunningham et al., 2007), and the OSNAP array at 53°N since 2014 (Lozier et al., 2017). These records show that the AMOC has large interannual variability, with periods of a weaker state (2004–2012; Smeed et al., 2014), followed by a recovery between 2014 and 2018 (Moat et al., 2020).

Projections of the AMOC state reveal a weakening over the 21st century (e.g., Collins et al., 2019, and references therein), partly due to an increase of heat-trapping greenhouse gases, especially anthropogenic carbon dioxide (Caesar et al., 2018; Gruber et al., 2019). Possible impacts of an AMOC weakening range from a cooling of the subpolar North Atlantic (Josey et al., 2018, and references therein), sea-level rise around the northeast coast of North America (e.g., Ezer, 2015), changes in the northern hemisphere weather and climate (e.g., Jackson et al., 2015), and marine productivity (Schmittner, 2005).

The increasing global mean surface temperature has been reported since the last century (Jones et al., 1999; Hartmann et al., 2013), and the projections for the 21st century are not

¹MOC is mathematically defined as the zonal integrated volume flux as a function of depth and latitude.

very optimistic (IPCC, 2021). The global ocean contributes to a large extent to the storage of heat due to its higher heat capacity than the atmosphere, absorbing more than 90 % of the excess heat (Rhein et al., 2013). The North Atlantic underwent the most significant warming from all ocean basins down to 2000 m (Levitus et al., 2012; Cheng et al., 2020) – the upper 700 m sustained the most significant increase in Ocean Heat Content (OHC), followed by the layer 700–2000 m (Zanna et al., 2019). In contrast, the upper 2000 m in the subpolar region has been cooling since the 1970s (the well known North Atlantic warming hole or cold blob; Rahmstorf et al., 2015). The emergence of the Atlantic warming hole has been linked to a slowdown of the AMOC, which leads to less ocean heat transport to the subpolar region (Rahmstorf et al., 2015; Caesar et al., 2018; Keil et al., 2020).

The increase of the global mean surface temperature is closely correlated with the concentration of anthropogenic carbon dioxide in the atmosphere (Barnett et al., 2005). Continuous measurements of atmospheric CO₂ at Mauna Loa, Hawaii, showed a solid increase since the 1950s, with an impressive record of 414.26 ppm in December 2020 (NOAA, 2022). The ocean’s greater capacity to store atmospheric CO₂ makes it an important sink for anthropogenic CO₂, playing a significant role in future climate conditions. Friedlingstein et al. (2020) estimated that the global oceans have uptake about 30 % of the total anthropogenic carbon emissions and more than 90 % of the anthropogenic heat since pre-industrial times (Rhein et al., 2013; Meyssignac et al., 2019). Thus, it means that the ocean has absorbed 118 ± 18 Pg ($1 \text{ Pg} = 10^{15} \text{ g}$) of anthropogenic carbon from the atmosphere since the industrial revolution until the mid-1990s (Sabine et al., 2004), followed by 34 ± 4 Pg by the end of 2007 (Gruber et al., 2019).

The continued increase in the ocean’s carbon concentration and warming will negatively impact the marine ecosystem. Among those impacts, ocean acidification and changes in oxygenation, nutrient levels, and primary production are already occurring (Hoegh-Guldberg et al., 2017; Kwiatkowski et al., 2020). Although historical datasets revealed a tight correlation between the heat and carbon uptakes, this correlation shows some divergences in projections for the 21st century (Mortenson et al., 2021; IPCC, 2021). The authors projected that the heat uptake would continue to rise despite the forecasted increase of anthropogenic CO₂; however, the carbon uptake will reach a constant rate by the last third of this century.

The carbon transport within the ocean occurs mainly through three mechanisms: the solubility pump, the biological pump, and the marine carbonate pump (Falkowski et al.,

2000). The solubility pump controls the transport of dissolved organic carbon from the surface down to the ocean's interior and is driven by the temperature gradient between the warm surface and colder deep waters. The biological pump depicts the fixation of carbon dioxide into the organic matter during photosynthesis and its export by the sinking of dead phytoplankton into the ocean's interior. In contrast, the marine carbonate pump counteracts the ocean's uptake of carbon dioxide once the formation of calcareous shells by microorganisms is accompanied by the release of dissolved CO_2 into the surrounding waters, leading to an increase in CO_2 concentration in the upper ocean and further reducing the ocean's CO_2 uptake. A change in any of the components of this delicate cycle will inevitably affect the atmospheric CO_2 concentration and the ocean's sequestration of carbon, and ultimately will influence the Earth's climate and marine ecosystems.

1.2. The North Atlantic Subtropical Gyre

Ocean gyres are large systems of ocean currents driven by the wind (Munk, 1950), covering $\sim 40\%$ of the Earth's surface. Mid-latitude westerlies and zonal trade winds in the subtropics regions force an anticyclonic subtropical circulation, known as the subtropical gyres. The subtropical gyres are constituted by strong western boundary currents, carrying warm waters from the tropics into the subpolar regions, contrasting with weaker and colder currents in the eastern part of the gyres. For this reason, the subtropical gyres are seen as a gateway between the tropics and the polar regions, where the heat transport compensates for the net radiation imbalance between those two regions.

Recent studies highlighted an additional role of the North Atlantic Subtropical Gyre (NASTG) in the Atlantic Meridional Overturning Circulation (Döös et al., 2019; Berglund, 2021). According to the authors, 70% of the water transported northward through the upper limb of the AMOC, the Gulf Stream, recirculates within the subtropical gyre up to 14 times before continuing northward. Over this process, the water becomes denser and deepens in the water column, thus creating a downward spiral and the necessary properties before entering the subpolar gyre.

The NASTG is bordered by the Gulf Stream in the west, characterized by great surface velocities and sharp temperature gradients (known as the Gulf Stream Front), and also by large transports of water, salt, heat, and nutrients from low to mid-latitudes (Pelegri & Csanady, 1991; Imawaki et al., 2013). South of Newfoundland, the Gulf Stream (GS)

splits into the North Atlantic Current (NAC) and the Azores Current (AzC) (Gould, 1985). The AzC and Canary Current (CC) limit the eastern part of the gyre, while the north- and southern limits of the NASTG are the NAC and North Atlantic Equatorial Current (NAEC), respectively (Siedler et al., 2001).

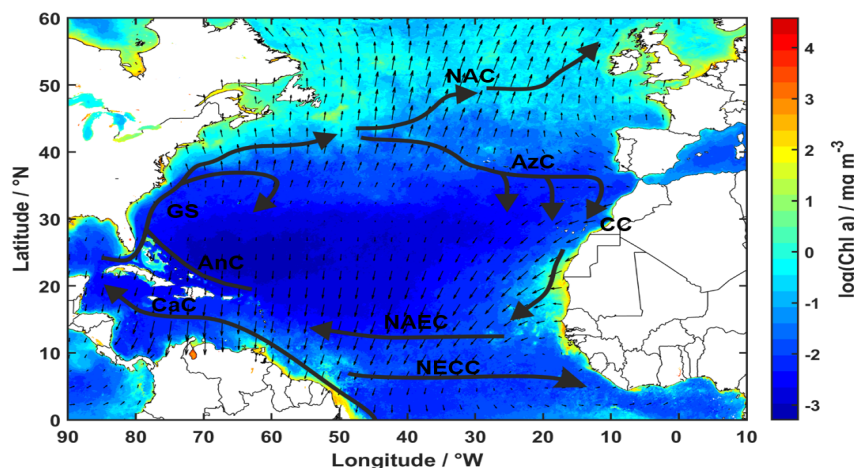


Figure 1.1. Global mean surface Chl *a* concentrations (indicated by the colorbar) from MODIS-Aqua (average for 2020, 4 km resolution) together with a schematic representation of the main currents at the surface of the North Atlantic Subtropical Gyre: Gulf Stream (GS), North Atlantic Current (NAC), Azores Current (AzC), Canary Current (CC), North Atlantic Equatorial Current (NAEC), North Atlantic Equatorial Countercurrent (NECC), Antilles Current (AnC), and Caribbean Current (CaC) (solid black lines; adapted from Daniault et al., 2016; Voelker et al., 2015). Superimposed is the long-term mean wind stress curl over the North Atlantic basin (small black arrows) calculated from the (SODA-POP v2.2.4 product; Carton & Giese, 2008; Giese & Ray, 2011). The Chl *a* data is available at <https://oceancolor.gsfc.nasa.gov/l3/>.

The prevailing wind pattern in the subtropical region induces convergence of Ekman transports towards the gyre’s center, resulting in downwelling or Ekman pumping (McClain & Firestone, 1993). Consequently, the nutricline deepens, suppressing the vertical supply of nutrients, and thus oligotrophic conditions are created in the central part of the subtropical gyres. Hence, these regions are often referred to as biological deserts once the biological production in these regions is low (Fig. 1.1).

The oligotrophic subtropical gyres account for about a quarter of the global primary production (Longhurst, 1998) and contribute to about 50% of global biological organic

carbon export from the surface to the deep ocean (Emerson et al., 1997). These regions are characterized by a deep and relatively stable thermo- and nutricline, and a shallow mixed layer, resulting in an environment strongly nutrient-limited for phytoplankton development (Chavez et al., 2011). Thus, nutrient supply into the euphotic layer in these regions occurs mainly through nitrate fixation, slow diffusion across the thermocline and mesoscale eddies (McGillicuddy et al., 1998; Mahaffey et al., 2003; Mahadevan, 2016). The seasonal cycle of Primary Production (PP) shows a bloom at the surface in winter and early spring due to the action of wind that deepens the mixed layer below the nutricline, supplying the necessary nutrients into the euphotic layer. In summer, the warming of the surface leads to a shallow mixed layer, and phytoplankton growth is significantly reduced. Once the nutrients at the surface are depleted, the primary production occurs at depths with a higher nutrient concentration, but still sufficient light, forming a Depth of Chlorophyll Maximum (DCM) at the lower end of the euphotic zone (Pérez et al., 2006).

The extension of the oligotrophic areas of the subtropical gyres might hint at the subtropical gyre’s variability. Using Chl *a* and Sea Surface Temperature (SST) satellite data since the 1990s, some studies addressed the variability and extension of the oligotrophic area (McClain et al., 2004; Polovina et al., 2008; Irwin & Oliver, 2009; Signorini et al., 2015). The NASTG has been shown to expand at a rate of $\sim 4\% \text{ year}^{-1}$ (e.g., McClain et al., 2004; Polovina et al., 2008; Irwin & Oliver, 2009), the fastest increase rate of all oligotrophic basins. Dave et al. (2015) analyzed the seasonality of the oligotrophic region in the North Atlantic, and they found out that the horizontal supply of nitrate is linked to the expansion and contraction of this area. Furthermore, marine productivity has been declining since the 1950s in the North Atlantic (Gregg et al., 2005; Boyce et al., 2010), associated with the rise of the mean SST in the oligotrophic areas. Global warming scenarios project an increase of vertical stratification at mid-latitudes, further hampering the nutrient inputs into the euphotic layer (Boyce et al., 2010). By the end of the 21st century, a decline in global primary production is likely to occur between 2 to 20 % (Steinacher et al., 2010).

1.3. The Azores Front-Current system

The current knowledge about the Azores Front-Current system was built upon several results of multiple projects and surveys over the last 60 years. Of these, the Kiel 276 mooring (Müller & Waniek, 2013), TOPOGULF (TOPOgraphic GULFstream; TOPOGULF Group,

1986), CANIGO (Canary Islands Azores Gibraltar Observation; Parrilla et al., 2002), Vivaldi '91 (Griffiths et al., 1992; Pollard et al., 1996), SEMAPHORE experiment (Eymard et al., 1996), World Ocean Circulation Experiment (WOCE) (Siedler et al., 2001), and Joint Global Ocean Flux Study (JGOFS) (Fasham, 2003) stand out.

In the northeastern Atlantic, the Azores Front-Current system forms the northeastern boundary of the North Atlantic Subtropical Gyre (Käse & Siedler, 1982; Gould, 1985), separating two different biogeochemical regimes (Longhurst, 1998; Fründt & Waniek, 2012): the warmer and saltier oligotrophic 18°C-mode water in the south and the colder and more productive Eastern North Atlantic Water in the north. The AzC is the main pathway of eastward transport into the Canary Basin. Observations and models show that east of Mid-Atlantic Ridge (MAR), the AzC forms three main branches: the easternmost branch flows into the Canary Basin and feeds the CC (Stramma, 1984; Stramma & Müller, 1989; New et al., 2001), and the other two branches recirculate into the North Atlantic Equatorial Current (NAEC) (Maillard & Käse, 1989). Additionally, the AzC recirculates in two westward flowing countercurrents – north (the Azores Countercurrent (AzCC) Onken, 1993) and south of the AzC jet (Cromwell et al., 1996; Alves & Colin de Verdière, 1999; Peliz et al., 2007; Barbosa Aguiar et al., 2011). The entire Azores Front-Current system, including the two counterflows, spans from 30° to 38°N.

The AzC flows eastward, east of the MAR, between 33° and 35°N, with velocities at surface exceeding 10 cm s⁻¹ decreasing to 5 cm s⁻¹ at 700 m (Stramma & Müller, 1989; Alves et al., 2002). Its transports varies both regional and temporally on seasonal to interannual timescales, from 8 to 18 Sv (1 Sv \equiv 10⁶ m³ s⁻¹) in the upper 1000 m (e.g., Gould, 1985; Klein & Siedler, 1989; Alves et al., 2002; Carracedo et al., 2014). The transports are higher in the western part close to the MAR than east of Madeira Island (Peliz et al., 2007). In situ observations had shown that the AzC's vertical structure penetrates as deep as 2000 m (Gould, 1985; Comas-Rodríguez et al., 2011). Thus, due to the presence of Mediterranean Water lenses (MEDDIES) in the region, the transports calculations are often obscured by those structures, leading to an overestimation of the transports (Alves et al., 2002).

Associated with the Azores Current is a high band of Eddy Kinetic Energy (EKE) at the surface observed using both drifter data (e.g., Richardson, 1983; Brügge, 1995; Fratantoni, 2001) and satellite altimetry (e.g., Le Traon et al., 1990; Barbosa Aguiar et al., 2011; Silva-Fernandes & Peliz, 2020). Values at the surface exceed 200 cm² s⁻² over the MAR (Richardson, 1983), decreasing eastward to 50 cm² s⁻² east of 16°W. The eddy field reveals

the meandering character of the Azores Front (AF)/AzC, which ultimately detached from the AzC and generated west/west-southwestward propagating eddies (Alves et al., 2002; Silva-Fernandes & Peliz, 2020). The dominant scales are of the order of 300 km, or larger, and last about 100 days (Le Traon & De Mey, 1994). The observed baroclinic instability along the jet is associated with the formation of those eddies (Kielmann & Käse, 1987; Alves & Colin de Verdière, 1999). Siedler et al. (1985, 2005) and Fründt et al. (2013), using mooring records, showed that the mean current is dominated by mesoscale events, with periods of 30 to 60 days, associated with the passage of the Azores frontal system through the Kiel 276 mooring.

Meridional transects of temperature and salinity along the Azores region have shown the existence of sharp gradients at sub-surface depths, which were attributed to the Azores Front (Käse et al., 1985; Schiebel et al., 2002; Pérez et al., 2003). Furthermore, those strong gradients were shown to be an important contributor to the subduction in the Northeast Atlantic (NEA) and also in the NASTG (Rudnick & Luyten, 1996; Paillet & Mercier, 1997; New et al., 2001), where weak southward ventilation is seen south of the Azores Current (Pollard et al., 1996; Robbins et al., 2000).

The Azores Front is very hard to detect at the surface. Gould (1985) observed that the AF has a thermal expression during winter, but its signature appeared several miles north of the AF. However, the cloud cover during winter makes the AF detection using satellite imagery difficult. In contrast, the AF is not detectable at the surface in summer due to the development of the seasonal thermocline, masking its thermal signal at the surface.

Different approaches have been used to study both the position and variability of the AF, including the location of the 15 °C-isotherm at 250 m (Fründt & Waniek, 2012) or 200 m (Frazão et al., 2022) and EKE at the surface (Volkov & Fu, 2011). However, to date, only one study assessed the long-term variability of the AF (Fründt & Waniek, 2012). Using a reanalysis product, the authors showed a poleward migration of the AF at a rate of 6 m day⁻¹ at 22°W between the late 1960s and 2009. Nevertheless, the lack of continuous monitoring of the AF makes it challenging to determine its driving mechanism(s) and the reasons behind this northward migration.

The Azores Front forms the northern border of the Eastern North Atlantic Subtropical Gyral Province (NAST-E), a region influenced by the westerly winds (Longhurst, 1998). There, the surface Chl *a* and the DCM show a high latitudinal and seasonal variability – the DCM deepens from spring to summer, and shallows during autumn, reaching 20–

40 m during the winter (Teira et al., 2005; Waniek et al., 2005; Fründt & Waniek, 2012). Conversely, the PP is minimal during summer but increases with the deepening of the mixed layer in autumn and reaches its maximum of 100–150 m in winter (Waniek et al., 2005; Fründt & Waniek, 2012).

Over the last 40 years, many cruises have taken place in the Azores region to understand the role of the AF on the biological pump (Fasham et al., 1985; Fernández & Pingree, 1996; Pérez et al., 2003; Teira et al., 2005, among others). Subtropical fronts, such as the Azores Front, are highly dynamic systems that can sustain a strong biological response due to their spatial and temporal characteristics (Mahadevan, 2016). For example, Fernández & Pingree (1996) reported high production levels in the frontal region, attributing it to the increased phytoplankton biomass. Contrarily, Teira et al. (2005) found no significant differences in primary production across the frontal system using a compilation of thirteen cruises spanning all seasons. However, Fründt & Waniek (2012) reported a difference in nutrient supply and PP north of the front due to shallower Mixed Layer Depth (MLD) compared to the south.

The vertical variability of the Azores Front and the seasonal and inter-annual variability of its position relative to the Kiel 276 mooring position was shown to affect the horizontal currents in the main thermocline (Siedler et al., 2005; Fründt et al., 2013), the productivity in the region (Schiebel et al., 2002), the export production (Brust & Waniek, 2010; Fründt & Waniek, 2012), and the composition and strength of the particle flux (Brust & Waniek, 2010; Brust et al., 2011; Stern et al., 2017, 2019; Pullwer & Waniek, 2020).

The permanence of the Azores Front throughout the year and its relevance for the biogeochemical cycles in the Northeast Atlantic make the AF-AzC system an attractive region to study the impact of climate change over the last century, mainly how does this region respond to accelerated warming and increased anthropogenic carbon dioxide in the atmosphere. For example, Fründt et al. (2015a), in an attempt to estimate the carbon uptake in the subtropical gyre, reconstructed the vertical distribution of Chl *a* in the AF region between 1871 and 2008 and estimated a reduction of 700 megatons in this region. The less carbon uptake by the ocean worldwide in the last century strongly impacts the biogeochemical cycles, and ultimately, sustains the accelerated warming of the oceans in the last and coming centuries.

2. Aims

Thousands of years ago, men looked at the vast oceans and thought the Earth was flat. But humankind's curiosity took them to venture into the unknown, leading to a starting point for exploration and understanding of the oceans. However, modern physical oceanography, as known today, started in the late 19th century with the first scientific expedition designed to explore the world's oceans and the seafloor. The Challenger Expedition took place between 1872 and 1876 and collected water samples, temperature, and currents measurements at 361 sites. The results obtained on this expedition inspired other scientists to study the oceans.

Nowadays, the amount of available data regarding physical, chemical, and biological oceanography is far too large, and the possibility of discoveries is endless. However, long records are still insufficient for a complete understanding of ocean circulation, especially concerning the availability of long records of current data.

The variability of water properties and currents in the ocean have timescales from seconds to millennia. Determining the scales of variability at which some phenomena in the ocean occur remains a great challenge. It is now recognized that humans accelerate some of the observed changes worldwide, both in the ocean and atmosphere (IPCC, 2021). However, one of the greatest challenges for the scientific community nowadays concerns how to distinguish the human influences from the natural variability of the ocean/atmosphere.

In this thesis, the water column in the Northeast subtropical Atlantic region has a central focus. This region has unique characteristics, such as (i) it is the northeastern border of the North Atlantic Subtropical Gyre, separating two distinct biogeochemical regimes; (ii) has the influence of the Azores Current, and (iii) the Mediterranean Water Outflow strongly influences the water column at intermediate depths.

In this context, the aims of this thesis were:

- (a) Determine the long-term variability of the Azores Front-Current system (**Frazão et al., 2022**). The knowledge on the Azores Current was mainly derived from synoptic observations since the 1960s and, more recently, using satellite data. However, the Azores Current's behavior on multi-decadal timescales is unknown;
- (b) Assess the variability of the Mediterranean Water Outflow properties along the western branch in the Northeast Atlantic (**Frazão & Waniek, 2021**);

- (c) Identify the temperature and current changes and the timescales below the main thermocline in the Northeast Atlantic (**Frazão et al., 2021**).
- (d) Assess the impact on CO₂ uptake in the Northeast Atlantic Subtropical Gyre by the determined variability of the physical properties studied in **Frazão et al. (2021)**, **Frazão & Waniek (2021)** and **Frazão et al. (2022)**.

It is instrumental in addressing these questions because of the largest reported changes in the North Atlantic circulation over the last century and millennium (e.g., Caesar et al., 2021). The GS underwent significant changes since the 1960s, partly due to accelerated warming of the oceans (Seidov et al., 2017, 2019) and weakening of the AMOC. The result of those changes in the Azores Current, as the extension branch of the GS in the NEA, were so far not studied. Thus, it is timely to explore the link between changes in the Azores Current and the Gulf Stream, which may shed some additional light on how the Azores Current is connected to the powerful changes in the Northwest Atlantic. Additionally, some studies link the AzC formation to the outflow of the Mediterranean Water through the β -plume mechanism (e.g., Jia, 2000; Volkov & Fu, 2010). Therefore, it is crucial to understand the Mediterranean Outflow Water variability along its western branch towards the North Atlantic interior.

Different datasets were used to assess the temporal and spatial variability of the water properties and currents to accomplish the described aims. As continuous current measurements on the Azores Current spanned only for 30 years (Siedler et al., 2005; Fründt et al., 2013; Müller & Waniek, 2013), an assimilation product (SODA-POP v2.2.4; Carton & Giese, 2008; Giese & Ray, 2011) was used to study the behavior of the Azores Current in the last 140 years (**Frazão et al., 2022**). Further, to understand the variability of the Mediterranean Water Outflow, a compilation of CTD profiles and Argo floats were used and compared with a quality-controlled dataset (EN4; Good et al., 2013) between 1981 and 2018 (**Frazão & Waniek, 2021**). Last, the currents and temperature changes below the main thermocline were assessed using a unique dataset constituted by quasi 30-year uninterrupted measurements in the Northeast Atlantic at the Kiel 276 mooring site (33°N, 22°W) (**Frazão et al., 2021**).

3. Methodological Approach

3.1. Datasets

3.1.1. Temperature and currents from the Kiel 276 mooring

The deep-sea mooring Kiel 276 (at a nominal position of 33°N, 22°W, Fig. 3.1 star) was located in the Madeira Basin, at approximately 5300 m depth (Waniek et al., 2005; Müller & Waniek, 2013). The moored instruments recorded currents and temperatures between April 4th, 1980 and April 21st, 2011 from near-surface down to the deep-sea, within 0.2° in latitude and longitude of the nominal mooring position.

Current measurements were performed by Aanderaa Recording Current Meters (RCM) 4/5 and 7/8, equipped with temperature and mostly near-surface pressure sensors. The RCM sensors have an accuracy of ± 0.2 bar in pressure, ± 0.05 °C in temperature, ± 0.1 cm s⁻¹ in velocity, and ± 0.5 ° in direction (Müller & Waniek, 2013). Temperature and current measurements were taken hourly and later two-hourly resolution (from 1987 forward). Unfortunately, the conductivity cells showed non-linear drifts, and therefore the salinity sensor could not be calibrated with sufficient accuracy.

The dataset used in this study consists on the acquisition of 27 records of temperature and current measurements below the main thermocline, around 1000 m, 1600 m, 3000 m, and 5000 m. The records' length varied between 6 and 24 months, with gaps of up to one week due to schedule arrangements for recovering and re-deployment of the moored instruments. Records' length, the deployment and recovery dates, and the depth of the instruments can be found in Table 1 of **Frazão et al. (2021)**. Longer gaps occasionally occurred due to, e.g., overturning of the instruments (caused by a strong MEDDY in deployment V276140, resulting in a data gap of 282 days between 1993 and 1994 at 1000 m and 1600 m), or malfunctioning of the instruments and errors during deployment (deployment V276200, resulting in a long gap of 300 days in 2000 at all depth levels). More details regarding each deployment are described in Müller & Waniek (2013).

3.1.2. CTD profiles and Argo floats

High-quality in-situ temperature, salinity, and dissolved oxygen CTD profiles were collected from different data centers to study the western branch of MOW, its variability and

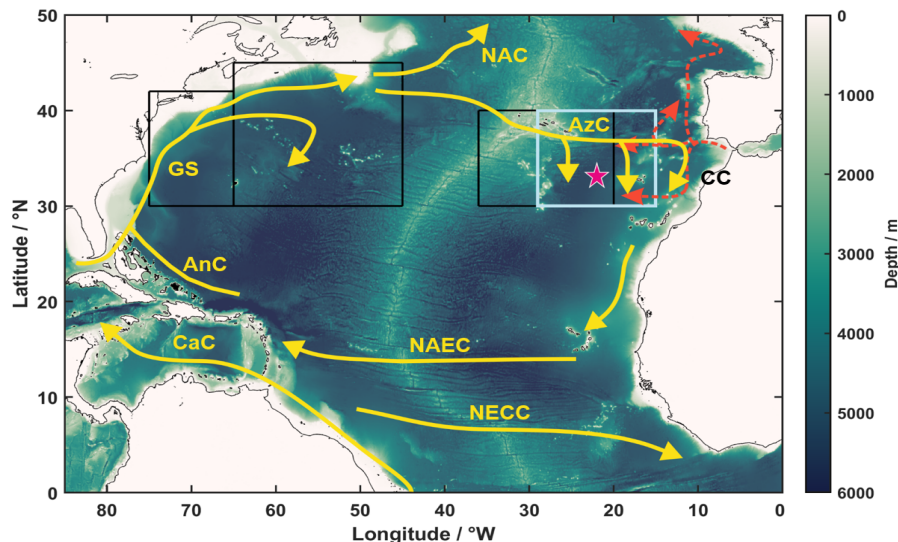


Figure 3.1. Working Areas used in the three publications: black (Frazão et al., 2022; Azores region between 30°N–40°N, 36°–20°W; Gulf Stream region between 30°–45°N, 75°–45°W), light blue (Frazão & Waniek, 2021; 30°–40°N, 29°–15°W), and star (Frazão et al., 2021; Kiel 276 mooring nominal position at 33°N, 22°W). Additionally, the main surface circulation of the North Atlantic Subtropical Gyre is also represented in yellow: Gulf Stream (GS), Azores Current (AzC), Canary Current (CC), North Atlantic Equatorial Current (NAEC), North Atlantic Equatorial Countercurrent (NECC), Antilles Current (AnC), Caribbean Current (CaC), and North Atlantic Current (NAC) (adapted from Daniault et al., 2016; Voelker et al., 2015). Orange arrays are a schematic representation of the main Mediterranean Water Outflow (MOW) pathways after exiting the Strait of Gibraltar (adapted from Carracedo et al., 2014; Daniault et al., 2016; de Pascual-Collar et al., 2019).

property changes since the 1980s in Northeast Atlantic. They include the World Ocean Database 2018 (WOD18) (Boyer et al., 2018, <https://www.ncei.noaa.gov/products/world-ocean-database>), PANGAEA data centre (<http://www.pangaea.de>), and other data centers (details of the cruises used are attached as the supplementary material of Frazão & Waniek, 2021). The study area is limited by the parallels 30°N and 40°N and by the meridians 29°W and 15°W (blue box in Fig. 3.1). Profiles shallower than 1500 m were excluded because the MOW influences in the NEA reaches depths of 1500 m (Iorga & Lozier, 1999a).

Additionally, data from Argo (2001–2018) and Biogeochemical Argo (BGC-Argo) floats

(2010–2018) were gathered to complement the CTD dataset, thus increasing both the spatial and temporal resolution of the final dataset. After the quality check (described in section 3.3.2), the final dataset used in **Frazão & Waniek (2021)** comprised 8839 (1158 CTD + 7681 Argo) temperature and salinity profiles and 1012 (628 CTD + 384 Bio-Argo) dissolved oxygen profiles. The dataset was used to estimate trends for potential temperature, salinity, dissolved oxygen, and density anomalies at the MOW’s core level (centered around 1000 m) between 1981 and 2018. Argo and BGC-Argo data is made freely available by the International Argo Program and can be retrieved at <http://argo.ucsd.edu>.

3.1.3. Objective analyses data

The UK Met Office Hadley Centre EN4 (version 4) dataset was used to compare the trends estimated using the hydrographic dataset (see section 3.1.2 and **Frazão & Waniek, 2021**). The EN4 dataset is a collection of quality-controlled temperature and salinity profiles on a global scale, covering the period from 1900 to present (Good et al., 2013). The final output is a monthly potential temperature and salinity objective analyses, with a 1° horizontal resolution and 42 vertical levels (Good et al., 2013), and bias correction according to Levitus et al. (2009). The potential temperature and salinity were extracted for the blue box in Fig. 3.1, between 900 m and 1200 m, between 1981 and 2018. The data is freely available at <https://www.metoffice.gov.uk/hadobs/en4/download-en4-2-1.html>.

3.1.4. Reanalysis data

Monthly temperature and velocity (zonal and meridional components) fields from the Simple Ocean Data Assimilation (SODA-POP) reanalysis (version 2.2.4 – Carton & Giese, 2008; Giese & Ray, 2011) were used to assess the long term variability of the Azores Current (AzC), Gulf Stream (GS), and Azores Front (AF) between 1871 and 2010 (**Frazão et al., 2022**). The ocean model is based on Parallel Ocean Programming (POP), and the ocean boundary conditions are given by 20CRv2 (Giese & Ray, 2011). Velocity and temperature data were extracted for the regions delimited by black in Fig. 3.1. Monthly outputs have a spatial resolution of $0.5^\circ \times 0.5^\circ$, with 40 depth levels. Carton & Giese (2008) and Giese & Ray (2011) describe the SODA-POP reanalysis product in more detail, including the assimilation data used and the forcing conditions. The monthly data is available at https://coastwatch.pfeg.noaa.gov/erddap/griddap/hawaii_d90f_20ee_c4cb.html.

3.2. Climate Indexes

3.2.1. North Atlantic Oscillation

The North Atlantic Oscillation (NAO) is the primary dominant mode of climate variability on an interannual to decadal scale in the North Atlantic (Marshall et al., 2001; Hurrell et al., 2003). Its direct and indirect (lagged) influence was reported on a broad range spectrum, from large-scale circulation in the North Atlantic basin (e.g., Visbeck et al., 2003), changes in the wind direction and water masses properties (e.g., Curry et al., 1998), to impacts on an ecosystem level (Ottersen et al., 2001; Drinkwater et al., 2003). The NAO is defined as a normalized index based on the sea level pressure anomalies between Lisbon, Portugal, and Stykkisholmur, Iceland (Hurrell, 1995). Once the NAO is more pronounced during wintertime (Marshall et al., 2001), the annual winter-NAO index (December to March) was used in **Frazaõ et al. (2022)** and **Frazaõ & Waniek (2021)**. The winter-NAO index was downloaded from <https://climatedataguide.ucar.edu/climate-data/hurrell-north-atlantic-oscillation-nao-index-station-based>.

3.2.2. Atlantic Multidecadal Oscillation

Opposite to the NAO, the Atlantic Multidecadal Oscillation (AMO) is a major pattern of SST variability in the North Atlantic, with an oscillation period of about 60 to 80 years (Schlesinger & Ramankutty, 1994; Kerr, 2000). Different phases of AMO have been shown to influence the rainfall and river flow in North America (Enfield et al., 2001), as well as an intensification (or weakening) of the severe Atlantic hurricanes (Goldenberg et al., 2001). AMO is defined as the detrended time series of the average SST in the North Atlantic basin (between the Equator and 70°N; Trenberth & Shea, 2006). The monthly AMO time-series used in **Frazaõ et al. (2022)** is accessible at <https://psl.noaa.gov/data/timeseries/AMO/>.

3.3. Validation and quality control

3.3.1. Temperature and currents time-series from the Kiel 276 mooring

For each deployment, the instruments depth was corrected according to the logs and pressure records at the top of the instruments, resulting in an estimation of the best estimate depth for each instrument. As the best estimate depths do not correspond to the nominal depths (1000 m, 1600 m, 3000 m, and 5000 m), the temperature records were adapted to the

nominal depths. A temperature offset was adapted for each deployment depth, comparing the initial (or final) 25-hour median RCM’s record to the closest CTD cast’s temperature value at the nominal depth taken during mooring turnarounds. At 5000 m, the temperature was not adapted to the nominal depths because not all CTD casts reached the 5000 m depth. The current records were not corrected to the nominal depths. In the last step, each record adapted to the respective nominal depth was low-pass filtered (35-hour half-power period) to remove the higher frequency signals. The resulting temperature and current time-series were daily averaged.

3.3.2. Quality control and monthly objective analyses fields from the in situ data

All profiles from the WOD18 dataset have associated quality control flags for every parameter (Boyer et al., 2018). Thus, only profiles with a “good quality data” flag were used. Subsequently, all profiles from the different data centers were checked for erroneous data, including density inversions, spikes and/or high noise profiles, systematic deviations in salinity, and missing temperature or salinity values. From this point on, the profiles flagged as bad were excluded.

Argo and BGC-Argo control assessment followed Wong et al. (2020). In addition, the selected Argo and BGC-Argo profiles went through the delayed mode quality control and were flagged as very good data.

The dissolved oxygen profiles were inspected for systematic shifts compared with a mean vertical profile averaged over the study domain (Fig. 3.1, blue box) using the World Ocean Atlas 2018 (WOA18) (Garcia et al., 2018).

Potential temperature (θ , referred to the surface) and potential density (σ_θ and σ_1 , referred to the surface and 1000 dbar, respectively) were determined for each profile (UNESCO, 1983). Each profile was then interpolated at 20-dbar pressure intervals between 600 and 1500 dbar. The obtained profiles were monthly interpolated over a regular grid of $2^\circ \times 2^\circ$ to obtain objective analyses field (Barnes, 1973), attributing to each profile a weight according to the distance from the grid points (assuming a 1° decorrelation length). The monthly objective analysis fields were calculated using the Matlab[®] script obtained from <https://www.mathworks.com/matlabcentral/fileexchange/28666-barnes-objective-analysis>.

The annual anomalies time-series were determined by subtracting the climatological

mean between 1981 and 2018 from the annual mean values. Then, the climatological mean was calculated for each property using all monthly mean values.

3.3.3. Azores Current, Gulf Stream, Azores Front and Ocean Heat Content

The variability of the Azores Current and Gulf Stream between 1871 and 2010 was analyzed by identifying the core of each current in the upper 1000 m. The AzC region was delimited between 36° and 20°W to avoid the influence of the MAR in the west, and the recirculation system east of 20°W (Barbosa Aguiar et al., 2011). In turn, the GS area was divided into sub-regions (75°–65°W, 65°–55°W, 55°–45°W) according to its dynamics and resilient position of the jet-like flow along the eastward US coast (Dong et al., 2019; Seidov et al., 2019). Finally, the position of both cores was delimited between the latitudes where the averaged velocity over the upper 1000 m was maximum at each sub-region (see Figs. 2a and 3a in **Frazão et al., 2022**).

The Azores Front position was determined as the latitude of the 15 °C-isotherm at 200 m depth between 30°W and 20°W. West of 30°W, the AF shows higher variability (standard deviation of up to 2° latitude) mainly due to the proximity to MAR. At the same time, east of 20°W, the AF position is more variable due to the Azores Current recirculation.

The integrated OHC was computed for the upper 400 m between 30°N–40°N and 30°W–20°W following the methodology of Levitus et al. (2012). Briefly, at each point of the grid and every depth level, the climatological mean was subtracted from each monthly temperature value. The climatological mean was calculated using all monthly fields between 1871 and 2010 at every standard depth level.

3.3.4. Vertical distribution of Chl *a* and CO₂ uptake estimates

Temperature fields covering the entire region of the NASTG between 10°–40°N and 80°–10°W were used to reconstruct Chl *a* hindcasts for the period 1871–2010. The method to reconstruct Chl *a* fields using in situ temperature and nitrate measurements was developed and applied at the Kiel 276 position (33°N, 22°W) by Fründt et al. (2015b). Briefly, the method consists of three main steps: (1) in situ nitrate measurements were fitted to in situ temperature using a first-order Gaussian equation, resulting in a temporally and vertically resolved nitrate field; (2) measured Chl *a* concentrations were also fitted to both temperature and nitrate, obtaining a first Chl *a* hindcast reconstruction. Last, (3) the

euphotic depth was calculated at each time, and the Chl *a* overshooting was removed for depths greater than the euphotic depth due to higher nitrate concentrations. More details regarding the method’s assumptions and equations used are described in Fründt et al. (2015b). Finally, the method was applied on the SODA-POP temperature fields (see section 3.1.4) for the entire subtropical NA, resulting in nitrate and Chl *a* time-series with a 0.5° horizontal resolution and 1 m vertical resolution for the upper 300 m.

The validation of the method developed by Fründt et al. (2015b) was extended to the closest position of the Bermuda Atlantic Time series Study (BATS) station (31.25°N, 64.25°W; Fig. 3.2), once BATS is the longest time-series of biogeochemical data in the North Atlantic. The BATS station, as part of the Joint Global Ocean Flux Study program to understand changes in the biogeochemical cycles on seasonal to decadal timescales, is located in the Sargasso Sea, 82 km southeast of the Bermuda. Monthly sampling took place since October 1988, and during winter an additional survey was done to resolve the spring-bloom period (Steinberg et al., 2001). The data from the BATS station is available at <http://bats.bios.edu/>.

The time-series of nitrate and Chl *a* measured in the upper 200 m at the BATS stations were used (Fig. 3.2a,b) to validate the method. Visual inspection shows that there is a good agreement between the calculated Chl *a* fields and the in situ data – higher Chl *a* concentrations at the surface are found in winter and early spring, a result of the spring-bloom, and a DCM is well defined between 60 and 120 m (Fig. 3.2b; Steinberg et al., 2001). Additionally, derived Chl *a* concentration at the surface from satellite ocean colour data was calculated at the closest point to the BATS station between 1997 and 2010 (Fig. 3.2c). Reconstructed Chl *a* concentrations at the surface reproduce the beginning and the end of the spring bloom (Fig. 3.2c), although occasionally the magnitude of the spring bloom is under- or overestimated. The correlation coefficient between the remotely measured Chl *a* and the calculated Chl *a* between 1997 and 2010 is 0.59. The ocean colour daily data was obtained from <https://cds.climate.copernicus.eu/cdsapp#!/dataset/satellite-ocean-colour?tab=form> (version 5.0.1), and averaged on a monthly basis.

The resulting temperature time-series at BATS, Kiel 276, and NASTG are presented as an averaged temperature of the upper 300 m. Additionally, the nitrate and Chl *a* time-series are shown as depth-integrated time-series of the upper 300 m.

The carbon uptake difference (ΔCU) was estimated for each point of the grid over the NASTG between 1871 and 2010 using $\Delta CU = \Delta_{Chl a} \times R \times A$, where $\Delta_{Chl a}$ is the difference

in integrated Chl *a* concentration between the surface and 300 m, $R = 50$ is the carbon/Chl *a* ratio, and $A = 2.04 \times 10^8 \text{ km}^2$ is the area of the NASTG (Polovina et al., 2008).

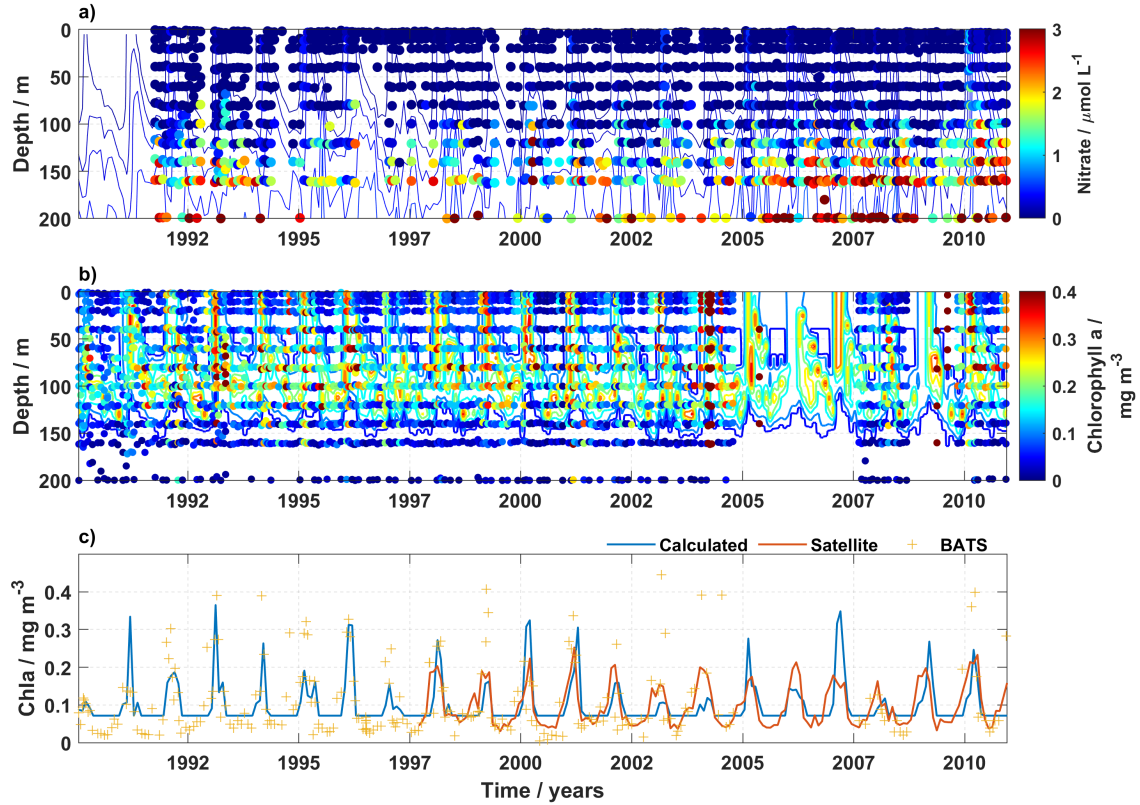


Figure 3.2. Comparison between the reconstructed vertical distributions (isolines in background) and the in situ measurements (colored circles) of nitrate (a) and Chl *a* (b) at the closest point of the BATS station (31.25°N , 64.25°W). (c) Validation of the calculated Chl *a* concentration at the surface (solid blue line) with the surface Chl *a* concentration measured remotely (solid orange line). In situ surface Chl *a* concentration measured during the surveys around the BATS station are also represented by a yellow cross.

4. Results and Discussion

4.1. Long-term variability of the Azores Front-Current system

The Azores Current is long recognized as a part of the NASTG (Gould, 1985). However, the existing studies in this region do not give a comprehensive picture of the underlying mechanisms of the Azores Front-Current system (Spall, 1990). To date, most modeling and synoptic descriptions focused mainly on the AzC's transports (Alves et al., 2002; Peliz et al., 2007; Carracedo et al., 2014, among others), its vertical structure (Stramma & Müller, 1989; Comas-Rodríguez et al., 2011), meandering of the AF-AzC (Siedler et al., 1985; Alves et al., 2002; Siedler et al., 2005), zonal EKE variability (Richardson, 1983; Le Traon et al., 1990; Le Traon & De Mey, 1994; Pingree, 1997; Barbosa Aguiar et al., 2011; Volkov & Fu, 2011; Silva-Fernandes & Peliz, 2020, among many others), and the formation of the AzC as a result of the water masses exchange in the Gulf of Cadiz, known as the β -plume mechanism (Jia, 2000; Özgökmen et al., 2001; Peliz et al., 2007; Kida et al., 2008). However, this latter hypothesis still cannot fully explain the observed features of the AzC. In addition, the Azores Current variability on a multi-decadal timescale is unexplored, and its connection to the large-scale circulation in the North Atlantic basin has not been inferred. Thus, using an assimilation product (SODA-POP version 2.2.4; for more details, see section 3.1.4), the long-term variability of the AzC and the AF was assessed between 1871 and 2010 and put in the context of changes in the large-scale circulation in the North Atlantic basin, mainly in the NASTG. The results are discussed in **Frazão et al. (2022)**.

In the last 140 years, the Azores Current underwent two periods of weakening: the first and most pronounced occurred between 1962 and 1983, with a reduction of 24% of the velocity, and a second period between 2000 and 2005 (Fig. 4.1a). Between those periods, the velocity slightly increased, confirmed by the Kiel 276 mooring measurements at 33°N, 22°W (Siedler et al., 2005; Fründt et al., 2013). However, the velocities never returned to the pre-1960s values.

The origin of the Azores Current is currently under debate. Early studies placed the origin of the Azores Current southeast of the Grand Banks region (40°N, 45°W) in the transition zone between the Gulf Stream (GS) and the NAC (Stommel et al., 1978; Gould, 1985; Klein & Siedler, 1989). There, the GS splits into three main branches: the NAC, a second branch entering the recirculation system south of the GS, and a third branch

flowing into the eastern Atlantic (Richardson, 2001; Schmitz & McCartney, 1993). The latter heads southeastward until it crosses the MAR and then flows eastward towards the Strait of Gibraltar. Thus, it may be expected that changes in the GS would ultimately be mirrored in the AzC (Frazão et al. 2022).

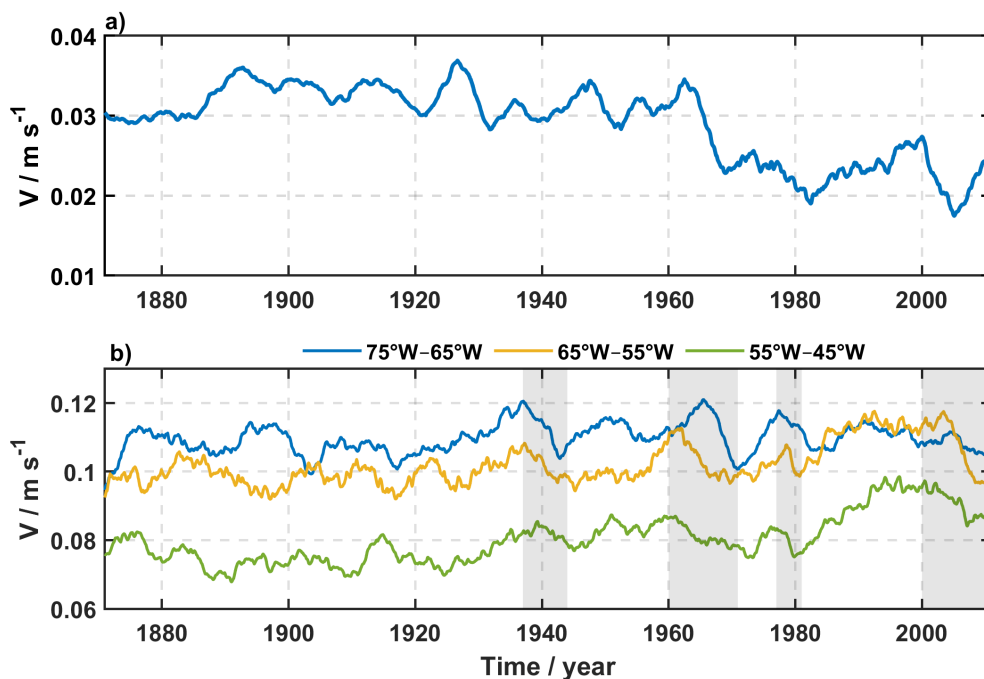


Figure 4.1. (a) Monthly vertical average absolute velocity (upper 1000 m) along the Azores Current core (between 32°N and 36°N, 36°W and 20°W). (b) Monthly vertical average absolute velocity (upper 1000 m) along the Gulf Stream core for each sub-region (western: 75°–65°W, solid blue line; central: 65°–55°W, solid yellow line; eastern: 55°–45°W, solid green line). All time-series are smoothed using a 60-months moving mean between 1871 and 2010 (adapted from Frazão et al., 2022).

The Gulf Stream has shown periods of intensification and weakening during the last century (Fig. 4.1b). The weakening that occurred during the 1960s and 1970s accounted for 10% in all sub-regions of the GS (Fig. 4.1b), was also described by Greatbatch et al. (1991) using a diagnosis model or Ezer (2015). Notably, the recent decline of the GS reported by Ezer (2015) or Dong et al. (2019) after 2000 is also present in the SODA-POP dataset (Fig. 4.1b).

The Azores Current and the Gulf Stream’s absolute velocity do not strongly correlate ($\rho > -0.5$ for the central and eastern regions, and $\rho = -0.1$ for the western region). Although a negative correlation coefficient between both currents emerged for the entire period, the correlation between the AzC and GS reversed to positive values after the 1960s (**Frazão et al., 2022**). Those weak correlations are possibly due to the different driving mechanisms that control both currents. While the bottom topography controls the western flank of the Gulf Stream (west of 65°W), the central and eastern parts of the Gulf Stream behave as a free baroclinic jet not constrained by the topography (Dong et al., 2019), similarly to the AzC. Reinforcing this line of argumentation, Andres et al. (2020) and Zhang et al. (2020) calculated different trends between the western and eastern parts of the Gulf Stream between 1993 and 2016. Additionally, the recirculation gyres north and south of the GS jet were shown to influence the position of the Gulf Stream jet (e.g., Marchese, 1999).

The Azores Front, the northern border of the Azores Current, showed a gradual poleward migration since the 1970s, at a rate of 12 m day^{-1} (Fig. 4.2). The AF’s north- and southward movements are hand-in-hand with the integrated OHC in the upper 400 m ($\rho = 0.92$; Fig. 4.2) and the AMO ($\rho = 0.69$; **Frazão et al., 2022**). Similarly, Seidov et al. (2019) found that the GS’s position variations strongly correlate with the AMO and OHC, with a higher correlation coefficient between the GS position and the OHC. Therefore, the thermal conditions observed in the North Atlantic basin (hence AMO and OHC) ultimately reflect the extension of the warmer subtropical water, as implied both in the AF and GS’s position definitions (Gould, 1985; Seidov et al., 2017).

The Azores Front lies in a region where the Ekman transports north and south of the Azores Current converge (Fründt & Waniek, 2012; Volkov & Fu, 2011). The position of this convergent zone is impacted by changes in the wind direction (Fründt & Waniek, 2012), affecting the position of the AF. The NAO is associated with altering the wind pattern in the North Atlantic (Visbeck et al., 2003). Both Volkov & Fu (2011) and Fründt & Waniek (2012) determined a lagged correlation between the NAO and the AF position of the order of months, likely caused by an adjustment of the upper water column to changes in the wind direction. However, on a multi-decadal timescale, the NAO does not seem to be linked with the variability of the AF position (**Frazão et al., 2022**). This lack of correlation between the Azores Front position and the NAO might be explained by the different definitions of the Azores Front (Volkov & Fu, 2011; Fründt & Waniek, 2012) and the expected stronger influence of the NAO at the surface instead of at sub-surface depths (Visbeck et al., 2003).

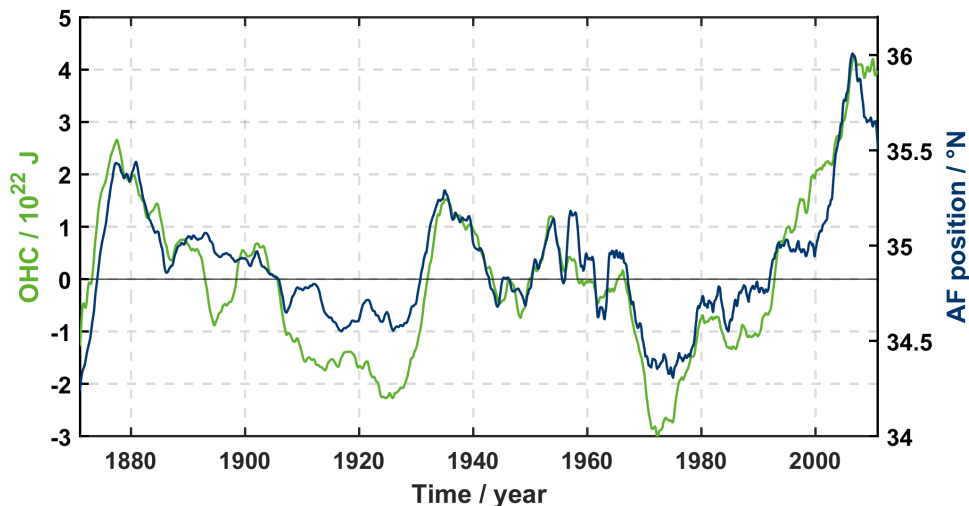


Figure 4.2. Monthly integrated Ocean Heat Content (OHC) in the NEA for the upper 400 m of the water column (solid green line), and the monthly AF position averaged between 30° and 20°W (solid blue line). Both time-series are 60-months smoothed (from **Frazão et al., 2022**).

Nevertheless, the results described in **Frazão et al. (2022)** are similar to the findings of Seidov et al. (2019), where the authors did not find any correlation between the NAO and the GS position on decadal and longer time scales, contradicting previous studies of Taylor & Stephens (1998) or Frankignoul et al. (2001).

It was shown that the Azores Current mirrors the changes observed along the Gulf Stream’s path, with a two-year lag (**Frazão et al., 2022**). Therefore, one may anticipate that both currents’ position and northern walls, the Gulf Stream North Wall (GSNW) (Taylor & Stephens, 1998) and the Azores Front, might also be connected. Fründt & Waniek (2012) calculated the lagged correlations between the AF and the GSNW and showed that the AF movements influence the drift of the GSNW with a lag of one year. Although the GS position is remarkably resilient on a decadal scale, the extension zone of the GS (east of 50°W) showed the largest northward propagation, mainly in recent decades (Wu et al., 2012; Seidov et al., 2019). Likewise, following the regime change of the Azores Current in the 1960s, the AzC’s core position displaced approximately 0.5° northward from the 1960s onwards (**Frazão et al., 2022**).

A change in the position of the delimiting currents of the subtropical gyres may pose

consequences so far unknown. Yang et al. (2020), using sea surface height and SST satellite data, observed that the subtropical gyres are moving poleward. However, the trends are insignificant for most gyres due to strong natural variability. Nevertheless, the authors proposed that the observed shifts are most likely to occur under global warming conditions. Siedler et al. (2005) and Fründt et al. (2013), using observations from the Kiel 276 mooring in the Madeira basin, suggested that the changes observed in the main thermocline are related to a possible displacement of the subtropical gyre, with the AzC's core position more southward in the 1990s than in the previous decades.

The 1950s and 1970s seem to be a critical period for changes in the North Atlantic circulation and water properties (e.g. Levitus, 1989; Levitus et al., 2012; Reverdin, 2010). In **Frazão et al. (2022)**, the authors proposed the existence of two transient periods, 1871–1959 and 1960–2010, where the driving mechanisms might be variable in time. Before the 1960s, the wind had a dominant role in the North Atlantic circulation, preferably over the AzC, GS and NAC, with the signals of GS and NAC better correlated compared with the GS and AzC. Roughly after the 1960s, the ongoing warming and consequent increase in the Ocean Heat Content (Fig. 4.2) led to stronger density gradients. As a result, the correlation between the Gulf Stream and the zero-line of the wind-stress curl reduced but increased with the AMO and the OHC, as for the Azores Current. By the end of the 20th century, the OHC pool south of the GS rapidly increased, and the GS deviated northward (Seidov et al., 2019). Concurrently, the strongest weakening of the AMOC was reported, resulting in a subpolar gyre strengthening (Zhang, 2008) and a decline of the GS and the AzC. Allegedly, the dipole observed by Zhang (2008), where a robust (weaker) AMOC induces a weaker (stronger) subpolar gyre, can be viewed as a seesaw in the Gulf Stream changes signal between the AzC and the NAC, depending on the behavior of the GS bifurcation region.

Attempts to derive the Azores Current and also the NASTG mean position using in-situ data were already done in the 1980s (Stramma & Siedler, 1988; Stramma & Isemer, 1988; Klein & Siedler, 1989). The authors noticed that the winter's AzC position is further north than in summer, attributing a seasonal characteristic to the AzC that was not found during the last century (**Frazão et al., 2022**). This might be attributed to the datasets used by those authors, which relied on discrete cruises taken before and during the 1980s. Later, Käse & Krauss (1996), in an effort to explain the origin of the AzC, proposed that this current was an extension of the Gulf Stream, forced by wind and buoyancy. They suggested

that the AzC flows south of the zero-line of wind stress curl; however, this hypothesis does not explain why its position does not change despite the region's large seasonal wind stress curl variations. Also, model simulations failed to reproduce an AzC forced by the wind stress (Jia, 2000; Paiva et al., 2000). Furthermore, Sverdrup dynamics only partly explains the zonal orientation of the Azores Current because the AzC axis is located south of the mean zero wind stress curl, and the resulting Ekman pumping in this region requires a southward transport (Townsend et al., 2000). Atmospheric forcing (hence, NAO) was shown to have little impact on the interannual variability of the Azores Current. However, for longer timescales (over 25 years), the winter NAO index and the annually-averaged AzC are positively correlated, with the NAO leading the signal of the AzC by 41 years (**Frazaõ et al., 2022**).

Recently, modeling studies considered the effect of water masses exchange in the Gulf of Cadiz (entrainment of Atlantic Central Water and outflow of the Mediterranean Water) and showed that a cyclonic recirculation is generated, which can explain the existence of the Azores Current and the Azores Countercurrent (Jia, 2000; Özgökmen et al., 2001; Kida et al., 2008; Volkov & Fu, 2010). These models rely on the dynamic concept of the β -plume mechanism (Stommel, 1982). However, some observational characteristics of the current appear to contradict this hypothesis – the jet's intensity and the higher transports west of Azores Islands than close to the Gulf of Cadiz. Using a more realistic model, Peliz et al. (2007) hypothesized that the wind forcing and the β -plume could explain the westward transport increase of the AzC. Lamas et al. (2010) provided the first observational evidence of the cyclonic recirculation west of the Gulf of Cadiz, combining both the β -plume and wind forcing. Although theoretically these models explain the existence of the Azores Current and Azores Countercurrent, there is a lack of observational evidence to refute or reinforce this hypothesis. Nevertheless, some authors showed that the extension of the MOW in the NEA is restricted to the south by the presence of the Azores Current (Sy, 1988; Ríos et al., 1992). Thus, it is important to understand the spatial and temporal variability of the MOW in the northeast Atlantic and then hypothesize how the MOW impacts the strength and position of the AzC.

4.2. Mediterranean Water Outflow in the Northeast Atlantic

The Mediterranean Water Outflow (MOW) salt tongue is a well-recognized feature flowing at mid-depths in the Northeast Atlantic as it is present in every climatological study (e.g., Lozier et al., 1995; Iorga & Lozier, 1999a,b; Bashmachnikov et al., 2015b). In the Gulf of Cadiz, the outflow of Mediterranean Water mixes with the surrounding North Atlantic Central Water to form the MOW. The Mediterranean Water entering the Strait of Gibraltar is a mixture of intermediate and deep waters – the Levantine Intermediate Water (LIW) and the Western Mediterranean Deep Water (WMDW). The resulting outflow is a high-saline and warm water mass that sinks in the Gulf of Cadiz until it reaches a buoyant depth of ~ 1000 dbar (Zenk, 1975; Ambar et al., 1976). After passing the Gulf of Cadiz, the MOW signature is found at mid-depths of the North Atlantic basin along two main advective-diffusive pathways: (i) northward, as an eastern boundary undercurrent across the western margin of the Iberian Peninsula, and into the western European continental slope (Reid, 1979; Bower et al., 2002); and (ii) westward, towards the central subtropical North Atlantic (Reid, 1978; Iorga & Lozier, 1999a). Additionally, the MOW also spreads southwestward, mainly in the form of MEDDIES generated in the proximity of Cape St. Vicent, south of Portugal (Armi & Zenk, 1984; Serra et al., 2005; Bashmachnikov et al., 2015a).

The vast extension of the MOW and its characteristic high salinity and temperature are a source of salt and heat into the North Atlantic Ocean (Zenk, 1975). The penetration of the diluted northward MOW’s branch as far as 50°N into the subpolar gyre (Lozier & Stewart, 2008; Sarafanov et al., 2008), an important region for the global overturning circulation, can impact the properties of the deep waters in the Northeast Atlantic (Sarafanov, 2009), which ultimately contribute to the thermohaline circulation. It was suggested in several studies that the salt input from the MOW could influence the different stages of the AMOC in the last glacial cycle (e.g., Voelker et al., 2006; Swingedouw et al., 2019; Sierro et al., 2020). Also, the presence of a westward pathway has been shown to strongly impact the upper layer dynamics (Jia, 2000; Kida et al., 2008). Thus, it is timely to understand the variability of the MOW’s properties along the western branch over time (thickness of the layer, temperature, salinity, dissolved oxygen) to perceive what role the MOW plays in the upper layer circulation on a multi-decadal timescale.

The variability of MOW properties at its core (~ 1000 – 1100 m) since 1980 were assessed

using two different datasets: daily temperature and velocity records at 1000 m from the Kiel 276 mooring in **Frazão et al. (2021)** (see section 3.1.1) and gridded objective analysis fields in **Frazão & Waniek (2021)** (see section 3.1.3, Fig. 3.1).

At the Kiel 276 mooring, the annual mean temperature increased by $0.03 \pm 0.01 \text{ }^\circ\text{C year}^{-1}$ at 1000 m between 1980 and 2009 (**Frazão et al., 2021**). Although gradual warming was observed over the entire period and within decades, the significant increase in temperature occurred from the 1980s to the 2000s (Fig. 6 in **Frazão et al., 2021**). Concurrently, the average speed, Mean Kinetic Energy (MKE) and Fluctuating Kinetic Energy (FKE) also intensified over the decades. 16 MEDDIES crossed the Kiel 276 mooring during this period, ten between 1980 and 2000 (Siedler et al., 2005), and six in the 2000s (**Frazão et al., 2021**). Siedler et al. (2005), using 20 years of Kiel 276 mooring records, suggested that the AF may act as a barrier to the MEDDIES propagation, in a way that a more southward (northward) position of the AF relative to the Kiel 276 mooring decrease (increase) the probability of MEDDIES crossing the mooring. As previously discussed, the AF has been migrating northward since the 1970s (**Frazão et al., 2022**). However, the number of MEDDIES that crossed the Kiel 276 has not increased over time. In fact, during the 1990s, the number of MEDDIES that crossed the mooring decreased by 50 % (Siedler et al., 2005). Thus, additionally to the possibility of the AF acting as a barrier to MEDDIES, there might be other processes that were not yet considered.

Along the western branch of Mediterranean Water Outflow, the temperature at the core decreased by $-0.015 \pm 0.007 \text{ }^\circ\text{C year}^{-1}$ and freshened by $-0.003 \pm 0.002 \text{ year}^{-1}$ between 1981 and 2018 (**Frazão & Waniek, 2021**). However, the freshening and cooling at the MOW level were also marked by periods of warming and salinification, especially after 2011 (Fig. 2 and Tab. 1 of **Frazão & Waniek, 2021**). The density at the core did not change significantly over time, indicating that the changes at the core level were density-compensated, as also shown by Potter & Lozier (2004). The dissolved oxygen concentration also decreased over the same period by $-0.426 \pm 0.276 \text{ } \mu\text{mol kg}^{-1} \text{ year}^{-1}$. This trend follows the reported deoxygenation at intermediate depths in the NEA, attributed to changes in the ventilation derived from both the solubility (due to temperature) and large-scale circulation (Johnson & Gruber, 2007; Stendardo & Gruber, 2012; Stendardo et al., 2015).

The observed variability at the MOW's core shows that changes occur at interannual to decadal timescales (**Frazão et al., 2021; Frazão & Waniek, 2021**). At the Kiel 276 site, seasonal variability of temperature and currents on a decadal and long-term scale is

negligible and highly influenced by the passage of MEDDIES across the mooring (**Frazão et al., 2021**). In the NEA, the variability of dissolved oxygen concentration at the MOW’s core is more evident on an inter-decadal timescale. The dissolved oxygen variability in the Mediterranean Sea on a multi-decadal timescale was attributed to the different deep water formation events, namely the Eastern Mediterranean Transient in the late 1980s and the western Mediterranean Transient in the mid-2000s (Mavropoulou et al., 2020). Furthermore, the decrease in oxygen concentration in the upper 1000 m worldwide due to increased temperature cannot be neglected in this context. Most likely, the weak deoxygenation reported by **Frazão & Waniek (2021)** might have been connected to the warmer outflow since the 1950s (Krahmann & Schott, 1998; Naranjo et al., 2017).

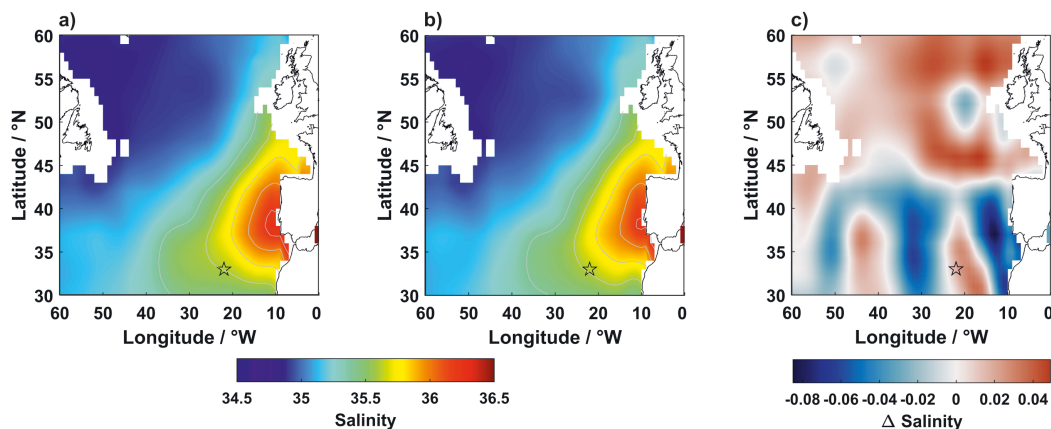


Figure 4.3. Salinity distribution averaged over the MOW’s core (1000–1100 m) from the WOA18 (Zweng et al., 2018) (a) between 1965–1974, and (b) 1985–1994. (c) Salinity difference between (a) and (b). The black star represents the location of the Kiel 276 mooring (adapted from **Frazão & Waniek, 2021**).

In the North Atlantic, the study of properties changes at intermediate depths has occupied a significant place in the literature since the 1980s (e.g., Levitus, 1989; Parrilla et al., 1994; Arbic & Owens, 2001). An extensive literature review of the salinity and temperature trends since the early 1940s at the MOW depths in the NA and the Mediterranean Sea basin is presented in Table 2 of **Frazão & Waniek (2021)**. The reported trends are not consistent over time, with some authors estimating warming (e.g., Potter & Lozier, 2004; Bozec et al., 2011, **Frazão et al., 2021**), cooling (Costoya et al., 2014, **Frazão & Waniek, 2021**), or no trends (Soto-Navarro et al., 2012). This disagreement depends not only on

the choice of the dataset but also the period, the depth levels, and the region (Table 2 in **Fraão & Waniek, 2021**). Trends calculated over a period longer than 20 years (i.e., on multi-decadal timescale) revealed lower values of the order of 10^{-3} , compared with decadal trends. Furthermore, different datasets imply different averaging, interpolation, and/or smoothing settings, thus influencing the calculated trend (e.g., Hurrell & Trenberth, 1999; Gregory et al., 2004, **Fraão & Waniek, 2021**).

In contrast to the trends estimated in the NEA, the Mediterranean Outflow in the Strait of Gibraltar/Gulf of Cadiz region has been gradually warming since the 1950s (e.g., Fusco et al., 2008; García-Lafuente et al., 2021). Thus, one might ask what drives the observed differences at intermediate depths in the NEA. The variability in the MOW properties in the NEA has been attributed to changes in the outflow properties (Potter & Lozier, 2004; Millot et al., 2006; Leadbetter et al., 2007) and to large-scale circulation that alters the pathway of MOW in the NEA (Lozier & Sindlinger, 2009; Bozec et al., 2011; Chaudhuri et al., 2011). Bozec et al. (2011) and Chaudhuri et al. (2011), using modeling results, showed that the preferential pathway of MOW shifted as a result of a large-circulation adjustment to external wind-forcing conditions, hence the predominant NAO-phase. **Fraão & Waniek (2021)**, using a combination of in situ data and a quality-controlled dataset (EN4), estimated the trends at the MOW’s core according to the predominant NAO phase. They showed that the detected trends in the NEA for the different periods of positive (negative) NAO-phase might be related to an expansion (retraction) of the MOW tongue, with the core properties lagging 7–8 years the NAO signal (Fig. 4.3a – negative NAO-phase, Fig. 4.3b – positive NAO-phase). Briefly, during a negative NAO-phase, the subpolar front moves westward, allowing the MOW to advance northward into the subpolar gyre, with the reverse situation for periods of positive NAO-phase (Lozier & Stewart, 2008; Chaudhuri et al., 2011, and Fig. 4.3c).

4.3. Deeper Northeast Atlantic

For a long time, physical oceanographers defined the deep ocean as approximately 1000 m, based on the assumption of the *level of no motion*. However, it is now recognized that the deep ocean is dynamic. The ocean basins deeper than 2000 m, corresponding roughly to half of the ocean volume, are sparsely sampled in space and time. The existing measurements of the deep global ocean were mainly derived from repeated oceanographic surveys, and

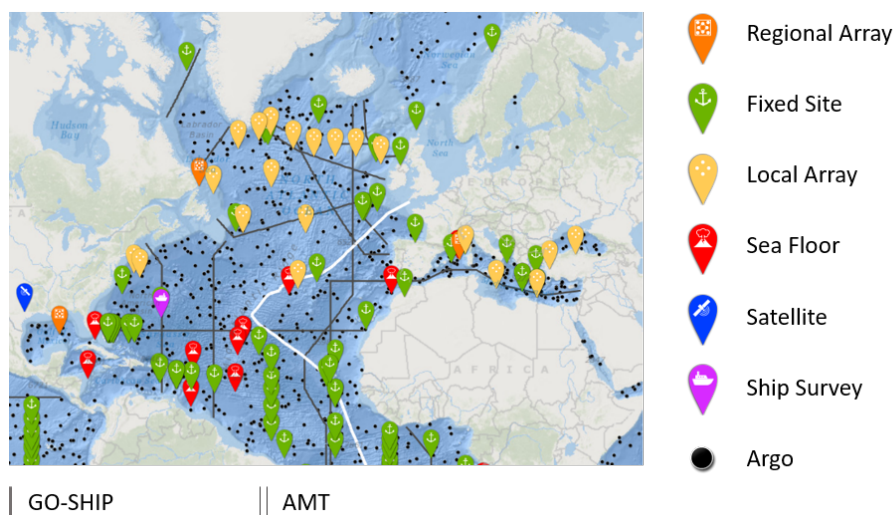


Figure 4.4. Deep-ocean observing platforms in the North Atlantic (adapted from the interactive map available online at <https://deeoceanobserving.org/deep-ocean-observations/>).

the accuracy and uncertainty of the data are strongly dependent on the time of sampling (Lyman & Johnson, 2014; Meyssignac et al., 2019). Among those programs, the JGOFS, WOCE, Global Ocean-Based Hydrographic Investigations Program (GO-SHIP), and Atlantic Meridional Transect (AMT) are the greatest contributors to the deep ocean knowledge nowadays (Fig. 4.4). In the NEA basin, the North East Atlantic Dynamics Study (NEADS) initiative placed a set of full-depth moorings starting in 1978 to describe the mean circulation and eddy kinetic fields along the entire water column (e.g., Dickson et al., 1982, 1985). Afterward, the 5300 m Kiel 276 mooring was placed in the Madeira Basin from 1980 until 2015 and recorded temperature and currents from the main thermocline depths to close to the seafloor (Müller & Waniek, 2013, and section 3.1.1 for more details). The 30-year record allowed to study the variability of temperature and currents on timescales from daily to seasonal, annual and long-term, in a region highly influenced by the presence of the AzC-AF system in the upper water column (Käse & Siedler, 1982, **Frazão et al., 2022**), the MOW and the passage of MEDDIES at intermediate depths (Armi & Zenk, 1984; Siedler et al., 2005, **Frazão & Waniek, 2021**), and the North Atlantic Deep Water (NADW) below 2000 m (Zhai et al., 2021).

At the Kiel 276 mooring, the deeper water column below 1600 m underwent different changes. At 1600 m, the temperature increased by $0.02 \pm 0.02 \text{ } ^\circ\text{C year}^{-1}$ but no long-term

trend at 3000 m between 1980 and 2009 (see Fig. 7 in **Frazão et al., 2021**). In addition, no seasonal signal in temperature emerged below 1000 m. The warming at 1600 m was gradual over decades but not significant. However, the warming was significant from the 1980s to the 2000s at 1600 m (see Fig. 6 in **Frazão et al., 2021**). This is in line with the temperature development in the upper thermocline at the same site (Fründt et al., 2013). Notwithstanding, the warming of the water column calculated at the Kiel 276 position is not restricted to the Madeira Basin. In the NEA, repeated hydrographic sections showed warming between 2000–3000 m and an abyssal cooling (Desbruyères et al., 2014), while the North Atlantic basin underwent the most considerable warming reported on the ocean basin scale in the upper 2000 m since the 1950s (Levitus et al., 2012).

The mean currents in the deep Madeira Basin are predominantly south/southwestward, with small amplitude (order of a few cm s^{-1} or not distinguishable from zero). Over the decades, the velocity intensified over the entire water column, and consequently, also the MKE increased decade by decade (Fründt et al., 2013, **Frazão et al., 2021**). Although the current variability is of the same order or higher as the mean current, the increase in FKE did not reach depths below 1000 m (Tab. 2 in **Frazão et al., 2021**).

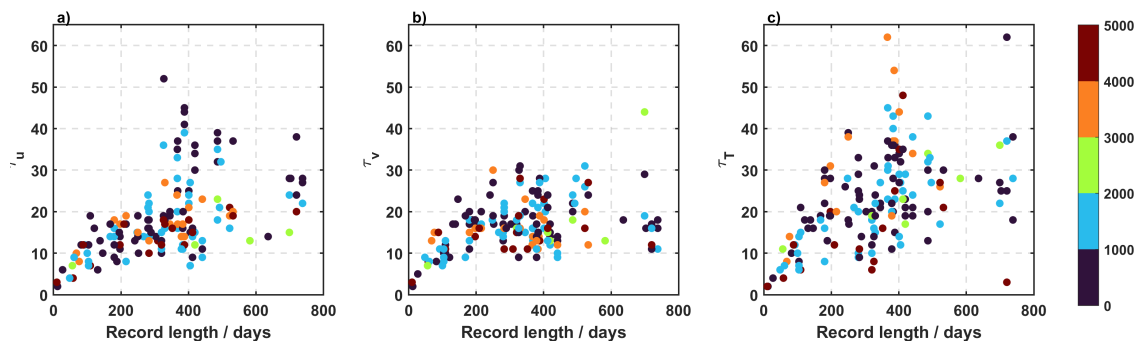


Figure 4.5. Integral Time Scale (τ , in days) based on individual deployments of the Kiel 276 mooring as a function of the record length for the (a) τ_u – zonal velocity component, (b) τ_v – meridional velocity component, and (c) τ_T – temperature. The depths of the instruments are color coded. Adapted from Müller & Waniek (2013) and **Frazão et al. (2021)**.

The Integral Time Scale (ITS) for both velocity components and temperature from the upper thermocline down to the seafloor (Fig. 4.5) showed no significant differences within depths (**Frazão et al., 2021**). They also revealed that the final level of the ITS is

reached around 30–40 days, hinting that mesoscale variability prevails in the entire water column. These mesoscale events are visible in the current records at all depth levels, and they are characterized by strong current events, which occur irregularly in time, last 1 to 3 months, and are often unidirectional with depth (Siedler et al., 1985; Müller & Siedler, 1992; Waniek et al., 2005). Siedler et al. (1985) attributed those events as the passage of the AF over the Kiel 276 mooring. Thus, the changes in the AzC-AF system reported in section 4.1 likely impact the region’s energy field, not only in the upper water column but also in the deepest part of the ocean.

4.4. Carbon uptake in the North Atlantic Subtropical Gyre

Long-term observatories placed in the west- and eastern basin of the North Atlantic Subtropical Gyral Province (NAST), such as BATS and European Station for Time-series in the Ocean, Canary Islands (ESTOC), and also the Kiel 276 mooring with sediment traps, allow continuous monitoring of the biogeochemical changes on seasonal to decadal timescales (e.g., Steinberg et al., 2001; Waniek et al., 2005; Neuer et al., 2007). However, those time-series are only operational since 1988 (BATS), 1994 (ESTOC), and 1980–2015 (Kiel 276 with sediment traps after 1993) and do not cover most significant changes in ocean circulation and water properties that occurred during the last century (see section 4.1). Thus, the method developed by Fründt et al. (2015b) was applied to reconstruct nitrate and Chl *a* vertical distribution between 1871 and 2010 at the Kiel 276 site, BATS station and for the North Atlantic subtropical basin (for more details, see section 3.3.4). The results are presented as the average temperature of the upper 300 m (hereafter referred only as mean temperature) and integrated nitrate and Chl *a* concentration in the upper 300 m (henceforth referred to as nitrate and Chl *a* concentration, respectively). Both BATS and the Kiel 276 sites are located at similar latitudes but on opposite sides of the NAST province, in the west- and eastern NAST provinces, respectively. The reconstructed fields at the ESTOC site are not analyzed here because of the additional nutrient source during summer due to the proximity to the upwelling region, resulting in greater variability in the nitrate and Chl *a* time-series not captured by the method (Cianca et al., 2012).

The average temperature showed large interannual variability on both sides of the North Atlantic subtropical basin, with periods of cooling before the 1900s and pronounced warming after the 1970s (solid grey lines in Fig. 4.6a,b). The temperature increased by

0.01 °C year⁻¹ at BATS and by 0.02 °C year⁻¹ at Kiel 276 site from the 1970s onward. Conversely, the nitrate concentration increased between 1880 and 1940 at BATS and from 1880 until 1910 at the Kiel 276 site and showed a marked decrease since the 1970s at both sites (dashed green lines in Fig. 4.6a,b). Thus, a warmer (colder) upper water column creates a stronger (weaker) gradient between the surface layer and underlying waters rich in nutrients, which suppress (enable) the nutrients supply through vertical mixing necessary for phytoplankton growth (Behrenfeld et al., 2006). This is also revealed by striking negative correlation coefficients between the average temperature and the nitrate concentration of -0.92 and -0.91 at Kiel 276 and BATS sites.

The Kiel 276 site is located close to the AF, a region with an enhanced biological response (Fernández & Pingree, 1996). The concentration of nutrients available in the upper water column is 2–3 times higher than at the BATS station (Fig. 4.6a,b), and a higher Chl *a* concentration is expected at the Kiel 276 site. However, the Chl *a* concentration is rather similar between the two sites (Fig. 4.6c,d). The variability of the Chl *a* concentration differs between the two regions ($\rho = 0.33$, $p < 0.05$), a result also confirmed by other authors between the west- and eastern NAST provinces (Cianca et al., 2012). Remarkably, the hydrography of both regions and the nutrients available in the euphotic zone contribute to this asymmetry (Palter et al., 2005; Cianca et al., 2012).

The annual nitrate cycle at both sites is linked to more nutrient availability during winter due to deeper winter mixing depths and fewer nutrients available in summer caused by increased stratification. Palter et al. (2005) showed that the spatial and temporal variability of the North Atlantic Subtropical Mode Water formation in the western Atlantic led to differences in the nutrients reservoir. The horizontal nutrient supply, though not as remarkable as the vertical supply, also plays an important role, especially at the borders of the subtropical gyre, contributing to the seasonal variability of the oligotrophic region of the NA (Dave et al., 2015). Additionally, the NAO has been linked to long-term changes in nutrient availability in the NA (Oschlies, 2001). However, as noted by the author, the influence of NAO in the nutrient supply differs in the west- and eastern basins of the NA, with no correlation found over the eastern Atlantic (Williams et al., 2000). Over the entire period, the Chl *a* concentration does not show any significant trend at both sites (Fig. 4.6c,d). Integrating over time, the carbon uptake at BATS and Kiel 276 sites was 3.3×10^6 mg C m⁻² and 4×10^6 mg C m⁻², respectively.

The average temperature in the upper 300 m, together with the nitrate and Chl *a*

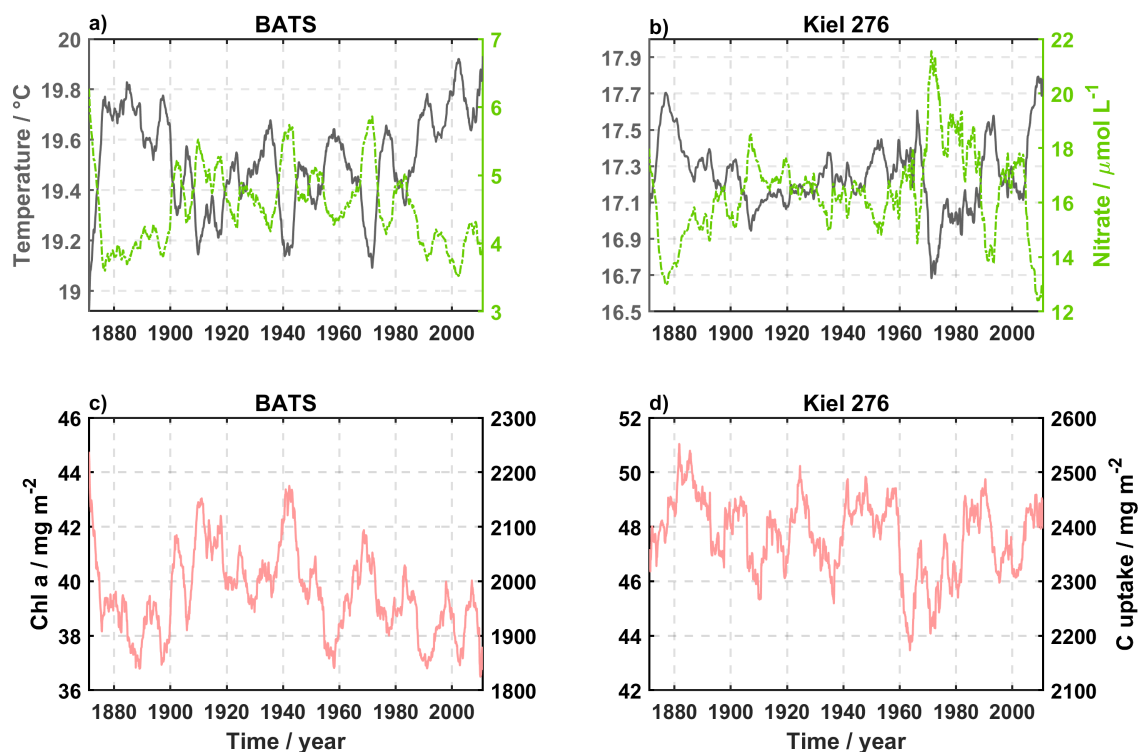


Figure 4.6. Averaged monthly temperature (solid gray line) and integrated nitrate concentration (dashed green line) in the upper 300 m at BATS (a) and Kiel 276 site (b). Monthly integrated Chl *a* and equivalent carbon uptake in the upper 300 m at BATS (c) and Kiel 276 site (d). The averaged monthly mean temperature was calculated using the SODA-POP v2.2.4 dataset at Kiel 276 and BATS positions (Carton & Giese, 2008; Giese & Ray, 2011). Carbon uptake was estimated at each site using a C/Chl *a* ratio of 50 (Fründt et al., 2015a). The time-series are smoothed with a 60-month moving mean filter.

concentration, and the solar radiation flux are presented in Fig. 4.7 for the entire North Atlantic subtropical basin. The mean temperature in the NASTG showed a marked increase after the 1970s at a rate of $0.016\text{ }^{\circ}\text{C year}^{-1}$ (Fig. 4.7b). Conversely, the nitrate concentration decreased by $-0.08\text{ }\mu\text{mol L}^{-1}\text{ year}^{-1}$ for the same period (Fig. 4.7c). At the Kiel 276 and BATS sites, the increase of temperature may be associated with an increased stratification over the entire NASTG, reducing the vertical supply of nitrate into the upper water column (Behrenfeld et al., 2006). Yamaguchi & Suga (2019) estimated an increase in stratification over the North Atlantic since the 1960s, especially during the summer season. The authors

determined a lagged negative correlation between detrended stratification and the NAO, denoting that during positive (negative) NAO-phases, stronger (weaker) winds lead to enhanced (reduced) stratification. This might explain why Lozier et al. (2011) found that the PP and water column stratification are weakly correlated in the NA on an interannual timescale, once their correlation was calculated between 1997 and 2009, a period of a more neutral NAO phase (Hurrell, 1995).

The Chl *a* concentration decline in the NASTG started earlier in the 1910s (Fig. 4.7d) and is consistent with the reported decline of marine primary production and Chl *a* concentration in the NA (Boyce et al., 2010). The nitrate concentration was at its highest values between 1910 and 1970 (Fig. 4.7b) and thus could not explain the early Chl *a* concentration decline. However, the average temperature in the NASTG seems to contribute to this early decline, with both time-series being highly negatively correlated (-0.94 , $p < 0.001$). This follows the findings of Martinez et al. (2009) between 1979 and 2005, where the authors find opposite trends between the development of SST and Chl *a* concentration. The overall decrease of Chl *a* concentration was $-0.009 \text{ mg m}^{-2} \text{ year}^{-1}$ between 1871 and 2010, similarly to Boyce et al. (2010) for the North Atlantic. However, the trend in Chl *a* concentration accelerated to $-0.016 \text{ mg m}^{-2} \text{ year}^{-1}$ from 1910s onwards.

In addition to the nutrient concentration in the euphotic zone, light availability is among the limiting factors controlling phytoplankton growth. The amount of solar radiation reaching the Earth's surface is variable over time, increasing in the early 20th century, followed by a decrease between the 1950s and 1980s (known as the global dimming period Wild, 2009). At BATS and Kiel 276 sites, no correlation was found between the solar radiation flux and the Chl *a* concentration. However, a closer inspection of both Chl *a* time-series reveals a decrease in the Chl *a* concentration in the first half of the dimming period at BATS and the early 1960s at Kiel 276 (Fig. 4.6c,d). In the NASTG, a correlation coefficient of 0.51 emerged between the annual mean solar radiation flux and the Chl *a* concentration (Fig. 4.7a,d). This correlation increases to 0.6 when the solar radiation flux leads the Chl *a* concentration by 13 years.

Thereby, the observed variability in the Chl *a* concentration may be a combination of both temperature, inducing stronger or weaker stratification periods, and the amount of solar radiation reaching the Earth's surface. The decrease in Chl *a* concentration is also consistent with the recent expansion of the oligotrophic region in the NA (McClain et al., 2004; Polovina et al., 2008; Irwin & Oliver, 2009). Additionally, changes in large-

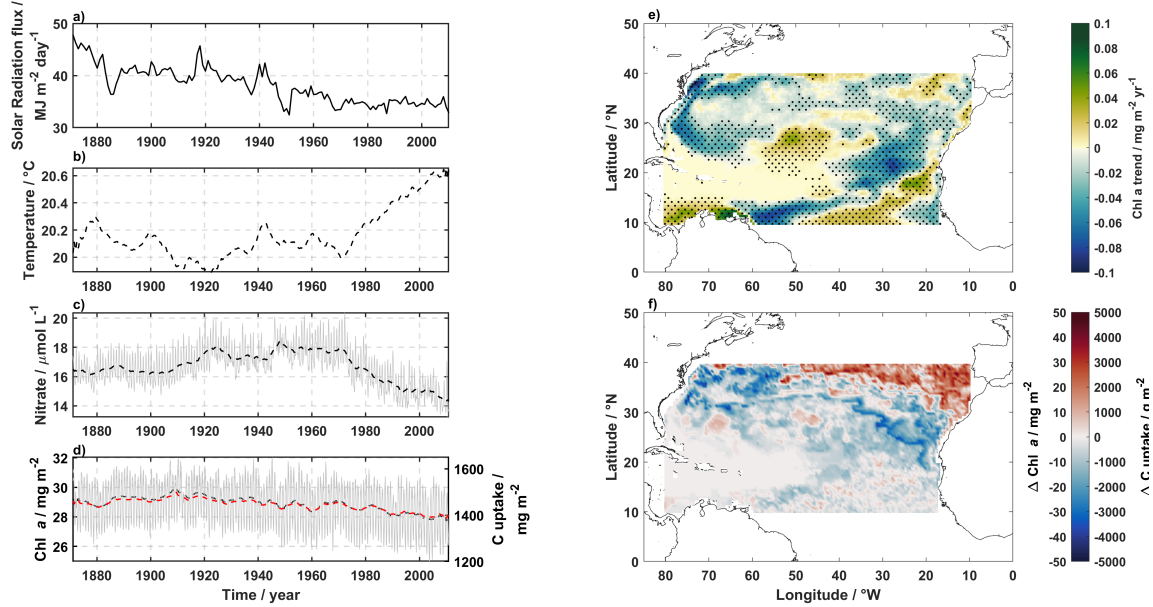


Figure 4.7. North Atlantic subtropical basin (a) annual mean solar radiation flux, (b) average water temperature, (c) integrated nitrate concentration and (d) integrated Chl *a* concentration (solid black line) and equivalent Carbon uptake concentration (solid red line) in the upper 300 m of the water column averaged over the entire North Atlantic subtropical basin between 10°–40°N and 80°–10°W. The grey solid lines in (b) and (c) are the monthly time-series. The time-series are smoothed with a 60-month moving filter. (e) Linear trend of the integrated Chl *a* concentration in the upper 300 m (dotted regions are statistically significant at $p < 0.001$). (f) Integrated Chl *a* difference between 2010 and 1871, and correspondent carbon uptake in the NASTG.

scale circulation are also responsible for the changes in temperature, nutrient availability, and ultimately Chl *a* concentration. The northward migration of the AF since the 1970s (Frazão et al., 2022) and the GSNW is linked to changes in the OHC (Frazão et al., 2022, Seidov et al., 2019, among others) and large-scale circulation. Thus, it is remotely possible that a reduction of the AMOC, linked with a weakening of the GS and two years later a weaker AzC, also impacts the Chl *a* concentration (Schmittner, 2005). A connection between reduced transports of the AMOC and a decline in the Chl *a* trend in the northern North Atlantic was proposed by Zhang et al. (2018).

The long-term variability of the Chl *a* concentration in the North Atlantic is not uniformly distributed in space, and its trends are variable according to the considered period

(e.g., Antoine et al., 2005; Gregg et al., 2005; Boyce et al., 2010). Thus, it is important to determine the long-term trends in Chl *a* and its spatial variability to understand the changes in the NASTG over the last century (Fig. 4.7e). The differences in integrated Chl *a* concentration and equivalent carbon uptake between 1871 and 2010 are presented in Fig. 4.7e,f. In the most oligotrophic region of the NASTG (i.e., the southwest corner of the NASTG; see the dark blue region in Fig. 1.1 for more details), the Chl *a* concentration and the carbon uptake did not change significantly over the last century. However, the surrounding areas showed a significant linear decrease in the Chl *a* concentration over the last century, except the Mid-Atlantic Ridge region (Fig. 4.7e), resulting in less carbon uptake in the North Atlantic Subtropical Gyral Province (Fig. 4.7f). North of the Azores Front and the Gulf Stream Front, the Chl *a* concentration increased over time, leading to the largest region in the North Atlantic of increased carbon uptake. Assuming a linear trend of carbon uptake between 1871–2010, a reduction of 617 Mt was calculated for the region in Fig. 4.7f, close to the estimated -700 Mt provided by Fründt et al. (2015a).

5. Summary and Outlook

This thesis describes changes in the circulation and properties of the water column in the Northeast Atlantic on different timescales. Thereby, different datasets were used to assess the variability of currents and water properties in the upper 1000 m, thus covering the Azores Current influence, the core of MOW at intermediate depths, and the deepest part of the water column below the MOW. Additionally, the reported differences in the circulation and water properties in the upper water column were linked to the dynamics of the biological production in the North Atlantic Subtropical Gyral Province region, estimating the differences in carbon uptake by the ocean over the last century.

On a multi-decadal timescale, the Azores Current underwent periods of intensification and weakening between 1871 and 2010. Most remarkable is the pronounced decline of the average velocity in the upper 1000 m after the 1960s, resulting in a reduction of 24 % of the velocity after the 1960s. Although a slight intensification occurred in the 1980s and 1990s, the Azores Current state at the end of 2010 was far weaker than the pre-1960s values. Similarly, the Gulf Stream velocity reduced in the 1960s and 1970s by 10 %. On the hypothesis that the Azores Current is a branch of the Gulf Stream in the eastern North Atlantic, the Azores Current's velocity variability seems to respond to the changes observed along the Gulf Stream pathway, with a time lag of 2 years (**Frazão et al., 2022**).

The northern border of the AzC, the AF, shows a gradual poleward migration since the 1970s, on a mean rate of 12 m day^{-1} . Contrarily to some studies, there was no correlation between the AF position and the NAO. However, the AF position is strongly correlated with the OHC in the upper 400 m and the AMO (**Frazão et al., 2022**), similarly with the Gulf Stream (Seidov et al., 2017, 2019).

The warming of the upper water column in the subtropical region of the North Atlantic also has repercussions at the biogeochemistry level. At the NASTG, the integrated nitrate concentration in the upper 300 m decreased since the 1970s, coincident with faster warming of the water column. Possibly associated with this warming is increased stratification, reducing the vertical supply of nutrients needed for phytoplankton growth. Indeed, the Chl *a* concentration declined for the same period. However, the decrease in Chl *a* concentration started in the early 20th century. Furthermore, the Chl *a* correlated negatively with the average temperature of the upper 300 m, confirming that this correlation is not only restricted to the rapid SST increase nor coincidental with the appearance of the satellite

observations (e.g., Behrenfeld et al., 2006; Martinez et al., 2009). Overall, the NASTG reduced its carbon uptake on average by 617 Mt ($1 \text{ Mt} = 10 \times 10^6 \text{ t}$) between 1871 and 2010.

Further down in the water column, the presence of MOW in the NEA revealed a large interannual variability of the water properties, and an overall freshening and cooling were calculated from the 1980s until 2018 (**Frazão & Waniek, 2021**). However, periods of warming and salinification were also detected. The changes between the two states of cooling/freshening and warming/salinification of the MOW are associated with large-scale circulation adjustments to external forcing. The NAO was found to induce preferential pathways of MOW after exiting the Strait of Gibraltar, thus ultimately affecting the properties of the water present during each NAO phase with a time lag of 7 to 8 years. Thereby, a positive (negative) NAO-phase might be related to the MOW tongue's expansion (retraction) (**Frazão & Waniek, 2021**).

The Kiel 276 mooring (33°N , 22°W) proved to be an excellent observatory over the last 30 years of the ocean state in the NEA. Warming was recorded as deep as 1600 m, and an intensification of the currents was observed in the entire water column between 1980 and 2009 (**Frazão et al., 2021**). Additionally, the FKE increased down to 1000 m over the same period, possibly related to an increase in the number of MEDDIES crossing the mooring position.

The ITS at the Kiel 276 for temperature and both velocity components showed that mesoscale events prevail in the entire water column, with no apparent differences between the upper and deeper parts (**Frazão et al., 2021**). Moreover, those mesoscale events are presented as strong current events irregularly in time, lasting one to three months, and are often unidirectional with depth (Siedler et al., 1985; Müller & Siedler, 1992; Waniek et al., 2005). They were identified as the passage of the AzC-AF system through the Kiel 276 site. Thus, it is likely that the changes occurred in the Northeast Atlantic over the last century (**Frazão et al., 2022**) also impacted the current and energy fields at greater depths.

Although the present results contribute to some extent to a more comprehensive picture of the variability in the Northeast Atlantic, a far more complete picture of NEA circulation and water properties changes is lacking. The regime change in the 1960s associated with a weakening of the AzC, followed by a northward displacement of its core remains a mystery. To understand the possible regime change involved in the weakening of the North Atlantic circulation, it is important to know first what are the drivers of the AzC. The reported

decline of the AzC and the GS might be a direct consequence of the AMOC slowdown.

The influence of the Mediterranean Water Outflow on the Azores Current variability still remains to be demonstrated with in-situ data. Although the existence of the β -plume with observational data was shown by Lamas et al. (2010), how does the outflow influence the positioning and strengthening of the Azores Current on longer time scales is still unknown. The first challenge to be overcome is correctly quantifying the outflow in the Strait of Gibraltar to better understand this issue.

Frazão & Waniek (2021) showed that external forcing (hence, NAO) induce large-scale circulation adjustments in the MOW spreading, thus creating preferential pathways for the MOW after exiting the Strait of Gibraltar (Bozec et al., 2011). At intermediate depths, different water masses are present in the North Atlantic besides MOW, such as Labrador Sea Water (LSW) and Antarctic Intermediate Water (AAIW). The LSW formation strongly correlates to the predominant NAO-phase (Curry et al., 1998), with its signal propagating into the subtropical Atlantic with a lag of seven years. Such time scales are comparable with the ones estimated by **Frazão & Waniek (2021)** for the MOW in the NEA. Additionally, Chaudhuri et al. (2011) showed, using a model simulation, that the intermediate circulation in the NA adjusted after an abrupt shift of the NAO-phase in 1996/97. Remains to be understood how the presence and extension of the different water masses at intermediate depths influence the extension of the MOW in the NEA and ultimately influence the positioning and strength of the Azores Current.

The gradual northward migration of the AF since the 1970s was shown to be tightly connected with the OHC and the AMO in the NEA (**Frazão et al., 2022**). This result might be another hint of the expansion of the oligotrophic regions, as described by several authors (e.g., Polovina et al., 2008; Irwin & Oliver, 2009). However, the datasets used by these authors are limited to the last 20–30 year of satellite observations. To determine whether these changes are warming-induced or natural variability of the subtropical gyre, a longer time-series of ~ 40 years is needed (Henson et al., 2010). Here, the application of the method developed by Fründt et al. (2013) to the North Atlantic Subtropical Gyral Province between 1871–2010 proved that the fine horizontal and vertical resolution of the method has great potential to study the biological production over the entire NA, and possibly extending the method to other gyres. The method could be used to better understand the dynamics of the DCM over the entire NAST, and how the different rates of warming in the North Atlantic basin (Seidov et al., 2017) could impact the biogeochemical cycles.

References

- Alves, M., Gaillard, F., Sparrow, M., Knoll, M., & Giraud, S. (2002). Circulation patterns and transport of the Azores Front-Current system. *Deep-Sea Research II*, *49*, 3983–4002. doi:[10.1016/S0967-0645\(02\)00138-8](https://doi.org/10.1016/S0967-0645(02)00138-8).
- Alves, M. L. G. R., & Colin de Verdière, A. (1999). Instability Dynamics of a Subtropical Jet and Applications to the Azores Front Current System: Eddy-Driven Mean Flow. *Journal of Physical Oceanography*, *29*, 837–864. doi:[10.1175/1520-0485\(1999\)029<0837:IDOASJ>2.0.CO;2](https://doi.org/10.1175/1520-0485(1999)029<0837:IDOASJ>2.0.CO;2).
- Ambar, I., Howe, M. R., & Abdullah, M. I. (1976). A Physical and Chemical Description of the Mediterranean Outflow in the Gulf of Cadiz. *Deutsche Hydrographische Zeitschrift*, *29*, 58–68. doi:[10.1007/BF02227031](https://doi.org/10.1007/BF02227031).
- Andres, M., Donohue, K. A., & Toole, J. M. (2020). The Gulf Stream’s path and time-averaged velocity structure and transport at 68.5°W and 70.3°W. *Deep-Sea Research I*, *156*, 103179. doi:[10.1016/j.dsr.2019.103179](https://doi.org/10.1016/j.dsr.2019.103179).
- Antoine, D., Morel, A., Gordon, H. R., Banzon, V. F., & Evans, R. H. (2005). Bridging ocean color observations of the 1980s and 2000s in search of long-term trends. *Journal of Geophysical Research*, *110*, C06009. doi:[10.1029/2004JC002620](https://doi.org/10.1029/2004JC002620).
- Arbic, B. K., & Owens, W. B. (2001). Climate Warming of Atlantic Intermediate Waters. *Journal of Climate*, *14*, 4091–4108. doi:[10.1175/1520-0442\(2001\)014<4091:CWOAIW>2.0.CO;2](https://doi.org/10.1175/1520-0442(2001)014<4091:CWOAIW>2.0.CO;2).
- Armi, L., & Zenk, W. (1984). Large Lenses of Highly Saline Mediterranean Water. *Journal of Physical Oceanography*, *14*, 1560–1576. doi:[10.1175/1520-0485\(1984\)014<1560:LLOHSM>2.0.CO;2](https://doi.org/10.1175/1520-0485(1984)014<1560:LLOHSM>2.0.CO;2).
- Barbosa Aguiar, A. C., Peliz, A. J., Cordeiro Pires, A., & Le Cann, B. (2011). Zonal structure of the mean flow and eddies in the Azores Current system. *Journal of Geophysical Research*, *116*, C02012. doi:[10.1029/2010JC006538](https://doi.org/10.1029/2010JC006538).
- Barnes, S. L. (1973). Mesoscale Objective Map Analysis Using Weighted Time-Series Observations. *NOAA Technical Memorandum ERL NSSL 62*; NOAA: Washington, DC, USA, (p. 66).
- Barnett, T. P., Pierce, D. W., AchutaRao, K. M., Gleckler, P. J., Santer, B. D., Gregory, J. M., & Washington, W. M. (2005). Penetration of Human-Induced Warming into the World’s Oceans. *Science*, *309*, 284–287. doi:[10.1126/science.1112418](https://doi.org/10.1126/science.1112418).

- Bashmachnikov, I., Neves, F., Calheiros, T., & Carton, X. (2015a). Properties and pathways of Mediterranean water eddies in the Atlantic. *Progress in Oceanography*, *137*, 149–172. doi:[10.1016/j.pocean.2015.06.001](https://doi.org/10.1016/j.pocean.2015.06.001).
- Bashmachnikov, I., Neves, F., Nascimento, Â., Medeiros, J., Ambar, I., Dias, J., & Carton, X. (2015b). Temperature–salinity distribution in the northeastern Atlantic from ship and Argo vertical casts. *Ocean Science*, *11*, 215–236. doi:[10.5194/os-11-215-2015](https://doi.org/10.5194/os-11-215-2015).
- Behrenfeld, M. J., O’Malley, R. T., Siegel, D. A., McClain, C. R., Sarmiento, J. L., Feldman, G. C., Milligan, A. J., Falkowski, P. G., Letelier, R. M., & Boss, E. S. (2006). Climate-driven trends in contemporary ocean productivity. *Nature*, *444*, 752–755. doi:[10.1038/nature05317](https://doi.org/10.1038/nature05317).
- Berglund, S. (2021). *Tracing pathways in the ocean circulation. A temperature and salinity perspective*. Ph.D. thesis Stockholm University.
- Bower, A. S., Serra, N., & Ambar, I. (2002). Structure of the Mediterranean Undercurrent and Mediterranean Water spreading around the southwestern Iberian Peninsula. *Journal of Geophysical Research*, *107*, 3161. doi:[10.1029/2001JC001007](https://doi.org/10.1029/2001JC001007).
- Boyce, D. G., Lewis, M. R., & Worm, B. (2010). Global phytoplankton decline over the past century. *Nature*, *466*, 591–596. doi:[10.1038/nature09268](https://doi.org/10.1038/nature09268).
- Boyer, T. P., Baranova, O. K., Coleman, C., Garcia, H. E., Grodsky, A., Locarnini, R. A., Mishonov, A. V., Paver, C. R., Reagan, J. R., Seidov, D., Smolyar, I. V., Weather, K., & Zweng, M. M. (2018). World Ocean Database 2018. *A.V. Mishonov, Technical Ed., NOAA Atlas NESDIS 87*, .
- Bozec, A., Lozier, M. S., Chassignet, E. P., & Halliwell, G. R. (2011). On the variability of the Mediterranean Outflow Water in the North Atlantic from 1948 to 2006. *Journal of Geophysical Research*, *116*, C09033. doi:[10.1029/2011JC007191](https://doi.org/10.1029/2011JC007191).
- Brügge, B. (1995). Near-surface mean circulation and kinetic energy in the central North Atlantic from drifter data. *Journal of Geophysical Research*, *100*, 20543–20554. doi:[10.1029/95JC01501](https://doi.org/10.1029/95JC01501).
- Brust, J., Schulz-Bull, D. E., Leipe, T., Chavagnac, V., & Waniek, J. J. (2011). Descending particles: From the atmosphere to the deep ocean – A time series study in the subtropical NE Atlantic. *Geophysical Research Letters*, *38*, L06603. doi:[10.1029/2010GL045399](https://doi.org/10.1029/2010GL045399).
- Brust, J., & Waniek, J. J. (2010). Atmospheric dust contribution to deep-sea particle fluxes in the subtropical Northeast Atlantic. *Deep-Sea Research I*, *57*, 988–998. doi:[10.1016/j.dsr.2010.04.011](https://doi.org/10.1016/j.dsr.2010.04.011).

- Bryden, H. L., Longworth, H. R., & Cunningham, S. A. (2005). Slowing of the Atlantic meridional overturning circulation at 25°N. *Nature*, *438*, 655–657. doi:[10.1038/nature04385](https://doi.org/10.1038/nature04385).
- Caesar, L., McCarthy, G. D., Thornalley, D. J. R., Cahill, N., & Rahmstorf, S. (2021). Current Atlantic Meridional Overturning Circulation weakest in the last millenium. *Nature Geoscience*, *14*, 118–120. doi:[10.1038/s41561-021-00699-z](https://doi.org/10.1038/s41561-021-00699-z).
- Caesar, L., Rahmstorf, S., Robinson, A., Feulner, G., & Saba, V. (2018). Observed fingerprint of a weakening Atlantic Ocean overturning circulation. *Nature*, *556*, 191–196. doi:[10.1038/s41586-018-0006-5](https://doi.org/10.1038/s41586-018-0006-5).
- Carracedo, L. I., Gilcoto, M., Mercier, H., & Pérez, F. F. (2014). Seasonal dynamics in the Azores–Gibraltar Strait region: A climatologically-based study. *Progress in Oceanography*, *122*, 116–130. doi:[10.1016/j.poccean.2013.12.005](https://doi.org/10.1016/j.poccean.2013.12.005).
- Carton, J. A., & Giese, B. S. (2008). A Reanalysis of Ocean Climate Using Simple Ocean Data Assimilation (SODA). *Monthly Weather Review*, *136*, 2999–3017. doi:[10.1175/2007MWR1978.1](https://doi.org/10.1175/2007MWR1978.1).
- Chaudhuri, A. H., Gangopadhyay, A., & Bisagni, J. J. (2011). Contrasting Response of the Eastern and Western North Atlantic Circulation to an Episodic Climate Event. *Journal of Physical Oceanography*, *41*, 1630–1638. doi:[10.1175/2011JPO4512.1](https://doi.org/10.1175/2011JPO4512.1).
- Chavez, F. P., Messié, M., & Pennington, J. T. (2011). Marine Primary Production in Relation to Climate Variability and Change. *Annual Review of Marine Science*, *3*, 227–260. doi:[10.1146/annurev.marine.010908.163917](https://doi.org/10.1146/annurev.marine.010908.163917).
- Cheng, L., Abraham, J., Zhu, J., Trenberth, K. E., Fasullo, J., Boyer, T., Locarnini, R., Zhang, B., Yu, F., Wan, L., Chen, X., Song, X., Liu, Y., & Mann, M. E. (2020). Record-Setting Ocean Warmth Continued in 2019. *Advances in Atmospheric Sciences*, *37*, 137–142. doi:[10.1007/s00376-020-9283-7](https://doi.org/10.1007/s00376-020-9283-7).
- Cianca, A., Godoy, J. M., Martin, J. M., Perez-Marrero, J., Rueda, M. J., Llinás, O., & Neuer, S. (2012). Interannual variability of chlorophyll and the influence of low-frequency climate modes in the North Atlantic subtropical gyre. *Global Biogeochemical Cycles*, *26*, GB2002. doi:[10.1029/2010GB004022](https://doi.org/10.1029/2010GB004022).
- Collins, M., Sutherland, M., Bouwer, L., Cheong, S.-M., Frölicher, T., Jacot des Combes, H., Koll Roxy, M., Losada, I., McInnes, K., Ratter, B., Rivera-Arriaga, E., Susanto, R. D., Swingedouw, D., & Tibig, L. (2019). Extremes, Abrupt Changes and Managing Risk. In H.-O. Pörtner, D. C. Roberts, V. Masson-Delmotte, P. Zhai, M. Tignor, E. Poloczanska, K. Mintenbeck, A. Alegría, M. Nicolai, A. Okem, J. Petzold, B. Rama, & N. M. Weyer (Eds.), *IPCC Special Report on the Ocean and Cryosphere in a Changing Climate* (pp. 589–655).

- Comas-Rodríguez, I., Hernández-Guerra, A., Fraile-Nuez, E., Martínez-Marrero, A., Benítez-Barrios, V. M., Pérez-Hernández, M. D., & Vélez-Belchí, P. (2011). The Azores Current System from a meridional section at 24.5°W. *Journal of Geophysical Research*, *116*, C09021. doi:[10.1029/2011JC007129](https://doi.org/10.1029/2011JC007129).
- Costoya, X., deCastro, M., & Gómez-Gesteira, M. (2014). Thermohaline trends in the Bay of Biscay from Argo floats over the decade 2004–2013. *Journal of Marine Systems*, *139*, 159–165. doi:[10.1016/j.jmarsys.2014.06.001](https://doi.org/10.1016/j.jmarsys.2014.06.001).
- Cromwell, D., Challenor, P. G., New, A. L., & Pingree, R. D. (1996). Persistent westward flow in the Azores Current as seen from altimetry and hydrography. *Journal of Geophysical Research*, *101*, 11923–11933. doi:[10.1029/96JC00609](https://doi.org/10.1029/96JC00609).
- Cunningham, S. A., Kanzow, T., Rayner, D., Baringer, M. O., Johns, W. E., Marotzke, J., Longworth, H. R., Grant, E. M., Hirschi, J. J.-M., Beal, L. M., Meinen, C. S., & Bryden, H. L. (2007). Temporal Variability of the Atlantic Meridional Overturning Circulation at 26.5°N. *Science*, *317*, 935–938. doi:[10.1126/science.1141304](https://doi.org/10.1126/science.1141304).
- Curry, R. G., McCartney, M. S., & Joyce, T. M. (1998). Oceanic transport of subpolar climate signals to mid-depth subtropical waters. *Nature*, *391*, 575–577. doi:[10.1038/35356](https://doi.org/10.1038/35356).
- Daniault, N., Mercier, H., Lherminier, P., Sarafanov, A., Falina, A., Zunino, P., Pérez, F. F., Rís, A. F., Ferron, B., Huck, T., Thierry, V., & Gladyshev, S. (2016). The northern North Atlantic Ocean mean circulation in the early 21st century. *Progress in Oceanography*, *146*, 142–158. doi:[10.1016/j.pocean.2016.06.007](https://doi.org/10.1016/j.pocean.2016.06.007).
- Dave, A. C., Barton, A. D., Lozier, M. S., & McKinley, G. A. (2015). What drives seasonal change in oligotrophic area in the subtropical North Atlantic? *Journal of Geophysical Research: Oceans*, *120*, 3958–3969. doi:[10.1002/2015JC010787](https://doi.org/10.1002/2015JC010787).
- Desbruyères, D. G., McDonagh, E. L., King, B. A., Garry, F. K., Blaker, A. T., Moat, B. I., & Mercier, H. (2014). Full-depth temperature trends in the northeastern Atlantic through the early 21st century. *Geophysical Research Letters*, *41*, 7971–7979. doi:[10.1002/2014GL061844](https://doi.org/10.1002/2014GL061844).
- Dickson, R. R., Gould, W. J., Gurbutt, P. A., & Killworth, P. D. (1982). A seasonal signal in ocean currents to abyssal depths. *Nature*, *295*, 193–198. doi:[10.1038/295193a0](https://doi.org/10.1038/295193a0).
- Dickson, R. R., Gould, W. J., Müller, T. J., & Maillard, C. (1985). Estimates of the Mean Circulation in the Deep (> 2000 m) Layer of the Eastern North Atlantic. *Progress in Oceanography*, *14*, 103–127. doi:[10.1016/0079-6611\(85\)90008-4](https://doi.org/10.1016/0079-6611(85)90008-4).
- Dong, S., Baringer, M. O., & Goni, G. J. (2019). Slow Down of the Gulf Stream during 1993–2016. *Scientific Reports*, *9*, 6672. doi:[10.1038/s41598-019-42820-8](https://doi.org/10.1038/s41598-019-42820-8).

- Döös, K., Berglund, S., Mcdougall, T., & Groeskamp, S. (2019). The spiralling North Atlantic Subtropical Gyre. EGU General Assembly 2020, Online, 2–8 May 2020, EGU2020-1459. doi:[10.5194/egusphere-egu2020-1459](https://doi.org/10.5194/egusphere-egu2020-1459).
- Drinkwater, K. F., Belgrano, A., Borja, A., Conversi, A., Edwards, M., Greene, C. H., Ottersen, G., Pershing, A. J., & Walker, H. (2003). The Response of Marine Ecosystems to Climate Variability Associated with the North Atlantic Oscillation. In J. W. Hurrell, Y. Kushnir, G. Ottersen, & M. Visbeck (Eds.), *In The North Atlantic Oscillation: Climatic Significance and Environmental Impact* (pp. 211–234). American Geophysical Union (AGU). doi:<https://doi.org/10.1029/134GM10>.
- Eakins, B. W., & Sharman, G. F. (2010). Volumes of the World’s Oceans from ETOPO1, NOAA National Geophysical Data Center, Boulder, CO. https://www.ngdc.noaa.gov/mgg/global/etopo1_ocean_volumes.html (accessed on 15.12.2021).
- Emerson, S., Quay, P., Karl, D., Winn, C., Tupas, L., & Landry, M. (1997). Experimental determination of the organic carbon flux from open-ocean surface waters. *Nature*, *389*, 951–954. doi:[10.1038/40111](https://doi.org/10.1038/40111).
- Enfield, D. B., Mestas-Nuñez, A. M., & Trimble, P. J. (2001). The Atlantic Multidecadal Oscillation and its relation to rainfall and river flows in the continental U.S. *Geophysical Research Letters*, *28*, 2077–2080. doi:[10.1029/2000GL012745](https://doi.org/10.1029/2000GL012745).
- Eymard, L., Planton, S., Durand, P., Le Visage, C., Le Traon, P. Y., Prieur, L., Weill, A., Hauser, D., Rolland, J., Pelon, J., Baudin, F., Bénech, B., Brenguier, J. L., Caniaux, G., De Mey, P., Dombrowski, E., Druilhet, A., Dupuis, H., Ferret, B., Flamant, C., Flamant, P., Hernandez, F., Jourdan, D., Katsaros, K., Lambert, D., Lefèvre, J. M., Le Borgne, P., Le Squere, B., Marsoin, A., Roquet, H., Tournadre, J., Troullet, V., Tychensky, A., & Zakardjian, B. (1996). Study of the air-sea interactions at the mesoscale: the SEMAPHORE experiment. *Annales Geophysicae*, *14*, 986–1015. doi:[10.1007/s00585-996-0986-6](https://doi.org/10.1007/s00585-996-0986-6).
- Ezer, T. (2015). Detecting changes in the transport of the Gulf Stream and the Atlantic overturning circulation from coastal sea level data: The extreme decline in 2009–2010 and estimated variations for 1935–2012. *Global and Planetary Change*, *129*, 23–36. doi:[10.1016/j.gloplacha.2015.03.002](https://doi.org/10.1016/j.gloplacha.2015.03.002).
- Falkowski, P., Scholes, R. J., Boyle, E., Canadell, J., Canfield, D., Elser, J., Gruber, N., Hibbard, K., Högberg, P., Linder, S., Machenzie, F. T., Moore III, B., Pedersen, T., Rosenthal, Y., Seitzinger, S., Smetacek, V., & Steffen, W. (2000). The Global Carbon Cycle: A Test of Our Knowledge of Earth as a System. *Science*, *290*, 291–296. doi:[10.1126/science.290.5490.291](https://doi.org/10.1126/science.290.5490.291).

- Fasham, M. J. (2003). *Ocean Biogeochemistry: The Role of the Ocean Carbon Cycle in Global Change*. Springer-Verlag Berlin Heidelberg.
- Fasham, M. J. R., Platt, T., Irwin, B., & Jones, K. (1985). Factors Affecting the Spatial Pattern of the Deep Chlorophyll Maximum in the Region of the Azores Front. *Progress in Oceanography*, *14*, 129–165. doi:[10.1016/0079-6611\(85\)90009-6](https://doi.org/10.1016/0079-6611(85)90009-6).
- Fernández, E., & Pingree, R. D. (1996). Coupling between physical and biological fields in the North Atlantic subtropical front southeast of the Azores. *Deep-Sea Research I*, *43*, 1369–1393. doi:[10.1016/S0967-0637\(96\)00065-9](https://doi.org/10.1016/S0967-0637(96)00065-9).
- Frankignoul, C., de Coëtlogon, G., Joyce, T. M., & Dong, S. (2001). Gulf Stream Variability and Ocean–Atmosphere Interactions. *Journal of Physical Oceanography*, *31*, 3516–3529. doi:[10.1175/1520-0485\(2002\)031<3516:GSVA0A>2.0.CO;2](https://doi.org/10.1175/1520-0485(2002)031<3516:GSVA0A>2.0.CO;2).
- Fratantoni, D. M. (2001). North Atlantic surface circulation during the 1990’s observed with satellite-tracked drifters. *Journal of Geophysical Research*, *106*, 22067–22093. doi:[10.1029/2000JC000730](https://doi.org/10.1029/2000JC000730).
- Frazão, H. C., Prien, R. D., Müller, T. J., Schulz-Bull, D. E., & Waniek, J. J. (2021). 30 years of temporal variability of temperature and currents below the main thermocline between 1980–2009 in the subtropical Northeast Atlantic (Kiel 276, 33°N, 22°W). *Journal of Marine Systems*, *217*, 103517. doi:[10.1016/j.jmarsys.2021.103517](https://doi.org/10.1016/j.jmarsys.2021.103517).
- Frazão, H. C., Prien, R. D., Schulz-Bull, D. E., Seidov, D., & Waniek, J. J. (2022). The forgotten Azores Current: a long-term perspective. *Frontiers in Marine Science*, (accepted). doi:[10.3389/fmars.2022.842251](https://doi.org/10.3389/fmars.2022.842251).
- Frazão, H. C., & Waniek, J. J. (2021). Mediterranean Water Properties at the Eastern Limit of the North Atlantic Subtropical Gyre Since 1981. *Oceans*, *2*, 266–280. doi:[10.3390/oceans2010016](https://doi.org/10.3390/oceans2010016).
- Friedlingstein, P., O’Sullivan, M., Jones, M. W., Andrew, R. M., Hauck, J., Olsen, A., Peters, G. P., Peters, W., Pongratz, J., Sitch, S., Le Quéré, C., Canadell, J. G., Ciais, P., Jackson, R. B., Alin, S., Aragão, L. E. O. C., Arneeth, A., Arora, V., Bates, N. R., Becker, M., Benoit-Cattin, A., Bittig, H. C., Bopp, L., Bultan, S., Chandra, N., Chevallier, F., Chini, L. P., Evans, W., Florentie, L., Forster, P. M., Gasser, T., Gehlen, M., Gilfillan, D., Gkritzalis, T., Gregor, L., Gruber, N., Harris, I., Hartung, K., Haverd, V., Houghton, R. A., Ilyina, T., Jain, A. K., Joetzjer, E., Kadono, K., Kato, E., Kitidis, V., Korsbakken, J. I., Landschützer, P., Lefèvre, N., Lenton, A., Lienert, S., Liu, Z., Lombardozzi, D., Marland, G., Metzl, N., Munro, D. R., Nabel, J. E. M. S., Nakaoka, S.-I., Niwa, Y., O’Brien, K., Ono, T., Palmer, P. I., Pierrot, D., Poulter, B., Resplandy, L., Robertson, E., Rödenbeck, C., Schwinger, J., Séférian, R., Skjelvan, I., Smith, A. J. P., Sutton, A. J., Tanhua, T., Tans, P. P., Tian, H., Tilbrook, B., van der Werf, G., Vuichard, N.,

- Walker, A. P., Wanninkhof, R., Watson, A. J., Willis, D., Wiltshire, A. J., Yuan, W., Yue, X., & Zaehle, S. (2020). Global carbon budget 2020. *Earth System Science Data*, *12*, 3269–3340. doi:[10.5194/essd-12-3269-2020](https://doi.org/10.5194/essd-12-3269-2020).
- Fründt, B., Dippner, J. W., Schulz-Bull, D. E., & Waniek, J. J. (2015a). Chlorophyll *a* reconstruction from in situ measurements: 2. Marked carbon uptake decrease in the last century. *Journal of Geophysical Research: Biogeosciences*, *120*, 246–260. doi:[10.1002/2014JG002692](https://doi.org/10.1002/2014JG002692).
- Fründt, B., Dippner, J. W., & Waniek, J. J. (2015b). Chlorophyll *a* reconstruction from in situ measurements: 1. Method description. *Journal of Geophysical Research: Biogeosciences*, *120*, 237–245. doi:[10.1002/2014JG002691](https://doi.org/10.1002/2014JG002691).
- Fründt, B., Müller, T. J., Schulz-Bull, D. E., & Waniek, J. J. (2013). Long-term changes in the thermocline of the subtropical Northeast Atlantic (33°N, 22°W). *Progress in Oceanography*, *116*, 246–260. doi:[10.1016/j.pocean.2013.07.004](https://doi.org/10.1016/j.pocean.2013.07.004).
- Fründt, B., & Waniek, J. J. (2012). Impact of the Azores Front Propagation on Deep Ocean Particle Flux. *Central European Journal of Geosciences*, *4*, 531–544. doi:[10.2478/s13533-012-0102-2](https://doi.org/10.2478/s13533-012-0102-2).
- Fusco, G., Artale, V., Cotroneo, Y., & Sannino, G. (2008). Thermohaline variability of Mediterranean Water in the Gulf of Cadiz, 1948–1999. *Deep-Sea Research I*, *55*, 1624–1638. doi:[10.1016/j.dsr.2008.07.009](https://doi.org/10.1016/j.dsr.2008.07.009).
- Garcia, H. E., Weather, K., Paver, C. R., Smolyar, I., Boyer, T. P., Locarnini, R. A., Zweng, M. M., Mishonov, A. V., Baranova, O. K., Seidov, D., & Reagan, J. (2018). World Ocean Atlas 2018, Volume 3: Dissolved Oxygen, Apparent Oxygen Utilization, and Oxygen Saturation.
- García-Lafuente, J., Sammartino, S., Huertas, I. E., Flecha, S., Sánchez-Leal, R. F., Naranjo, C., Nadal, I., & Bellanco, M. J. (2021). Hotter and Weaker Mediterranean Outflow as a Response to Basin-Wide Alteration. *Frontiers in Marine Science*, *8*, 613444. doi:[10.3389/fmars.2021.613444](https://doi.org/10.3389/fmars.2021.613444).
- Giese, B. S., & Ray, S. (2011). El Niño variability in simple ocean data assimilation (SODA), 1871–2008. *Journal of Geophysical Research*, *116*, C02024. doi:[10.1029/2010JC006695](https://doi.org/10.1029/2010JC006695).
- Goldenberg, S. B., Landsea, C. W., Mestas-Núñez, A. M., & Gray, W. M. (2001). The Recent Increase in Atlantic Hurricane Activity: Causes and Implications. *Science*, *293*, 474–479. doi:[10.1126/science.1060040](https://doi.org/10.1126/science.1060040).
- Good, S. A., Martin, M. J., & Rayner, N. A. (2013). EN4: Quality controlled ocean temperature and salinity profiles and monthly objective analyses with uncertainty estimates. *Journal of Geophysical Research: Oceans*, *118*, 6704–6716. doi:[10.1002/2013JC009067](https://doi.org/10.1002/2013JC009067).

- Gould, W. J. (1985). Physical Oceanography of the Azores Front. *Progress in Oceanography*, *14*, 167–190. doi:[10.1016/0079-6611\(85\)90010-2](https://doi.org/10.1016/0079-6611(85)90010-2).
- Greatbatch, R. J., Fanning, A. F., & Goulding, A. D. (1991). A Diagnosis of Interpentadal Circulation Changes in the North Atlantic. *Journal of Geophysical Research*, *96*, 22009–22023. doi:[10.1029/91JC02423](https://doi.org/10.1029/91JC02423).
- Gregg, W. W., Casey, N. W., & McClain, C. R. (2005). Recent trends in global ocean chlorophyll. *Geophysical Research Letters*, *32*, L03606. doi:[10.1029/2004GL021808](https://doi.org/10.1029/2004GL021808).
- Gregory, J. M., Banks, H. T., Stott, P. A., Lowe, J. A., & Palmer, M. D. (2004). Simulated and observed decadal variability in ocean heat content. *Geophysical Research Letters*, *31*, L15312. doi:[10.1029/2004GL020258](https://doi.org/10.1029/2004GL020258).
- Griffiths, G., Cunningham, S., Griffiths, M., Pollard, R. T., Leach, H., Holley, S., Paylor, T., Haine, T. W. N., Ríos, A., Alderson, S. G., Lowry, R. K., Smith, P., Preston, M., Gwilliam, T. J. P., Smithers, J., Keene, S., Hemmings, J., & Anderson, T. R. (1992). CTD oxygen, tracer and nutrient data from *RRS Charles Darwin* Cruises 58/59 in the NE Atlantic as part of Vivaldi '91. Institute of Oceanographic Sciences Deacon Laboratory, Report No. 296, 51 pp.
- Gruber, N., Clement, D., Carter, B. R., Feely, R. A., van Heuven, S., Hoppema, M., Ishii, M., Key, R. M., Kozyr, A., Lauvset, S. K., Monaco, C. L., Mathis, J. T., Murata, A., Olsen, A., Perez, F. F., Sabine, C. L., Tanhua, T., & Wanninkhof, R. (2019). The oceanic sink for anthropogenic CO₂ from 1994 to 2007. *Science*, *363*, 1193–1199. doi:[10.1126/science.aau5153](https://doi.org/10.1126/science.aau5153).
- Hartmann, D. L., Klein Tank, A. M. G., Rusticucci, M., Alexander, L. V., Brönnimann, S., Charabi, Y., Dentener, F. J., Dlugokencky, E. J., Easterling, D. R., Kaplan, A., Soden, B. J., Thorne, P. W., Wild, M., & Zhai, P. M. (2013). Observations: Atmosphere and Surface. In T. F. Stocker, D. Qin, G.-K. Plattner, M. Tignor, S. K. Allen, J. Boschung, A. Nauels, Y. Xia, V. Bex, & P. M. Midgley (Eds.), *Climate Change 2013: The Physical Science Basis. Contribution of Working Group I to the Fifth Assessment Report of the Intergovernmental Panel on Climate Change* (pp. 159–254). Cambridge University Press, Cambridge, United Kingdom and New York, NY, US.
- Henson, S. A., Sarmiento, J. L., Dunne, J. P., Bopp, L., Lima, I., Doney, S. C., John, J., & Beaulieu, C. (2010). Detection of anthropogenic climate change in satellite records of ocean chlorophyll and productivity. *Biogeosciences*, *7*, 621–640. doi:[10.5194/bg-7-621-2010](https://doi.org/10.5194/bg-7-621-2010).
- Hoegh-Guldberg, O., Poloczanska, E. S., Skirving, W., & Dove, S. (2017). Coral Reef Ecosystems under Climate Change and Ocean Acidification. *Frontiers in Marine Science*, *4*, 158. doi:[10.3389/fmars.2017.00158](https://doi.org/10.3389/fmars.2017.00158).

- Hurrell, J. W. (1995). Decadal Trends in the North Atlantic Oscillation: Regional Temperatures and Precipitation. *Science*, *269*, 676–679. doi:[10.1126/science.269.5224.676](https://doi.org/10.1126/science.269.5224.676).
- Hurrell, J. W., Kushnir, Y., Ottersen, G., & Visbeck, M. (2003). An Overview of the North Atlantic Oscillation. In *The North Atlantic Oscillation: Climatic Significance and Environmental Impact* (pp. 1–35). American Geophysical Union (AGU). doi:<https://doi.org/10.1029/134GM01>.
- Hurrell, J. W., & Trenberth, K. E. (1999). Global Sea Surface Temperature Analyses: Multiple Problems and Their Implications for Climate Analysis, Modeling, and Reanalysis. *Bulletin of the American Meteorological Society*, *80*, 2661–2678. doi:[10.1175/1520-0477\(1999\)080<2661:GSSTAM>2.0.CO;2](https://doi.org/10.1175/1520-0477(1999)080<2661:GSSTAM>2.0.CO;2).
- Imawaki, S., Bower, A. S., Beal, L., & Qiu, B. (2013). Western boundary currents. In G. Siedler, S. M. Griffies, & J. A. Church (Eds.), *Ocean Circulation and Climate: A 21st Century Perspective* (pp. 305–338). Academic Press.
- Iorga, M. C., & Lozier, M. S. (1999a). Signatures of the Mediterranean outflow from a North Atlantic climatology 1. Salinity and density fields. *Journal of Geophysical Research*, *104*, 25985–26009. doi:[10.1029/1999JC900115](https://doi.org/10.1029/1999JC900115).
- Iorga, M. C., & Lozier, M. S. (1999b). Signatures of the Mediterranean outflow from a North Atlantic climatology 2. Diagnostic velocity fields. *Journal of Geophysical Research*, *104*, 26011–26029. doi:[10.1029/1999JC900204](https://doi.org/10.1029/1999JC900204).
- IPCC (2021). *Climate Change 2021: The Physical Science Basis. Contribution of Working Group I to the Sixth Assessment Report of the Intergovernmental Panel on Climate Change* [Masson-Delmotte, V. and Zhai, P. and Pirani, A. and Connors, S. L. and Péan, C. and Berger, S. and Caud, N. and Chen, Y. and Goldfarb, L. and Gomis, M. I. and Huang, M. and Leitzell, K. and Lonnoy, E. and Matthews, J. B. R. and Maycock, T. K. and Waterfield, T. and Yelekci, O. and Yu, R. and Zhou, B. (eds)]. Cambridge University Press. In Press.
- Irwin, A. J., & Oliver, M. J. (2009). Are ocean deserts getting larger? *Geophysical Research Letters*, *36*, L18609. doi:[10.1029/2009GL039883](https://doi.org/10.1029/2009GL039883).
- Jackson, L. C., Kahana, R., Graham, T., Ringer, M. A., Woollings, T., Mecking, J. V., & Wood, R. A. (2015). Global and European climate impacts of a slowdown of the AMOC in a high resolution GCM. *Climate Dynamics*, *45*, 3299–3316. doi:[10.1007/s00382-015-2540-2](https://doi.org/10.1007/s00382-015-2540-2).
- Jia, Y. (2000). Formation of an Azores Current Due to Mediterranean Overflow in a Modeling Study of the North Atlantic. *Journal of Physical Oceanography*, *30*, 2342–2358. doi:[10.1175/1520-0485\(2000\)030<2342:FOAACD>2.0.CO;2](https://doi.org/10.1175/1520-0485(2000)030<2342:FOAACD>2.0.CO;2).

- Johns, W. E., Baringer, M. O., Beal, L. M., Cunningham, S. A., Kanzow, T., Bryden, H. L., Hirschi, J. J. M., Marotzke, J., Meinen, C. S., Shaw, B., & Curry, R. (2011). Continuous, Array-Based Estimates of Atlantic Ocean Heat Transport at 26.5°N. *Journal of Climate*, *24*, 2429–2449. doi:[10.1175/2010JCLI3997.1](https://doi.org/10.1175/2010JCLI3997.1).
- Johnson, G. C., & Gruber, N. (2007). Decadal water mass variations along 20°W in the Northeast Atlantic Ocean. *Progress in Oceanography*, *73*, 277–295. doi:[10.1016/j.pocean.2006.03.022](https://doi.org/10.1016/j.pocean.2006.03.022).
- Jones, P. D., New, M., Parker, D. E., Martin, S., & Rigor, I. G. (1999). Surface air temperature and its changes over the past 150 years. *Reviews of Geophysics*, *37*, 173–199. doi:[10.1029/1999RG900002](https://doi.org/10.1029/1999RG900002).
- Josey, S. A., Hirschi, J. J.-M., Sinha, B., Duchez, A., Grist, J. P., & Marsh, R. (2018). The Recent Atlantic Cold Anomaly: Causes, Consequences, and Related Phenomena. *Annual Review of Marine Science*, *10*, 475–501. doi:[10.1146/annurev-marine-121916-063102](https://doi.org/10.1146/annurev-marine-121916-063102).
- Käse, R. H., & Krauss, W. (1996). The Gulf Stream, the North Atlantic Current, and the Origin of the Azores Current. In W. Krauss (Ed.), *The Warmwatersphere of the North Atlantic Ocean* (pp. 291–337). Gebrüder Borntraeger, Berlin.
- Käse, R. H., & Siedler, G. (1982). Meandering of the subtropical front south-east of the Azores. *Nature*, *300*, 245–246. doi:[10.1038/300245a0](https://doi.org/10.1038/300245a0).
- Käse, R. H., Zenk, W., Sanford, T. B., & Hiller, W. (1985). Currents, Fronts and Eddy Fluxes in the Canary Basin. *Progress in Oceanography*, *14*, 231–257. doi:[10.1016/0079-6611\(85\)90013-8](https://doi.org/10.1016/0079-6611(85)90013-8).
- Keil, P., Mauritsen, T., Jungclaus, J., Hedemann, C., Olonscheck, D., & Ghosh, R. (2020). Multiple drivers of the North Atlantic warming hole. *Nature Climate Change*, *10*, 667–671. doi:[10.1038/s41558-020-0819-8](https://doi.org/10.1038/s41558-020-0819-8).
- Kerr, R. A. (2000). A North Atlantic Climate Pacemaker for the Centuries. *Science*, *288*, 1984–1985. doi:[10.1126/science.288.5473.1984](https://doi.org/10.1126/science.288.5473.1984).
- Kida, S., Price, J. F., & Yang, J. (2008). The Upper-Oceanic Response to Overflows: A Mechanism for the Azores Current. *Journal of Physical Oceanography*, *38*, 880–895. doi:[10.1175/2007JP03750.1](https://doi.org/10.1175/2007JP03750.1).
- Kielmann, J., & Käse, R. H. (1987). Numerical Modeling of Meander and Eddy Formation in the Azores Current Frontal Zone. *Journal of Physical Oceanography*, *17*, 529–541. doi:[10.1175/1520-0485\(1987\)017<0529:NMOMAE>2.0.CO;2](https://doi.org/10.1175/1520-0485(1987)017<0529:NMOMAE>2.0.CO;2).
- Klein, B., & Siedler, G. (1989). On the Origin of the Azores Current. *Journal of Geophysical Research*, *94*, 6159–6168. doi:[10.1029/JC094iC05p06159](https://doi.org/10.1029/JC094iC05p06159).

- Krahmann, G., & Schott, F. (1998). Longterm increases in Western Mediterranean salinities and temperatures: anthropogenic and climatic sources. *Geophysical Research Letters*, *25*, 4209–4212. doi:[10.1029/1998GL900143](https://doi.org/10.1029/1998GL900143).
- Kwiatkowski, L., Torres, O., Bopp, L., Aumont, O., Chamberlain, M., Christian, J. R., Dunne, J. P., Gehlen, M., Ilyina, T., John, J. G., Lenton, A., Li, H., Lovenduski, N. S., Orr, J. C., Palmieri, J., Santana-Falcón, Y., Schwinger, J., Séférian, R., Stock, C. A., Tagliabue, A., Takano, Y., Tjiputra, J., Toyama, K., Tsujino, H., Watanabe, M., Yamamoto, A., Yool, A., & Ziehn, T. (2020). Twenty-first century ocean warming, acidification, deoxygenation, and upper-ocean nutrient and primary production decline from CMIP6 model projections. *Biogeosciences*, *17*, 3439–3470. doi:[10.5194/bg-17-3439-2020](https://doi.org/10.5194/bg-17-3439-2020).
- Lamas, L., Peliz, Á., Ambar, I., Barbosa Aguiar, A., Maximenko, N., & Teles-Machado, A. (2010). Evidence of time-mean cyclonic cell southwest of Iberian Peninsula: The Mediterranean Outflow-driven β -plume? *Geophysical Research Letters*, *37*, L12606. doi:[10.1029/2010GL043339](https://doi.org/10.1029/2010GL043339).
- Le Traon, P.-Y., & De Mey, P. (1994). The eddy field associated with the Azores Front east of the Mid-Atlantic Ridge as observed by the Geosat altimeter. *Journal of Geophysical Research*, *99*, 9907–9923. doi:[10.1029/93JC03513](https://doi.org/10.1029/93JC03513).
- Le Traon, P.-Y., Rouquet, M. C., & Boissier, C. (1990). Spatial Scales of Mesoscale Variability in the North Atlantic as Deduced From Geosat Data. *Journal of Geophysical Research*, *95*, 20267–20285. doi:[10.1029/JC095iC11p20267](https://doi.org/10.1029/JC095iC11p20267).
- Leadbetter, S. J., Williams, R. G., McDonagh, E. L., & King, B. A. (2007). A twenty year reversal in water mass trends in the subtropical North Atlantic. *Geophysical Research Letters*, *34*, L12608. doi:[10.1029/2007GL029957](https://doi.org/10.1029/2007GL029957).
- Levitus, S. (1989). Interpentadal Variability of Temperature and Salinity at Intermediate Depths of the North Atlantic Ocean, 1970–1974 Versus 1955–1959. *Journal of Geophysical Research*, *94*, 16125–16131. doi:[10.1029/JC094iC11p16125](https://doi.org/10.1029/JC094iC11p16125).
- Levitus, S., Antonov, J. I., Boyer, T. P., Baranova, O. K., Garcia, H. E., Locarnini, R. A., Mishonov, A. V., Reagan, J. R., Seidov, D., Yarosh, E. S., & Zweng, M. M. (2012). World ocean heat content and thermosteric sea level change (0–2000 m), 1955–2010. *Geophysical Research Letters*, *39*, L10603. doi:[10.1029/2012GL051106](https://doi.org/10.1029/2012GL051106).
- Levitus, S., Antonov, J. I., Boyer, T. P., Locarnini, R. A., Garcia, H. E., & Mishonov, A. V. (2009). Global ocean heat content 1955–2008 in light of recently revealed instrumentation problems. *Geophysical Research Letters*, *36*, L07608. doi:[10.1029/2008GL037155](https://doi.org/10.1029/2008GL037155).
- Longhurst, A. (1998). *Ecological Geography of the Sea*. San Diego, California: Academic Press.

- Lozier, M. S. (2012). Overturning in the North Atlantic. *Annual Reviews Marine Science*, 4, 291–315. doi:[10.1146/annurev-marine-120710-100740](https://doi.org/10.1146/annurev-marine-120710-100740).
- Lozier, M. S., Bacon, S., Bower, A. S., Cunningham, S. A., Femke de Jong, M., de Steur, L., deYoung, B., Fischer, J., Gary, S. F., Greenan, B. J. W., Heimbach, P., Holliday, N. P., Houpert, L., Inall, M. E., Johns, W. E., Johnson, H. L., Karstensen, J., Li, F., Lin, X., Mackay, N., Marshall, D. P., Mercier, H., Myers, P. G., Pickart, R. S., Pillar, H. R., Straneo, F., Thierry, V., Weller, R. A., Williams, R. G., Wilson, C., Yang, J., Zhao, J., & Zika, J. D. (2017). Overturning in the Subpolar North Atlantic Program: A New International Ocean Observing System. *Bulletin of the American Meteorological Society*, 98, 737–752. doi:[10.1175/BAMS-D-16-0057.1](https://doi.org/10.1175/BAMS-D-16-0057.1).
- Lozier, M. S., Dave, A. C., Palter, J. B., Gerber, L. M., & Barber, R. T. (2011). On the relationship between stratification and primary productivity in the North Atlantic. *Geophysical Research Letters*, 38, L18609. doi:[10.1029/2011GL049414](https://doi.org/10.1029/2011GL049414).
- Lozier, M. S., Owens, W. B., & Curry, R. G. (1995). The climatology of the North Atlantic. *Progress in Oceanography*, 36, 1–44. doi:[10.1016/0079-6611\(95\)00013-5](https://doi.org/10.1016/0079-6611(95)00013-5).
- Lozier, M. S., & Sindlinger, L. (2009). On the Source of Mediterranean Overflow Water Property Changes. *Journal of Physical Oceanography*, 39, 1800–1817. doi:[10.1175/2009JPO4109.1](https://doi.org/10.1175/2009JPO4109.1).
- Lozier, M. S., & Stewart, N. M. (2008). On the Temporally Varying Northward Penetration of Mediterranean Overflow Water and Eastward Penetration of Labrador Sea Water. *Journal of Physical Oceanography*, 38, 2097–2103. doi:[10.1175/2008JPO3908.1](https://doi.org/10.1175/2008JPO3908.1).
- Lyman, J. M., & Johnson, G. C. (2014). Estimating Global Ocean Heat Content Changes in the Upper 1800 m since 1950 and the Influence of Climatology Choice. *Journal of Climate*, 27, 1945–1957. doi:[10.1175/JCLI-D-12-00752.1](https://doi.org/10.1175/JCLI-D-12-00752.1).
- Mahadevan, A. (2016). The Impact of Submesoscale Physics on Primary Production of Plankton. *Annual Review of Marine Science*, 8, 161–184. doi:[10.1146/annurev-marine-010814-015912](https://doi.org/10.1146/annurev-marine-010814-015912).
- Mahaffey, C., Williams, R. G., Wolff, G. A., Mahowald, N., Anderson, W., & Woodward, M. (2003). Biogeochemical signatures of nitrogen fixation in the eastern North Atlantic. *Geophysical Research Letters*, 30, 1300. doi:[10.1029/2002GL016542](https://doi.org/10.1029/2002GL016542).
- Maillard, C., & Käse, R. (1989). The near-surface flow in the subtropical gyre south of the Azores. *Journal of Geophysical Research*, 94, 16133–16140. doi:[10.1029/JC094iC11p16133](https://doi.org/10.1029/JC094iC11p16133).
- Marchese, P. J. (1999). Variability in the Gulf Stream recirculation gyre. *Journal of Geophysical Research*, 104, 29549–29560. doi:[10.1029/1999JC900254](https://doi.org/10.1029/1999JC900254).

- Marshall, J., Kushnir, Y., Battisti, D., Chang, P., Czaja, A., Dickson, R., Hurrell, J., McCartney, M., Saravanan, R., & Visbeck, M. (2001). North Atlantic climate variability: phenomena, impacts and mechanisms. *International Journal of Climatology*, *21*, 1863–1898. doi:[10.1002/joc.693](https://doi.org/10.1002/joc.693).
- Martinez, E., Antoine, D., D'ortenzio, F., & Gentili, B. (2009). Climate-Driven Basin-Scale Decadal Oscillations of Oceanic Phytoplankton. *Science*, *326*, 1253–1256. doi:[10.1126/science.1177012](https://doi.org/10.1126/science.1177012).
- Mavropoulou, A.-M., Vervatis, V., & Sofianos, S. (2020). Dissolved oxygen variability in the Mediterranean Sea. *Journal of Marine Systems*, *208*, 103348. doi:[10.1016/j.jmarsys.2020.103348](https://doi.org/10.1016/j.jmarsys.2020.103348).
- McClain, C. R., & Firestone, J. (1993). An Investigation of Ekman Upwelling in the North Atlantic. *Journal of Geophysical Research*, *98*, 12327–12339. doi:[10.1029/93JC00868](https://doi.org/10.1029/93JC00868).
- McClain, C. R., Signorini, S. R., & Christian, J. R. (2004). Subtropical gyre variability observed by ocean-color satellites. *Deep-Sea Research II*, *51*, 281–301. doi:[10.1016/j.dsr2.2003.08.002](https://doi.org/10.1016/j.dsr2.2003.08.002).
- McGillicuddy, D. J., Robinson, A. R., Siegel, D. A., Jannasch, H. W., Johnson, R., Dickey, T. D., McNeil, J., Michaels, A. F., & Knap, A. H. (1998). Influence of mesoscale eddies on new production in the Sargasso Sea. *Nature*, *394*, 263–266. doi:[10.1038/28367](https://doi.org/10.1038/28367).
- Meyssignac, B., Boyer, T., Zhao, Z., Hakuba, M. Z., Landerer, F. W., Stammer, D., Köhl, A., Kato, S., L'Ecuyer, T., Ablain, M., Abraham, J. P., Blazquez, A., Cazenave, A., Church, J. A., Cowley, R., Cheng, L., Domingues, C. M., Giglio, D., Gouretski, V., Ishii, M., Johnson, G. C., Killick, R. E., Legler, D., Llovel, W., Lyman, J., Palmer, M. D., Piotrowicz, S., Purkey, S. G., Roemmich, D., Roca, R., Savita, A., Schuckmann, K. v., Speich, S., Stephens, G., Wang, G., Wijffels, S. E., & Zilberman, N. (2019). Measuring Global Ocean Heat Content to Estimate the Earth Energy Imbalance. *Frontiers in Marine Science*, *6*, 432. doi:[10.3389/fmars.2019.00432](https://doi.org/10.3389/fmars.2019.00432).
- Millot, C., Candela, J., Fuda, J.-L., & Tber, Y. (2006). Large warming and salinification of the Mediterranean outflow due to changes in its composition. *Deep-Sea Research II*, *53*, 656–666. doi:[10.1016/j.dsr.2005.12.017](https://doi.org/10.1016/j.dsr.2005.12.017).
- Moat, B. I., Smeed, D. A., Frajka-Williams, E., Desbruyères, D. G., Beaulieu, C., Johns, W. E., Rayner, D., Sanchez-Franks, A., Baringer, M. O., Volkov, D., Jackson, L. C., & Bryden, H. L. (2020). Pending recovery in the strength of the meridional overturning circulation at 26°N. *Ocean Science*, *16*, 863–874. doi:[10.5194/os-16-863-2020](https://doi.org/10.5194/os-16-863-2020).
- Mortenson, E., Lenton, A., Shadwick, E. H., Trull, T. W., Chamberlain, M. A., & Zhang, X. (2021). Divergent trajectories of ocean warming and acidification. *Environmental Research Letters*, *16*, 124063. doi:[10.1088/1748-9326/ac3d57](https://doi.org/10.1088/1748-9326/ac3d57).

- Müller, T. J., & Siedler, G. (1992). Multi-year current time series in the eastern North Atlantic Ocean. *Journal of Marine Research*, *50*, 63–98. doi:[10.1357/002224092784797755](https://doi.org/10.1357/002224092784797755).
- Müller, T. J., & Waniek, J. J. (2013). KIEL276 Time Series Data from Moored Current Meters 33°N, 22°W, 5285 m water depth. March 1980 - April 2011. Background Information and Data Compilation. GEOMAR Report Nr. 13. doi:[10.3289/GEOMAR_REP_NS_13_2013](https://doi.org/10.3289/GEOMAR_REP_NS_13_2013).
- Munk, W. H. (1950). On the wind-driven ocean circulation. *Journal of Atmospheric Sciences*, *7*, 80–93. doi:[10.1175/1520-0469\(1950\)007<0080:OTWDOC>2.0.CO;2](https://doi.org/10.1175/1520-0469(1950)007<0080:OTWDOC>2.0.CO;2).
- Naranjo, C., García-Lafuente, J., Sammartino, S., Sánchez-Garrido, J. C., Sánchez-Leal, R., & Bellanco, M. J. (2017). Recent changes (2004–2016) of temperature and salinity in the Mediterranean outflow. *Geophysical Research Letters*, *44*, 5665–5672. doi:[10.1002/2017GL072615](https://doi.org/10.1002/2017GL072615).
- Neuer, S., Cianca, A., Helmke, P., Freudenthal, T., Davenport, R., Meggers, H., Knoll, M., Santana-Casiano, J. M., González-Davila, M., Rueda, M.-J., & Llinás, O. (2007). Biogeochemistry and hydrography in the eastern subtropical North Atlantic gyre. Results from the European time-series station ESTOC. *Progress in Oceanography*, *72*, 1–29. doi:[10.1016/j.pocean.2006.08.001](https://doi.org/10.1016/j.pocean.2006.08.001).
- New, A. L., Jia, Y., Coulibaly, M., & Dengg, J. (2001). On the role of the Azores Current in the ventilation of the North Atlantic Ocean. *Progress in Oceanography*, *48*, 163–194. doi:[10.1016/S0079-6611\(01\)00004-0](https://doi.org/10.1016/S0079-6611(01)00004-0).
- NOAA (2022). Trends in Atmospheric Carbon Dioxide – Mauna Loa, Hawaii. <https://gml.noaa.gov/ccgg/trends/mlo.html> (accessed on 06.01.2022).
- Onken, R. (1993). The Azores Countercurrent. *Journal of Physical Oceanography*, *23*, 1638–1646. doi:[10.1175/1520-0485\(1993\)023<1638:TAC>2.0.CO;2](https://doi.org/10.1175/1520-0485(1993)023<1638:TAC>2.0.CO;2).
- Oschlies, A. (2001). NAO-induced long-term changes in nutrient supply to the surface waters of the North Atlantic. *Geophysical Research Letters*, *28*, 1751–1754. doi:[10.1029/2000GL012328](https://doi.org/10.1029/2000GL012328).
- Ottersen, G., Planque, B., Belgrano, A., Post, E., Reid, P. C., & Stenseth, N. C. (2001). Ecological effects of the North Atlantic Oscillation. *Oecologia*, *128*, 1–14. doi:[10.1007/s004420100655](https://doi.org/10.1007/s004420100655).
- Özgökmen, T. M., Chassignet, E. P., & Rooth, C. G. H. (2001). On the Connection between the Mediterranean Outflow and the Azores Current. *Journal of Physical Oceanography*, *31*, 461–480. doi:[10.1175/1520-0485\(2001\)031<0461:OTCBTM>2.0.CO;2](https://doi.org/10.1175/1520-0485(2001)031<0461:OTCBTM>2.0.CO;2).

- Paillet, J., & Mercier, H. (1997). An inverse model of the eastern North Atlantic general circulation and thermocline ventilation. *Deep-Sea Research I*, *44*, 1293–1328. doi:[10.1016/S0967-0637\(97\)00019-8](https://doi.org/10.1016/S0967-0637(97)00019-8).
- Paiva, A. M., Chassignet, E. P., & Mariano, A. J. (2000). Numerical simulations of the North Atlantic subtropical gyre: sensitivity to boundary conditions. *Dynamics of Atmospheres and Oceans*, *32*, 209–237. doi:[10.1016/S0377-0265\(00\)00048-8](https://doi.org/10.1016/S0377-0265(00)00048-8).
- Palter, J. B., Lozier, M. S., & Barber, R. T. (2005). The effect of advection on the nutrient reservoir in the North Atlantic subtropical gyre. *Nature*, *437*, 687–692. doi:[10.1038/nature03969](https://doi.org/10.1038/nature03969).
- Parrilla, G., Lavín, A., Bryden, H., García, M., & Millard, R. (1994). Rising temperatures in the subtropical North Atlantic Ocean over the past 35 years. *Nature*, *369*, 48–51. doi:[10.1038/369048a0](https://doi.org/10.1038/369048a0).
- Parrilla, G., Neuer, S., Le Traon, P. Y., & Fernández-Suarez, E. (2002). Topical studies in oceanography: Canary Islands Azores Gibraltar Observations (CANIGO) Volume 1: Studies in the northern Canary Islands basin. *Deep-Sea Research Part II*, *49*, 3409–3413. doi:[10.1016/S0967-0645\(02\)00104-2](https://doi.org/10.1016/S0967-0645(02)00104-2).
- de Pascual-Collar, Á., Sotillo, M. G., Levier, B., Aznar, R., Lorente, P., Amo-Baladrón, A., & Álvarez-Fanjul, E. (2019). Regional circulation patterns of Mediterranean Outflow Water near the Iberian and African continental slopes. *Ocean Science*, *15*, 565–582. doi:[10.5194/os-15-565-2019](https://doi.org/10.5194/os-15-565-2019).
- Pelegri, J. L., & Csanady, G. T. (1991). Nutrient Transport and Mixing in the Gulf Stream. *Journal of Geophysical Research*, *96*, 2577–2583. doi:[10.1029/90JC02535](https://doi.org/10.1029/90JC02535).
- Peliz, A., Dubert, J., Marchesiello, P., & Teles-Machado, A. (2007). Surface circulation in the Gulf of Cadiz: Model and mean flow structure. *Journal of Geophysical Research*, *112*, C11015. doi:[10.1029/2007JC004159](https://doi.org/10.1029/2007JC004159).
- Pérez, F. F., Gilcoto, M., & Ríos, A. F. (2003). Large and mesoscale variability of the water masses and the deep chlorophyll maximum in the Azores Front. *Journal of Geophysical Research*, *108*, 3215. doi:[10.1029/2000JC000360](https://doi.org/10.1029/2000JC000360).
- Pérez, V., Fernández, E., Marañón, E., Morán, X. A. G., & Zubkov, M. V. (2006). Vertical distribution of phytoplankton biomass, production and growth in the Atlantic subtropical gyres. *Deep-Sea Research I*, *53*, 1616–1634. doi:[10.1016/j.dsr.2006.07.008](https://doi.org/10.1016/j.dsr.2006.07.008).
- Pingree, R. D. (1997). The eastern subtropical gyre (North Atlantic): flow rings recirculations structure and subduction. *Journal of the Marine Biological Association of the United Kingdom*, *77*, 573–624. doi:[10.1017/S0025315400036109](https://doi.org/10.1017/S0025315400036109).

- Pollard, R. T., Griffiths, M. J., Cunningham, S. A., Read, J. F., Pérez, F. F., & Ríos, A. F. (1996). Vivaldi 1991 - A study of the formation, circulation and ventilation of Eastern North Atlantic Central Water. *Progress in Oceanography*, *37*, 167–192. doi:[10.1016/S0079-6611\(96\)00008-0](https://doi.org/10.1016/S0079-6611(96)00008-0).
- Polovina, J. J., Howell, E. A., & Abecassis, M. (2008). Ocean's least productive waters are expanding. *Geophysical Research Letters*, *35*, L03618. doi:[10.1029/2007GL031745](https://doi.org/10.1029/2007GL031745).
- Potter, R. A., & Lozier, M. S. (2004). On the warming and salinification of the Mediterranean outflow waters in the North Atlantic. *Geophysical Research Letters*, *31*, L01202. doi:[10.1029/2003GL018161](https://doi.org/10.1029/2003GL018161).
- Pullwer, J., & Waniek, J. J. (2020). Particulate trace metal fluxes in the center of an oceanic desert: Northeast Atlantic subtropical gyre. *Journal of Marine Systems*, *212*, 103447. doi:[10.1016/j.jmarsys.2020.103447](https://doi.org/10.1016/j.jmarsys.2020.103447).
- Rahmstorf, S., Box, J. E., Feulner, G., Mann, M. E., Robinson, A., Rutherford, S., & Schaffernicht, E. J. (2015). Exceptional twentieth-century slowdown in Atlantic Ocean overturning circulation. *Nature Climate Change*, *5*, 475–480. doi:[10.1038/NCLIMATE2554](https://doi.org/10.1038/NCLIMATE2554).
- Reid, J. L. (1978). On the Middepth Circulation and Salinity Field in the North Atlantic Ocean. *Journal of Geophysical Research*, *83*, 5063–5067. doi:[10.1029/JC083iC10p05063](https://doi.org/10.1029/JC083iC10p05063).
- Reid, J. L. (1979). On the contribution of the Mediterranean Sea outflow to the Norwegian-Greenland Sea. *Deep-Sea Research*, *26*, 1199–1223. doi:[10.1016/0198-0149\(79\)90064-5](https://doi.org/10.1016/0198-0149(79)90064-5).
- Reverdin, G. (2010). North Atlantic Subpolar Gyre Surface Variability (1895–2009). *Journal of Climate*, *23*, 4571–4584. doi:[10.1175/2010JCLI3493.1](https://doi.org/10.1175/2010JCLI3493.1).
- Rhein, M., Rintoul, S. R., Aoki, S., Campos, E., Chambers, D., Feely, R. A., Gulev, S., Johnson, G. S., Josey, S. A., Kostianoy, A., Mauritzen, C., Roemmich, D., & Talley, L. D. (2013). Observations: Ocean. In T. F. Stocker, D. Qin, G.-K. Plattner, M. Tignor, S. K. Allen, J. Boschung, A. Nauels, Y. Xia, V. Bex, & P. M. Midgley (Eds.), *Climate Change 2013: The Physical Science Basis. Contribution of Working Group I to the Fifth Assessment Report of the Intergovernmental Panel on Climate Change* (pp. 255–316). Cambridge, GB: Cambridge University Press.
- Richardson, P. L. (1983). Eddy Kinetic Energy in the North Atlantic From Surface Drifters. *Journal of Geophysical Research*, *88*, 4355–4367. doi:[10.1029/JC088iC07p04355](https://doi.org/10.1029/JC088iC07p04355).
- Richardson, P. L. (2001). Florida Current, Gulf Stream, and Labrador Current. In J. H. Steele (Ed.), *Encyclopedia of ocean sciences* (pp. 554–563). Oxford: Academic Press. (2nd ed.). doi:[10.1016/B978-012374473-9.00357-X](https://doi.org/10.1016/B978-012374473-9.00357-X).

- Ríos, A. F., Pérez, F. F., & Fraga, F. (1992). Water masses in the upper and middle North Atlantic Ocean east of the Azores. *Deep-Sea Research*, *39*, 645–658. doi:[10.1016/0198-0149\(92\)90093-9](https://doi.org/10.1016/0198-0149(92)90093-9).
- Robbins, P. E., Price, J. F., Owens, W. B., & Jenkins, W. J. (2000). The Importance of Lateral Diffusion for the Ventilation of the Lower Thermocline in the Subtropical North Atlantic. *Journal of Physical Oceanography*, *30*, 67–89. doi:[10.1175/1520-0485\(2000\)030<0067:TIOLDF>2.0.CO;2](https://doi.org/10.1175/1520-0485(2000)030<0067:TIOLDF>2.0.CO;2).
- Rudnick, D. L., & Luyten, J. R. (1996). Intensive surveys of the Azores Front 1. Tracers and dynamics. *Journal of Geophysical Research*, *101*, 923–939. doi:[10.1029/95JC02867](https://doi.org/10.1029/95JC02867).
- Sabine, C. L., Feely, R. A., Gruber, N., Key, R. M., Lee, K., Bullister, J. L., Wanninkhof, R., Wong, C. S., Wallace, D. W. R., Tilbrook, B., Millero, F. J., Peng, T.-H., Kozyr, A., Ono, T., & Rios, A. F. (2004). The Oceanic Sink for Anthropogenic CO₂. *Science*, *305*, 367–371. doi:[10.1126/science.1097403](https://doi.org/10.1126/science.1097403).
- Sarafanov, A. (2009). On the effect of the North Atlantic Oscillation on temperature and salinity of the subpolar North Atlantic intermediate and deep waters. *ICES Journal of Marine Science*, *66*, 1448–1454. doi:[10.1093/icesjms/fsp094](https://doi.org/10.1093/icesjms/fsp094).
- Sarafanov, A., Falina, A., Sokov, A., & Demidov, A. (2008). Intense warming and salinification of intermediate waters of southern origin in the eastern subpolar North Atlantic in the 1990s to mid-2000s. *Journal of Geophysical Research*, *113*, C12022. doi:[10.1029/2008JC004975](https://doi.org/10.1029/2008JC004975).
- Schiebel, R., Waniek, J., Zeltner, A., & Alves, M. (2002). Impact of the Azores Front on the distribution of planktic foraminifers, shelled gastropods, and coccolithophorids. *Deep-Sea Research II*, *49*, 4035–4050. doi:[10.1016/S0967-0645\(02\)00141-8](https://doi.org/10.1016/S0967-0645(02)00141-8).
- Schlesinger, M. E., & Ramankutty, N. (1994). An oscillation in the global climate system of period 65–70 years. *Nature*, *367*, 723–726. doi:[10.1038/367723a0](https://doi.org/10.1038/367723a0).
- Schmittner, A. (2005). Decline of the marine ecosystem caused by a reduction in the Atlantic overturning circulation. *Nature*, *434*, 628–633. doi:[10.1038/nature03476](https://doi.org/10.1038/nature03476).
- Schmitz, W. J., & McCartney, M. S. (1993). On the North Atlantic Circulation. *Reviews of Geophysics*, *31*, 29–49. doi:[10.1029/92RG02583](https://doi.org/10.1029/92RG02583).
- Seidov, D., Mishonov, A., Reagan, J., & Parsons, R. (2017). Multidecadal variability and climate shift in the North Atlantic Ocean. *Geophysical Research Letters*, *44*, 4985–4993. doi:[10.1002/2017GL073644](https://doi.org/10.1002/2017GL073644).
- Seidov, D., Mishonov, A., Reagan, J., & Parsons, R. (2019). Resilience of the Gulf Stream path on decadal and longer timescales. *Scientific Reports*, *9*, 11549. doi:[10.1038/s41598-019-48011-9](https://doi.org/10.1038/s41598-019-48011-9).

- Serra, N., Ambar, I., & Käse, R. H. (2005). Observations and numerical modelling of the Mediterranean outflow splitting and eddy generation. *Deep-Sea Research II*, *52*, 383–408. doi:[10.1016/j.dsr2.2004.05.025](https://doi.org/10.1016/j.dsr2.2004.05.025).
- Siedler, G., Armi, L., & Müller, T. J. (2005). Meddies and decadal changes at the Azores Front from 1980 to 2000. *Deep-Sea Research II*, *52*, 583–604. doi:[10.1016/j.dsr2.2004.12.010](https://doi.org/10.1016/j.dsr2.2004.12.010).
- Siedler, G., Church, J., & Gould, J. (2001). *Ocean Circulation & Climate: Observing and Modelling the Global Ocean*. International Geophysics Series, Vol. 77. Elsevier.
- Siedler, G., Zenk, W., & Emery, W. J. (1985). Strong Current Events Related to a Sub-tropical Front in the Northeast Atlantic. *Journal of Physical Oceanography*, *15*, 885–897. doi:[10.1175/1520-0485\(1985\)015<0885:SCERTA>2.0.CO;2](https://doi.org/10.1175/1520-0485(1985)015<0885:SCERTA>2.0.CO;2).
- Sierro, F. J., Hodell, D. A., Andersen, N., Azibei, L. A., Jimenez-Espejo, F. J., Bahr, A., Flores, J. A., Ausin, B., Rogerson, M., Lozano-Luz, R., Lebreiro, S. M., & Hernandez-Molina, F. J. (2020). Mediterranean Overflow Over the Last 250 kyr: Freshwater Forcing From the Tropics to the Ice Sheets. *Paleoceanography and Paleoclimatology*, *35*, e2020PA003931. doi:[10.1029/2020PA003931](https://doi.org/10.1029/2020PA003931).
- Signorini, S. R., Franz, B. A., & McClain, C. R. (2015). Chlorophyll variability in the oligotrophic gyres: mechanisms, seasonality and trends. *Frontiers in Marine Science*, *2*. doi:[10.3389/fmars.2015.00001](https://doi.org/10.3389/fmars.2015.00001).
- Silva-Fernandes, S. M., & Peliz, A. J. (2020). The Turbulent Structure of the Azores Current System: A Statistical Analysis. *Journal of Geophysical Research: Oceans*, *125*, e2020JC016327. doi:[10.1029/2020JC016327](https://doi.org/10.1029/2020JC016327).
- Smeed, D. A., McCarthy, G. D., Cunningham, S. A., Frajka-Williams, E., Rayner, D., Johns, W. E., Meinen, C. S., Baringer, M. O., Moat, B. I., Duchez, A., & Bryden, H. L. (2014). Observed decline of the Atlantic meridional overturning circulation 2004–2012. *Ocean Sciences*, *10*, 29–38. doi:[10.5194/os-10-29-2014](https://doi.org/10.5194/os-10-29-2014).
- Soto-Navarro, J., Criado-Aldeanueva, F., Sánchez-Garrido, J. C., & García-Lafuente, J. (2012). Recent thermohaline trends of the Atlantic waters inflowing to the Mediterranean Sea. *Geophysical Research Letters*, *39*, L01604. doi:[10.1029/2011GL049907](https://doi.org/10.1029/2011GL049907).
- Spall, M. A. (1990). Circulation in the Canary Basin: A Model/Data Analysis. *Journal of Geophysical Research*, *95*, 9611–9628.
- Steinacher, M., Joos, F., Frölicher, T. L., Bopp, L., Cadule, P., Cocco, V., Doney, S. C., Gehlen, M., Lindsay, K., Moore, J. K., Schneider, B., & Segschneider, J. (2010). Projected 21st century decrease in marine productivity: a multi-model analysis. *Biogeosciences*, *7*, 979–1005. doi:[10.5194/bg-7-979-2010](https://doi.org/10.5194/bg-7-979-2010).

- Steinberg, D. K., Carlson, C. A., Bates, N. R., Johnson, J., Rodney, Michaels, A. F., & Knap, A. H. (2001). Overview of the US JGOFS Bermuda Atlantic Time-series Study (BATS): a decade-scale look at ocean biology and biogeochemistry. *Deep-Sea Research II*, *48*, 1405–1447. doi:[10.1016/S0967-0645\(00\)00148-X](https://doi.org/10.1016/S0967-0645(00)00148-X).
- Stendardo, I., & Gruber, N. (2012). Oxygen trends over five decades in the North Atlantic. *Journal of Geophysical Research*, *117*, C11004. doi:[10.1029/2012JC007909](https://doi.org/10.1029/2012JC007909).
- Stendardo, I., Kieke, D., Rhein, M., Gruber, N., & Steinfeldt, R. (2015). Interannual to decadal oxygen variability in the mid-depth water masses of the eastern North Atlantic. *Deep-Sea Research I*, *95*, 85–98. doi:[10.1016/j.dsr.2014.10.009](https://doi.org/10.1016/j.dsr.2014.10.009).
- Stern, J., Dellwig, O., & Waniek, J. J. (2017). Deep-sea fluxes of barium and lithogenic trace elements in the subtropical northeast Atlantic. *Deep Sea Research Part I*, *122*, 72–80. doi:[10.1016/j.dsr.2017.02.002](https://doi.org/10.1016/j.dsr.2017.02.002).
- Stern, J., Kaiser, D., Przibilla, A., Schulz-Bull, D. E., & Waniek, J. J. (2019). Trace metals and persistent organic pollutants fingerprint on the particle flux in the deep subtropical NE Atlantic. *Marine Pollution Bulletin*, *145*, 506–516. doi:[10.1016/j.marpolbul.2019.06.001](https://doi.org/10.1016/j.marpolbul.2019.06.001).
- Stommel, H. (1982). Is the South Pacific helium-3 plume dynamically active? *Earth and Planetary Science Letters*, *61*, 63–67. doi:[10.1016/0012-821X\(82\)90038-3](https://doi.org/10.1016/0012-821X(82)90038-3).
- Stommel, H., Niiler, P., & Anati, D. (1978). Dynamic topography and recirculation of the North Atlantic. *Journal of Marine Research*, *36*, 449–468.
- Stramma, L. (1984). Geostrophic transport in the Warm Water Sphere of the eastern subtropical North Atlantic. *Journal of Marine Research*, *42*, 537–558. doi:[10.1357/002224084788506022](https://doi.org/10.1357/002224084788506022).
- Stramma, L., & Isemer, H.-J. (1988). Seasonal variability of meridional temperature fluxes in the eastern North Atlantic Ocean. *Journal of Marine Research*, *46*, 281–299. doi:[10.1357/002224088785113577](https://doi.org/10.1357/002224088785113577).
- Stramma, L., & Müller, T. J. (1989). Some Observations of the Azores Current and the North Equatorial Current. *Journal of Geophysical Research*, *94*, 3181–3186. doi:[10.1029/JC094iC03p03181](https://doi.org/10.1029/JC094iC03p03181).
- Stramma, L., & Siedler, G. (1988). Seasonal Changes in the North Atlantic Subtropical Gyre. *Journal of Geophysical Research*, *93*, 8111–8118. doi:[10.1029/JC093iC07p08111](https://doi.org/10.1029/JC093iC07p08111).
- Swingedouw, D., Colin, C., Eynaud, F., Ayache, M., & Zaragosi, S. (2019). Impact of freshwater release in the Mediterranean Sea on the North Atlantic climate. *Climate Dynamics*, *53*, 3893–3915. doi:[10.1007/s00382-019-04758-5](https://doi.org/10.1007/s00382-019-04758-5).

- Sy, A. (1988). Investigation of large-scale circulation patterns in the central North Atlantic: the North Atlantic Current, the Azores Current, and the Mediterranean Water plume in the area of the Mid-Atlantic Ridge. *Deep-Sea Research*, 35, 383–413. doi:[10.1016/0198-0149\(88\)90017-9](https://doi.org/10.1016/0198-0149(88)90017-9).
- Taylor, A. H., & Stephens, J. A. (1998). The North Atlantic Oscillation and the latitude of the Gulf Stream. *Tellus A: Dynamic Meteorology and Oceanography*, 50, 134–142. doi:[10.3402/tellusa.v50i1.14517](https://doi.org/10.3402/tellusa.v50i1.14517).
- Teira, E., Mouriño, B., Marañón, E., Pérez, V., Pazó, M. J., Serret, P., de Armas, D., Escáñez, J., Woodward, E. M. S., & Fernández, E. (2005). Variability of chlorophyll and primary production in the Eastern North Atlantic Subtropical Gyre: potential factors affecting phytoplankton activity. *Deep-Sea Research I*, 52, 569–588. doi:[10.1016/j.dsr.2004.11.007](https://doi.org/10.1016/j.dsr.2004.11.007).
- TOPOGULF Group (1986). TOPOGULF—A joint programme initiated by IFREMER, Brest and IfM, Kiel – Data Report. Vol. 1. Bericht aus dem Institut für Meereskunde, Kiel, 154. 183 pp.
- Townsend, T. L., Hurlburt, H. E., & Hogan, P. J. (2000). Modeled Sverdrup flow in the North Atlantic from 11 different wind stress climatologies. *Dynamics of Atmospheres and Oceans*, 32, 373–417. doi:[10.1016/S0377-0265\(00\)00052-X](https://doi.org/10.1016/S0377-0265(00)00052-X).
- Trenberth, K. E., & Shea, D. J. (2006). Atlantic hurricanes and natural variability in 2005. *Geophysical Research Letter*, 33, L12704. doi:[10.1029/2006GL026894](https://doi.org/10.1029/2006GL026894).
- UNESCO (1983). Algorithms for Computation of Fundamental Properties of Seawater. *UNESCO Tech. Pap. Mar. Sci*, 44, 1–53. doi:[10.25607/OBP-1450](https://doi.org/10.25607/OBP-1450).
- Visbeck, M., Chassignet, E. P., Curry, R. G., Delworth, T. L., Dickson, R. R., & Krahnmann, G. (2003). The Ocean’s Response to North Atlantic Oscillation Variability. In *The North Atlantic Oscillation: Climatic Significance and Environmental Impact* (pp. 113–145). American Geophysical Union (AGU). doi:<https://doi.org/10.1029/134GM06>.
- Voelker, A. H. L., Colman, A., Olack, G., Waniek, J. J., & Hodell, D. (2015). Oxygen and hydrogen isotope signatures of Northeast Atlantic water masses. *Deep Sea Research Part II: Topical Studies in Oceanography*, 116, 89–106. doi:[10.1016/j.dsr2.2014.11.006](https://doi.org/10.1016/j.dsr2.2014.11.006).
- Voelker, A. H. L., Lebreiro, S. M., Schönfeld, J., Cacho, I., Erlenkeuser, H., & Abrantes, F. (2006). Mediterranean outflow strengthening during northern hemisphere coolings: A salt source for the glacial Atlantic? *Earth and Planetary Science Letters*, 245, 39–55. doi:[10.1016/j.epsl.2006.03.014](https://doi.org/10.1016/j.epsl.2006.03.014).

- Volkov, D. L., & Fu, L.-L. (2010). On the Reasons for the Formation and Variability of the Azores Current. *Journal of Physical Oceanography*, *40*, 2197–2220. doi:[10.1175/2010JP04326.1](https://doi.org/10.1175/2010JP04326.1).
- Volkov, D. L., & Fu, L.-L. (2011). Interannual variability of the Azores Current strength and eddy energy in relation to atmospheric forcing. *Journal of Geophysical Research*, *116*, C11011. doi:[10.1029/2011JC007271](https://doi.org/10.1029/2011JC007271).
- Waniek, J. J., Schulz-Bull, D. E., Blanz, T., Prien, R. D., Oschlies, A., & Müller, T. J. (2005). Interannual variability of deep water particle flux in relation to production and lateral sources in the northeast Atlantic. *Deep-Sea Research Part I*, *52*, 33–50. doi:[10.1016/j.dsr.2004.08.008](https://doi.org/10.1016/j.dsr.2004.08.008).
- Wild, M. (2009). Global dimming and brightening: A review. *Journal of Geophysical Research*, *114*, D00D16. doi:[10.1029/2008JD011470](https://doi.org/10.1029/2008JD011470).
- Williams, R. G., McLaren, A. J., & Follows, M. J. (2000). Estimating the convective supply of nitrate and implied variability in export production over the North Atlantic. *Global Biogeochemical Cycles*, *14*, 1299–1313. doi:[10.1029/2000GB001260](https://doi.org/10.1029/2000GB001260).
- Wong, A., Keeley, R., Carval, T., & Argo Data Management Team (2020). Argo Quality Control Manual for CTD and Trajectory Data. doi:[10.13155/33951](https://doi.org/10.13155/33951).
- Wu, L., Cai, W., Zhang, L., Nakamura, H., Timmermann, A., Joyce, T., McPhaden, M. J., Alexander, M., Qiu, B., Visbeck, M., Chang, P., & Giese, B. (2012). Enhanced warming over the global subtropical western boundary currents. *Nature Climate Change*, . doi:[10.1038/NCLIMATE1353](https://doi.org/10.1038/NCLIMATE1353).
- Yamaguchi, R., & Suga, T. (2019). Trend and Variability in Global Upper-Ocean Stratification Since the 1960s. *Journal of Geophysical Research: Oceans*, *124*, 8933–8948. doi:[10.1029/2019JC015439](https://doi.org/10.1029/2019JC015439).
- Yang, H., Lohmann, G., Krebs-Kanzow, U., Ionita, M., Shi, X., Sidorenko, D., Gong, X., Chen, X., & Gowan, E. J. (2020). Poleward Shift of the Major Ocean Gyres Detected in a Warming Climate. *Geophysical Research Letters*, *47*, e2019GL085868. doi:[10.1029/2019GL085868](https://doi.org/10.1029/2019GL085868).
- Zanna, L., Khatiwala, S., Gregory, J. M., Ison, J., & Heimbach, P. (2019). Global reconstruction of historical ocean heat storage and transport. *PNAS*, *116*, 1126–1131. doi:[10.1073/pnas.1808838115](https://doi.org/10.1073/pnas.1808838115).
- Zenk, W. (1975). On the Mediterranean outflow west of Gibraltar. *Meteor-Forschungsergebnisse A*, *16*, 35–43.

-
- Zhai, Y., Yang, J., Wan, X., & Zou, S. (2021). The Eastern Atlantic Basin Pathway for the Export of the North Atlantic Deep Waters. *Geophysical Research Letters*, *48*, e2021GL095615. doi:[10.1029/2021GL095615](https://doi.org/10.1029/2021GL095615).
- Zhang, M., Zhang, Y., Shu, Q., Zhao, C., Wang, G., Wu, Z., & Qiao, F. (2018). Spatiotemporal evolution of the chlorophyll *a* trend in the North Atlantic Ocean. *Science of the Total Environment*, *612*, 1141–1148. doi:[10.1016/j.scitotenv.2017.08.303](https://doi.org/10.1016/j.scitotenv.2017.08.303).
- Zhang, R. (2008). Coherent surface-subsurface fingerprint of the Atlantic meridional overturning circulation. *Geophysical Research Letters*, *35*, L20705. doi:[10.1029/2008GL035463](https://doi.org/10.1029/2008GL035463).
- Zhang, W.-Z., Chai, F., Xue, H., & Oey, L.-Y. (2020). Remote sensing linear trends of the Gulf Stream from 1993 to 2016. *Ocean Dynamics*, *70*, 701–712. doi:[10.1007/s10236-020-01356-6](https://doi.org/10.1007/s10236-020-01356-6).
- Zweng, M. M., Reagan, J. R., Seidov, D., Boyer, T. P., Locarnini, R. A., Garcia, H. E., Mishonov, A. V., Baranova, O. K., Weathers, K., Paver, C. R., & Smolyar, I. (2018). World Ocean Atlas 2018, Volume 2: Salinity. *A. Mishonov Technical Ed., NOAA Atlas NESDIS 82*, (p. 50).

Contributions to the manuscripts

Publication I

Frazão, H. C., R. D. Prien, D. E. Schulz-Bull, D. Seidov & J. J. Waniek (2022). The forgotten Azores Current: a long-term perspective. Accepted in *Frontiers in Marine Science*. doi: 10.3389/fmars.2022.842251

This work was conceptualized by J.J. Waniek and H.C. Frazão. H. C. Frazão processed the SODA-POP data, ran the analysis, produced the figures, and wrote the manuscript. R.D. Prien contributed with the visualization; D. E. Schulz-Bull and J. J. Waniek secured the funding. J. J. Waniek and D. Seidov supervised the work. All authors reviewed the manuscript. Approximate contribution to this work by H. C. Frazão of 90 %.

Publication II

Frazão, H. C. & J. J. Waniek (2021). Mediterranean Water Properties at the Eastern Limit of the North Atlantic Subtropical Gyre Since 1981. *Oceans*, 2, 266–280. doi: 10.3390/oceans2010016

This work was conceptualized by H. C. Frazão and J. J. Waniek. H. C. Frazão collected and processed the entire dataset, and wrote all versions of the manuscript. J. J. Waniek secured the funding, supervised the study, and reviewed all versions. Approximate contribution to this work by H. C. Frazão of 90 %.

Publication III

Frazão, H. C., R. D. Prien, T. J. Müller, D. E. Schulz-Bull & J. J. Waniek (2021). 30 years of temporal variability of temperature and currents below the main thermocline between 1980–2009 in the subtropical Northeast Atlantic (Kiel 276, 33°N, 22°W). *Journal of Marine Systems*, 217, 103517. doi: 10.1016/j.jmarsys.2021.103517.

H. C. Frazão ran all the analysis, prepared the graphs, and wrote the manuscript. R. D. Prien helped with the analysis; T. J. Müller and J. J. Waniek supervised the work, and led the cruises assigned to the deployments and recovery of Kiel 276 mooring. J. J. Waniek secured the funding. The manuscript was revised by all authors. Approximate contribution to this work by H. C. Frazão of 75 %.

Publication I

Full Research Paper, *Frontiers in Marine Science*, 2022

The forgotten Azores Current: a long-term perspective

Helena C. Frazão, Ralf D. Prien, Detlef E. Schulz-Bull, Dan Seidov, Joanna J. Waniek

Submitted: 23 December 2021; Accepted: 05 April 2022

doi: 10.3389/fmars.2022.842251

Abstract The Atlantic Meridional Overturning Circulation (AMOC) and its surface limb, the Gulf Stream, are in their weakest state since the last millennium. The consequences of this weakening in the Northeast Atlantic are not yet known. We show that the slowdown of the Gulf Stream in the 1960s, 1970s, and after 2000 may have caused a delayed weakening of the Azores Current. Concurrently, the Azores Front associated with the Azores Current migrated northward since the 1970s due to gradual changes in the Atlantic Multidecadal Oscillation and ocean heat content. We argue that the AMOC slowdown is also detectable in the low-energy region of the Northeast Atlantic and that the dynamics of Azores Current tightly connects to that of the dynamics of the Gulf Stream and AMOC on decadal and longer time scales.

The forgotten Azores Current: a long-term perspective

Helena C. Frazão*, Ralf Dieter Prien, Detlef Eckart Schulz-Bull, Dan Seidov, Joanna Jadwiga Waniek

Original Research, *Front. Mar. Sci. – Physical Oceanography*, Submitted on: 23 Dec 2021, Edited by: Ming Li

Reviewed by: Manuel Bensi, Tal Ezer

DOI: 10.3389/fmars.2022.842251

Typesetter: Typesetter 2

Manuscript Id: 842251

[View in Review Forum](#)

STATUS

Displayed is the current article status and the action required from you.

Article Stage: In Production
Article Status: Typesetter pending to produce the author's proof.
Action required from you: [Please proceed to pay the article publication fee.](#)

HISTORY

Date	Updates
06 Apr 2022	Corresponding Author Helena C. Frazão re-submitted manuscript.
05 Apr 2022	Production Office Frontiers Production Office uploaded file(s). Typesetting initiated. Production Office Frontiers Production Office uploaded file(s). Article accepted for publication.

The forgotten Azores Current: a long-term perspective

1 **Helena C. Frazão^{1*}, Ralf D. Prien¹, Detlef E. Schulz-Bull¹, Dan Seidov², Joanna J. Waniak¹**

2 ¹Leibniz Institute for Baltic Sea Research Warnemünde, Department of Marine Chemistry, Seestraße
3 15, D-18119 Rostock, Germany

4 ² National Centers for Environmental Information, NOAA, Silver Spring, Maryland, USA

5 *** Correspondence:**

6 Helena C. Frazão

7 helena.frazao@io-warnemuende.de

8

9 **Keywords: Azores Current, Azores Front, Gulf Stream, North Atlantic Circulation, Atlantic**
10 **Multidecadal Oscillation, Ocean Heat Content, North Atlantic**

11 **Abstract**

12 The Atlantic Meridional Overturning Circulation (AMOC) and its surface limb, the Gulf Stream, are
13 in their weakest state since the last millennium. The consequences of this weakening in the Northeast
14 Atlantic are not yet known. We show that the slowdown of the Gulf Stream in the 1960s, 1970s, and
15 after 2000 may have caused a delayed weakening of the Azores Current. Concurrently, the Azores
16 Front associated with the Azores Current migrated northward since the 1970s due to gradual changes
17 in the Atlantic Multidecadal Oscillation and ocean heat content. We argue that the AMOC slowdown
18 is also detectable in the low-energy region of the Northeast Atlantic and that the dynamics of Azores
19 Current tightly connects to that of the dynamics of the Gulf Stream and AMOC on decadal and longer
20 time scales.

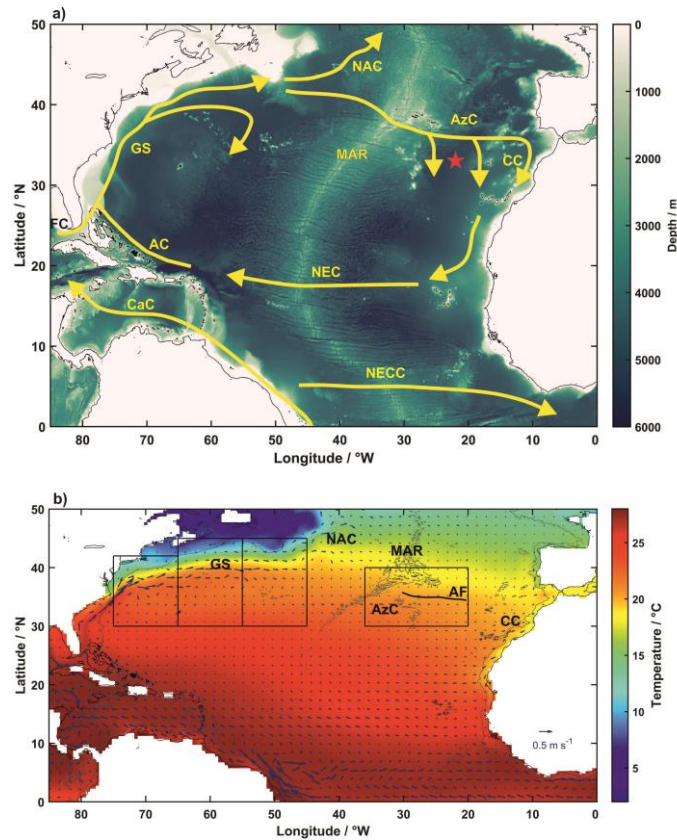
21

22 **1 Introduction**

23 Over the last century, multiple changes in large-scale circulation and water properties were reported in
24 the North Atlantic. Among them, the most intriguing and alarming are the recent slowdown of the
25 Atlantic Meridional Overturning Circulation (AMOC) (Bryden et al., 2005; Caesar et al., 2021) and an
26 increase in ocean heat content (OHC) in the upper 2000 m of the water column since the mid-20th
27 century (Levitus et al., 2012). The Intergovernmental Panel on Climate Change (IPCC) projects a very
28 likely weakening of the AMOC over the 21st century in comparison to its pre-industrial state (Collins

29 et al., 2013) under warmer climate conditions, at least partially caused by increased anthropogenic
 30 carbon dioxide concentration in the atmosphere (Caesar et al., 2018).

31 The AMOC strength depends, among other factors, on the Gulf Stream's strength and position (de
 32 Coëtlogon et al., 2006; Joyce & Zhang, 2010). Since the 1990s, Gulf Stream transports have strongly
 33 declined (Ezer, 2015; Dong et al., 2019). Ocean warming and the AMOC slowing are supposed to be
 34 linked to the recent Gulf Stream decline, which may cause sea-level rise along the U.S. East Coast
 35 (Ezer et al., 2003). However, quantifying the Gulf Stream slowdown from direct current observations
 36 is still difficult to achieve (Rossby et al., 2014; Andres et al., 2020). Additionally, Gulf Stream
 37 variability and pathway have been associated with the North Atlantic Oscillation (NAO) (e.g., Joyce
 38 et al., 2000; Zhang et al., 2020), warming in the southeast region of the Gulf Stream (Seidov et al.,
 39 2019) and the Atlantic Multidecadal Oscillation (AMO) phase (Nigam et al., 2018). Moreover, the
 40 reconstructions of the Gulf Stream transport and some modeling efforts revealed a weakening of the
 41 Gulf Stream during the 1960s and 1970s (Greatbatch et al., 1991; Ezer, 2015). However, possible
 42 consequences of an AMOC slowdown for the circulation and thermohaline structure in the mid-latitude
 43 of the Northeastern Atlantic have not yet been sufficiently studied. A new focus on this part of the
 44 North Atlantic Ocean is needed because of the dependence of the Azores Current, as the major pathway
 45 of eastward transport into the recirculation in the Canary Basin, on the AMOC dynamics (Fig. 1a). The
 46 Azores Current is weaker than the Gulf Stream, with kinetic energy values exceeding $200 \text{ cm}^2 \text{ s}^{-2}$ at the
 47 surface between the Mid-Atlantic Ridge (MAR) and 29°W (Barbosa Aguiar et al., 2011), falling in the
 48 lower energy band (Garçon et al., 2001). Therefore, being a much weaker current, the Azores Current
 49 might be more sensitive to AMOC variability than the more powerful Gulf Stream current system and
 50 thus not as easily discovered.



51
 52 **Fig. 1. North Atlantic circulation at the surface.** (a) Schematic representation of the North Atlantic
 53 Subtropical Gyre currents at the surface: Caribbean Current (CaC), Florida Current (FC), Antilles

54 Current (AC), Gulf Stream (GS), North Atlantic Current (NAC), Azores Current (AzC), Canary
 55 Current (CC), North Atlantic Equatorial Current (NEC), and North Atlantic Equatorial Counter Current
 56 (NECC). Mid-Atlantic Ridge (MAR) and the Kiel 276 mooring (red star) are also identified (adapted
 57 from Tomczak & Godfrey, 1994 and Danialt et al., 2016). **(b)** Mean temperature and mean velocity
 58 at 5 m depth in the North Atlantic basin from the SODA-POP v2.2.4 (Carton & Giese, 2008; Giese &
 59 Ray, 2011) averaged between 1871 and 2010. Black boxes show our study domains in the Gulf Stream
 60 (between 75°W and 45°W, divided into three 10° sub-zones) and in the Azores Current (between 36°W
 61 and 20°W). A thin grey line depicts the 2000 m-isobath. The time-averaged annual position of the
 62 Azores Front (AF) position is represented by a thick black line between 30°W and 20°W for the period
 63 1871-2010.

64

65 The Azores Current originates near the Grand Banks (40°N, 45°W), where the Gulf Stream splits into
 66 two main branches – the North Atlantic Current and the Azores Current (Fig. 1). It then flows south-
 67 eastward until it crosses the MAR at approximately 34°N, 37°W, and then turns eastward as a coherent
 68 jet towards the Strait of Gibraltar. East of the Mid-Atlantic Ridge, the Azores Current forms three main
 69 branches, the easternmost branch heads into the Canary Basin and feeds the Canary Current (Stramma,
 70 1984; New et al., 2001; Fig. 1), while the other two branches recirculate into the North Equatorial
 71 Current (Maillard & Käse, 1989; Fig. 1). Furthermore, the Azores Current recirculates in two westward
 72 countercurrents – (i) north (known as the Azores Countercurrent; Onken, 1993) and (ii) south of the
 73 Azores Current core (Peliz et al., 2007; Barbosa Aguiar et al., 2011). The Azores Current's core is
 74 located between 33°N and 36°N east of MAR (Fig. 1b, Fig. 2), transporting 10–12 Sv (1 Sv = 10⁶ m³ s⁻¹)
 75 eastward in the upper 1000 m (e.g., Käse & Siedler, 1982). The Azores Current surface velocity and
 76 transports decrease eastwards (Peliz et al., 2007). Consequently, the eddy field along the Azores
 77 Current jet varies zonally (Barbosa Aguiar et al., 2011; Silva-Fernandes & Peliz, 2020).

78 The Azores Current and its associated thermohaline Azores Front comprise the northeast boundary of
 79 the North Atlantic subtropical gyre. Importantly, the Azores Front-Current system separates two
 80 different biogeochemical regimes (Fründt & Waniek, 2012) – the cold and more productive temperate
 81 Eastern North Atlantic Water in the north and the warm and oligotrophic 18 °C-mode water south of
 82 the Azores Current. The changes in this system may be, therefore, critical for the long-term alteration
 83 of the biogeochemical regime in this region. Unfortunately, the existing analyses of the structure and
 84 variability of the Azores Front-Current system using hydrographic data are limited to the last 40 years
 85 and mainly based on quasi-synoptic surveys and drifters (e.g., Onken, 1993; Alves et al., 2002) or the
 86 Kiel 276 mooring data located at 33°N, 22°W (30 years of current and temperature measurements
 87 Siedler et al., 2005; Fründt et al., 2013; Frazão et al., 2021; Fig. 1 red star). To date, most studies
 88 described the Azores Current's transports (e.g., Alves et al., 2002; Peliz et al., 2007, among others), the
 89 spatial and vertical structure of the Azores Current (Stramma & Müller, 1989; Comas-Rodríguez et al.,
 90 2011), its meandering characteristic (e.g., Siedler et al., 1985; Alves et al., 2002), and the zonal
 91 variability of the Kinetic Energy (e.g., Richardson, 1983; Le Traon & De May, 1994; Volkov & Fu,
 92 2011; Silva-Fernandes & Peliz, 2020). The interest in the Azores Current has recently increased as
 93 satellite altimeter data became available, allowing far better monitoring of the Azores Current surface
 94 signature and mesoscale variability (Barbosa Aguiar et al., 2011; Silva-Fernandes & Peliz, 2020).
 95 There are some modeling studies of the Azores Current, but their main focus remained on the possible
 96 link between the Azores Current system and the Mediterranean Outflow Water (MOW) based on the
 97 dynamical concept of the β -plume mechanism (Jia, 2000; Kida et al., 2008; Volkov & Fu, 2010), rather
 98 than on a potential link between the Azores Current and AMOC. Yet, the driving mechanisms for the
 99 Azores Current are not fully understood. Spall (1990), using a numerical model, analyzed the
 100 circulation in the Canary basin and concluded that the model misrepresented the position of the Azores

101 Current and its transports. Nevertheless, he could not explain why the model did not adequately
 102 represent the Azores Current since the dominant forcing mechanisms at the time were not determined.
 103 However, little progress has been made since Spall (1990), and some hypotheses have been put forward
 104 without reaching a general consensus. The latest hypothesis formulates that a combined effect of the
 105 wind and the β -plume mechanism might drive Azores Current (Peliz et al., 2007; Lamas et al., 2010).
 106 However, the NAO, as the primary mode associated with changes in the wind field over the North
 107 Atlantic Ocean, has shown to have little influence on the Azores Current magnitude (Volkov & Fu,
 108 2011). Siedler et al. (2005) argued that the Azores Current's axis during the 1990s was further south
 109 than in the 1980s. Nonetheless, those links were calculated over periods shorter than 30 years, and the
 110 long-term influence of the NAO over the Azores Current is not yet known.

111 Understanding the multi-decadal variability of the Azores Current and its importance in a wider
 112 circulation context of the North Atlantic subtropical gyre is currently far from complete. Here we
 113 explore the link between the Gulf Stream and the Azores Current, the latter as an extension of the Gulf
 114 Stream in the eastern subtropical Atlantic (Richardson, 2001; Schmitz & McCartney, 1993).
 115 Furthermore, we consider a possible link between the reported slowdown of the Gulf Stream
 116 (Greatbatch et al., 1991; Ezer, 2015; Dong et al., 2019) and a decline in the Azores Current strength.

117

118 2 Materials and Methods

119 We used monthly temperature and velocity data from the Simple Ocean Data Assimilation reanalysis
 120 (SODA-POP v2.2.4) in the Gulf Stream (30°N–50°N, 75°W–45°W; Fig. 1b) and at the Azores Current
 121 regions (30°N–40°N, 36°W–20°W; Fig. 1b) between 1871–2010 (Carton & Giese, 2008; Giese & Ray,
 122 2011). The SODA assimilation is performed sequentially in a 10-day cycle, with corrections applied
 123 incrementally at every time step. Output variables are averaged every 5 days and mapped onto a
 124 uniform global 0.5°×0.5° horizontal grid using the horizontal grid spherical coordinate remapping and
 125 interpolation package of Jones (1999). The ocean model is based on Parallel Ocean Programming
 126 (POP; Smith et al. (1992) with an average horizontal resolution of 0.25°×0.4° and 40 vertical levels.
 127 The surface boundary conditions are provided by the Twentieth Century Atmospheric Reanalysis
 128 product (20CRv2; Compo et al., 2011). From 20CRv2, the surface wind stress is used for the surface
 129 momentum flux; additionally, the heat and freshwater fluxes are calculated using the solar radiation,
 130 2 m air temperature, cloud cover, 10 m wind speed, specific humidity, and precipitation (Giese & Ray,
 131 2011). SODA-POP assimilates all available hydrographic profile data from the World Ocean Database
 132 2009 (Boyer et al., 2009), including CTD, buoys, moorings, and expendable bathythermograph (XBT)
 133 and mechanical bathythermograph (MBT). The temperature obtained from XBT and MBT was
 134 corrected following Levitus et al. (2009). Surface temperature data is provided by the International
 135 Comprehensive Ocean-Atmosphere Data Set (ICOADS 2.5); however, other datasets are also used (for
 136 more details about the additional datasets used, see Giese & Ray, 2011). The monthly property fields
 137 (temperature, salinity, velocity) used in this study have a spatial resolution of 0.5°×0.5°, with 40 depth
 138 levels.

139 We further divided the Gulf Stream region into three 10° longitude zones, 75°W–65°W, 65°W–55°W,
 140 and 55°W–45°W, according to the Gulf Stream behavior and resilient position of the jet-like flow
 141 (Dong et al., 2019; Seidov et al., 2019) (see the areas shown by three boxes in the Gulf Stream region
 142 Fig. 1b; note that the third of the three areas is already in the extension zone; Seidov et al., 2019).

143 The circulation pattern west of the Madeira Islands shows recirculation both north and south of the
 144 Azores Current (Barbosa Aguiar et al., 2011). Thus, we constrained the study area around the Azores
 145 Current between 36°W and 20°W and limited the analysis to its core (between 32°N and 36°N, Fig.

146 2). Additionally, the Azores Current's dynamics and eddy energy at the surface show a zonal variation
 147 along its pathway towards the Strait of Gibraltar (Barbosa Aguiar, 2011; Silva-Fernandes & Peliz,
 148 2020). East of the MAR, those authors further divided the Azores Current into three main regions
 149 according to the surface variability of eddy kinetic energy: 36°W–28°W, 28°W–24°W, and
 150 24°W–20°W. In this study, we followed the same partition suggested by those authors and accessed
 151 the dynamic of the Azores Current in the three sub-regions.

152 Monthly zonal and meridional velocity fields were used to calculate the absolute velocity for both
 153 Azores Current and Gulf Stream. The Azores Current and Gulf Stream cores were identified by the
 154 latitudes at each sub-region with the maximum averaged velocity in the upper 1000 m for the entire
 155 period (Fig. 3a, 4a), once the higher transports for both currents occur in the upper 1000 m (Käse &
 156 Siedler, 1982; Pelegrí & Csanady, 1991).

157 To map the northern boundary of the Azores Current, we define the Azores Front latitude using the
 158 established criterion of 15 °C-isotherm coordinates at 200 m depth between 30°W and 20°W (Gould,
 159 1985; Fig. 6). West of 30°W, the Azores Front position shows higher variability, with a standard
 160 deviation of up to 2° in latitude. Therefore, we calculated the Azores Front position between 30°W and
 161 20°W, where the Azores Front variability is less than 1.5°.

162 The integrated Ocean Heat Content (OHC) time-series in the upper 400 m was calculated following
 163 Levitus et al. (2012). The temperature anomaly fields were obtained by subtracting the climatological
 164 temperature (the temperature averaged over the entire period from 1871 to 2010) from the SODA-POP
 165 monthly temperature data. Häkkinen et al. (2016) showed a good agreement between the OHC
 166 calculated using the SODA-POP dataset and the OHC time-series determined by Levitus et al. (2012).

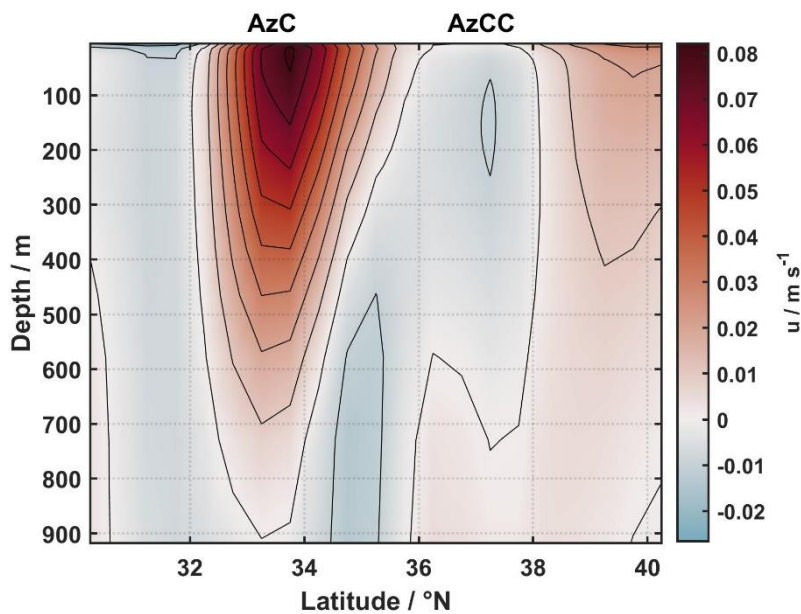
167 To better understand the long-term variability of the Azores Current and Front, it is instrumental to
 168 find their links, if any, to the major ocean-atmosphere interaction patterns in the North Atlantic Ocean
 169 – the North Atlantic Oscillation and the Atlantic Multidecadal Oscillation. The NAO is the dominant
 170 pattern in the North Atlantic Ocean, associated with altering the wind pattern, large-scale circulation,
 171 and water properties (Visbeck et al., 2003), affecting the upper water column even at the Mediterranean
 172 Water depths (e.g., Frazão & Waniek, 2021). The AMO, on the other hand, is the major pattern of the
 173 sea surface temperature variability and thus provides a fundamental description of the climate pattern
 174 in the North Atlantic Ocean. Therefore, we investigated the possible connection between the Azores
 175 Front position and the most dominant climate patterns in the North Atlantic, the winter NAO and the
 176 AMO. The latter has an oscillation period of about 60–80 years (Schlesinger & Ramankutty, 1994),
 177 meaning our time-series are sufficiently long to explore a possible link, if any, between AMO and the
 178 Azores Front. We used the unsmoothed detrended Atlantic Multidecadal Oscillation index (AMO)
 179 (available at <https://psl.noaa.gov/data/timeseries/AMO/>) and the North Atlantic Oscillation index
 180 (retrieved from [https://climatedataguide.ucar.edu/climate-data/hurrell-north-atlantic-oscillation-nao-](https://climatedataguide.ucar.edu/climate-data/hurrell-north-atlantic-oscillation-nao-index-station-based)
 181 [index-station-based](https://climatedataguide.ucar.edu/climate-data/hurrell-north-atlantic-oscillation-nao-index-station-based)). The correlation coefficients between AMO, OHC, and the Azores Front position
 182 were calculated using the monthly time-series smoothed with a 60-months running mean.
 183

184 2.1 Validation of the Azores Current system in the SODA-POP dataset

185 First, we evaluated how well the SODA-POP dataset represents the Azores Current. The surface
 186 circulation of the North Atlantic Subtropical Gyre averaged between 1871 and 2010 is depicted in Fig.
 187 1b. As this figure attests, the SODA-POP reproduces the surface circulation in the subtropical North
 188 Atlantic quite well, with all major currents of the subtropical gyre resolved. It is known that models
 189 often misrepresent the Azores Current (e.g., New et al., 2001). Therefore, at this first step, we estimated

190 the mean circulation in the Azores Current region (see Fig. 1b) and its transports, this time from the
 191 SODA reanalysis.

192 The average zonal velocity shows a well-defined eastward jet located between 32° and 35°N in the
 193 upper 1000 m comprising the Azores Current, bordered by two countercurrents south and north of the
 194 Azores Current jet (Fig. 2). North of the Azores Current, the Azores Countercurrent (AzCC in Fig. 2)
 195 appear between 36° and 38°N, a sub-surface intensified jet (Onken, 1993; Comas-Rodríguez et al.,
 196 2011). Also, the SODA-POP velocity components were previously used to fill the gaps in the Kiel 276
 197 mooring dataset (Fründt et al., 2013). The authors compared the SODA-POP annual zonal and
 198 meridional velocities with the Kiel 276 velocity measurements at 240 m and 500 m, and they concluded
 199 that the difference in variance between the two datasets is less than the natural variances estimated for
 200 this region (for more details, see Fründt et al., 2013). The estimated zonal transports within the Azores
 201 Current jet varied zonally, with higher transports close to the MAR (mean of 14 ± 6 Sv west of 35°W),
 202 decreasing towards the Strait of Gibraltar (mean of 8 ± 4 Sv at 20°W). Our estimates agree with
 203 reported values estimated using observational data – e.g., Gould (1985) estimated a total volume
 204 transport of 10 to 12 Sv, Alves et al. (2002) reported transports of 11 to 18 Sv, and Comas-Rodríguez
 205 et al. (2011) estimated a mean transport of 13.9 Sv at 24.5°W; and also with models (Peliz et al. (2007)
 206 calculated an Azores Current transport of about 16 Sv west of 30°W and 8 Sv east of 20°W).



207

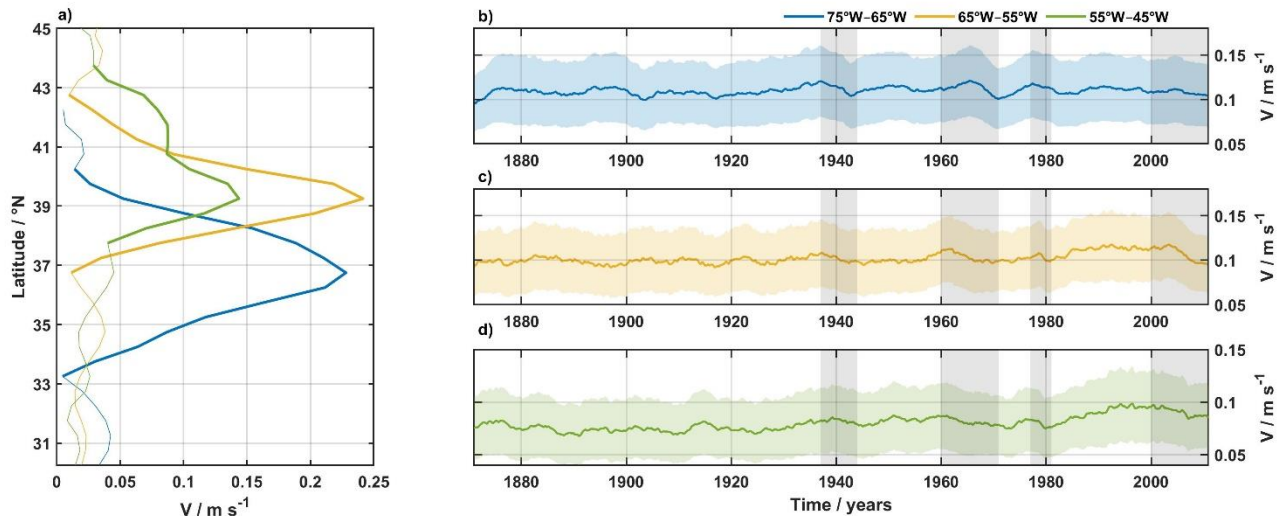
208 **Fig. 2. The Azores Current System.** Average of the zonal velocity component at the Azores Current
 209 region between 36°W and 20°W (see Fig. 1b) for the period 1871 and 2010. Positive values indicate
 210 eastward flow. The Azores Current (AzC) and Azores Countercurrent (AzCC; Onken, 1993) cores are
 211 identified.

212

213 Fründt & Waniek (2012) compared the Azores Front position at 22°W calculated using the SODA-
 214 POP temperature fields with the Azores Front position retrieved from the observations in fourteen
 215 research cruises in the Azores region. A good agreement is found between the observed Azores Front
 216 position and the one calculated from SODA-POP, with the differences between both positions not
 217 exceeding 0.5°, corresponding to the horizontal resolution of the SODA-POP dataset (for more details,
 218 the reader is referred to Fründt & Waniek (2012) and their fig. 2).

219 3 Azores Current as a part of the extended Gulf Stream region

220 The Gulf Stream's velocity time-series averaged along the core latitudes for the upper 1000 m are
 221 shown in Fig. 3b-d. The Gulf Stream absolute velocity for all regions demonstrates larger variability
 222 on inter-annual and decadal time scales, with the selected areas behaving quite differently (Fig. 3b-d).
 223 Stronger variability in the Gulf Stream region occurs mainly on shorter time and spatial scales because
 224 the mesoscale activity in the western Atlantic sector is stronger than in the eastern Atlantic sector (Le
 225 Traon, 1991; Garçon et al., 2001). Also, the Gulf Stream jet is marked by strong mesoscale activity
 226 and the meanders intensifying towards the Gulf Stream extension region.



227

228 **Fig. 3. The Gulf Stream.** (a) Meridional profiles of the absolute velocity averaged in the upper 1000 m
 229 for each sub-region along the Gulf Stream: western (75°W–65°W, blue line), central (65°W–55°W,
 230 yellow line), and eastern/extension (55°W–45°W, green line) zones. The Gulf Stream cores are marked
 231 with a thicker line for each region. (b) Averaged monthly time-series of absolute velocity at the western
 232 Gulf Stream, (c) central Gulf Stream region, and (d) extension Gulf Stream region inside the core in
 233 the upper 1000 m between 1871 and 2010. Colored shadowed areas in (b), (c), and (d) represent the
 234 standard deviation. Shadow grey areas mark the periods of velocity decrease of the Gulf Stream.
 235 Absolute velocity was calculated from the monthly zonal and meridional velocity fields from SODA-
 236 POP v2.2.4 (Carton & Giese, 2008; Giese & Ray, 2011). The time-series are smoothed with a 60-
 237 months running mean.

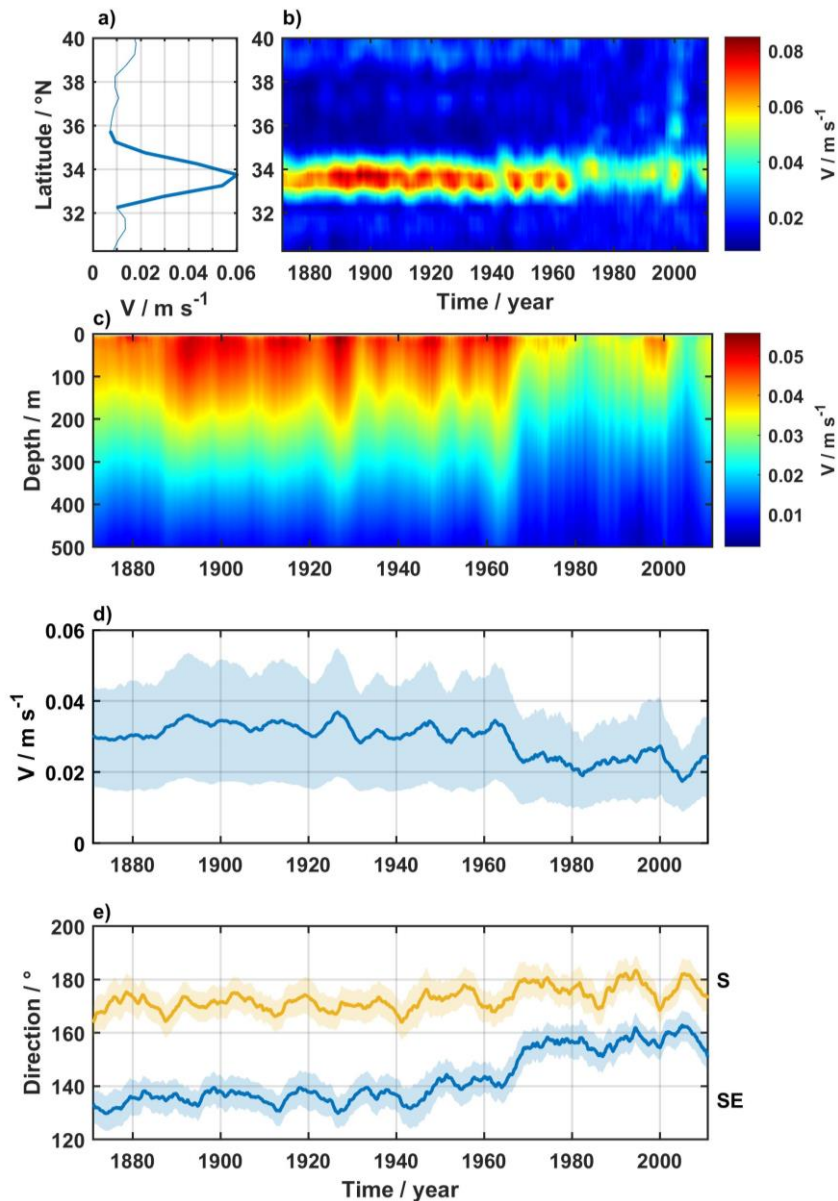
238

239 Periods of Gulf Stream intensification (1920–1930, the 1950s, 1980–2000) and weakening (end of the
 240 1930s and beginning of the 1940s, 1960–1970, and after 2000) are similar in all three regions, although
 241 the intensity of strengthening and weakening varied (Fig. 3b-d). The most pronounced Gulf Stream
 242 weakening episodes occurred between the 1960s and 1970s (accounting for 10% across the Gulf
 243 Stream pathway) and after 2000 in all sub-regions (Fig. 3b-d). During the 1980s and 1990s, the velocity
 244 increased in both the Gulf Stream's central and extension zone and simultaneously decreased in the
 245 western zone. Nevertheless, overall Gulf Stream weakening was observed in all sub-regions after the
 246 1990s, agreeing with the most recent literature (e.g., Ezer, 2015; Dong et al., 2019).

247

248 4 Weakening of the Azores Current

249 The mean flow of the Azores Current showed a well-defined jet before the mid-1960s, with a maximum
 250 velocity at 34°N (Fig. 2, 4b). At the end of the 1960s, however, the Azores Current experienced a
 251 drastic change, with a decrease in the jet's velocity, and its axis moved roughly 0.5° northward (Fig.
 252 4b). In the current's core, the Azores Current velocity exceeds 0.10 m s⁻¹ at the surface, with a sub-
 253 surface maximum of up to 0.11 m s⁻¹ at 15 m, and the vertically averaged velocity reaches 0.04 m s⁻¹
 254 (Fig. 4c, d).



255
 256 **Fig. 4. The Azores Current.** (a) Average absolute velocity in the upper 1000 m along the Azores
 257 Current region (30°N–40°N, 36°W–20°W, Fig. 1). A thicker line represents the Azores Current core.
 258 (b) Average absolute velocity in the upper 1000 m in the region between 36°W and 20°W for the
 259 period 1871–2010. Higher velocities between 32° and 36°N indicate the Azores Current jet. (c)
 260 Vertical variation of the mean absolute velocity averaged between the core latitudes over the entire
 261 period. (d) Time-series of the monthly absolute velocity averaged inside the Azores Current core (a)

262 in the upper 1000 m. Shadowed area is the calculated standard deviation of the absolute velocity in the
 263 Azores Current region. (e) Time-series of the Azores Current's average direction in the upper 300 m
 264 (solid blue line) and at the layer 300–1000 m (solid yellow line) between the latitudes of the Azores
 265 Current core (a). Blue and Yellow shadowed areas are the calculated standard deviation of the mean
 266 direction flow in the upper 300 m and between 300–1000 m, respectively. The absolute velocity was
 267 calculated from the monthly zonal and meridional velocity fields from SODA-POP v2.2.4 (Carton &
 268 Giese, 2008; Giese & Ray, 2011). All time-series are smoothed using a 60-months running mean.

269

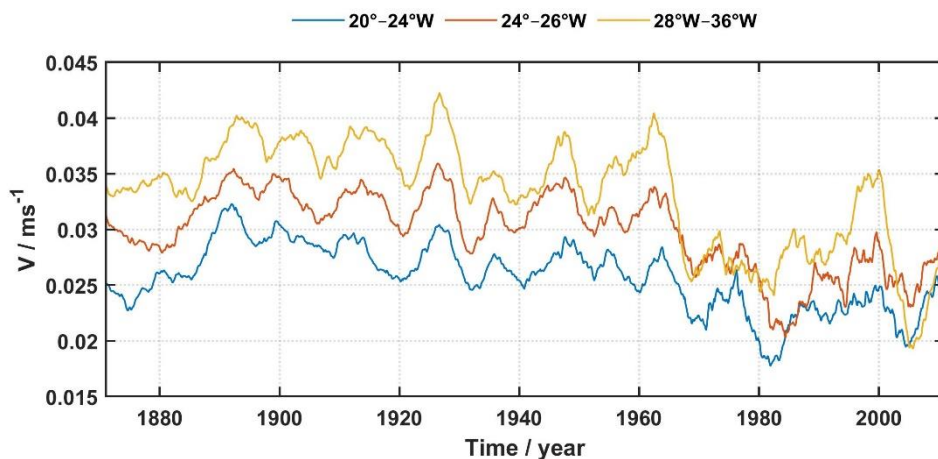
270 Over the last century, the Azores Current was in its stronger state between 1890 and 1960. Then, in the
 271 late 1960s, the velocity began decreasing in the upper 500 m, and by 1969 the core with the higher
 272 velocities raised from 300 m to 200 m, coinciding with the northward migration of the Azores Current
 273 jet (Fig. 4c). The time-averaged direction of the flow in the Azores Current's core is predominantly
 274 southeast (142°) in the upper 300 m and directed to the south below (172°). Concurrently with the
 275 velocity decrease, the flow's direction in the upper 300 m turned from 136° to 154° after the 1960s
 276 (Fig. 4e). A change in the flow's direction in the upper thermocline (at 240 m and 500 m) was also
 277 observed by Fründt et al. (2013) at the Kiel 276 site, where the authors reported a divergent flow
 278 between the two depth levels after 2000. They suggested that a northward displacement of the North
 279 Atlantic Subtropical Gyre could result in an altered current regime. However, here we found that the
 280 altered current regime started before during the 1960s, and it affected the upper 600 m of the Azores
 281 Current's core.

282 The vertically-averaged velocity inside the Azores Current core in the upper 1000 m varies on
 283 interannual and inter-decadal scales (Fig. 4d). Variations on the annual scale were insignificant and
 284 therefore are not shown. The Azores Current velocity time-series is marked by two periods of
 285 weakening: the most pronounced decrease started in 1962 and continued until 1983, and a shorter event
 286 occurred between 2000 and 2005. Although the current speed increased slightly in the 1980s and 1990s,
 287 and afterward, at the end of the time-series, the Azores Current never returned to its pre-1960s state
 288 (Fig. 4b-d). The acceleration of the Azores Current after the 1980s, and also in the second half of the
 289 2000s, is confirmed by the current measurements taken close to the Azores Current jet, at the Kiel 276
 290 mooring (33°N , 22°W) between 1980 and 2009, where almost daily continuous observations showed
 291 an increase in the current speed in the upper 1000 m from the 1980s to 2000s (Siedler et al., 2005;
 292 Fründt et al., 2013; Frazão et al., 2021). At this site, according to the authors, the velocity noticeably
 293 increased on a decadal scale, especially in the transition from the 1980s to the 1990s. From the end of
 294 the 1990s until 2004, a decrease in the velocity in the upper thermocline (upper 500 m) was observed,
 295 followed by a significant increase until 2009 (Fründt et al., 2013). Mean current speeds averaged over
 296 1000 m prior to and after 1960 are 0.03 m s^{-1} and 0.02 m s^{-1} (Fig. 4d), respectively, resulting in a
 297 substantial Azores Current reduction of 24% after the 1960s.

298 Interannual variability of the Azores Current has been shown to be only mildly impacted by the wind
 299 (Volkov & Fu, 2010). Calculation of the correlation between the winter NAO and the intensity of the
 300 Azores Current did not result in a significant correlation that could explain the interannual variability
 301 of the Azores Current. However, for timescales over 20 years or longer, the correlation between the
 302 winter NAO and the annual Azores Current velocity is significant and positive and has a maximum for
 303 the NAO leading the Azores Current velocity by 41 years ($\rho = 0.45$, $p < 0.05$; not shown). Similarly,

304 Ezer & Dangendorf (2022) calculated positive correlation coefficients on multi-decadal timescales and
 305 long-term trends between the sea level and the NAO in the Azores Current region.

306 The three regions of Azores Current are highly correlated ($\rho > 0.8$, $p < 0.05$), and the average velocity
 307 at the core increase towards the MAR (Fig. 5), a result consistent with other observations and models
 308 (e.g., Peliz et al., 2007). The correlation between the sub-regions along the Azores Current time-series
 309 has a maximum with a lag of three months between them, with the easternmost region leading the
 310 western. The increase of the Azores Current's velocity at the beginning of the time-series starts earlier
 311 in the easternmost region (1875), and it is followed by the central and then western regions until 1893.
 312 In the following period up to 1962, the three areas behave similarly. The drastic weakening along the
 313 Azores Current pathway occurred almost synchronously in the western and central zones (starting in
 314 1962), while the changes in the easternmost area lagged the other two by about one year. In the 1960s,
 315 the strong decline of the average velocity at the core occurred in the western region close to the MAR
 316 (accounting for up 19%), while in the central and eastern zones, the decrease of the average velocity at
 317 the core accounted for 15% (Fig. 5).



318
 319 **Fig. 5. The Azores Current sub-regions.** Monthly absolute velocity averaged inside the core of the
 320 Azores Current (between 32° and 36°N) in the upper 1000 m between 1871 and 2010. The Azores
 321 Current is divided into three sub-regions according to the eddy kinetic energy dynamic at the surface
 322 (Barbosa Aguiar et al., 2011; Silva-Fernandez & Peliz, 2020): western (36°W–28°W, yellow line),
 323 central (28°W–24°W, orange line), and eastern (24°W–20°W, blue line). All time-series are smoothed
 324 with a 60-months running mean.

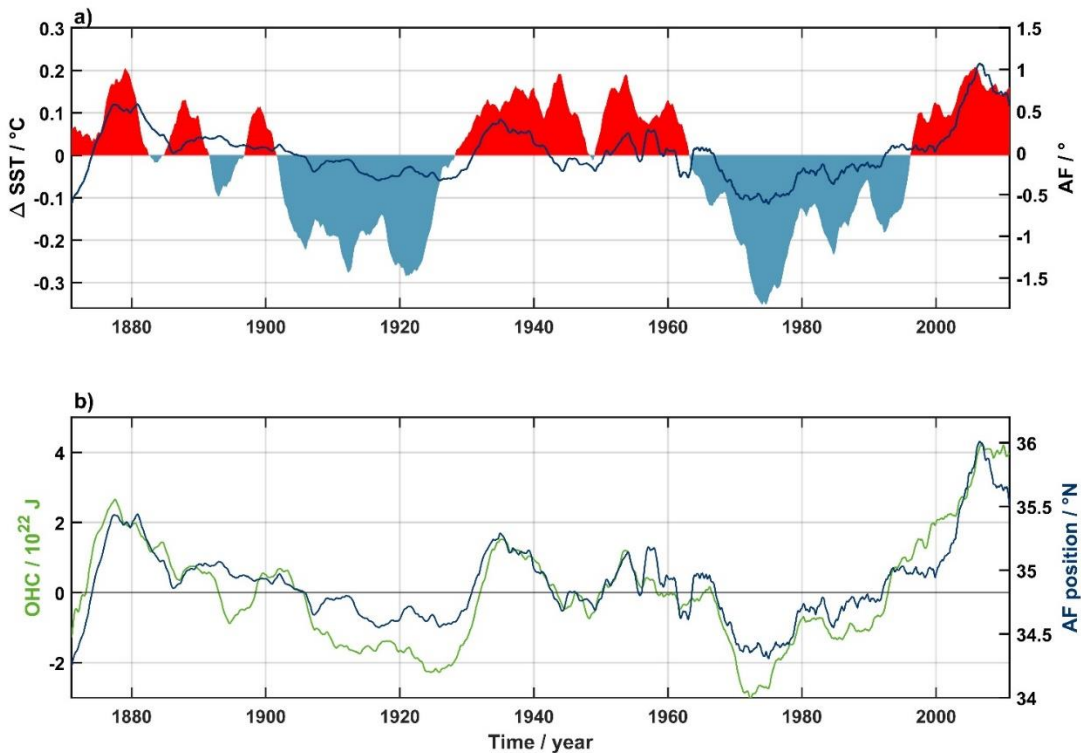
325
 326 Comparing the Gulf Stream and Azores Current velocity series reveals a striking similarity between
 327 the periods of weakening (during the 1960s and after 2000) and strengthening (during the 1980s and
 328 1990s, Fig. 3b-d, 4d). The correlations between the Gulf Stream (Fig. 3b-d) and the Azores Current
 329 absolute velocity (Fig. 4d) show a striking negative value (significant at $p < 0.05$). The highest negative
 330 correlations are found between the Azores Current and the central and eastern Gulf Stream time-series
 331 ($\rho > -0.5$), while between the western Gulf Stream and Azores Current, the correlation is weak yet still
 332 negative ($\rho = -0.1$). The latter weaker correlation is possibly due to the different driving mechanisms
 333 that control both currents – while the western flank of the Gulf Stream (west of 65°W) is constrained

334 by the shelf (shallower than 200 m), the central and eastern flanks are not topography-constrained and
 335 behave as a free jet (Dong et al., 2019), similarly to the Azores Current.

336 Interesting to note is the change of the correlation signal throughout the last century. Before the drastic
 337 weakening of the Azores Current in the 1960s, the correlation coefficient between the Azores Current
 338 and all regions of the Gulf Stream is significant and negative. The opposite situation is observed after
 339 the 1960s, with the correlation coefficients between both currents reversing to a positive value.
 340 However, the correlation between the two currents had almost ceased after 2000 (it is not yet clear to
 341 us what caused this sudden drop in correlation).

342 5 Azores Front

343 The Azores Front position shows large inter-annual and decadal variability; however, it does not have
 344 a significant seasonality (not shown in Fig. 6). The Azores Front position shows slight variation around
 345 the mean before the 2000s ($34.9^{\circ}\text{N} \pm 0.5^{\circ}$), with periods of southward (1880–1925, 1935–1948, 1957–
 346 1974, 2006–2010) and northward (1871–1880, 1926–1934, 1975–2005) migration (Fig. 6). Notably,
 347 the progressive northward Azores Front migration starting in the mid-1970s and continuing until 2005,
 348 at an estimated rate of $\approx 12 \text{ m day}^{-1}$, is twice as high as estimated by Fründt & Waniek (2012) at 22°W
 349 for the period 1966–2007.



350

351 **Fig. 6. The Azores Front.** (a) Monthly detrended Azores Front position (solid dark blue line)
 352 superimposed on the Atlantic Multidecadal Oscillation index (shaded areas: positive phase in red;
 353 negative phase in blue). (b) Monthly Azores Front position (solid dark blue line) and integrated OHC
 354 in the upper 400 m (solid green line; details on the OHC calculation are given in Data & Methods).
 355 The Azores Front position is an average of all the Azores Front positions between 30°W and 20°W .

356 The monthly detrended time-series was calculated by removing the linear trend for the entire period.
 357 All time-series are smoothed with a 60-months running mean.

358

359 North and south of the Azores Current, the meridional Ekman transport forms a convergence zone
 360 within which the Azores Front lies (Fründt & Waniek, 2012). Changes in the wind direction impact
 361 the position of the convergence zone, which ultimately alters the Azores Front position. The correlation
 362 between the winter NAO index and the annual mean Azores Front position was not significant at any
 363 confidence level (and therefore is not shown). This result is similar to the findings in Seidov et al.
 364 (2019), where they did not find a significant correlation between the Gulf Stream thermal front and
 365 NAO. Although some authors already showed the NAO impact on the Azores Front position, with the
 366 Azores Front lagging NAO from months to years (Fründt & Waniek, 2012; Volkov & Fu, 2011), NAO
 367 does not seem to be the main driver of the Azores Front variability for the period 1871–2010, as it was
 368 not the main driver of the Gulf Stream position either on the decadal and longer time scale (Seidov et
 369 al., 2017). There may be several reasons why we did not find a significant correlation between the
 370 NAO and the Azores Front position. First, the different definitions used to determine the Azores Front
 371 position, either using eddy kinetic energy at the surface (Volkov & Fu, 2011), the temperature at 250 m
 372 (Fründt & Waniek, 2012) or 200 m in this study. Second, NAO effects seen in Azores Front are
 373 expected to be lagging at 200 m and stronger at the surface due to the adjustment of the water column
 374 to atmospheric forcing (Visbeck et al., 2003). Finally, even though Fründt & Waniek (2012) and
 375 Volkov & Fu (2011) determined significant correlations for shorter periods, Fründt & Waniek (2012)
 376 noticed that the correlation between NAO and Azores Front at 22°W changed after 2003. Moreover,
 377 Williams et al. (2000) found that the correlation between NAO and nutrient supply in the eastern
 378 Atlantic is not significant, in contrast to the western and central Atlantic basin between 1968 and 1993.

379 The Azores Front position, together with the AMO and the OHC in the upper 400 m, are presented in
 380 Fig. 6. The Azores Front position shows similar behavior as the AMO (Fig. 6a), but the similarity
 381 between the Azores Front position and OHC is even more striking (Fig. 6b). Periods of increase
 382 (decrease) in OHC are consistent with a northward (southward) propagation of the Azores Front (Fig.
 383 6b). The correlation coefficient between Azores Front and AMO is 0.69, and between Azores Front
 384 and OHC is 0.92, both at 0-lag and significant at the 95% confidence level. The correlation coefficient
 385 between the AMO and the Azores Front position is maximum at 0.7, with the AMO leading the Azores
 386 Front position by 13 months. The Azores Front definition used partly implies the high correlation
 387 between Azores Front and AMO and OHC as this delimits the extension of warmer subtropical waters
 388 and mirrors the thermal conditions of the upper water column in this part of the Northeast Atlantic.

389 **6 Discussion and Implications**

390 The use of assimilation products, like the one in this study, helps to analyze the basin-scale ocean
 391 circulation in general, and in our case – with a special focus on the northern border of the North Atlantic
 392 subtropical gyre. Our analysis so far points to the close though time-lagged connection between the
 393 Gulf Stream climatology and dynamics and the Azores Current behavior – an extension of the Gulf
 394 Stream in the Northeast Atlantic. We found that the Azores Current responds to the changes in all three
 395 sections of the Gulf Stream, with the signal of weakening or strengthening of the Gulf Stream traveling
 396 toward the Azores Current within two years, most likely driven by the observed decline in the central
 397 and extension parts of the Gulf Stream current. Indeed, the Azores Current weakening in the 1960s and
 398 1970s (Fig. 4d) was observed two years after the weakening of the Gulf Stream started (Fig. 3).

399 While no sufficient data is available for the North Atlantic before the 1980s, there were some attempts
 400 to reconstruct the circulation using hydrographic data. For example, Greatbatch et al. (1991), using a
 401 diagnostic model, showed that the Gulf Stream transport was reduced by 30% in the early 1970s
 402 compared to the mid-1950s, and Ezer & Dangendorf (2020) employed a global reconstruction of the
 403 sea level and discovered similar weakening in the 1960s and 1970s. Levitus (1989) hypothesized that
 404 this weakening might be due to density changes in the subsurface of the North Atlantic. Our analysis
 405 follows this line of argument. The most recent weakening in the Gulf Stream region and Azores Current
 406 (after 2000) also allegedly links to a new slowdown of the AMOC (Bryden et al., 2005; Caesar et al.,
 407 2021). Ezer (2015) and Ezer & Dangendorf (2020) suggested that AMOC weakening might be linked
 408 to the Gulf Stream slowdown both in the 1960s/1970s and late 2000s. Possibly, slowing down of the
 409 AMOC, which may relate, at least partially, to reduced Gulf Stream transports east of the U.S. coast,
 410 leads to a delayed weakening of the Azores Current in the eastern North Atlantic. However, different
 411 views of the variability in the Gulf Stream transport arose in the last decade, where some authors
 412 advocate that the Gulf Stream transport is not declining (e.g., Rossby et al., 2014; 2019) and neither is
 413 the AMOC (e.g., Willis, 2010; Moat et al., 2020). For example, Rossby et al. (2014; 2019) did not
 414 detect a long-term change in the Gulf Stream along the Oleander line. Nonetheless, as pointed out by
 415 Ezer (2015), the part of the Gulf Stream in the Oleander line (near 70.3°W) does not correlate with the
 416 AMOC nor the Florida Current due to the eddies and meandering of the Gulf Stream. The AMOC
 417 transports calculated at 26°N with the SODA-POP dataset are close to the observational AMOC
 418 transports, with an increasing trend in the AMOC transports since the 1960s (Tett et al., 2014).
 419 Additionally, AMOC transports estimated at mid- and higher latitudes show larger interannual
 420 variability, with alternating periods of stronger and weaker AMOC (e.g., Bryden et al., 2005; Willis,
 421 2010; Moat et al., 2020). As noted by Moat et al. (2020), it is still difficult to assess with certainty
 422 whether the AMOC is recovering or not, partly due to the short time-series of continuous
 423 measurements.

424 The regional differences in the Gulf Stream velocity may possibly be attributed to the behavior of the
 425 Gulf Stream jet at its different parts. For example, southwest of Cape Hatteras, the jet is strongly
 426 controlled by bottom topography, while east of Cape Hatteras, where the Gulf Stream separates from
 427 the continental shelf and slope, the flow becomes a free baroclinic jet not constrained by topography
 428 (Dong et al., 2019). Different trends were also found between the eastern and western parts of the Gulf
 429 Stream between 1993 and 2016 (e.g., Andres et al., 2020; Zhang et al., 2020), reinforcing the zonal
 430 behavior between the extension and the western zone of the Gulf Stream. Additionally, the presence
 431 of cold and warm recirculation gyres north and south of the Gulf Stream, respectively, has been shown
 432 to influence the position of the Gulf Stream jet (e.g., Marchese, 1999).

433 The baroclinic instability along the Azores Current jet leads to the formation of large mesoscale
 434 anticyclonic structures north and cyclonic eddies south of the jet, with diameters on the order of 200 km
 435 and timespans of 40 to 100 days (Müller & Siedler, 1992; Alves et al., 2002). The three-month lag
 436 between the Azores Current sub-regions is of the same order as the relevant timescales associated with
 437 the meandering of the Azores Front-Current system (Siedler et al., 1985; Müller & Siedler, 1992). In
 438 fact, Silva-Fernandes & Peliz (2020) determined the number of eddies in the last 25 years in the Azores
 439 Current region. They showed that most of the eddies expected to be associated with the Azores Current
 440 have a lifetime of 16 weeks, 54% of these were cyclonic, i.e., propagating westward. Those cyclonic
 441 eddies were shown to propagate westward with a combination of Rossby waves and advective flow
 442 characteristics (Pingree & Sinha, 2001).

443 Our interpretation of the results in Fig. 5 is inherently incomplete as we cannot offer a satisfying
 444 conclusion on how the variability evident in the time-series can be explained fully and through which

445 processes it may be forced and maintained. Indeed, the speed maxima in different segments of the
446 Azores Current are not synchronized universally throughout the entire time of the analyzed record.
447 Sometimes they are synchronized, sometimes obviously and even strikingly desynchronized, and being
448 anything between these two extremes during other time intervals. Nevertheless, we provide this result
449 to encourage a discussion that may shed a better light than what we can currently offer in our analysis.

450 The 1960s seem to be a turning point for changes in the North Atlantic circulation and water properties
451 from the 1950s to the 1970s, as reported in a number of studies (e.g., Levitus, 1989a, b; Greatbatch et
452 al., 1991; Grey et al., 2000; Reverdin, 2010; Yeager & Danabasoglu, 2014). During this period, we
453 found a northward displacement of the Azores Current's jet by 0.5° starting in the late 1960s (Fig. 4b),
454 a change in the signal of the correlation coefficient between the Azores Current and the Gulf Stream
455 in the 1960s, and gradual poleward migration of the Azores Front starting in the 1970s. We offer a
456 working hypothesis that the existence of two transient periods, before and after the 1960s, was driven
457 by some mechanisms that were variable in time. That is, before the 1960s, the wind had a preponderant
458 role in the North Atlantic circulation, namely over the Gulf Stream, North Atlantic Current, and Azores
459 Current, with the signal between the North Atlantic Current and the Gulf Stream better correlated than
460 with the Azores Current. However, after roughly the 1960s, the ongoing surface warming began (Fig.
461 6), and the Gulf Stream became stronger influenced by increasing density differences between the
462 warm and cold recirculation gyres, south and north of the Gulf Stream jet, respectively. By that time,
463 the correlation between the Gulf Stream path (and possibly the Gulf Stream strength) with the zero line
464 of the wind stress curl reduced and, in contrast, increased with the AMO (Nigam et al., 2018; Seidov
465 et al., 2019). After the onset of surface warming, the OHC began to rise, controlled by a combination
466 of the surface warming and the circulation pattern, and started to play a more critical role, leading to a
467 stronger correlation between the AMO and OHC and the Azores Current and the Gulf Stream. The
468 largest increase of OHC was observed in the North Atlantic in the upper 2000 m (Levitus et al., 2012)
469 and is concentrated in the warm recirculation gyre of the Gulf Stream (Seidov et al., 2017). After 2000,
470 the OHC pool south of the Gulf Stream increased very quickly, and therefore, the Gulf Stream path
471 deviated northward quite strongly. At that time, the largest weakening of AMOC was reported (e.g.,
472 Ezer 2015; Caesar et al., 2021). As a result, the subpolar gyre strengthened (Zhang, 2008),
473 accompanied by a coincident weakening of the Gulf Stream and Azores Current. It seems that the
474 dipole observed by Zhang (2008), where a stronger (weaker) AMOC induces a weaker (stronger)
475 subpolar gyre, can also be viewed as a seesaw in the Gulf Stream changes signal between the North
476 Atlantic Current and the Azores Current, depending on the Gulf Stream behavior in the bifurcation
477 zone between the two major current systems in the North Atlantic Ocean. However, this hypothesis is
478 very difficult to verify, so we provide our explanation for a discussion rather than a definitive
479 conclusion. Perhaps the best way to prove or disprove the relative role of surface warming and its
480 consequences and the wind stress over the North Atlantic would be through numerical hindcast
481 experiments that could compare the Gulf Stream and the Azores Current connection with and without
482 the 20th-century surface warming. Nevertheless, this hypothesis is far beyond the scope of our research
483 and requires further investigation.

484 Global and regional models often misrepresent the Azores Current, e.g., New et al. (2001), because of
485 the difficulties of adequately resolving the Mediterranean Outflow, especially close to the Gulf of
486 Cadiz (Jia, 2000). The difficulty in properly represent the Azores Current might be one of the reasons
487 why its role in decadal and longer-term variability of the North Atlantic large-scale circulation was
488 underestimated and, therefore, did not attract much attention. Recently, Jia (2000), Özgökmen et al.
489 (2001), and Kia et al. (2008) proposed that the effect of water mass exchange in the Gulf of Cadiz
490 between the Atlantic Central Water and the Mediterranean Outflow (known as the β -plume
491 mechanism) could impact the upper-ocean circulation. In particular, it may lead to a cyclonic

492 recirculation consisting of the Azores Current and the Azores Countercurrent in the north. However,
 493 this hypothesis does not explain some observational characteristics of the Azores Current, namely the
 494 intensity of the jet and the higher transports west of the Azores islands far from the Gulf of Cadiz
 495 (source region). Although the temporal and spatial distribution of MOW in the Northeast Atlantic
 496 varies through time (Bozec et al., 2011; Frazão & Waniek, 2021) and ultimately could influence the
 497 Azores Current positioning, it is not yet conclusive, and addressing this issue may require further
 498 research.

499 The northward propagation of the Azores Front position from the 1970s until the mid-2000 is similar
 500 to the finding that the variations of the Gulf Stream position correlate with AMO and OHC but not
 501 with NAO (Seidov et al., 2017; 2019). Several publications have shown that the sea surface path of the
 502 Gulf Stream correlates with the NAO (e.g., Joyce et al., 2000; Gangopadhyay et al., 2016; Watelet et
 503 al., 2017), and we do not dispute those findings. However, Seidov et al. (2019) indicate that the
 504 observed Gulf Stream North Wall (GSNW) position west of 50°W is very resilient and is only mildly
 505 impacted by the overall North Atlantic atmospheric variability. Even at the extension zone, i.e., east of
 506 50°W, where the Gulf Stream branches into the North Atlantic Current and the Azores Current, the
 507 correlation with the NAO is not significant. Instead, they showed that the strongest correlation of the
 508 GSNW position east of 50°W is between the AMO and ocean heat content on decadal and longer time
 509 scales. A detailed discussion of the weaker dependence of the Gulf Stream path on NAO compared
 510 with AMO and OHC can be found in Seidov et al. (2019). Notwithstanding, other authors also found
 511 a strong correlation between the Gulf Stream northward excursion and the AMO index (e.g., Nigam et
 512 al., 2018; Ezer & Dangendorf, 2020). Therefore, it can be argued that a gradual change in the AMO
 513 and the OHC over the upper 400 m in the 1970s (Fig. 6) coincided with the poleward displacement of
 514 the Azores Front and also the Gulf Stream path, both defined via a temperature index (Seidov et al.,
 515 2019). Although both AMO and OHC are highly coherent ($\rho = 0.77$, $p < 0.05$), as pointed out by Seidov
 516 et al. (2017) for the North Atlantic basin, they are not linearly connected because the OHC depends on
 517 both thermal conditions at the surface (hence AMO) and the Ekman pumping (Seidov et al., 2019b).
 518 Thus, since OHC depends on both the sea surface temperature and the wind stress curl, there is a better
 519 correlation between the OHC and the current's dynamics (Seidov et al., 2019).

520 The poleward migration of the Azores Front, as the border separating the waters with higher biological
 521 productivity in the north from the waters with lower productivity in the south, is coherent with an
 522 expansion of the oligotrophic areas of the main gyres (Polovina et al., 2008). Additionally, the Azores
 523 Front movements have been shown to influence not only the primary production in the region but also
 524 affect the export production in the Northeast Atlantic (e.g., Waniek et al., 2005; Fründt & Waniek,
 525 2012; Fründt et al., 2015; Stern et al., 2017; 2019). Marine productivity decline in the oligotrophic
 526 regions since the 1990s (Boyce et al., 2010) is associated with rising sea surface temperature
 527 (Behrenfeld et al., 2006; Martinez et al., 2009). It is projected to further decline by up to 20% by the
 528 end of the 21st century (Steinacher et al., 2010). In a first attempt, Fründt et al. (2015) estimated a
 529 700 megaton reduction of carbon uptake over the North Atlantic subtropical region between 1871 and
 530 2008. Nevertheless, the understanding of the future impact of a northward expansion of the subtropical
 531 gyre on the biogeochemical cycles in this region requires further investigation.

532 The northward propagation of both the Azores Current jet and the Azores Front after the 1970s poses
 533 the question of whether the subtropical gyre is moving northward as an entity or the subtropical gyre
 534 is simply expanding. Answering this question is critical for understanding the subtropical gyre
 535 dynamics as a competitor to AMOC internal variability. Northward migration of the entire subtropical
 536 gyre would have forced the relocation of the main surface currents, leading to drastic changes in the
 537 basin-wide circulation. In connection with this problem, several studies have been exploring the size

538 and intensity of the North Atlantic subpolar gyre (Koul et al., 2020). Depending on the employed
539 methodology, some authors have shown a decline in size and strength (e.g., Häkkinen & Rhines, 2004),
540 while others did not find any significant change (e.g., Daniault et al., 2011). Unfortunately, the time-
541 series in these studies are too short to conclude with greater certainty whether a northward shift of the
542 northern limit of the subtropical gyre does lead to a shrinkage of the subpolar gyre. Yang et al. (2020),
543 using observational data analysis and numerical modeling, showed a poleward shift of the main ocean
544 gyres. They argue that such a poleward shift was likely caused by global warming in the last four
545 decades, coupled with a displacement of the extratropical atmospheric circulation.

546 Regardless of the overall change in the size or the northward propagation of the northern border only,
547 we are now confident that the Atlantic Meridional Overturning Circulation, Gulf Stream, and Azores
548 Current slowdown are tightly connected and are the parts of a larger picture of the North Atlantic
549 circulation variability on the decadal and longer time scale. The bottom line here is that we confidently
550 show that the changes in large-scale circulation reflected in the Gulf Stream and AMOC
551 weakening/strengthening pattern are detectable in the low energy region of the northeastern Atlantic,
552 embracing the biogeochemically very important regions of the Azores Current and its thermohaline
553 front.

554 **7 Conflict of Interest**

555 The authors declare that the research was conducted in the absence of any commercial or financial
556 relationships that could be construed as a potential conflict of interest.

557 **8 Author Contributions**

558 Conceptualization: HCF, JJW; Methodology: HCF, JJW; Visualization: HCF, RDP; Funding
559 acquisition: JJW, DSB; Supervision: JJW, DS; Writing – original draft: HCF; Writing – review &
560 editing: HCF, RDP, DSB, DS, JJW

561 **9 Funding**

562 This work was funded by the German Research Foundation grant, WA 2175/5-1 (JJW), and by the
563 Leibniz Institute for Baltic Sea Research Warnemünde (DSB, RP, HCF).

564 **10 Acknowledgments**

565 We thank the three reviewers for their valuable comments to improve the manuscript.

566 **Data Availability Statement**

567 The SODA-POP v2.2.4 is freely available at https://coastwatch.pfeg.noaa.gov/erddap/griddap/hawaii_d90f_20ee_c4cb.html. The unsmoothed detrended Atlantic Multidecadal Oscillation index
568 (AMO) was downloaded from <https://psl.noaa.gov/data/timeseries/AMO/>; the North Atlantic
569 Oscillation index is freely available at [https://climatedataguide.ucar.edu/climate-data/hurrell-north-
570 atlantic-oscillation-nao-index-station-based](https://climatedataguide.ucar.edu/climate-data/hurrell-north-atlantic-oscillation-nao-index-station-based).
571

572 **References**

- 573 Alves, M., Gaillard, F., Sparrow, M., Knoll, M. & Giraud, S. (2002), Circulation patterns and transport of
574 the Azores front-current system. *Deep-Sea Research II*, 49, 3983–4002. doi: 10.1016/S0967-
575 0645(02)00138-8
- 576 Andres, M., Donohue, K. A., Toole, J. M. (2020), The Gulf Stream's path and time-averaged velocity
577 structure and transport at 68.5°W and 70.3°W. *Deep-Sea Research Part I*, 156, 103179. doi:
578 10.1016/j.dsr.2019.103179
- 579 Barbosa Aguiar, A. C., Peliz, A. J., Cordeiro Pires, A. & Le Cann, B. (2011), Zonal structure of the mean
580 flow and eddies in the Azores current system. *Journal of Geophysical Research*, 116, C02012. doi:
581 10.1029/2010JC006538
- 582 Behrenfeld, M. J., O'Malley, R. T., Siegel, D. A., McClain, C. R., Sarmiento, J. L., Feldman, G. C. et al.
583 (2006), Climate-driven trends in contemporary ocean productivity. *Nature*, 444, 752–555. doi:
584 10.1038/nature05317
- 585 Boyce, D. G., Lewis, M. R. & Worm, B. (2010), Global phytoplankton decline over the past century.
586 *Nature*, 446, 591–596. doi: 10.1038/nature09268
- 587 Boyer, T. P., Antonov, J. I., Baranova, O. K., Garcia, H. E., Johnson, D. R., Locarnini, R. A. et al. (2009),
588 *World Ocean Database 2009*, S. Levitus, Ed., NOAA Atlas NESDIS 66, U.S. Gov. Printing Office,
589 Wash., D.C., 216 pp.
- 590 Bozec, A., Lozier, M. S., Chassignet, E. P. & Halliwell, G. R. (2011), On the variability of the
591 Mediterranean Outflow Water in the North Atlantic from 1948 to 2006. *Journal of Geophysical Research*,
592 116, C09033. doi: 10.1029/2011JC007191
- 593 Bryden, H. L., Longworth, H. R. & Cunningham, S. A. (2005), Slowing of the Atlantic meridional
594 overturning circulation at 25°N. *Nature*, 438, 655–657. doi: 10.1038/nature04385
- 595 Caesar, L., Rahmstorf, S., Robinson, A., Feulner, G. & Saba, V. (2018), Observed fingerprint of a
596 weakening Atlantic Ocean overturning circulation. *Nature*, 556, 191–196. doi: 10.1038/s41586-018-0006-
597 5
- 598 Caesar, L., McCarthy, G. D., Thornalley, D. J. R., Cahill, N. & Rahmstorf, S. (2021), Current Atlantic
599 Meridional Overturning Circulation weakest in the last millennium, *Nature Geoscience*, 14, 118–120. doi:
600 10.1038/s41561-021-00699-z
- 601 Carton, J. A. & Giese, B. S. (2008), A reanalysis of ocean climate using Simple Ocean Data Assimilation
602 (SODA). *Monthly Weather Review*, 136, 2999–3017. doi: 10.1175/2007MWR1978.1
- 603 Collins, M., Knutti, R., Arblaster, J., Dufresne, J.-L., Fichet, T., Friedlingstein, P., Gao, X., Gutowski,
604 W. J., Johns, T., Krinner, G., Shongwe, M., Tebaldi, C., Weaver, A. J., Wehner, M. (2013), Long-term
605 Climate Change: Projections, Commitments and Irreversibility. In *Climate Change 2013: The Physical
606 Science Basis Contribution of Working Group I to the Fifth Assessment Report of the Intergovernmental
607 Panel on Climate Change* [Stocker, T. F., Qin, D., Plattner, G.-K., Tignor, M., Allen, S. K., Boschung, J.,
608 Nauels, A., Xia, Y., Bex, V. and Midgley, P. M. (eds)]. Cambridge University Press, Cambridge, United
609 Kingdom and New York, NY, USA.
- 610 Comas-Rodríguez, I., Hernández-Guerra, A., Fraile-Nuez, E., Martínez-Marrero, A., Benítez-Barrios, V.
611 M., Pérez-Hernández, M. D. et al. (2011), The Azores Current System from a meridional section at
612 24.5°W. *Journal of Geophysical Research*, 116, C09021. doi: 10.1029/2011JC007129
- 613 Compo, G. P., Whitaker, J. S., Sardeshmukh, P. D., Matsui, N., Allan, R. J., Yin, X. et al. (2011), The
614 Twentieth Century Reanalysis Project. *Quarterly Journal of the Royal Meteorological Society*, 137, 1–28.
615 doi: 10.1002/qj.776
- 616 Daniault, N., Mercier, H. & Lherminier, P. (2011), The 1992–2009 transport variability of the East
617 Greenland-Irminger current at 60°N. *Geophysical Research Letters*, 38, L07601. doi:
618 10.1029/2011GL046863
- 619 Daniault, N., Mercier, H., Lherminier, P., Sarafanov, A., Falina, A., Zunino, P. et al. (2016). The northern
620 North Atlantic Ocean mean circulation in the early 21st century. *Progress in Oceanography*, 146, 142–
621 158. doi: 10.1016/j.pocean.2016.06.007
- 622 de Coëtlogon, G., Frankignoul, C., Bentsen, M., Delon, C., Haak, H., Masina, S. et al. (2006), Gulf Stream
623 variability in five oceanic general circulation models. *Journal of Physical Oceanography*, 36, 2119–2135.
624 doi: 10.1175/JPO2963.1

- 625 Dong, S., Baringer, M. O. & Goni, G. J. (2019), Slow down of the Gulf Stream during 1993–2016.
 626 *Scientific Reports*, 9, 6672. doi: 10.1038/s41598-019-42820-8
- 627 Ezer, T., Atkinson, L. P., Corlett, W. B., Blanco, J. L. (2013), Gulf Stream's induced sea level rise and
 628 variability along the U.S. mid-Atlantic coast. *Journal of Geophysical Research*, 118(2), 685–697. doi:
 629 10.1002/jgrc.20091
- 630 Ezer, T. (2015), Detecting changes in the transport of the Gulf Stream and the Atlantic Overturning
 631 circulation from coastal sea level data: The extreme decline in 2009–2010 and estimated variations for
 632 1935–2012. *Global and Planetary Change*, 129, 23–36. doi: 10.1016/j.gloplacha.2015.03.002
- 633 Ezer, T. & Dangendorf, S. (2020), Global sea level reconstruction for 1990–2015 reveals regional
 634 variability in ocean dynamics and an unprecedented long weakening in the Gulf Stream flow since the
 635 1990s. *Ocean Science*, 16, 997–1016. doi: 10.5194/os-16-997-2020
- 636 Ezer, T. & Dangendorf, S. (2022), Spatiotemporal variability of the ocean since 1900: testing a new
 637 analysis approach using global sea level reconstruction. *Ocean Dynamics*, 72, 79–97. doi:
 638 10.1007/s10236-021-01494-5
- 639 Frazão, H. C., Prien, R. D., Müller, T. J., Schulz-Bull, D. E. & Waniek, J. J. (2021), 30 years of temporal
 640 variability of temperature and currents below the main thermocline between 1980–2009 in the subtropical
 641 Northeast Atlantic (Kiel 276, 33°N, 22°W). *Journal of Marine Systems*, 217, 103517. doi:
 642 10.1016/j.jmarsys.2021.103517
- 643 Frazão, H. C. & Waniek, J. J. (2021), Mediterranean water properties at the eastern limit of the North
 644 Atlantic subtropical gyre since 1981. *Oceans*, 2, 266–280. doi: 10.3390/oceans2010016
- 645 Fründt, B. & Waniek, J. J. (2012), Impact of the Azores front propagation on deep ocean particle flux.
 646 *Central European Journal of Geosciences*, 4, 531–544. doi: 10.2478/s13533-012-0102-2
- 647 Fründt, B., Müller, T. J., Schulz-Bull, D. E. & Waniek, J. J. (2013), Long-term changes in the thermocline
 648 of the subtropical Northeast Atlantic (33°N, 22°W). *Progress in Oceanography*, 116, 246–260. doi:
 649 10.1016/j.pocean.2013.07.004
- 650 Fründt, B., Dippner, J. W. Schulz-Bull, D. E. & Waniek, J. J. (2015), Chlorophyll a reconstruction from in
 651 situ measurements: 2. Marked carbon uptake decrease in the last century. *Journal of Geophysical
 652 Research: Biogeosciences*, 120, 246–253. doi: 10.1002/2014JG002692
- 653 Gangopadhyay, A., Chaudhuri, A. H., Taylor, A. H. (2016), On the Nature of Temporal Variability of the
 654 Gulf Stream Path from 75°W to 55°W. *Earth Interactions*, 20, 1–17. doi: 10.1175/EI-D-15-0025.1
- 655 Garçon, V. G., Oschlies, A., Doney, S. C., McGillicuddy, D. & Waniek, J. (2001), The role of mesoscale
 656 variability on plankton dynamics in the North Atlantic. *Deep-Sea Research II*, 48, 2199–2226. doi:
 657 10.1016/S0967-0645(00)00183-1
- 658 Giese, B. S. & Ray, S. (2011), El Niño variability in simple ocean data assimilation (SODA), 1871–2008.
 659 *Journal of Geophysical Research*, 116, C02024. doi: 10.1029/2010JC006695
- 660 Gould, W. J. (1985), Physical Oceanography of the Azores Front. *Progress in Oceanography*, 14, 167–
 661 190. doi: 10.1016/0079-6611(85)90010-2
- 662 Greatbatch, R. J., Fanning, A. F., Goulding, A. D. & Levitus, S. (1991), A diagnosis of Interpentadal
 663 circulation changes in the North Atlantic. *Journal of Geophysical Research*, 96, 22009–22023. doi:
 664 10.1029/91JC02423
- 665 Grey, S. M., Haines, K., Troccoli, A. (2000), A Study of Temperature Changes in the Upper North
 666 Atlantic: 1950–94. *Journal of Climate*, 13, 2697–2711. doi: 10.1175/1520-
 667 0442(2000)013<2697:ASOTCI>2.0.CO;2
- 668 Häkkinen, S. & Rhines, P. B. (2004), Decline of subpolar North Atlantic circulation during the 1990s.
 669 *Science*, 304, 555–559. doi: 10.1126/science.1094917
- 670 Häkkinen, S., Rhines, P. B. & Worthen, D. L. (2016), Warming of the Global Ocean: Spatial Structure and
 671 Water-Mass Trends. *Journal of Climate* 29(13), 4949–4963. doi: 10.1175/JCLI-D-15-0607.1
- 672 Jia, Y. (2000), Formation of an Azores current due to Mediterranean Overflow in a modeling study of the
 673 North Atlantic. *Journal of Physical Oceanography*, 30, 2342–2358. doi:10.1175/1520-
 674 0485(2000)030<2342:FOACD>2.0.CO;2
- 675 Jones, P. W. (1999), First- and second-order conservative remapping schemes for grids in spherical
 676 coordinates. *Monthly Weather Review*, 127, 2204–2210. doi: 10.1175/1520-
 677 0493(1999)127<2204:FASOCR>2.0.CO;2

- 678 Joyce, T. M., Deser, C., Spall, M. A. (2000), The Relation between Decadal Variability of Subtropical
679 Mode Water and the North Atlantic Oscillation. *Journal of Climate*, 13, 2550–2569. doi: 10.1175/1520-
680 0442(2000)013<2550:TRBDVO>2.0.CO;2
- 681 Joyce, T. M. & Zhang, R. (2010), On the path of the Gulf Stream and the Atlantic Meridional Overturning
682 Circulation. *Journal of Climate*, 23, 3146–3154. doi: 10.1175/2010JCLI3310.1
- 683 Käse, R. H. & Siedler, G. (1982), Meandering of the subtropical front south-east of the Azores. *Nature*,
684 300, 245–246. doi: 10.1038/300245a0
- 685 Koul, V., Tesday, J.-E., Bersch, M., Hátún, H., Brune, S., Borchert, L. et al. (2020). Unraveling the choice
686 of the north Atlantic subpolar gyre index. *Scientific Reports*, 10, 1005. doi: 10.1038/s41598-020-57790-5
- 687 Lamas, L., Peliz, Á., Ambar, I., Barbosa Aguiar, A., Maximenko, N., Teles-Machado, A. (2010), Evidence
688 of time-mean cyclonic cell southwest of Iberian Peninsula: The Mediterranean Outflow-driven β -plume?
689 *Geophysical Research Letters*, 37, L12606. doi: 10.1029/2010GL043339
- 690 Le Traon, P. Y. (1991), Time scales of mesoscale variability and their relationship with space scales in the
691 North Atlantic. *Journal of Marine Research*, 49, 467–492. doi: 10.1357/002224091784995828
- 692 Le Traon, P.-Y. & De Mey, P. (1994), The eddy field associated with the Azores Front east of the Mid-
693 Atlantic Ridge as observed by the Geosat altimeter. *Journal of Geophysical Research*, 99(C5), 9907–9923.
694 doi: 10.1029/93JC03513
- 695 Levitus, S. (1989a), Interpentadal variability of temperature and salinity at intermediate depths of the
696 North Atlantic Ocean, 1970–1974 versus 1955–1959. *Journal of Geophysical Research*, 94, 6091–6131.
697 doi: 10.1029/JC094iC05p06091
- 698 Levitus, S. (1989b), Interpentadal Variability of Salinity in the Upper 150 m of the North Atlantic Ocean,
699 1970–1974 Versus 1955–1959. *Journal of Geophysical Research*, 94(C7), 9679–9685. doi:
700 10.1029/JC094iC07p09679
- 701 Levitus, S., Antonov, J. I., Boyer, T. P., Locarnini, R. A., Garcia, H.E., Mishonov, A. V. (2009), Global
702 ocean heat content 1955–2008 in light of recently revealed instrumentation problems. *Geophysical*
703 *Research Letters*, 36, L07608. doi: 10.1029/2008GL037155
- 704 Levitus, S., Antonov, J. I., Boyer, T. P., Baranova, O. K., Garcia, H. E., Locarnini, R. A et al. (2012),
705 World ocean heat content and thermocline sea level change (0–2000 m), 1955–2010. *Geophysical*
706 *Research Letters*, 39, L10603, doi:10.1029/2012GL051106
- 707 Maillard, C. & Käse, R. (1989), The near-surface flow in the subtropical gyre south of the Azores. *Journal*
708 *of Geophysical Research*, 94(C11), 16133–16140. doi:10.1029/JC094iC11p16133
- 709 Marchese, P. J. (1999), Variability in the Gulf Stream recirculation gyre. *Journal of Geophysical*
710 *Research*, 14 (C12), 29549–29560. doi: 10.1029/1999JC900254
- 711 Martinez, E., Antoine, D., D'Ortenzio, F., Gentili, B. (2009), Climate-Driven Basin-Scale Decadal
712 Oscillations of Oceanic Phytoplankton. *Science*, 326, 1253–1256. doi: 10.1126/science.1177012
- 713 Moat, B. I., Smeed, D. A., Frajka-Williams, E., Desbruyères, D. G., Beaulieu, C., Johns, W. E. et al.
714 (2020), Pending recovery in the strength of the meridional overturning circulation at 26°N. *Ocean Science*,
715 16, 863–874. doi: 10.5194/os-16-863-2020
- 716 Müller, T. J. & Siedler, G. (1992), Multi-year current time series in the eastern North Atlantic Ocean.
717 *Journal of Marine Research*, 50, 63–98. doi: 10.1357/002224092784797755
- 718 New, A. L., Jia, Y., Coulibaly, M. & Dengg, J. (2001), On the role of the Azores current in the ventilation
719 of the North Atlantic Ocean. *Progress in Oceanography* 48, 163–194. doi:10.1016/S0079-6611(01)00004-
720 0
- 721 Nigam, S., Ruiz-Barradas, A., Chafik, L. (2018), Gulf Stream Excursions and Sectional Detachments
722 Generate the Decadal Pulses in the Atlantic Multidecadal Oscillation. *Journal of Climate*, 31, 2853–2870.
723 doi: 10.1175/JCLI-D-17-0010.1
- 724 Onken, R. (1993), The Azores countercurrent. *Journal of Physical Oceanography*, 23, 1638–1646. doi:
725 10.1175/1520-0485(1993)023<1638:TAC>2.0.CO;2
- 726 Özgökmen, T. M., Chassignet, E. P. & Rooth, C. G. H. (2001), On the Connection between the
727 Mediterranean Outflow and the Azores Current. *Journal of Physical Oceanography*, 31(2), 461–480. doi:
728 10.1175/1520-0485(2001)031<0461:OTCBTM>2.0.CO;2
- 729 Pelegrí, J. L. & Csanady, G. T. (1991), Nutrient transport and mixing in the Gulf Stream. *Journal of*
730 *Geophysical Research*, 96, 2577–2583. doi:10.1029/90JC02535

- 731 Peliz, A., Dubert, J., Marchesiello, P. & Teles-Machado, A. (2007), Surface circulation in the Gulf of
 732 Cadiz: Model and mean flow structure. *Journal of Geophysical Research*, 12, C11015. doi:
 733 10.1029/2007JC004159
- 734 Pingree, R. & Sinha, B. (2001), Westward moving waves or eddies (*Storms*) on the Subtropical/Azores
 735 Front near 32.5°N? Interpretation of the Eulerian currents and temperature records at mooring 155
 736 (35.5°W) and 156 (34.4°W). *Journal of Marine Systems*, 29, 239–276. doi: 10.1016/S0924-
 737 7963(01)00019-7
- 738 Polovina, J. J., Howell, E. A. & Abecassis, M. (2008), Ocean's least productive waters are expanding.
 739 *Geophysical Research Letters*, 35, L03618. doi: 10.1029/2007GL031745
- 740 Reverdin, G. (2010), North Atlantic Subpolar Gyre Surface Variability (1895-2009). *Journal of Climate*,
 741 23, 4571–4584. doi: 10.1175/2010JCLI3493.1
- 742 Richardson, P. L. (1983), Eddy Kinetic Energy in the North Atlantic From Surface Drifters. *Journal of*
 743 *Geophysical Research*, 88/C7, 4355–4367. doi: 10.1029/JC088iC07p04355
- 744 Richardson, P. L. (2001), Florida Current, Gulf Stream, and Labrador Current. In J. H. Steele (Ed.),
 745 *Encyclopedia of ocean sciences* (2nd Ed., pp. 554-563). Oxford: Academic Press. doi: 10.1016/B978-
 746 012374473-9.00357-X
- 747 Rossby, T., Flagg, C. N., Donohue, K., Sanchez-Franks, A., Lillibridge, J. (2014), On the long-term
 748 stability of Gulf Stream transport based on 20 years of direct measurements. *Geophysical Research*
 749 *Letters*, 41, 114-120. doi: 10.1002/2013GL058636
- 750 Rossby, T., Flagg, C. N., Donohue, K., Fontana, S., Curry, R. Andres, M. et al. (2019), Oleander is more
 751 than a flower: Twenty-five years of oceanography aboard a merchant vessel. *Oceanography*, 32(3), 126–
 752 137. doi: 10.5670/oceanog.2019.319
- 753 Schlesinger, M. E. & Ramankutty, N. (1994), An oscillation in the global climate system of period 65–
 754 years. *Nature*, 367, 723–726. doi: 10.1038/367723a0
- 755 Schmitz, W. J. Jr. & McCartney, M. S. (1993), On the North Atlantic Circulation. *Reviews of Geophysics*,
 756 31(1), 29–49. doi: 10.1029/92RG02583
- 757 Seidov, D., Mishonov, A., Reagan, J. & Parsons, R. (2017), Multidecadal variability and climate shift in
 758 the North Atlantic Ocean. *Geophysical Research Letters*, 44, 4985–4993. doi:10.1002/2017GL073644
- 759 Seidov, D., Mishonov, A., Reagan, J. & Parsons, R. (2019), Resilience of the Gulf Stream path on decadal
 760 and longer timescales. *Scientific Reports*, 9, 11549. doi: 10.1038/s41598-019-48011-9
- 761 Seidov, D., Mishonov, A., Reagan, J. & Parsons, R. (2019b), Eddy-Resolving In Situ Ocean Climatologies
 762 of Temperature and Salinity in the Northwest Atlantic Ocean. *Journal of Geophysical Research: Oceans*,
 763 124, 41–58. doi: 10.1029/2018JC014548
- 764 Siedler, G., Zenk, W., Emery, W. J. (1985), Strong Current Events Related to a Subtropical Front in the
 765 Northeast Atlantic. *Journal of Physical Oceanography*, 15, 885–897. doi: 10.1175/1520-
 766 0485(1985)015<0885:SCERTA>2.0.CO;2
- 767 Siedler, G., Armi, L. & Müller, T. J. (2005), Meddies and decadal changes at the Azores front from 1980
 768 to 2000. *Deep-Sea Research II*, 52, 583–604. doi: 10.1016/j.dsr2.2004.12.010
- 769 Silva-Fernandes, S. M. & Peliz, A. J. (2020), The turbulent structure of the Azores current system: a
 770 statistical analysis. *Journal of Geophysical Research: Oceans*, 125, e2020JC016327. doi:
 771 10.1029/2020JC016327
- 772 Smith, R. D., Dukowicz, J. K., Malone, R. C. (1992), Parallel ocean general circulation modeling.
 773 *Physical D*, 60, 38-61. doi: 10.1016/0167-2789(92)90225-C
- 774 Spall, M. A. (1990), Circulation in the Canary Basin: A model/data analysis. *Journal of Geophysical*
 775 *Research*, 95, 9611–9628
- 776 Steinacher, M., Joos, F., Frölicher, T. L., Bopp, L., Cadule, P., Cocco, V. et al. (2010), Projected 21st
 777 century decrease in marine productivity: a multi-model analysis. *Biogeosciences*, 7, 979–1005. doi:
 778 10.5194/bg-7-979-2010
- 779 Stern, J., Dellwig, O. & Waniek, J. J. (2017), Deep-sea fluxes of barium and lithogenic trace elements in
 780 the subtropical northeast Atlantic. *Deep-Sea Research I*, 122, 72–80. doi: 10.1016/j.dsr.2017.02.002
- 781 Stern, J., Kaiser, D., Przibilla, A., Schulz-Bull, D. E. & Waniek, J. J. (2019), Trace metals and persistent
 782 organic pollutants fingerprint on the particle flux in the deep subtropical NE Atlantic. *Marine Pollution*
 783 *Bulletin*, 145, 508–516. doi: 10.1016/j.marpolbul.2019.06.001

- 784 Stramma, L. (1984), Geostrophic transport in the Warm Water Sphere of the eastern subtropical North
 785 Atlantic. *Journal of Marine Research*, 42(3), 537–558. doi: 10.1357/002224084788506022
 786 Stramma, L. & Müller, T. J. (1989), Some Observations of the Azores Current and the North Equatorial
 787 Current. *Journal of Geophysical Research*, 94(C3), 3181–3186. doi: 10.1029/JC094iC03p03181
 788 Tett, S. F. B., Sherwin, T. J., Shrivastava, A., Browne, O. (2014), How Much Has the North Atlantic Ocean
 789 Overturning Circulation Changed in the Last 50 Years? *Journal of Climate*, 27, 6325–6342. doi:
 790 10.1175/JCLI-D-12-00095.1
 791 Tomczak, M. & Godfrey, J. S. (1994). *Regional Oceanography: An Introduction*. Pergamon, 437 pp. doi:
 792 10.1016/C2009-0-14825-0
 793 Visbeck, M., Chassignet, E. P., Curry, R. G., Delworth, T. L., Dickson, R. R. & Krahnemann, G. (2003), The
 794 ocean's response to North Atlantic Oscillation variability. *Geophysical Monograph-American Geophysical*
 795 *Union*, 134, 113–146. doi: 10.1029/134GM06
 796 Volkov, D. L. & Fu, L.-L. (2010), On the reasons for the formation and variability of the Azores current.
 797 *Journal of Physical Oceanography*, 40, 2197–2220. doi: 10.1175/2010JPO4326.1
 798 Volkov, D. L. & Fu, L.-L. (2011), Interannual variability of the Azores current strength and eddy energy
 799 in relation to atmospheric forcing. *Journal of Geophysical Research*, 116, C11011. doi:
 800 10.1029/2011JC007271
 801 Waniek, J. J., Schulz-Bull, D. E., Blanz, T., Prien, R. D., Oschlies, A. & Müller, T. J. (2005), Interannual
 802 variability of deep water particle flux in relation to production and lateral sources in the northeast Atlantic.
 803 *Deep-Sea Research I*, 52, 33–50. doi: 10.1016/j.dsr.2004.08.008
 804 Watelet, S., Beckers, J.-M., Barth, A. (2017), Reconstruction of the Gulf Stream from 1940 to the Present
 805 and Correlation with the North Atlantic Oscillation. *Journal of Physical Oceanography*, 47, 2741–2754.
 806 doi: 10.1175/JPO-D-17-0064.1
 807 Williams, R. G., McLaren, A. J. & Follows, M. J. (2000), Estimating the convective supply of nitrate and
 808 implied variability in export production over the North Atlantic. *Global Biogeochemical Cycles*, 14, 1299–
 809 1313. doi: 10.1029/2000GB001260
 810 Willis, J. K. (2010), Can in situ floats and satellite altimeters detect long-term changes in Atlantic Ocean
 811 overturning? *Geophysical Research Letters*, 37, L06602. doi: 10.1029/2010GL042372
 812 Yang, H., Lohmann, G., Krebs-Kanzow, U., Ionita, M., Shi, X., Sidorenko, D. et al. (2020), Poleward shift
 813 of the major ocean gyres detected in a warming climate. *Geophysical Research Letters*, 47,
 814 e2019GL085868. doi: 10.1029/2019GL085868
 815 Yeager, S. & Danabasoglu, G. (2014), The Origins of Late-Twentieth-Century Variations in the Large-
 816 Scale North Atlantic Circulation. *Journal of Climate*, 27, 3222–3247. doi: 10.1175/JCLI-D-13-00125.1
 817 Zhang, R. (2008), Coherent surface-subsurface fingerprint of the Atlantic meridional overturning
 818 circulation. *Geophysical Research Letters*, 35, L20705. doi: 10.1029/2008GL035463
 819 Zhang, W.-Z., Chai, F., Xue, H., Oey, L.-Y. (2020), Remote sensing linear trends of the Gulf Stream from
 820 1993 to 2016. *Ocean Dynamics*, 70, 701–712. doi: 10.1007/s10236-020-01356-6
 821

Publication II

Full Research Paper, *Oceans*, 2021, 2, 266–280

Mediterranean Water Properties at the Eastern Limit of the North Atlantic Subtropical Gyre Since 1981

Helena C. Frazão, & Joanna J. Waniek



Submitted: 18 December 2020; Accepted: 15 March 2021

doi: 10.3390/oceans2010016

Abstract A high-quality hydrographic CTD and Argo float data was used to study the property changes along the westward branch of the Mediterranean Outflow Water (MOW) in the northeast Atlantic between 1981 and 2018. In this period, the temperature and salinity are marked by periods of cooling/freshening and warming/salinification. Since 1981, the MOW properties at the core decreased by $-0.015 \pm 0.07 \text{ }^\circ\text{C year}^{-1}$ and $-0.003 \pm 0.002 \text{ year}^{-1}$. The different phases of the North Atlantic Oscillation (NAO) influence the main propagation pathways of the MOW into the North Atlantic basin, thus affecting the trends determined within different NAO-phases. The temperature and salinity show a strong correlation with NAO, with NAO leading the properties by 8 and 7 years, respectively, indicating a delayed response of the ocean to different forcing conditions. A decrease in oxygen concentration ($-0.426 \pm 0.276 \text{ } \mu\text{mol kg}^{-1} \text{ year}^{-1}$) was calculated for the same period; however, no connection with the NAO was found.

Article

Mediterranean Water Properties at the Eastern Limit of the North Atlantic Subtropical Gyre Since 1981

Helena C. Frazão *  and Joanna J. Waniek 

Leibniz Institute for Baltic Sea Research Warnemünde, Seestraße 15, 18119 Rostock, Germany;
joanna.waniek@io-warnemuende.de

* Correspondence: helena.frazao@io-warnemuende.de

Abstract: A high-quality hydrographic CTD and Argo float data was used to study the property changes along the westward branch of the Mediterranean Outflow Water (MOW) in the northeast Atlantic between 1981 and 2018. In this period, the temperature and salinity are marked by periods of cooling/freshening and warming/salinification. Since 1981, the MOW properties at the core decreased by $-0.015 \pm 0.07 \text{ }^\circ\text{C year}^{-1}$ and $-0.003 \pm 0.002 \text{ year}^{-1}$. The different phases of the North Atlantic Oscillation (NAO) influence the main propagation pathways of the MOW into the North Atlantic basin, thus affecting the trends determined within different NAO-phases. The temperature and salinity show a strong correlation with NAO, with NAO leading the properties by 8 and 7 years, respectively, indicating a delayed response of the ocean to different forcing conditions. A decrease in oxygen concentration ($-0.426 \pm 0.276 \text{ } \mu\text{mol kg}^{-1} \text{ year}^{-1}$) was calculated for the same period; however, no connection with the NAO was found.

Keywords: Mediterranean Outflow Water; North Atlantic Oscillation; Northeast Atlantic; time-series



Citation: Frazão, H.C.; Waniek, J.J. Mediterranean Water Properties at the Eastern Limit of the North Atlantic Subtropical Gyre Since 1981. *Oceans* **2021**, *2*, 266–280. <https://doi.org/10.3390/oceans2010016>

Academic Editor: Michael W. Lomas

Received: 18 December 2020

Accepted: 9 March 2021

Published: 15 March 2021

Publisher's Note: MDPI stays neutral with regard to jurisdictional claims in published maps and institutional affiliations.



Copyright: © 2021 by the authors. Licensee MDPI, Basel, Switzerland. This article is an open access article distributed under the terms and conditions of the Creative Commons Attribution (CC BY) license (<https://creativecommons.org/licenses/by/4.0/>).

1. Introduction

The Mediterranean Water flows out of the Strait of Gibraltar and mixes with the surrounding North Atlantic Central Water in the Gulf of Cadiz to form the Mediterranean Outflow Water (MOW). MOW is a high-salinity and warm water mass that enters the Gulf of Cadiz and sinks until it reaches a buoyant depth around 1000 dbar [1,2]. To the west of the Gulf of Cadiz, MOW spreads into the North Atlantic by two main advective-diffusive pathways (Figure 1a): northward, as an eastern boundary undercurrent following the western margin of the Iberian Peninsula into the western European continental slope [3,4] and westward, into the subtropical Northeast Atlantic [5,6]. MOW also spreads south-westward, mainly through the influence of Mediterranean Water lenses formed in the proximity of Cape St. Vicent [7], also known as Meddies [8–11]. Although the north- and westward pathways contribute more to the spreading of MOW into the North Atlantic than the southwestern branch [12], its flow along the Gulf of Cadiz is guided by the local topography [13] and influenced by tides [14]. A more detailed description of the complex outflow and its spreading dynamics can be found, for example, in Figure 10 of de Pascual-Collar [15].

As an anomalously warm and saline water mass at intermediate depths, MOW is an important source of salt and heat in the eastern North Atlantic [1]. Reid [3] showed that the penetration of Mediterranean Water into higher latitudes, mainly Nordic Seas, a critical region in the context of the global overturning circulation, might impact the deep water formation in the Northeast Atlantic, and ultimately alter the thermohaline circulation [16].

The water column in the North Atlantic down to 2000 m has been warming since the second half of the last century [17]. Until the 1980s, most studies showed warming at intermediate depths [18,19]. However, after the 1980s, the warming along the western branch reported so far by Potter & Lozier [19] reversed to cooling [20] and, during the last decade (2002–2010), no significant trend was found [21]. In contrast, the MOW along the

northward flow continued to warm until 2001 [22] and showed cooling and freshening afterwards until 2013 [23].

The variability of MOW’s temperature and salinity in the Northeast Atlantic (NEA) has been attributed to (i) changes in the properties of the outflow waters [19,20,24] and (ii) basin-wide circulation changes that alter the preferential pathways of the MOW after exiting the Strait of Gibraltar [25–27]. Lozier & Sindlinger [25] showed that changes in the source waters have little impact on interannual to decadal property variations observed at the MOW. However, Chaudhuri et al. [27] and Bozec et al. [26] pointed out that changes in the preferential pathways of MOW can be attributed to the observed properties changes, despite the warming of the Mediterranean Outflow reported in some studies [28,29].

The North Atlantic Oscillation (NAO), as the primary mode of atmospheric variability in the North Atlantic, is connected to changes in properties and transports on different time scales, even at depths of intermediate waters [28,30]. The influence of NAO on the main pathways of MOW was identified by Bozec et al. [26] and Chaudhuri et al. [27], with a particular focus on the penetration of Mediterranean Waters into the subpolar gyre [25,31].

In this study, a dataset comprising hydrographic data and Argo float data was used to assess the variability of the MOW’s properties at the core (1000–1100 dbar) in the northeastern border of the subtropical gyre between 1981 and 2018 (Figure 1a). First, we analyzed the scales of temporal changes in MOW properties in the core over 38 years. Second, the changes observed in the in situ time-series were compared with a global gridded product (EN4) [32]. Finally, we investigated the NAO’s influence on the variability of the temperature and salinity at the MOW core.

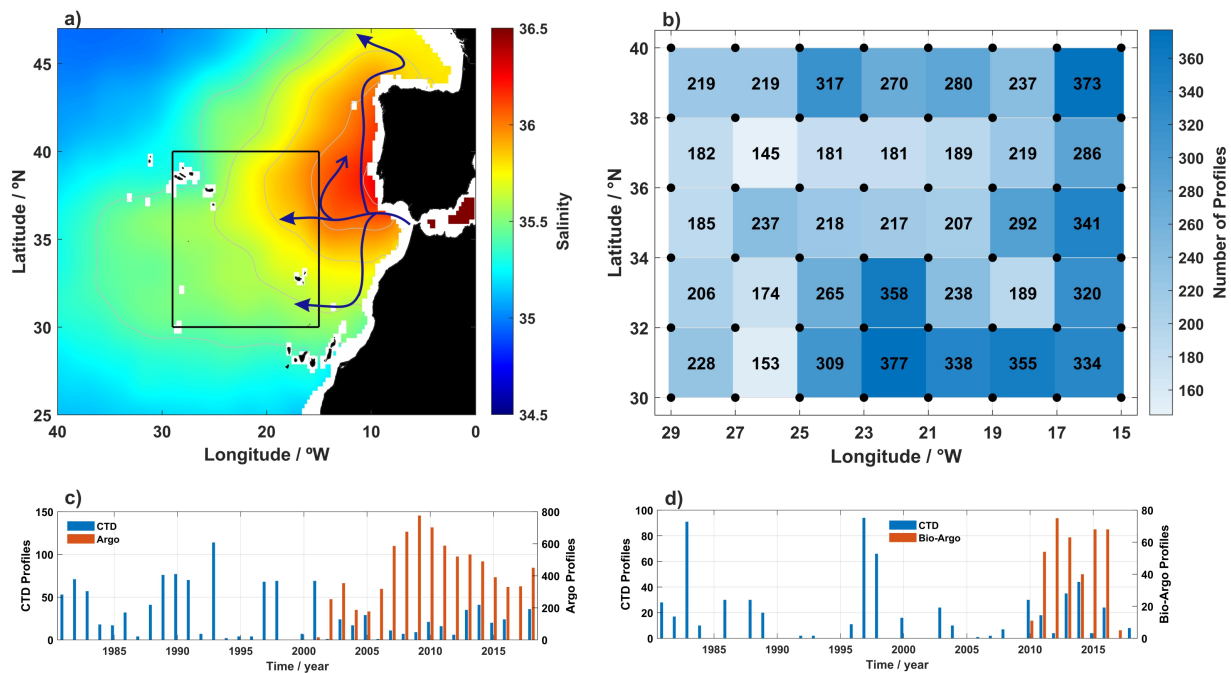


Figure 1. (a) Climatological distribution of the salinity at 1000 m from the World Ocean Atlas (WOA18) [33]. Dark blue lines are a schematic representation of the main pathways of the Mediterranean Outflow Water after exiting the Strait of Gibraltar in the eastern part of the subtropical gyre (adapted from [12,15,34]). The black box delimits the study area. (b) Number of temperature and salinity profiles for each box of the 2° × 2° grid over the study domain in (a). Temporal distribution of temperature and salinity profiles obtained with CTD and Argo floats (c) and oxygen profiles acquired by CTD and Bio-Argo floats (d) for each year.

2. Data and Methods

2.1. Temperature, Salinity and Oxygen Time-Series

High-quality temperature, salinity, and dissolved oxygen profiles were extracted for a grid delimited by 30° N–40° N, and 29° W–15° W in the Northeast Atlantic between 1981–2018 (Figure 1a, black box). The hydrographic data were gathered from the World Ocean Database 2018 (WOD18, www.nodc.noaa.gov, accessed on 19 October 2019), PANGAEA World Data Centre (<http://www.pangaea.de>, accessed on 20 October 2019) and other data centres. For more details of the additional profiles used, see Table S1 in the Supplementary Materials. In addition, data from Argo and Bio-Argo floats was used for the period 2001–2018 and 2010–2017, respectively. The introduction of the Argo array in the early 2000s provided the first systematic and homogeneous sampling network of the ocean interior, improving both temporal and spatial resolution of ocean properties [35].

The quality assessment of the WOD18 profiles followed Wong et al. [36]. Only profiles that passed the Argo and Bio-Argo delayed-mode quality control and marked as very good data were used [37]. Additionally, salinity and temperature profiles were checked for erroneous data (i.e., density inversions, spikes and high noise profiles, systematic deviations in salinity, and missing salinity or temperature). All profiles flagged with erroneous data were removed. Dissolved oxygen data were inspected for systematic shifts relative to a mean vertical profile from the World Ocean Atlas 2018 (WOA18) [38] averaged over the region of interest in Figure 1a (black box). Since we are interested in the depths where MOW settles, profiles shallower than 1500 m were excluded. From the total of 10,592 (1716 CTD + 8876 Argo) salinity and temperature profiles and of 1222 (788 CTD + 434 Bio-Argo) dissolved oxygen profiles available in the study area, 8839 (1158 CTD + 7681 Argo, 83%) salinity and temperature profiles, and 1012 (628 CTD + 384 Bio-Argo, 83%) dissolved oxygen profiles were left (Figure 1c,d) after carrying out the described quality procedures.

Potential temperature referenced to the surface (θ , hereafter referred as temperature) and potential density (σ_θ —correspond to the surface, σ_1 —correspond to 1000 dbar) were derived for each profile [39]. In the northeast Atlantic (NEA), at intermediate levels, the MOW lies between σ_1 of 31.8 and 32.25 kg m⁻³ [10,12]. Temperature, salinity, potential density, and dissolved oxygen were interpolated at 20-dbar pressure intervals between 600–1500 dbar. The resulting profiles were then interpolated over a regular grid of 2° × 2° on a monthly basis, using the individual profiles data weighted according to the distance from the grid points (Figure 1b, black dots), assuming a 1° (≈110 km) decorrelation length scale used in the objective analysis in this study [40,41]. Integral time scales in the NEA are in the order of 30 to 40 days at 1000 m, indicating that the dominant processes at this depth are of the order of a month [42]. Therefore, the monthly averages of temperature and salinity calculated from the profiles can be assumed as statistically independent [42,43]. Thus, the annual property time-series at the core of MOW were obtained averaging the monthly mean fields over the entire study area (black box in Figure 1a) between 1000 and 1100 dbar [19,44] for both CTD and Argo datasets (Supplementary Figure S1). Anomalies were determined by subtracting the climatological mean calculated over the study area for the period 1981–2018 using all the monthly means, from the annual mean values to create anomaly property time-series of the MOW (Figure 2).

The resulting time-series were fitted using a least-square linear fit to compute the linear trends. Significant trends at 95% confidence level and confidence intervals (estimated with a t-student test) are given in bold in Table 1. The confidence intervals were calculated using the effective number of degrees of freedom [45]. The anomaly time-series were detrended to calculate the lagged correlation coefficients with the NAO. To compare the estimated trends using CTD and Argo data, we used the UK Met Office EN4 product [32] and extracted temperature and salinity for the black box of Figure 1a between 900 m and 1200 m. The EN4 resulting time-series are presented in Supplementary Figure S2.

Table 1. Estimated temperature and salinity trends and confidence intervals between 1981 and 2018, calculated for the study domain in Figure 1a. The trends were determined using only CTD data, Argo floats, combined (CTD/Argo) dataset, and EN4 dataset. Trends were calculated for each decade, and also according to NAO-phase periods. The NAO periods are divided as follows: 1981–1996 corresponds to a predominantly positive NAO; 1997–2010 comprises a period of transition from a strongly negative NAO phase (in 1996) to neutral values in the following years; and 2011–2018 corresponds to a transition of a strongly negative NAO in 2010 to a positive phase afterwards. Once the last period coincides with the last decade, the values are not repeated. Trends significant at 95% confidence level are in bold. The variance explained by the least-square linear trend (r^2) is presented in brackets. n.a. = not applicable.

	Temperature / °C year ⁻¹				Salinity / year ⁻¹			
	CTD	Argo	CTD/Argo	EN4	CTD	Argo	CTD/Argo	EN4
Decadal periods								
1981–1990	−0.022 ± 0.043 (0.13)	n.a.	−0.022 ± 0.043 (0.13)	−0.009 ± 0.012 (0.31)	−0.006 ± 0.011 (0.15)	n.a.	−0.006 ± 0.011 (0.15)	−0.001 ± 0.003 (0.08)
1991–2000	0.022 ± 0.046 (0.06)	n.a.	0.013 ± 0.036 (0.09)	−0.021 ± 0.011 (0.84)	0.009 ± 0.010 (0.29)	n.a.	0.007 ± 0.010 (0.27)	−0.005 ± 0.003 (0.79)
2001–2010	−0.017 ± 0.108 (0.03)	0.026 ± 0.049 (0.16)	0.006 ± 0.047 (0.01)	0.017 ± 0.015 (0.62)	−0.006 ± 0.019 (0.10)	0.003 ± 0.009 (0.08)	−0.001 ± 0.010 (0.01)	0.002 ± 0.002 (0.48)
2011–2018	0.050 ± 0.040 (0.71)	0.025 ± 0.013 (0.79)	0.024 ± 0.013 (0.79)	0.015 ± 0.009 (0.72)	0.007 ± 0.008 (0.49)	0.005 ± 0.003 (0.84)	0.005 ± 0.002 (0.85)	0.003 ± 0.002 (0.64)
NAO-phase periods								
1981–1996	−0.038 ± 0.021 (0.71)	n.a.	−0.038 ± 0.021 (0.71)	−0.008 ± 0.005 (0.64)	−0.009 ± 0.005 (0.70)	n.a.	−0.009 ± 0.005 (0.70)	−0.001 ± 0.001 (0.26)
1997–2010	−0.021 ± 0.053 (0.01)	0.026 ± 0.049 (0.16) ^a	−0.008 ± 0.028 (0.04)	0.013 ± 0.008 (0.67)	−0.007 ± 0.010 (0.15)	0.003 ± 0.009 (0.08) ^a	−0.003 ± 0.006 (0.02)	0.003 ± 0.002 (0.70)
Long-term mean								
1981–2018	−0.015 ± 0.007 (0.37)	0.007 ± 0.014 (0.03) ^b	−0.015 ± 0.007	−0.002 ± 0.003 (0.07)	−0.004 ± 0.002 (0.45)	$−4.86 \times 10^{-4} \pm 0.003$ (0.01) ^b	−0.003 ± 0.002	$−2.1 \times 10^{-4} \pm$ 4×10^{-4} (0.01)

^a The temporal coverage of the Argo dataset starts in 2001. Thus, the trend is calculated for 2001–2010. ^b period 2001–2018.

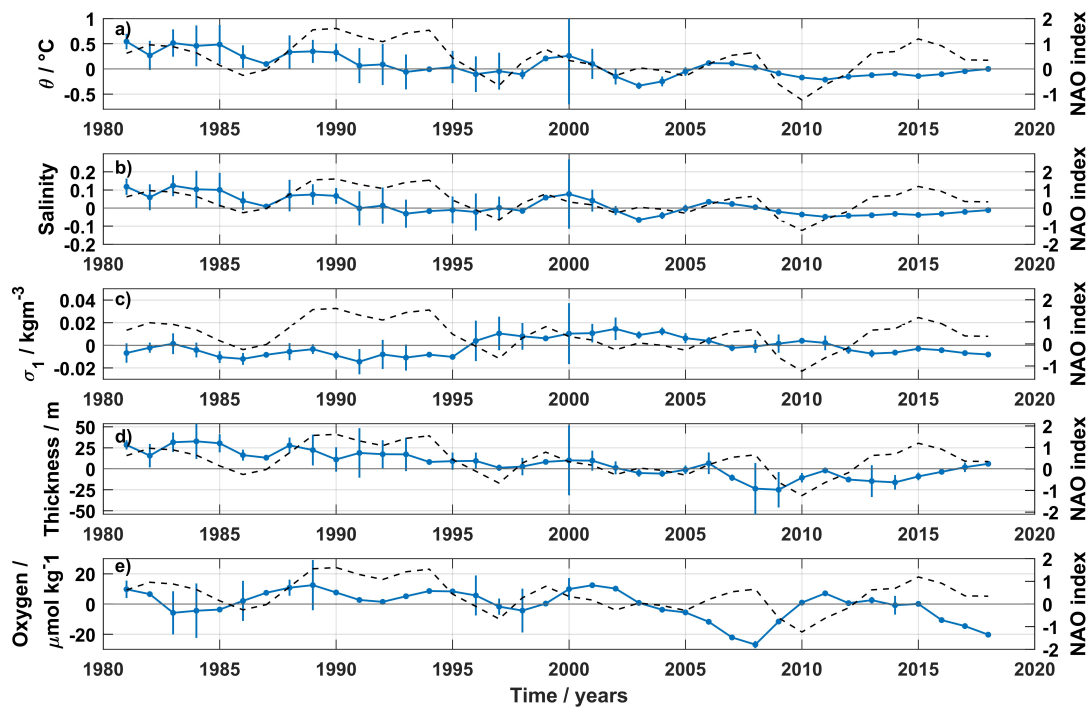


Figure 2. Annual mean anomaly time-series (1981–2018) of potential temperature (a), salinity (b), potential density (σ_1 , corresponding to 1000 dbar) (c), thickness (d) and dissolved oxygen (e) averaged at the core of MOW (between 1000 and 1100 dbar). Black dashed line is the 3-years moving mean NAO-winter index [46]. The annual anomalies were averaged over the entire study area in Figure 1a and smoothed using a 3-year moving average. Error bars represent the standard error of the mean. Points without error bars were interpolated using a 3-point mean filter.

2.2. North Atlantic Oscillation (NAO)

The North Atlantic Oscillation is the most dominant mode of interannual to decadal-scale atmospheric variability in the North Atlantic basin [47]. In this study, the winter NAO-index (December to March) was used. It is a normalized index based on the sea level pressure anomalies between Lisbon and Iceland [46].

3. Results

3.1. Interannual Variability of MOW's Properties Core

Annual mean anomaly time-series of the MOW's properties at the core are presented in Figure 2. Interannual variability (expressed as the standard deviation) is particularly striking in temperature and salinity until 2005, and in dissolved oxygen until 2010, and it is reduced afterwards (Figure 2). The variability calculated before the introduction of Argo and Bio-Argo floats might be overestimated due to the lower number of CTD profiles (Figure 1c,d), together with a sparse spatial and temporal resolution (Supplementary Figure S1).

At the MOW core, the temperature and salinity decreased over the period 1981–2018 (Figure 2a,b). However, the cooling and freshening observed were not persistent over time. Before the Argo era, the temperature and salinity decreased until 1996, followed by warming and salinification until 2000. When considering the separate datasets, after 2000, both CTD and Argo time-series differ during the first decade—the temperature and salinity time-series from CTD show a decrease until 2005, followed by a slight increase until 2010,

while the time-series using only Argo floats show the opposite behavior (Supplementary Figure S1), similar to observations presented by Soto-Navarro et al. [21] west of the Iberian Peninsula region. However, from 2010 onwards, both time-series converge to similar values with a slight increase in temperature and salinity (Supplementary Figure S1). The differences between both datasets are probably due to the different spatial and seasonal coverage of each dataset (see Supplementary Figure S1). While the Argo dataset has a more uniform temporal and spatial distribution throughout the year (Supplementary Figure S1c,d), the CTD were mostly obtained during spring and summer months (twice as many as in autumn/winter; Supplementary Figure S1b). Together with the uneven temporal resolution, the spatial distribution of the CTD profiles fails to be as homogeneous as the one provided by the Argo floats (Supplementary Figure S1a,c).

Examination of the CTD/Argo data shows, on a decadal scale, the mean temperature and salinity were highest in the 1980s (9.302 ± 0.099 °C and 35.754 ± 0.024), decreased afterwards (8.936 ± 0.144 °C and 35.677 ± 0.033 in the 1990s to 8.852 ± 0.040 °C and 35.655 ± 0.008 in the 2000s to 8.819 ± 0.019 °C and 35.641 ± 0.004 after 2011). Regarding the trends over decades, although both CTD/Argo and EN4 datasets showed a decrease in temperature and salinity during the 1980s, the trends are not significant (Table 1). In the 1990s and the 2000s, only the EN4 product shows significant trends, with freshening and cooling during the 1990s, reversing to warming and salinification after 2000. Although the combined dataset and the EN4 product disagree on the sign of the trends in the 1990s, all datasets agree with significant warming and salinification after 2010 (Table 1). The difference in trends calculated using the EN4 and the combined datasets can be attributed to various reasons. Some authors (e.g., [48,49]) attribute these differences to the data analysis methods, the way that scarce data are averaged and also to the techniques used to fill the gaps in time-series. For instance, before the Argo era, the CTD dataset's spatial coverage was too scarce and we did not interpolate the properties for all the points of the grid. Opposite to our approach, the objective analysis in the EN4 dataset combines a background climatology of the ocean state with the available profiles to calculate the temperature and salinity fields [32].

The density anomaly of the MOW core has almost no interannual variability before 1995. After 1995, the density increased over ten years, decreasing to 1980s values after 2011 (Figure 2c). Overall, the time-series shows no trends for the whole period, suggesting that the changes observed at the core are density-compensated [19].

The amount of MOW (defined here as the distance between the isopycnals $\sigma_1 = 31.8$ and $\sigma_1 = 32.25$ kg m⁻³) decreased by -1.12 ± 0.41 m year⁻¹ during the period 1981–2018. More MOW was present in the NEA until the beginning of 2000s, followed by a period of almost below-average values until 2016 (Figure 2d). In the NEA, the MOW's thickness decreases westward from the Gulf of Cadiz. We calculated a mean thickness of 470 m at 30° W and 570 m at 15° W. Our values are somewhat different from Bashmachnikov et al. [44], who calculated 400 m thickness at 30°W and ≈ 800 m at 15°W. The authors estimated the percentage of MOW in the water column, and they identified three cores of MOW, reaching deeper than 1600 m. Our estimations of MOW's thickness are restricted to the thickness between the main and the lower core of MOW [10], disregarding the mixing between the lower core of MOW and the upper North Atlantic Deep Water in the NEA. Year-to-year variability is more remarkable at the upper limit ($\sigma_1 = 31.8$ kg m⁻³) rather than the lower limit of MOW ($\sigma_1 = 32.25$ kg m⁻³), due to the different circulation dynamics above and below the MOW [10,12,50]. While the subtropical recirculation controls the upper limit, the lower limit is influenced by the Labrador Sea Water (LSW) circulation from the north and the Antarctic Intermediate Water (AAIW) from the south. After 2006, the upper limit's mean position deepened, reaching a more stable position after 2013. The deepening of the $\sigma_1 = 31.8$ -isopycnal might be a response to the extreme winter mixing event in 2005, leading to the formation of denser central water, that spread over the regions off the Iberian Peninsula to North Africa in the following years [51]. The lower limit was deeper until 1996, followed by 13 years with a shallower position. A thin (thicker) LSW might explain

the deepening (uplift) of the lower limit in the 1980s (1990s), allowing (restricting) the expansion of MOW into the central North Atlantic [52]. However, the authors estimated an approximate 6-years transit time of the LSW into the central Atlantic. Thus, the deepening (shallowing) of the lower limit in the 1980s (late 1990s) might be explained by thin (thicker) LSW formed during the 1970s (beginning of the 1990s). The upper limit deepened on a rate of 0.51 ± 0.37 dbar year⁻¹, while the $\sigma_1 = 32.25$ kg m⁻³ isopycnal shallowed by -0.58 ± 0.45 dbar year⁻¹ over the period 1981–2018.

The dissolved oxygen concentration decreased by -0.426 ± 0.276 $\mu\text{mol kg}^{-1}$ year⁻¹ between 1981–2018. Before 2000, the annual mean oxygen concentration at the MOW core shows low variability on an interannual scale. After 2002, the oxygen concentration decreases to a minimum in 2008. Although a weak long-term trend was estimated, the mean oxygen concentration shows more variability on a decadal-scale than on the interannual scale (Figure 2e). In a recent study, Mavropoulou et al. [53] analyzed the oxygen concentration in the Mediterranean basin, and they did not find a long-term trend since the 1960s. However, they noticed that the oxygen varied instead on an inter-decadal scale, attributing those changes to the significant deep water formation events in the eastern Mediterranean basin (known as the Eastern Mediterranean Transient in the late 1980s until mid-1990s) and in the western Mediterranean basin (the Western Mediterranean Transient between 2004–2006) [54]. In the NEA, deoxygenation at intermediate levels was also reported [55–57], and it was attributed to large scale changes in circulation as well as ventilation in connection with solubility. Additionally, a link between warming and a decrease in oxygen concentration on a global scale in the upper 1000 m layer was reported by Helm et al. [58] and Schmidtko et al. [59]. In our case, the observed weak decrease in oxygen concentration might be connected with the warming of the outflow waters in the Strait of Gibraltar [28,29].

3.2. NAO Impact at MOW Core Properties

The impact of NAO in the North Atlantic has been studied intensively in the last few decades, with reported changes in large-scale circulation, water mass properties, as well as on the ecosystems level. Although the effect of NAO affects the upper water column primarily, some authors observed the influence of NAO in water mass changes and properties at intermediate depths [28,30,52].

The temperature and salinity anomaly time-series at the core show a correlation with the NAO, with correlation coefficients of 0.38 and 0.29 (both with $p < 0.05$), respectively (Figures 2a,b and 3a). However, the effect of NAO at such depths is not immediate, and it is “felt” with delay. The strongest correlation between temperature and salinity anomalies with NAO occur with a lag of 8 (0.51, $p < 0.05$) and 7 years (0.45, $p < 0.05$), respectively, with both properties lagging the NAO (Figure 3a).

The cross-correlation between the anomaly time-series from the EN4 gridded product and NAO are presented in Figure 3b. Although there are differences between these time-series and the combined CTD/Argo dataset (see Supplementary Figure S3), the maximum correlation coefficients are observed for the same time-lag in temperature (7 years, $\rho = 0.57$, $p < 0.05$) and salinity (8 years, $\rho = 0.44$, $p < 0.05$). Time-scales of the same order were interpreted by Eden & Willebrand [60] as a delayed baroclinic ocean response to the NAO. The density anomaly at the core and the NAO are strongly correlated at 0 lag (-0.50 , $p < 0.05$) and at 7 years (-0.41 , $p < 0.05$), supporting the delayed response of the ocean to NAO.

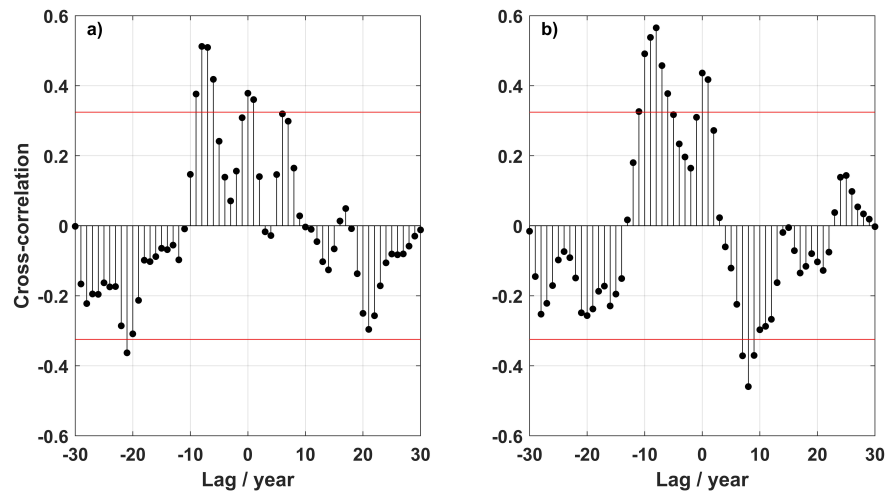


Figure 3. (a) Cross-correlation between the North Atlantic Oscillation and the CTD/Argo temperature detrended anomaly time-series, and the EN4 temperature anomaly time-series (b). The cross-correlation was calculated using 3-years running mean of both NAO-winter index and the annual mean temperature anomaly time-series. Red lines represent the upper and lower 95% confidence bounds.

4. Discussion

We have shown that the changes in the MOW's properties at the core (temperature, salinity and dissolved oxygen) and also the MOW's thickness changed in the last 40 years, at inter-annual to decadal time-scales.

The outflow of the Mediterranean Water through the Strait of Gibraltar is mainly composed of a mixture of intermediate and deep waters—the Levantine Intermediate Water (LIW) and the Western Mediterranean Deep Water (WMDW). The LIW is formed through open-sea convection in the eastern Mediterranean basin and flows across the Strait of Sicily into the western basin [61]. The WMDW is formed in the Gulf of Lion by winter deep convection [62] and flows through the Strait of Gibraltar. Recently, Millot et al. [24] showed that the Tyrrhenian Deep Water (TDW) contributed to the outflow water composition after the 2000s.

Since 1981, we estimated cooling of $-0.015 \pm 0.007 \text{ } ^\circ\text{C year}^{-1}$ and freshening by $-0.003 \pm 0.002 \text{ year}^{-1}$ at the core of MOW in the northeast Atlantic using the CTD/Argo dataset (Table 1). Over the recent years, most trends estimated for the MOW's properties in the North Atlantic were calculated for time-series shorter than 20 years, with just a few studies using time-series longer than 40 years (Table 2). Until the early 1980s, the trends calculated in the NEA showed clear warming and salinification at intermediate depths (Table 2), following the warming and salinification of the Mediterranean waters. However, after the 1980s, some authors reported cooling and freshening (e.g., [20,23]), or no trends at all (Table 1 in [21]) in the NEA, while the waters in the Mediterranean basin continued to warm and get saltier.

The calculated trends in the NEA after the 1980s contradict the warming and salinification of the intermediate and deep waters in the Mediterranean basin reported since the 1950s, as well as for the outflow waters into the North Atlantic (Table 2). One reason might be the dilution of the outflow waters at the Strait of Gibraltar. In the NEA, the highest percentage of around 50–60% of MOW is found at the main core layer of MOW (900 m–1000 m) [44]. However, the percentage of MOW at the core decreases substantially westward, reaching values below 40% for the lower core south of the Azores region [44]. Also, Fiúza et al. [63] estimated that the lower core dilutes 0.06/100 km in salinity and 0.05 $^\circ\text{C}/100 \text{ km}$ in temperature for the northward pathways along the western Iberian Peninsula. A careful inspection of the trends calculated for the Mediterranean basin and

also for the outflow waters reveals that those trends are of the order of 10^{-3} for periods longer than 20 years (Table 2). Considering that after MOW leaves the Strait of Gibraltar, the outflow waters experience strong mixing in the Gulf of Cadiz region, it is possible that the trends calculated for the NEA over such long periods might be not significant or even reversed. Leadbetter et al. [20] suggested that the warming observed between 1981 and 2005 was due to change in the source water, as also reported by Millot et al. [24]. However, Lozier & Sindlinger [25] using a box model showed that source water changes have almost no impact on interannual to decadal variability of MOW's properties. In the same study, the authors suggested that changes in the North Atlantic basin circulation alter the main pathways of MOW, and in consequence, the properties of MOW.

To investigate whether the different NAO phases would possibly influence the detection of different MOW core properties, we divided the properties time-series into different periods. Between 1981 and 1996, the NAO was predominantly in a positive phase. During this period, the MOW core cooled and freshened (Table 1). After the negative NAO in 1997, the NAO index was rather neutral until 2010, and the MOW's properties at the core do not show any significant trend for the combined dataset (Table 1). Using the EN4 dataset, the MOW core during this period was warmer and saltier. In contrast, after the NAO negative phase in 2010, the NAO return to a more positive phase, and the MOW core warmed and became saltier (Table 1).

The reverse of trends at the MOW core in the NEA seems to be an indirect response to the NAO-phase, in a way that a positive (negative) NAO phases induce a more westward (northward) MOW propagation. Thus, the trends detected in our study area might be related to the expansion/retraction of the MOW tongue. The mean salinity distribution around the MOW core during a period of predominantly negative NAO (1965–1974) and positive NAO (1985–1994) are presented in Figure 4a,b, together with the salinity difference between the two periods (Figure 4c). Since the changes at the MOW core in the NEA are density-compensated, only the salinity is shown. During a negative NAO-phase, the expansion of the MOW tongue westward is more restricted compared with the positive NAO-phase (Figure 4a,b, red colours). In contrast, the salinity is higher along the northward pathway of MOW during a negative NAO-phase. The difference between the two periods enables a better view of the dynamic of MOW in the NEA. A negative anomaly of salinity appears along the westward pathway of MOW in contrast with a positive anomaly along the northward MOW pathway (Figure 4c). The northward penetration of MOW was already studied by several authors (e.g., [25,31,64]). These authors showed that during periods of negative (positive) NAO-phase, the Subpolar Front shifts westward (eastward), allowing (blocking) the penetration of the MOW into higher latitude, into the Subpolar gyre. Also, Chaudhuri et al. [27] and Bozec et al. [26], using model simulations, showed that under different NAO-phases, the circulation and distribution of water masses at intermediate depths in the North Atlantic is different. At times of a positive NAO-phase, the flow of MOW into higher latitudes is blocked, and a westward extension of the MOW tongue is observed [26,27] (Figure 4b). The warming and salinification of MOW reported by Potter & Lozier [19] and Leadbetter et al. [20] covered a long period of negative NAO in the 1950s and 1960s shifting to a positive phase in the late 1970s [65]. In contrary, the cooling and freshening calculated by Leadbetter et al. [20] at 36° N after 1981 comprise a time-span of positive and neutral values of NAO (after a strongly negative NAO in 1996). Also, during the neutral phase of NAO in the 2000s, no trends were determined in the NEA (Table 1 in [21]).

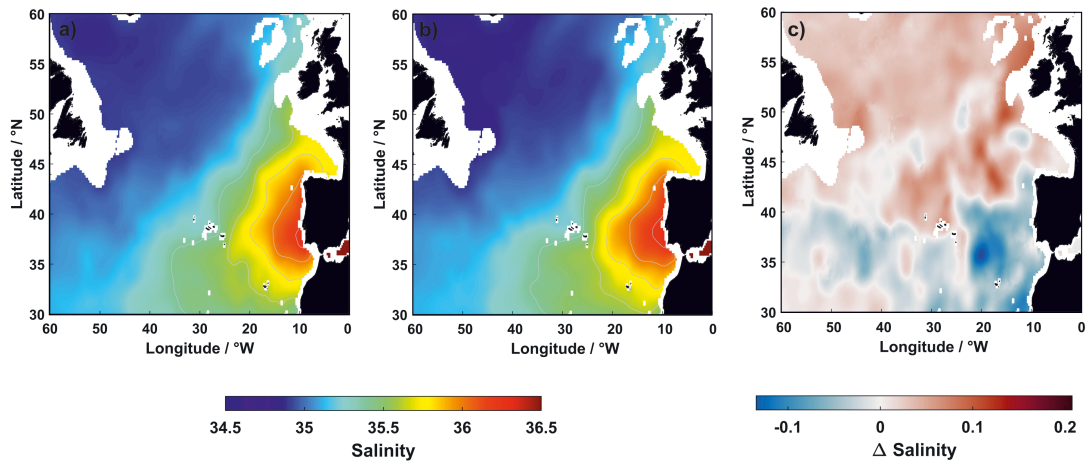


Figure 4. (a) Salinity distribution averaged at the core of Mediterranean Outflow Water (MOW) (1000–1100 m) from the World Ocean Atlas (WOA18 in [33]) between 1965–1974 and (b) between 1985–1994. (c) Salinity difference between the periods 1965–1974 and 1985–1994.

Table 2. Summary of in situ potential temperature and salinity trends in the Northeast Atlantic basin, at the Strait of Gibraltar and in the Mediterranean Sea. The period refers to the considered time span for which the trends were calculated. The dataset gives the source used. n.s.: trends are not significant; n.a. not applicable in the considered study.

Area	Period	Dataset	Depth Range (m)	Trend		Reference
				Temperature	Salinity	
North Atlantic basin						
30°–40° N; 20°–5° W	1955–1993	CTD	1150	0.101 °C/decade	0.0283/decade	[19]
32°–42° N; 25°–10° W	1955–2003	HYDROBASE2	1100	0.119 °C/decade	0.024/decade	[26]
28°–42° N; 24°–5° W	2002–2010	Argo	600–1200	n.s.	n.s.	[21]
Kiel 276 (33° N, 22° W)	1980–2009	Mooring	1000	0.03 °C/y ^a	n.a.	[42]
Bay of Biscay/43°30′–43°54′ N; 3°47′ W	1995–2003	CTD	700–1000	0.023 °C/y	0.005/y	[22]
Bay of Biscay/43.5–48° N; 10°–1° W	2004–2013	Argo	600–1200	–0.011 °C/y	–0.005/y	[23]
24.5° N; 35°–25° W	1957–2004	CTD	900–1750	0.0014 °C/y	–0.0002/y	[66]
53° N; 25°–15° W	1992–2002	CTD	27.45 < σ_0 < 27.65	0.049 °C/y	0.0088/y	[64]
32°S–36° N	1920–1990	CTD	1000–2000	0.005 °C/y	n.d.	[18]
Gulf of Cadiz/35.5°–37° N; 9°–5.9° W	1948–1999	MEDATALAS II + WOD2005	700–1400	0.16°/decade	0.05/decade	[67]
Strait of Gibraltar						
Espartel sill/35°51.70′ N; 5°58.60′ W	2004–2010	Mooring	≈360	0.0017 °C/y	–0.0022/y	[21]
	2005–2009	Mooring	≈360	0.0091 °C/y	–0.0056/y	[68]
	2005–2016	Mooring	≈360	0.0069 °C/y	0.0013/y	[29]
Eastern Strait	2009–2014	CTD	WMDW	0.009 °C/y	0.003/y	[69]
Mediterranean basin						
Western Mediterranean	1943–2000	Medatlas 2002	600–bottom	0.002 °C/y	9.2×10^{-4} /y	[70]
Western Mediterranean	1943–2015	Medatlas + RADMED	600–bottom	0.004 °C/y	0.001/y	[71]
MEDOC area	1969–1987	CTD	1850–2050	0.0027 °C/y	0.0019/y	[72]
Balearic Sea	1996–2005	CTD	600–bottom	0.011 °C/y	0.003/y	[73]
Africa–42° N; 0°–10° E	1909–1955	NODC + CTD	2000	8.19×10^{-4} °C/y	3.88×10^{-4}	[74]
	1955–1989	NODC + CTD	2000	0.0016 °C/y	9.45×10^{-4}	[74]
Western basin	1959–1994	CTD	2000–bottom	0.0036 °C/y ^a	0.0011/y	[75]
38°–46° N; 0°–10° E	1955–2006	CTD + Argo	WMDW	0.0036 °C/y	0.0015/y	[76]
DYFAMED site/WMDW	1995–2004	MEDATALAS II	400–1200	0.012 °C/y	0.0043/y	[77]
DYFAMED site	1995–2004	CTD	1800	0.0054 °C/y	0.002/y	[78]
DYFAMED site	1995–2005	CTD	1974	0.005 °C/y	0.0022/y	[79]
Gulf of Lion	1960–1994	CTD	1000–bottom	0.0016 °C/y	8×10^{-4} /y	[28]
Gulf of Lion	2009–2013	Mooring + Buoy + CTD	1000–2300	0.0032 °C/y	0.0033/y	[80]
Tyrrhenian sea	1996–2001	Mooring	>3000	0.016 °C/y	0.008/y	[81]
Ligurian Sea	1950–1973	CTD	300–400	0.0068 °C/y	0.0018/y	[75]
Western basin/LIW	1943–2000	CTD	500	0.004 °C/y	0.0011/y	[82]
Western basin/LIW	1943–2000	CTD	200–600	0.0005 °C/y	13×10^{-4} /y	[70]
41°–42° N; 5°–7.5° E	1990–2005	CTD + Argo	500–600	n.s.	9.17×10^{-4}	[76]
Levantine Basin/LIW	1979–2014	CTD	≈150–350	0.03 °C/y	0.005/y	[83]

^a Trend was calculated using in situ temperature.

5. Conclusions

In the Northeast Atlantic, the MOW experience periods of cooling/freshening and warming/salinification from 1981 onwards, after a prolonged period of warming and salinification since the 1950s. The temperature and salinity increased in the last decade (2011 onwards), after a long period of cooling and freshening (1981–1996). The opposite trends at the MOW core seems to be related to the different phases of NAO. During a prolonged positive NAO-phase (1981–1996), the temperature and salinity decreased. In contrast, warming and salinification were observed after the NAO-phase changed from negative to positive (from 2011 onwards). The different direction of trends detected in the NEA can be interpreted as an adjustment of the large scale circulation at intermediate depths in response to the NAO-phase, insofar a positive NAO-phase induce a more westward MOW propagation in opposition to a negative NAO-phase, where the MOW propagation is preferentially northward. However, the NAO-phase effect at intermediate depths leads the changes at the core properties by 7–8 years. The oxygen concentration at the core also decreased after 1981, but no connection to the NAO was found. The oxygen concentration at the MOW shows more inter-decadal variability, most likely linked to the variability on decadal-scale, associated with the different deep water formation events in the Mediterranean Sea. Also, the decrease in oxygen concentration might be connected to the warming of the outflow waters, which decreases the solubility of oxygen. However, we should point out that the effect of biological activity on dissolved oxygen levels was not considered.

The results presented here indicate weak cooling and freshening over the entire period in both datasets (CTD/Argo and EN4 product) for the region studied. It is important to note that the trends calculated are averaged for the entire box in Figure 1a, and might not translate all the dynamics in the study area or in a different (sub)domain. Although the results for the individual periods or decades are partly contradicting each other, they highlight the importance of a careful choice of the dataset for analyzing climate signals at mid-depths.

Supplementary Materials: The following are available online at <https://www.mdpi.com/2673-1924/2/1/16/s1>, Figure S1. (a) Number of temperature and salinity CTD profiles for each box of the $2^\circ \times 2^\circ$ grid over the study domain in Figure 1a. (b) Histogram with the number of CTD profiles per season. (c) Same as (a) but for the number of Argo floats. (d) Same as (b) but with respect to the number of Argo floats. Figure S2. Annual mean potential temperature (a), salinity (b), potential density (with reference to 1000 dbar) (c), thickness (d), and dissolved oxygen concentration (e) averaged at the core of MOW (between 1000 and 1100 dbar). The blue time-series were calculated using only CTD profiles, and the red time-series were determined using only Argo/Bio-Argo profiles. Black dashed time-series are the 3-years moving mean winter NAO-index. The annual means were averaged over the entire domain of Figure 1a and smoothed with a 3-years running mean. Error bars represent the standard error of the mean. Points without error bars were interpolated using a 3-point moving mean filter. Figure S3. Annual mean potential temperature (a), and salinity (b) averaged at the core of MOW (between 1000 and 1100 dbar). The blue time-series were calculated using the combined CTD and Argo profiles, and the yellow time-series were determined using the EN4 gridded product. The annual means were averaged over the entire domain of Figure 1a and smoothed with a 3-years running mean. Error bars represent the standard error of the mean. Points without error bars were interpolated using a 3-point moving mean filter. Table S1. Hydrographic data used from cruises in the Northeast Atlantic within the study domain of Figure 1a obtained from the PANGAEA, ICES repository, CCHDO, and BODC data centres for the period 1981–2018. The date format includes the month and year.

Author Contributions: Conceptualization H.C.F.; data analysis H.C.F.; writing—original draft preparation, H.C.F.; writing—review and editing, H.C.F., J.J.W.; funding acquisition, J.J.W. All authors have read and agreed to the published version of the manuscript.

Funding: J.J.W. thanks the Deutsche Forschungsgemeinschaft (DFG) for many years of financial support for cruises in the study area during various projects (WA2175/1-1 to 2175/5-1).

Data Availability Statement: Argo data were collected and made freely available by the International Argo Programme and the national programmes that contribute to it. The Argo Programme is part of the Global Ocean Observation System. Objective analysis fields were obtained from the UK Met Office EN4 product (<http://www.metoffice.gov.uk/hadobs/en4/>, accessed on 18 October 2020).

Acknowledgments: We thank the many investigators who contribute to the databases and all people on board of numerous cruises used in this study. We also thank the three anonymous reviewers for valuable suggestions to improve our study.

Conflicts of Interest: The authors declare no conflict of interest. The funders had no role in the design of the study; in the collection, analyses, or interpretation of data; in the writing of the manuscript, or in the decision to publish the results.

Abbreviations

The following abbreviations are used in this manuscript:

AAIW	Antarctic Intermediate Water
CTD	Conductivity, Temperature, Depth
LIW	Levantine Intermediate Water
LSW	Labrador Sea Water
MOW	Mediterranean Outflow Water
NAO	North Atlantic Oscillation
NEA	Northeast Atlantic
TDW	Tyrrhenian Deep Water
WMDW	Western Mediterranean Deep Water
WOA	World Ocean Atlas
WOD	World Ocean Database

References

- Zenk, W. On the Mediterranean outflow west of Gibraltar. *Meteor-Forschungsergebnisse A* **1975**, *16*, 35–43.
- Ambar, I.; Howe, M.R.; Abdullah, M.I. A Physical and Chemical Description of the Mediterranean Outflow in the Gulf of Cadiz. *Dtsch. Hydrogr. Z.* **1976**, *29*, 58–68. [[CrossRef](#)]
- Reid, J.L. On the contribution of the Mediterranean Sea outflow to the Norwegian-Greenland Sea. *Deep-Sea Res. Part A Oceanogr. Res. Pap.* **1979**, *26*, 1199–1223. [[CrossRef](#)]
- Bower, A.S.; Serra, N.; Ambar, I. Structure of the Mediterranean Undercurrent and Mediterranean Water spreading around the southwestern Iberian Peninsula. *J. Geophys. Res.* **2002**, *107*, 3161. [[CrossRef](#)]
- Reid, J.L. On the Middepth Circulation and Salinity Field in the North Atlantic Ocean. *J. Geophys. Res.* **1978**, *83*, 5063–5067. [[CrossRef](#)]
- Iorga, M.C.; Lozier, M.S. Signatures of the Mediterranean outflow from a North Atlantic climatology: 1. Salinity and density fields. *J. Geophys. Res.* **1999**, *104*, 25985–26009. [[CrossRef](#)]
- Serra, N.; Ambar, I.; Käse, R.H. Observations and numerical modelling of the Mediterranean outflow splitting and eddy generation. *Deep-Sea Res. II* **2005**, *52*, 383–408. [[CrossRef](#)]
- Armi, L.; Zenk, W. Large Lenses of Highly Saline Mediterranean Water. *J. Phys. Oceanogr.* **1984**, *14*, 1560–1576. [[CrossRef](#)]
- Richardson, P.L.; McCartney, M.S.; Maillard, C. A search for meddies in historical data. *Dyn. Atmos. Ocean.* **1991**, *15*, 241–265. [[CrossRef](#)]
- van Aken, H.M. The hydrography of the mid-latitude Northeast Atlantic Ocean II: The intermediate water masses. *Deep-Sea Res. I* **2000**, *47*, 789–824. [[CrossRef](#)]
- Siedler, G.; Armi, L.; Müller, T.J. Meddies and decadal changes at the Azores Front from 1980 to 2000. *Deep-Sea Res. II* **2005**, *52*, 583–604. [[CrossRef](#)]
- Carracedo, L.I.; Gilcoto, M.; Mercier, H.; Pérez, F.F. Seasonal dynamics in the Azores-Gibraltar Strait region: A climatologically-based study. *Prog. Oceanogr.* **2014**, *122*, 116–130. [[CrossRef](#)]
- Sánchez-Leal, R.F.; Bellanco, M.J.; Fernández-Salas, L.M.; García-Lafuente, J.; Gasser-Rubinat, M.; González-Pola, C.; Hernández-Molina, F.J.; Pelegrí, J.L.; Peliz, A.; Relvas, P.; et al. The Mediterranean Overflow in the Gulf of Cadiz: A rugged journey. *Sci. Adv.* **2017**, *3*, eaao0609. [[CrossRef](#)] [[PubMed](#)]
- Izquierdo, A.; Mikolajewicz, U. The role of tides in the spreading of Mediterranean Outflow waters along the southwestern Iberian margin. *Ocean. Model.* **2019**, *133*, 27–43. [[CrossRef](#)]
- de Pascual-Collar, Á.; Sotillo, M.G.; Levier, B.; Aznar, R.; Lorente, P.; Amo-Baladrón, A.; Álvarez-Fanjul, E. Regional circulation patterns of Mediterranean Outflow Water near the Iberian and African continental slopes. *Ocean Sci.* **2019**, *15*, 565–582. [[CrossRef](#)]

16. Candela, J. Chapter 5.7 Mediterranean water and global circulation. In *Ocean Circulation and Climate*; Siedler, G., Church, J., Gould, J., Eds.; Academic Press: Cambridge, MA, USA, 2001; Volume 77, pp. 417–429. [CrossRef]
17. Levitus, S.; Antonov, J.I.; Boyer, T.P.; Stephens, C. Warming of the World Ocean. *Science* **2000**, *287*, 2225–2229. [CrossRef]
18. Arbic, B.K.; Owens, W.B. Climatic Warming of Atlantic Intermediate Waters. *J. Clim.* **2001**, *14*, 4091–4108. [CrossRef]
19. Potter, R.A.; Lozier, M.S. On the warming and salinification of the Mediterranean outflow waters in the North Atlantic. *Geophys. Res. Lett.* **2004**, *31*, L01202. [CrossRef]
20. Leadbetter, S.J.; Williams, R.G.; McDonagh, E.L.; King, B.A. A twenty year reversal in water mass trends in the subtropical North Atlantic. *Geophys. Res. Lett.* **2007**, *34*, L12608. [CrossRef]
21. Soto-Navarro, J.; Criado-Aldeanueva, F.; Sánchez-Garrido, J.C.; García-Lafuente, J. Recent thermohaline trends of the Atlantic waters inflowing to the Mediterranean Sea. *Geophys. Res. Lett.* **2012**, *39*, L01604. [CrossRef]
22. González-Pola, C.; Lavín, A.; Vargas-Yáñez, M. Intense warming and salinity modification of intermediate water masses in the northeastern corner of the Bay of Biscay for the period 1992–2003. *J. Geophys. Res.* **2005**, *110*, C05020. [CrossRef]
23. Costoya, X.; deCastro, M.; Gómez-Gesteira, M. Thermocline trends in the Bay of Biscay from Argo floats over the decade 2004–2013. *J. Mar. Syst.* **2014**, *139*, 159–165. [CrossRef]
24. Millot, C.; Candela, J.; Fuda, J.L.; Tber, Y. Large warming and salinification of the Mediterranean outflow due to changes in its composition. *Deep-Sea Res. I* **2006**, *53*, 656–666. [CrossRef]
25. Lozier, M.S.; Sindlinger, L. On the Source of Mediterranean Overflow Water Property Changes. *J. Phys. Oceanogr.* **2009**, *39*, 1800–1817. [CrossRef]
26. Bozec, A.; Lozier, M.S.; Chassignet, E.P.; Halliwell, G.R. On the variability of the Mediterranean Outflow Water in the North Atlantic from 1948 to 2006. *J. Geophys. Res.* **2011**, *116*, C09033. [CrossRef]
27. Chaudhuri, A.H.; Gangopadhyay, A.; Bisagni, J.J. Contrasting Response of the Eastern and Western North Atlantic Circulation to an Episodic Climate Event. *J. Phys. Oceanogr.* **2011**, *41*, 1630–1638. [CrossRef]
28. Krahnmann, G.; Schott, F. Longterm increases in Western Mediterranean salinities and temperatures: Anthropogenic and climatic sources. *Geophys. Res. Lett.* **1998**, *25*, 4209–4212. [CrossRef]
29. Naranjo, C.; García-Lafuente, J.; Sammartino, S.; Sánchez-Garrido, J.C.; Sánchez-Leal, R.; Jesús Bellanco, M. Recent changes (2004–2016) of temperature and salinity in the Mediterranean outflow. *Geophys. Res. Lett.* **2017**, *44*, 5665–5672. [CrossRef]
30. Dickson, R.; Lazier, J.; Meincke, J.; Rhines, P.; Swift, J. Long-term coordinated changes in the convective activity of the North Atlantic. *Prog. Oceanogr.* **1996**, *38*, 241–295. [CrossRef]
31. Lozier, M.S.; Steward, N.M. On the Temporally Varying Northward Penetration of Mediterranean Overflow Water and Eastward Penetration of Labrador Sea Water. *J. Phys. Oceanogr.* **2008**, *38*, 2097–2103. [CrossRef]
32. Good, S.A.; Martin, M.J.; Rayner, N.A. EN4: Quality controlled ocean temperature and salinity profiles and monthly objective analyses with uncertainty estimates. *J. Geophys. Res. Ocean.* **2013**, *118*, 6704–6716. [CrossRef]
33. Zweng, M.M.; Reagan, J.R.; Seidov, D.; Boyer, T.P.; Locarnini, R.A.; Garcia, H.E.; Mishonov, A.V.; Baranova, O.K.; Weathers, K.; Paver, C.R.; et al. *World Ocean Atlas 2018, Volume 2: Salinity*; NOAA Atlas NESDIS 82; NOAA: Washington, DC, USA, 2018; p. 50.
34. Daniault, N.; Mercier, H.; Lherminier, P.; Sarafanov, A.; Falina, A.; Zunino, P.; Pérez, F.F.; Ríos, A.F.; Ferron, B.; Huck, T.; et al. The northern North Atlantic Ocean mean circulation in the early 21st century. *Prog. Oceanogr.* **2016**, *146*, 142–158. [CrossRef]
35. Wong, A.; Wijffels, S.E.; Riser, S.C.; Pouliquen, S.; Hosoda, S.; Roemmich, D.; Gilson, J.; Johnson, G.C.; Martini, K.; Murphy, D.J.; et al. Argo Data 1999–2019: Two Million Temperature-Salinity Profiles and Subsurface Velocity Observations From a Global Array of Profiling Floats. *Front. Mar. Sci.* **2020**, *7*, 700. [CrossRef]
36. Wong, A.; Keeley, R.; Carval, T.; Argo Data Management Team. *Argo Quality Control Manual for CTD and Trajectory Data*; Ifremer: Brest, France, January 2020. [CrossRef]
37. Argo. Argo float data and metadata from Global Data Assembly Centre (Argo GDAC). *SEANOE* **2000**. [CrossRef]
38. Garcia, H.E.; Weather, K.; Paver, C.R.; Smolyar, I.; Boyer, T.P.; Locarnini, R.A.; Zweng, M.M.; Mishonov, A.V.; Baranova, O.K.; Seidov, D.; et al. *World Ocean Atlas 2018, Volume 3: Dissolved Oxygen, Apparent Oxygen Utilization, and Oxygen Saturation*; A. Mishonov Technical Editor; NOAA Atlas NESDIS 83; NOAA: Washington, DC, USA, 2018; p. 38.
39. UNESCO. Algorithms for Computation of Fundamental Properties of Seawater. *UNESCO Tech. Pap. Mar. Sci.* **1983**, *44*, 1–53.
40. Barnes, S.L. *Mesoscale Objective Map Analysis Using Weighted Time-Series Observations*; NOAA Technical Memorandum ERL NSSL 62; NOAA: Washington, DC, USA, 1973.
41. Pierce, S. Stephen Pierce (2020). Barnes Objective Analysis. 2010. Available online: <https://www.mathworks.com/matlabcentral/fileexchange/28666-barnes-objective-analysis> (accessed on 15 November 2020).
42. Frazão, H.C.; Prien, R.D.; Müller, T.J.; Schulz-Bull, D.E.; Waniek, J.J. 30 years of temporal variability of temperature and currents below the main thermocline between 1980–2009 in the subtropical Northeast Atlantic (Kiel 276, 33°N, 22°W). *J. Mar. Syst.* **2021**, *217*, 103517. [CrossRef]
43. Müller, T.J.; Waniek, J.J. *KIEL276 Time Series Data from Moored Current Meters 33°N, 22°W, 5285 m Water Depth. March 1980–April 2011. Background Information and Data Compilation*; GEOMAR Report Nr. 13; GEOMAR: Kiel, Germany, 2013. [CrossRef]
44. Bashmachnikov, I.; Nascimento, A.; Neves, F.; Menezes, T.; Koldunov, N.V. Distribution of intermediate water masses in the subtropical northeast Atlantic. *Ocean. Sci.* **2015**, *11*, 803–827. [CrossRef]
45. Thomson, R.E.; Emery, W.J. Chapter 3—Statistical Methods and Error Handling. In *Data Analysis Methods in Physical Oceanography*, 3rd ed.; Thomson, R.E., Emery, W.J., Eds.; Elsevier: Amsterdam, The Netherlands, 2014; pp. 219–311. [CrossRef]

46. Hurrell, J. The Climate Data Guide: Hurrell North Atlantic Oscillation (NAO) Index (Station-Based). 2020. Available online: <https://climatedataguide.ucar.edu/climate-data/hurrell-north-atlantic-oscillation-nao-index-station-based> (accessed on 4 March 2020).
47. Hurrell, J.; Kushnir, Y.; Ottersen, G.; Visbeck, M. An overview of the North Atlantic oscillation. *Geophys. Monogr. Am. Geophys. Union* **2003**, *134*, 1–36.
48. Hurrell, J.W.; Trenberth, K.E. Global Sea Surface Temperature Analyses: Multiple Problems and Their Implications for Climate Analysis, Modeling, and Reanalysis. *Bull. Am. Meteorol. Soc.* **1999**, *80*, 2661–2678. [[CrossRef](#)]
49. Gregory, J.M.; Banks, H.T.; Stott, P.A.; Lowe, J.A.; Palmer, M.D. Simulated and observed decadal variability in ocean heat content. *Geophys. Res. Lett.* **2004**, *31*, L15312. [[CrossRef](#)]
50. Käse, R.; Zenk, W. Structure of the Mediterranean Water and meddy characteristics in the northeastern Atlantic. In *The Warmwatersphere of the North Atlantic Ocean*; Krauss, W., Ed.; Gebrüder Borntraeger: Berlin, Germany, 1996; pp. 365–395.
51. Somavilla, R.; González-Pola, C.; Rodriguez, C.; Josey, S.A.; Sánchez, R.F.; Lavín, A. Large changes in the hydrographic structure of the Bay of Biscay after the extreme mixing of winter 2005. *J. Geophys. Res.* **2009**, *114*, C01001. [[CrossRef](#)]
52. Curry, R.G.; McCartney, M.S.; Joyce, T.M. Oceanic transport of subpolar climate signals to mid-depth subtropical waters. *Nature* **1998**, *391*, 575–577. [[CrossRef](#)]
53. Mavropoulou, A.M.; Vervatis, V.; Sofianos, S. Dissolved oxygen variability in the Mediterranean Sea. *J. Mar. Syst.* **2020**, *208*, 103348. [[CrossRef](#)]
54. Schroeder, K.; Chiggiato, J.; Bryden, H.L.; Borghini, M.; Ismail, S.B. Abrupt climate shift in the Western Mediterranean Sea. *Sci. Rep.* **2016**, *6*, 23009. [[CrossRef](#)]
55. Johnson, G.C.; Gruber, N. Decadal water mass variations along 20°W in the Northeastern Atlantic Ocean. *Prog. Oceanogr.* **2007**, *73*, 277–295. [[CrossRef](#)]
56. Stendardo, I.; Gruber, N. Oxygen trends over five decades in the North Atlantic. *J. Geophys. Res.* **2012**, *117*, C11004. [[CrossRef](#)]
57. Stendardo, I.; Kieke, D.; Rhein, M.; Gruber, N.; Steinfeldt, R. Interannual to decadal oxygen variability in the mid-depth water masses of the eastern North Atlantic. *Deep-Sea Res. I* **2015**, *95*, 85–98. [[CrossRef](#)]
58. Helm, K.P.; Bindoff, N.L.; Church, J.A. Observed decreases in oxygen content of the global ocean. *Geophys. Res. Lett.* **2011**, *38*, L23602. [[CrossRef](#)]
59. Schmidtko, S.; Stramma, L.; Visbeck, M. Decline in global oceanic oxygen content during the past five decades. *Nature* **2017**, *542*, 335–339. [[CrossRef](#)]
60. Eden, C.; Willebrand, J. Mechanism of Interannual to Decadal Variability of the North Atlantic Circulation. *J. Clim.* **2001**, *14*, 2266–2280. [[CrossRef](#)]
61. Katz, E.J. The Levantine Intermediate Water between the Strait of Sicily and the Strait of Gibraltar. *Deep-Sea Res.* **1972**, *19*, 507–520. [[CrossRef](#)]
62. Stommel, H. Deep winter-time convection in the Western Mediterranean Sea. In *Studies in Physical Oceanography*; Gordon, A.L., Ed.; Gordon and Breach: New York, NY, USA, 1972; Volume 2, pp. 207–218.
63. Fiúza, A.F.G.; Hamann, M.; Ambar, I.; Díaz del Río, G.; González, N.; Cabanas, J.M. Water masses and their circulation off western Iberian during May 1993. *Deep-Sea Res. I* **1998**, *45*, 1127–1160. [[CrossRef](#)]
64. Sarafanov, A.; Falina, A.; Sokov, A.; Demidov, A. Intense warming and salinification of intermediate waters of southern origin in the eastern subpolar North Atlantic in the 1990s to mid-2000s. *J. Geophys. Res.* **2008**, *113*, C12022. [[CrossRef](#)]
65. Hurrell, J. Decadal trends in the North Atlantic Oscillation: Regional temperatures and precipitation. *Science* **1995**, *269*, 676–679. [[CrossRef](#)] [[PubMed](#)]
66. Cunningham, S.A.; Alderson, S. Transatlantic temperature and salinity changes at 24.5°N from 1957 to 2004. *Geophys. Res. Lett.* **2007**, *34*, L14606. [[CrossRef](#)]
67. Fusco, G.; Artale, V.; Cotroneo, Y.; Sannino, G. Thermohaline variability of Mediterranean Water in the Gulf of Cadiz, 1948–1999. *Deep-Sea Res. I* **2008**, *55*, 1624–1638. [[CrossRef](#)]
68. García-Lafuente, J.; Delgado, J.; Sánchez Román, A.; Soto, J.; Carracedo, L.; Díaz del Río, G. Interannual variability of the Mediterranean outflow observed in Espartel sill, western Strait of Gibraltar. *J. Geophys. Res. Ocean.* **2009**, *114*, C10018. [[CrossRef](#)]
69. Naranjo, C.; Sammartino, S.; García-Lafuente, J.; Bellanco, M.J.; Taupier-Letage, I. Mediterranean waters along and across the Strait of Gibraltar, characterization and zonal modification. *Deep. Sea Res. Part I* **2015**, *105*, 41–52. [[CrossRef](#)]
70. Vargas-Yáñez, M.; Zunino, P.; Benali, A.; Delpy, M.; Pastre, F.; Moya, F.; García-Martínez, M.D.C.; Tel, E. How much is the western Mediterranean really warming and salting? *J. Geophys. Res. Ocean.* **2010**, *115*, C04001. [[CrossRef](#)]
71. Vargas-Yáñez, M.; García-Martínez, M.C.; Moya, F.; Balbín, R.; López-Jurado, J.L.; Serra, M.; Zunino, P.; Pascual, J.; Salat, J. Updating temperature and salinity mean values and trends in the Western Mediterranean: The RADMED project. *Prog. Oceanogr.* **2017**, *157*, 27–46. [[CrossRef](#)]
72. Leaman, K.D.; Schoot, F.A. Hydrographic Structure of the Convection Regime in the Gulf of Lions: Winter 1987. *J. Phys. Oceanogr.* **1991**, *21*, 575–598. [[CrossRef](#)]
73. López-Jurado, J.L.; González-Pola, C.; Vélez-Belchí, P. Observation of an abrupt disruption of the long-term warming trend at the Balearic Sea, western Mediterranean Sea, in summer 2005. *Geophys. Res. Lett.* **2005**, *32*, L24606. [[CrossRef](#)]
74. Rohling, E.J.; Bryden, H.L. Man-induced salinity and temperature increases in the Western Mediterranean Deep Water. *J. Geophys. Res.* **1992**, *97*, 11191–11198. [[CrossRef](#)]

75. Béthoux, J.P.; Gentili, B. The Mediterranean Sea, coastal and deep-sea signatures of climatic and environmental changes. *J. Mar. Syst.* **1996**, *7*, 383–394. [[CrossRef](#)]
76. Smith, R.O.; Bryden, H.L.; Stansfield, K. Observations of new western Mediterranean deep water formation using Argo floats 2004–2006. *Ocean. Sci.* **2008**, *4*, 133–149. [[CrossRef](#)]
77. Grignon, L.; Smeed, D.A.; Bryden, H.L.; Schroeder, K. Importance of the variability of hydrographic preconditioning for deep convection in the Gulf of Lion, NW Mediterranean. *Ocean. Sci.* **2010**, *6*, 573–586. [[CrossRef](#)]
78. Schröder, K.; Gasparini, G.P.; Tangherlini, M.; Astraldi, M. Deep and intermediate water in the western Mediterranean under the influence of the Eastern Mediterranean Transient. *Geophys. Res. Lett.* **2006**, *33*, L21607. [[CrossRef](#)]
79. Marty, J.C.; Chiavérini, J. Hydrological changes in the Ligurian Sea (NW Mediterranean, DYFAMED site) during 1995–2007 and biogeochemical consequences. *Biogeosciences* **2010**, *7*, 2117–2128. [[CrossRef](#)]
80. Houpert, L.; Durrieu de Madron, X.; Testor, P.; Bosse, A.; D’Ortenzio, F.; Bouin, M.N.; Dausse, D.; Le Goff, H.; Kunesch, S.; Labaste, M.; et al. Observations of open-ocean deep convection in the northwestern Mediterranean Sea: Seasonal and interannual variability of mixing and deep water masses for the 2007–2013 Period. *J. Geophys. Res. Ocean.* **2016**, *121*, 8139–8171. [[CrossRef](#)]
81. Fuda, J.L.; Etiopie, G.; Millot, C.; Favali, P.; Calcara, M.; Smriglio, G.; Boschi, E. Warming, salting and origin of the Tyrrhenian Deep Water. *Geophys. Res. Lett.* **2002**, *29*, 1898. [[CrossRef](#)]
82. Zunino, P.; Vargas-Yárñez, M.; Moya, F.; García-Martínez, M.C.; Plaza, F. Deep and intermediate layer warming in the western Mediterranean: Water mass changes and heaving. *Geophys. Res. Lett.* **2009**, *36*, L20608. [[CrossRef](#)]
83. Ozer, T.; Gertman, I.; Kress, N.; Silverman, J.; Herut, B. Interannual thermohaline (1979–2014) and nutrient (2002–2014) dynamics in the Levantine surface and intermediate water masses, SE Mediterranean Sea. *Glob. Planet. Chang.* **2017**, *151*, 60–67. [[CrossRef](#)]

Supplementary Materials: Mediterranean Water properties at the eastern limit of the North Atlantic Subtropical Gyre since 1981

Helena C. Frazão and Joanna J. Waniek

1. Introduction

The supporting information includes three additional figures (Figures S1–S3) to complement the results shown and one additional table (Table S1) with complementary information regarding the CTD profiles in addition to the WOD18 used in this study.

In Figure S1 we present a summary of the spatial and temporal distribution of both CTD and Argo datasets in the study domain of Figure 1a.

In Figure S2 we present the time-series of temperature, salinity, potential density (σ_t), thickness, and dissolved oxygen calculated using only CTD profiles (1981–2018) and Argo/Bio-Argo floats (2001–2018; 2010–2017 for the dissolved oxygen).

In Figure S3 we compare the temperature and salinity time-series from two different datasets: EN4 gridded product from UK Met Office [1], and the dataset used in this study.

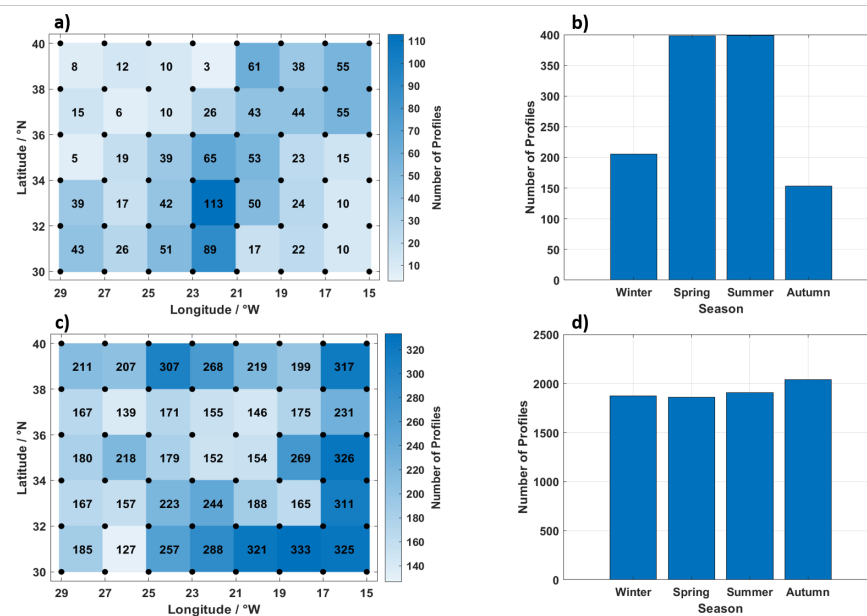


Figure S1. (a) Number of temperature and salinity CTD profiles for each box of the $2^\circ \times 2^\circ$ grid over the study domain in Figure 1(a). (b) Histogram with the number of CTD profiles per season. (c) Same as (a) but for the number of Argo floats. (d) Same as (b) but with respect to the number of Argo floats.

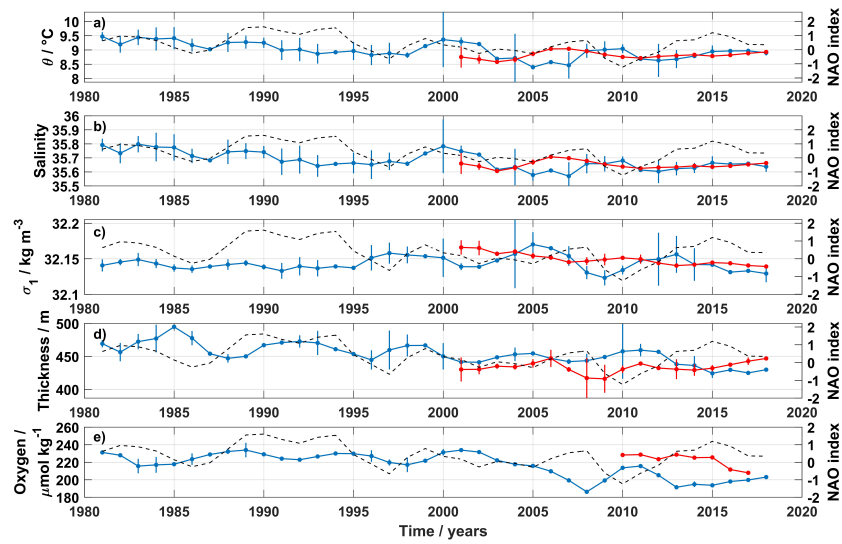


Figure S2. Annual mean potential temperature (a), salinity (b), potential density (with reference to 1000 dbar) (c), thickness (d), and dissolved oxygen concentration (e) averaged at the core of MOW (between 1000 and 1100 dbar). The blue time-series were calculated using only CTD profiles, and the red time-series were determined using only Argo/Bio-Argo profiles. Black dashed time-series are the 3-years moving mean winter NAO-index [DJFM, 2]. The annual means were averaged over the entire domain of Figure 1a and smoothed with a 3-years running mean. Error bars represent the standard error of the mean. Points without error bars were interpolated using a 3-point moving mean filter.

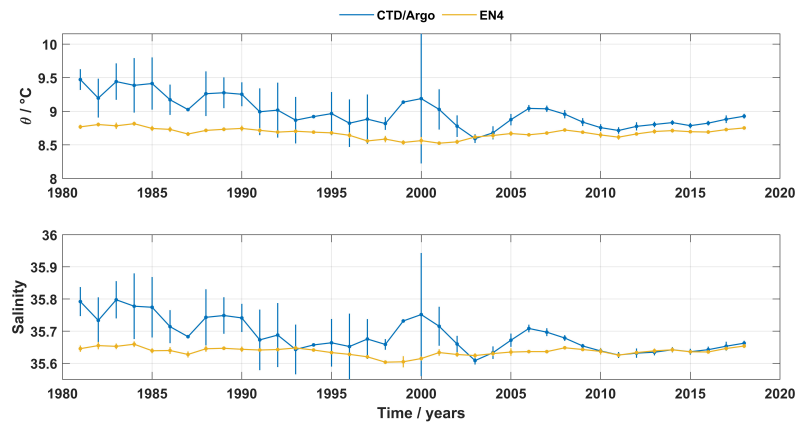


Figure S3. Annual mean potential temperature (a), and salinity (b) averaged at the core of MOW (between 1000 and 1100 dbar). The blue time-series were calculated using the combined CTD and Argo profiles, and the yellow time-series were determined using the EN4 gridded product [? ?]. The annual means were averaged over the entire domain of Figure 1a and smoothed with a 3-years running mean. Error bars represent the standard error of the mean. Points without error bars were interpolated using a 3-point moving mean filter.

Table S1. Hydrographic data used from cruises in the Northeast Atlantic within the study domain of Figure 1.a obtained from the PANGAEA, ICES repository, CCHDO, and BODC data centres for the period 1981–2018. The date format includes the month and year.

Cruise	Research Vessel	Date	Number of Profiles	Reference
D117	RRS Discovery	Jan-Feb/1981	2	https://www.bodc.ac.uk/data/bodc_database/ctd/
316N19810516	Knorr	May-Jun/1981	8	https://cchdo.ucsd.edu/cruise/316N19810516
06PO		Mar-Apr/1982	9	ICES repository
06MT		Oct/1984	1	ICES repository
M9/2	Meteor	Jan/1989	9	https://doi.org/10.1594/PANGAEA.880023
M10/1	Meteor	Apr/1989	3	https://doi.pangaea.de/10.1594/PANGAEA.62022
NAPP90-1	Tyro	Apr-May/1990	15	https://doi.pangaea.de/10.1594/PANGAEA.817065
M14/1	Meteor	Sep/1990	1	https://doi.pangaea.de/10.1594/PANGAEA.880027
03OC240_2	Oceanus	May-Jun/1991	3	https://doi.pangaea.de/10.1594/PANGAEA.290745
07AL991_3	Alexander von Humboldt	Sep-Oct/1991	11	https://doi.org/10.1594/PANGAEA.290774
90MD46_1	Dmitry Mendelejev	Sep-Nov/1991	17	https://cchdo.ucsd.edu/cruise/90MD46_1
32OC254_4	Oceanus	Dez/1992	1	https://cchdo.ucsd.edu/cruise/32OC254_4
POS200	Poseidon	Apr&Jul/1993	10	https://doi.pangaea.de/10.1594/PANGAEA.914338
3175MB93	Malcolm Baldrige	Jul-Aug/1993	5	https://doi.pangaea.de/10.1594/PANGAEA.290789
90CT40_1	Professor Multanosvskiy	Sep-Oct/1993	15	https://doi.pangaea.de/10.1594/PANGAEA.293942
90P431_1	Professor Shtokman	Oct/1993	26	https://cchdo.ucsd.edu/cruise/90P431_1
CD83	Charles Darwin	Dec/1993	2	https://doi.org/10.1594/PANGAEA.805824
POS202	Poseidon	Sep/1994	2	https://doi.pangaea.de/10.1594/PANGAEA.93019
POS212/2	Poseidon	Sep/1995	3	https://doi.pangaea.de/10.1594/PANGAEA.93018 https://doi.pangaea.de/10.1594/PANGAEA.93125 https://doi.pangaea.de/10.1594/PANGAEA.93126 https://doi.pangaea.de/10.1594/PANGAEA.93128
POS212/4	Poseidon	Oct/1995	1	https://doi.pangaea.de/10.1594/PANGAEA.817060
DCM	Tydeman	Aug/1996	1	https://doi.pangaea.de/10.1594/PANGAEA.761693
M37/2	Meteor	Jan/1997	10	https://doi.org/10.1594/PANGAEA.816974
POS231/3	Poseidon	Aug/1997	2	https://doi.pangaea.de/10.1594/PANGAEA.816971
POS233	Poseidon	Sep/1997	6	https://doi.pangaea.de/10.1594/PANGAEA.93298 https://doi.pangaea.de/10.1594/PANGAEA.93300 https://doi.pangaea.de/10.1594/PANGAEA.93301 https://doi.pangaea.de/10.1594/PANGAEA.93302 https://doi.pangaea.de/10.1594/PANGAEA.93304 https://doi.pangaea.de/10.1594/PANGAEA.93306
MERLIM	Pelagia	Mar/1998	2	https://doi.pangaea.de/10.1594/PANGAEA.817093
CAMBIO598	RV Thalassa	Apr-May/1998	5	https://www.seanoe.org/data/00298/40905/
74DI233_1	Discovery	May/1998	1	https://cchdo.ucsd.edu/cruise/74DI233_1

Table S1. Continuation.

M42/1b	Meteor	Jul/1998	6	https://doi.pangaea.de/10.1594/PANGAEA.92975 https://doi.pangaea.de/10.1594/PANGAEA.92977 https://doi.pangaea.de/10.1594/PANGAEA.92981 https://doi.pangaea.de/10.1594/PANGAEA.92983 https://doi.pangaea.de/10.1594/PANGAEA.92985 https://doi.pangaea.de/10.1594/PANGAEA.92987
06GA350A_1	Gauss	May/2000	1	https://doi.pangaea.de/10.1594/PANGAEA.290787
FICARAM II	R/V Hespérides	Apr/2001	2	https://cchdo.ucsd.edu/cruise/29HE20010305
ARQ	Arquipelago	Jul/2003	2	https://doi.pangaea.de/10.1594/PANGAEA.326113 https://doi.pangaea.de/10.1594/PANGAEA.326112
M60/5	Meteor	Apr/2004	10	https://www.tib.eu/en/suchen/id/awi:doi~10.2312%252Fcr_m60/a
D282	Discovery	Jul/2004	7	https://doi.pangaea.de/10.1594/PANGAEA.265173 https://doi.pangaea.de/10.1594/PANGAEA.265175 https://doi.pangaea.de/10.1594/PANGAEA.265176 https://doi.pangaea.de/10.1594/PANGAEA.265177 https://doi.pangaea.de/10.1594/PANGAEA.265179 https://doi.pangaea.de/10.1594/PANGAEA.265165 https://doi.pangaea.de/10.1594/PANGAEA.265166
CD171	RRS Charles Darwin	May-Jun/2005	21	https://www.bodc.ac.uk/data/
POS349	Poseidon	Apr/2007	5	http://dx.doi.org/10.2312/cr_po349^a
PE278	Pelagia	Oct/2007	1	https://doi.pangaea.de/10.1594/PANGAEA.897976
POS366/2	Poseidon	May/2008	1	https://doi.pangaea.de/10.1594/PANGAEA.729612
POS377	Poseidon	Dec/2008	6	https://doi.pangaea.de/10.1594/PANGAEA.729612
POS383	Poseidon	Apr-May/2009	9	https://doi.pangaea.de/10.1594/PANGAEA.729612
POS404	Poseidon	Sep/2010	19	http://dx.doi.org/10.2312/cr_po404^a
POS418/1	Poseidon	Jul/2011	6	https://doi.pangaea.de/10.1594/PANGAEA.890525
POS432	Poseidon	May/2012	4	http://oceanrep.geomar.de/id/eprint/27465^a
POS452	Poseidon	May/2013	2	http://dx.doi.org/10.2312/cr_po452^a
POS459	Poseidon	Sep/2013	10	http://dx.doi.org/10.2312/cr_po459^a
POS470	Poseidon	May-Jun/2014	31	http://dx.doi.org/10.3289/CR_POS470^a
POS471/1	Poseidon	Jun/2014	10	https://doi.pangaea.de/10.1594/PANGAEA.890578
POS485	Poseidon	May/2015	17	http://dx.doi.org/10.3289/CR_POS485^a
MSM48	Maria S. Merian	Nov/2015	3	https://doi.pangaea.de/10.1594/PANGAEA.860823
POS501	Poseidon	Jun/2016	24	http://dx.doi.org/10.3289/CR_POS_501^a
POS521	Poseidon	Mar/2018	27	J. J. Waniek (not published)
POS523	Poseidon	May/2018	9	https://doi.pangaea.de/10.1594/PANGAEA.903400

^aReference to the cruise report.

References

1. Good, S.A.; Martin, M.J.; Rayner, N.A. EN4: Quality controlled ocean temperature and salinity profiles and monthly objective analyses with uncertainty estimates. *J. Geophys. Res. Ocean.* **2013**, *118*, 6704–6716. doi:10.1002/2013JC009067.
2. Hurrell, J. The Climate Data Guide: Hurrell North Atlantic Oscillation (NAO) Index (Station-Based). 2020. Available online: <https://climatedataguide.ucar.edu/climate-data/hurrell-north-atlantic-oscillation-nao-index-station-based> (accessed on March 4, 2020).

Publication III

Full Research Paper, *Journal of Marine Systems*, 2021, 217, 103517

30 years of temporal variability of temperature and currents below the main thermocline between 1980–2009 in the subtropical Northeast Atlantic (Kiel 276, 33°N, 22°W)

Helena C. Frazão, Ralf D. Prien, Thomas J. Müller, Detlef E. Schulz-Bull, Joanna J. Waniak

Submitted: 25 August 2020; Accepted: 31 January 2021

doi: 10.1016/j.jmarsys.2021.103517

Abstract Data from the deep-sea mooring Kiel 276 (33°N, 22°W), 5300 m water depth in the northeast Atlantic, was used to investigate the temporal variability of temperature and currents below the main thermocline (1000 m, 1600 m, 3000 m, 5000 m) in the 30-year period (between 1980 and 2009). Daily averages were the basis to assess the temperature and currents changes, as well as kinetic energy, from annual to decadal and long-term scales. Below the main thermocline, no seasonal signal was identified for both, temperature and currents, during the 30 years. The record-length linear temperature trends at 1000 m and 1600 m are 0.03 ± 0.01 °C year⁻¹ and 0.02 ± 0.02 °C year⁻¹, respectively. The mean currents also intensified within the decades in the entire water column, and as a consequence, the mean kinetic energy increased. The fluctuating kinetic energy increased on a decadal scale only at 1000 m, as a possible consequence of the increase in the strength of Mediterranean Water lenses (MEDDIES) that crossed the mooring site. During the period 2001–2009, six MEDDIES crossed the Kiel 276 site, in addition to the 10 MEDDIES identified earlier during the previous 20 years, between 1980 and 2000 (Siedler et al., 2005). The integral time scales are of the same order in all depths (between 30 to 40 days), indicating that events occur on similar time scales, with mesoscale signals dominating and being present within the entire water column.



30 years of temporal variability of temperature and currents below the main thermocline between 1980–2009 in the subtropical Northeast Atlantic (Kiel 276, 33°N, 22°W)

H.C. Frazão^{a,*}, R.D. Prien^a, T.J. Müller^b, D.E. Schulz-Bull^a, J.J. Waniek^a

^a Leibniz Institute for Baltic Sea Research Warnemünde, Seestraße 15, 18119 Rostock, Germany

^b GEOMAR Helmholtz Centre for Ocean Research Kiel, Düsterbrokerweg 20, 24105 Kiel, Germany

ARTICLE INFO

Dataset link: <https://doi.pangaea.de/10.1594/PANGAEA.836686>, <http://tds0.ifremer.fr/thredds/catalog/CORIOLIS-OCEANSITES-GDAC-OB S/DATA/K276/catalog.htm>

Keywords:

Decadal and interannual variability
Northeast Atlantic
Madeira Basin

ABSTRACT

Data from the deep-sea mooring Kiel 276 (33°N, 22°W), 5300 m water depth in the northeast Atlantic, was used to investigate the temporal variability of temperature and currents below the main thermocline (1000 m, 1600 m, 3000 m, 5000 m) in the 30-year period (between 1980 and 2009). Daily averages were the basis to assess the temperature and currents changes, as well as kinetic energy, from annual to decadal and long-term scales. Below the main thermocline, no seasonal signal was identified for both, temperature and currents, during the 30 years. The record-length linear temperature trends at 1000 m and 1600 m are 0.03 ± 0.01 °C year⁻¹ and 0.02 ± 0.02 °C year⁻¹, respectively. The mean currents also intensified within the decades in the entire water column, and as a consequence, the mean kinetic energy increased. The fluctuating kinetic energy increased on a decadal scale only at 1000 m, as a possible consequence of the increase in the strength of Mediterranean Water lenses (MEDDIES) that crossed the mooring site. During the period 2001–2009, six MEDDIES crossed the Kiel 276 site, in addition to the 10 MEDDIES identified earlier during the previous 20 years, between 1980 and 2000 (Siedler et al., 2005). The integral time scales are of the same order in all depths (between 30 to 40 days), indicating that events occur on similar time scales, with mesoscale signals dominating and being present within the entire water column.

1. Introduction

In the last two decades of the 20th century, extensive observational surveys (e.g. Joint Global Ocean Flux Study, JGOFS and the World Ocean Circulation Experiment, WOCE) took place to study the ocean's role in global and regional climate variability, atmosphere–ocean interactions and marine bio-geochemistry. Within those campaigns, many time-series stations worldwide were established and run for different periods providing an understanding of natural variability in the ocean, at different spatial and temporal scales (Karl et al., 2003). The launch of the Argo program at the beginning of the 2000s provided an increase of the number of observations worldwide, becoming the largest systematic and global sampling network of the ocean up to date (IPCC, 2014b). The contributions from both observations and modelling efforts provided evidence of changes in ocean variability at seasonal to inter-decadal scales (IPCC, 2014a, and references therein; e.g. Desbruyères et al. (2014) for the Northeast Atlantic).

An increase in Earth's surface temperature has been recorded since the last century (Jones et al., 1986, 1999; IPCC, 2014a). In parallel, the

surface warming extended to the upper levels of the global ocean and an increase of ocean heat content in the upper 700 m has been reported since 1971, especially in the North Atlantic (Levitus et al., 2009; IPCC, 2014b; Cheng et al., 2019). Some studies (e.g. Church et al., 2011; Levitus et al., 2012; Cheng et al., 2019) showed that during the last 50 years about 93% of the Earth's excess heat energy had been absorbed by oceans, leading to an increase of the ocean heat content even at depths of 2000 m.

The extension of the warming in the deep and abyssal ocean is difficult to determine due to a lack of in situ measurements sufficiently close distributed both in space and time (IPCC, 2014b). Models have been used together with in situ data to assess the warming at the deep and abyssal ocean; however, reports of ocean warming deeper than 2000 m are still rare, uncertain and challenging (Desbruyères et al., 2014, 2016; Zanna et al., 2019). Repeated hydrographic sections in the Northeast Atlantic showed warming at the layer 2000 m–3000 m and an abyssal cooling in the subtropical region (Desbruyères et al., 2014).

* Corresponding author.

E-mail address: helena.frazao@io-warnemuende.de (H.C. Frazão).

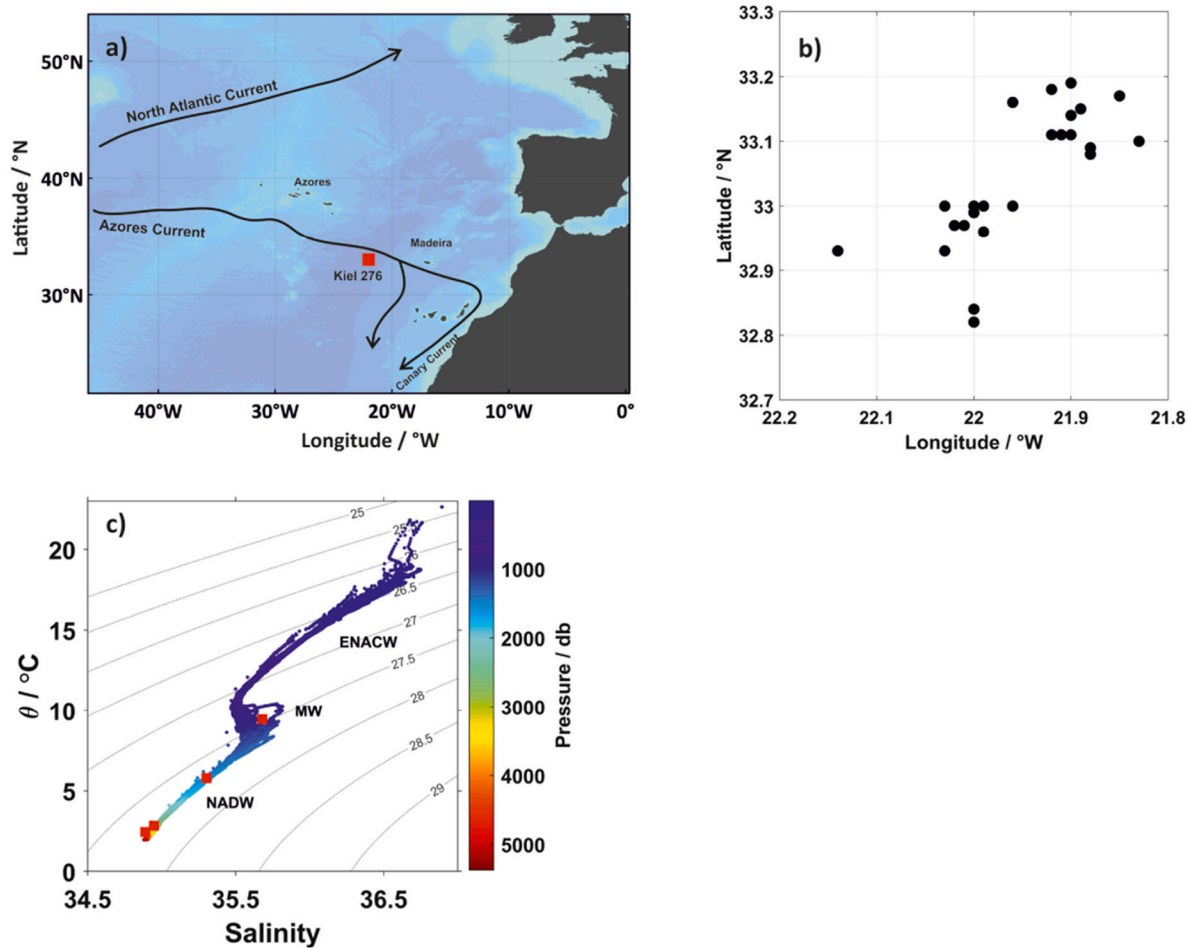


Fig. 1. Kiel 276 location. (a) Nominal position of the mooring Kiel 276, together with a schematic representation of the main upper ocean currents in the region: North Atlantic Current, Azores Current and Canary Current (Stocker, 2013). (b) Position of the individual deployments between 1980 and 2011 (see Table 1 for more details). (c) θ -S diagram of the deployment CTDs at Kiel 276 positions, with the indication of the main water masses present in the water column: ENACW (Eastern North Atlantic Central Water), MOW (Mediterranean Outflow Water), NADW (North Atlantic Deep Water) (adapted from Siedler et al., 2005, their Fig. 4). The red squares on the θ -S diagram correspond to the current meter levels used in this study (1000 m, 1600 m, 3000 m and 5000 m).

The deep-sea mooring Kiel 276 was placed at 33°N, 22°W at the Madeira Basin, the northeastern part of the North Atlantic subtropical gyre (Fig. 1a). It was operated from April 1980 until April 2011, recording temperature and currents at different depth levels, covering the major water masses from below the mixed layer (250 m) to 50 m above the bottom (Müller and Waniek, 2013). In the upper water column, between 30°N and 38°N, the Azores Current and the permanent Azores thermohaline front highly influence the local hydrodynamics (Käse and Siedler, 1982; Fründt and Waniek, 2012; Fründt et al., 2013) down to depths of 2000 m (Gould, 1985). Beneath the main thermocline, from 600 m to 1300 m, the Mediterranean Water Outflow through the Gibraltar Strait prevails (Armi and Zenk, 1984, and Fig. 1c). This water mass is characterised by density compensated temperature and salinity anomalies of $\Delta T = 2\text{--}3$ °C and $\Delta S = 1\text{--}2$, respectively (Siedler et al., 2005; Fusco et al., 2008). Associated with the Mediterranean Water tongue, there are high temperature (maximum near 13 °C) and haline (maximum around 36.5) water lenses or eddies, also known as MEDDIES (Zenk and Armi, 1990). The North Atlantic Deep Water found below the Mediterranean Water (Tomczak and Godfrey, 1994; Voelker et al., 2015) is identified by temperatures between 1.5–4 °C and salinities of 34.8–35 (Emery and Meincke, 1986, and Fig. 1c). Rudiments of Antarctic Bottom Water (−0.9–1.7 °C, 34.64–34.72; Emery and Meincke, 1986) are occasionally found close to the bottom (Saunders, 1987).

Previous studies using shorter time-series from Kiel 276 showed that (i) mean currents averaged over the available record lengths, of

maximum 25 years, were weak and decrease with depth, from less than 10 cm s^{-1} close to the surface to 1 cm s^{-1} close to the bottom (Dickson et al., 1985; Müller and Siedler, 1992; Waniek et al., 2005; Fründt et al., 2013), (ii) eddy variability resulting from baroclinic instability of the Azores Current dominates the mean flow at all depth levels (Siedler et al., 1985; Müller and Siedler, 1992; Siedler et al., 2005), and (iii) eddy features at the core of the Mediterranean Outflow Water contribute significantly to the variability at all depth levels (Siedler et al., 2005). Decadal and long-term changes in the upper thermocline (at 240 m and 500 m) at the Kiel 276 mooring were analysed by Fründt et al. (2013) for the period 1980–2009. These authors reported warming at both depth levels and change in the current regime after 2000, compared with the 1980s and the 1990s.

In our study, daily averages of temperature and currents from the Kiel 276 mooring are examined at depths below the main thermocline (1000 m, 1600 m, 3000 m and 5000 m) for the moorings deployed between 1980 and 2011. With this study, we seek to verify if the deeper water column underwent similar changes like the ones reported by Fründt et al. (2013) in the main thermocline. The 30-year dataset is almost continuous and allows to assess whether temperature changes (e.g. Levitus et al., 2000; Potter and Lozier, 2004) or current changes (Hu et al., 2020; Yang et al., 2020) reported on a larger temporal and spatial scale in the Northeast Atlantic can be detected at a single point located at the northeastern boundary of the subtropical gyre. Temperature and current variability below the main thermocline is assessed on different spatial scales, from annual to long-term.

Table 1

Summary of the Kiel 276 mooring data (1980–2011): numbers in parentheses indicate the deployment and recovery days (day 0 is the decimal day corresponding to 01-Jan-1980, 00:00:00 UTC), stars mark occasionally missing data for a single parameter (* – temperature; ** – currents). Data available from pressure sensor are marked by p in parenthesis, next to the best estimated deployment depth of the respective instrument. Instrument's (best estimated) deployment depths and position are also listed. Instruments' deployment depths were consistently re-estimated for all deployments between 1980 and 2011 by Müller and Waniek (2013), and may differ from those given in earlier papers (e.g. Siedler et al., 2005). A strong MEDDY caused overturning of the V276140 deployment resulting in missing data for 282 days for the upper levels. The complete mooring malfunction during deployment V276200 resulted in missing data for 300 days. Only the records used in the study are listed. For the statistical analysis from annual to decadal scales, the records from mooring V276270 were used until December 31st, 2009. For additional details, see Müller and Waniek (2013).

Number	Deployment		Position	Instrument depth [m]
	Start	End		
V264010	04.04.1980 (94)	12.10.1980 (285)	33.102°N, 21.848°W	942, 3025, 4812
V276010	21.10.1980 (294)	23.07.1981 (569)	33.165°N, 21.848°W	1004, 1107, 1611
V276020	31.07.1981 (577)	25.02.1982 (786)	33.075°N, 21.884°W	1170, 3034
V276030	09.03.1982 (798)	13.04.1983 (1198)	33.195°N, 21.898°W	1057, 1564
V276040	23.04.1983 (1208)	15.10.1983 (1383)	33.177°N, 21.917°W	1081, 1587, 3013, 5237*
V276050	24.10.1983 (1392)	21.10.1984 (1755)	33.180°N, 21.923°W	1176, 1679, 3068*, 5236*
V276060	30.10.1984 (1764)	12.11.1985 (2142)	33.158°N, 21.955°W	1177, 1680, 3092, 5241**
V276070	21.11.1985 (2151)	27.10.1986 (2491)	33.142°N, 21.960°W	1065, 1168, 1672, 3085*, 5237
V276080	05.11.1986 (2500)	02.11.1987 (2862)	33.112°N, 21.918°W	1074, 1177**, 1680, 3070, 5231**
V276090A	10.11.1987 (2870)	20.09.1988 (3185)	33.090°N, 21.875°W	950, 1051, 1141, 1555, 2966, 5239
V276100	18.01.1989 (3305)	23.10.1989 (3583)	33.107°N, 21.897°W	1120*, 1726, 3116, 5231
V276110	31.10.1989 (3591)	21.09.1990 (3916)	33.103°N, 21.905°W	1070, 1173, 1676, 3086*, 5266*
V276120	29.09.1990 (3924)	23.01.1992 (4405)	33.149°N, 21.888°W	941, 1044, 1547, 2967
V276130	01.02.1992 (4414)	07.07.1993 (4936)	32.922°N, 22.136°W	1026, 1129, 3019, 5229
V276140	11.07.1993 (4940)	17.09.1994 (5373)	32.994°N, 22.002°W	1018, 1121, 1624, 3037
V276150	20.09.1994 (5376)	11.10.1995 (5762)	32.957°N, 22.022°W	969, 1075, 3002, 5226
V276160	16.10.1995 (5767)	22.06.1996 (6017)	33.002°N, 21.964°W	996, 1603, 3012, 5213
V276170	30.06.1996 (6025)	04.08.1997 (6425)	33.000°N, 22.000°W	1019, 1624, 3045, 5232
V276180	09.08.1997 (6430)	21.01.1999 (6960)	32.992°N, 21.998°W	1020, 1625, 3052, 5225
V276190	21.01.1999 (6966)	10.04.2000 (7405)	32.968°N, 22.008°W	1020, 1624, 3025
V276210	04.02.2001 (7705)	16.02.2002 (8082)	32.925°N, 22.025°W	999, 1608, 3016, 5222**
V276220	24.02.2002 (8090)	17.04.2003 (8507)	32.868°N, 22.029°W	930, 1548, 2992, 5223(p)
V276230	24.04.2003 (8514)	13.03.2004 (8838)	32.828°N, 22.003°W	979, 1588, 3013, 5214(p)
V276240	19.03.2004 (8844)	03.05.2005 (9254)	32.818°N, 22.000°W	1049, 1600, 2996, 5220
V276250	10.05.2005 (9261)	07.04.2007 (9958)	33.000°N, 21.998°W	983, 1542(p), 2957, 5211
V276260	16.04.2007 (9969)	26.04.2009 (10709)	33.000°N, 22.000°W	943, 1506, 2933
V276270	28.04.2009 (10711)	21.04.2011 (11434)	32.959°N, 21.993°W	989, 1546, 2958, 5209

2. Data & methods

2.1. Dataset

The mooring Kiel 276 was operated in the Northeast Atlantic, within the Madeira Basin, at a nominal position of 33°N, 22°W, at approximately 5300 m water depth (Fig. 1a; Siedler et al., 2005; Waniek et al., 2005; Fründt et al., 2013). The moored instruments recorded temperature and currents between April 4th, 1980 and April 21st, 2011 from near-surface layer down to the bottom layer, within 0.2° in latitude and 0.2° in longitude of the nominal mooring position (Fig. 1b, Table 1; Müller and Waniek, 2013).

Current measurements were performed by Aanderaa Recording Current Meters RCM 4/5 and RCM 7/8 (AANDERAA Instruments, 1978, 1987), additionally equipped with temperature and, mostly at near-surface, pressure sensors. The RCM sensors have accuracies of ± 0.2 bar in pressure, ± 0.05 °C in temperature, ± 0.1 cm s⁻¹ in velocity and $\pm 5^\circ$ in direction (AANDERAA Instruments, 1978, 1987). Temperature and current measurements were taken with an hourly and later (from 1987 onwards) two-hourly resolution. In the first deployments, conductivity was measured in the Mediterranean Water level (around 1000 m). However, the conductivity cells showed non-linear drifts, which could not be calibrated because salinity data were only available from the CTD measurements during deployment and recovery phases. For further details of the individual mooring deployments see Müller and Waniek (2013).

In this study, only records of current meters from below the main thermocline were used, which were deployed at depth levels around 1000 m, 1600 m, 3000 m and 5000 m (Table 1). The details of the dataset used in this study are compiled in Table 1. The length of the deployments used in this study varied between 6 and 24 months (Table 1). Between the deployments, there are gaps of up to one week,

caused by schedules for recovering and re-deploying the moored instruments. Occasionally, longer gaps occurred as well due to instrument failure (see Müller and Waniek, 2013, for more details). Records from the deployment V276140, during which a strong MEDDY caused overturning of the mooring, were lost, resulting in a data gap of 282 days (between 1993–1994) at 1000 m and 1600 m. Due to malfunction of the instruments and errors during the deployment V276200, a long gap of 300 days occurred in 2000 at all depth levels (Table 1 and Figs. 3, 4).

2.2. Methods

The depths of the instruments slightly differ over time due to mooring modifications and/or changes in the scientific focus (Table 1 and Müller and Waniek, 2013). In a first step, the depths of instruments for each deployment were corrected according to actual water depth, deployment logs and pressure records of the top instrument. In a second step, best estimates of the instrument depths were achieved by matching in a least-square sense the median of the first 25 h of moored (normalised) pressure and (normalised) temperature sensor data to the CTD profiles obtained at the start of the respective mooring deployment. Normalised pressure and temperature sensor data were based on the RCM sensor's measurement range. The method takes into account that the start of the moored sensor records is not necessarily coherent with high-frequency variability inherent in any CTD profile taken close to the mooring site. It provides best depth estimates that are internally consistent for all 27 deployments (see Müller and Waniek, 2013, for more details), but they may differ from estimates presented in earlier studies (e.g. Siedler et al., 2005).

For the present study, current and temperature records were adapted from instrument depths to nominal depths to form combined time-series at the nominal depths as follows: mean currents in the Northeast

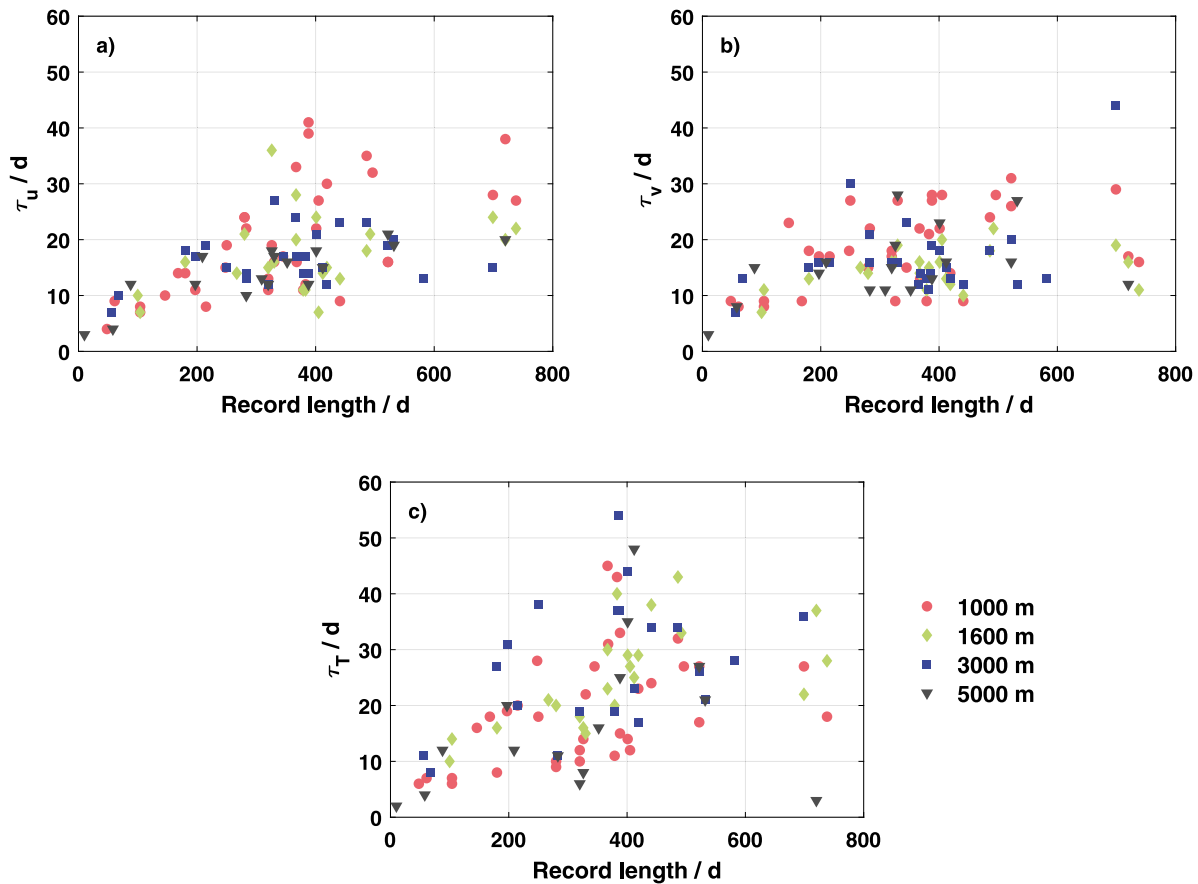


Fig. 2. Integral Time Scales based on individual deployments. Integral Time Scales (τ , in days) as a function of record length for the (a) zonal velocity component τ_u , (b) meridional velocity component τ_v and (c) temperature τ_T . The different symbols and colours indicate different depth levels: red circles — 1000 m, green diamonds — 1600 m, blue squares — 3000 m and grey triangles — 5000 m.

Atlantic deeper than 1000 m are dominated by low modes and generally have weak vertical gradients over 50 m (see Müller and Siedler, 1992). Consequently, we did not correct current records to nominal depths when combining them to a single series at a nominal depth.

Temperature variability in the vertical is assumed not to change significantly in the deep ocean on vertical scales of 50 m. However, the mean temperature may change over such distance. Therefore, temperature records were offset adapted from deployment depths (Table 1) to nominal depths by comparing the initial (or final) 25-hour median of the RCM record to the closest CTD cast's temperature value at nominal depth taken during mooring turnarounds. Next, record parts that show a vertical displacement of the instrument by more than 50 m (according to pressure records) were removed. The resulting data loss is less than 0.5% of the total time-series, and it is not significant for the long-term analysis. The temperature records at 5000 m are of low resolution and accuracy, and are by no means continuous (Fig. 3d). Also, not all CTD casts reached 5000 m depth because of cable problems. Therefore, temperature records around 5000 m were not adapted to the 5000 m level.

Finally, each record was low-pass filtered (35 h half power period) to remove (local) inertial and higher frequency signals. Daily averages then build the base for the analysis of the combined current and temperature time series at (common) nominal depths.

The low-pass filtered daily means of the two current components and temperature were used to calculate means for the low-frequency part of the time series and its associated variance, standard deviation, integral time scale (ITS, defined as the first zero-crossing of the auto-correlation function), and the mean kinetic (MKE) and the fluctuating part of energy (FKE) per unit mass function (see Müller and Waniek, 2013). Here, MKE and FKE are defined through the currents' mean

speed (\bar{u} and \bar{v}) and associated fluctuations around the mean (u' and v') (Reynolds, 1895, Eqs. (1) and (2)).

$$MKE = 0.5 \times (\bar{u}^2 + \bar{v}^2) \quad (1)$$

$$FKE = 0.5 \times (\overline{u'^2} + \overline{v'^2}) \quad (2)$$

Statistics of low pass filtered daily averages from individual deployments can be found in Müller and Waniek (2013). Here, we present statistics for the combined records for monthly and annual means, three decadal means (1980–1989, 1990–1999, 2000–2009, Table 2) and the long-term mean over the whole period (LTM, 1980–2009, Table 2). Also, temperature and current ranges for the daily averages are presented in Table 2. The temperature record of the deployment V27603 at 3000 m could not be calibrated either using the deployment or the recovery CTD cast, as the maximum depth of the CTD was shallower (Müller and Waniek, 2013, their table 3.2). Therefore, this record was excluded from all the statistical analysis. For the statistical analysis from annual to decadal scales, the records of the mooring V276270 were used until December 31st, 2009. 95% confidence intervals were estimated on annual, decadal and long term scales using a t-student test.

Annual cycles over the entire period were calculated using monthly means of temperature, absolute velocity and its components, once they can be assumed to be statistically independent (see section 3.1 for more details). At 5000 m, temperature and velocity components annual cycles were not determined due to the long gaps in the record.

MEDDIES were identified by a strong temperature increase ($T > 2.5\sigma$, corresponding to $\Delta T > 1.28$ °C) combined with an increase and change in the direction of currents (for more details see discussion in Siedler et al., 2005, their section 3). Since the conductivity cells

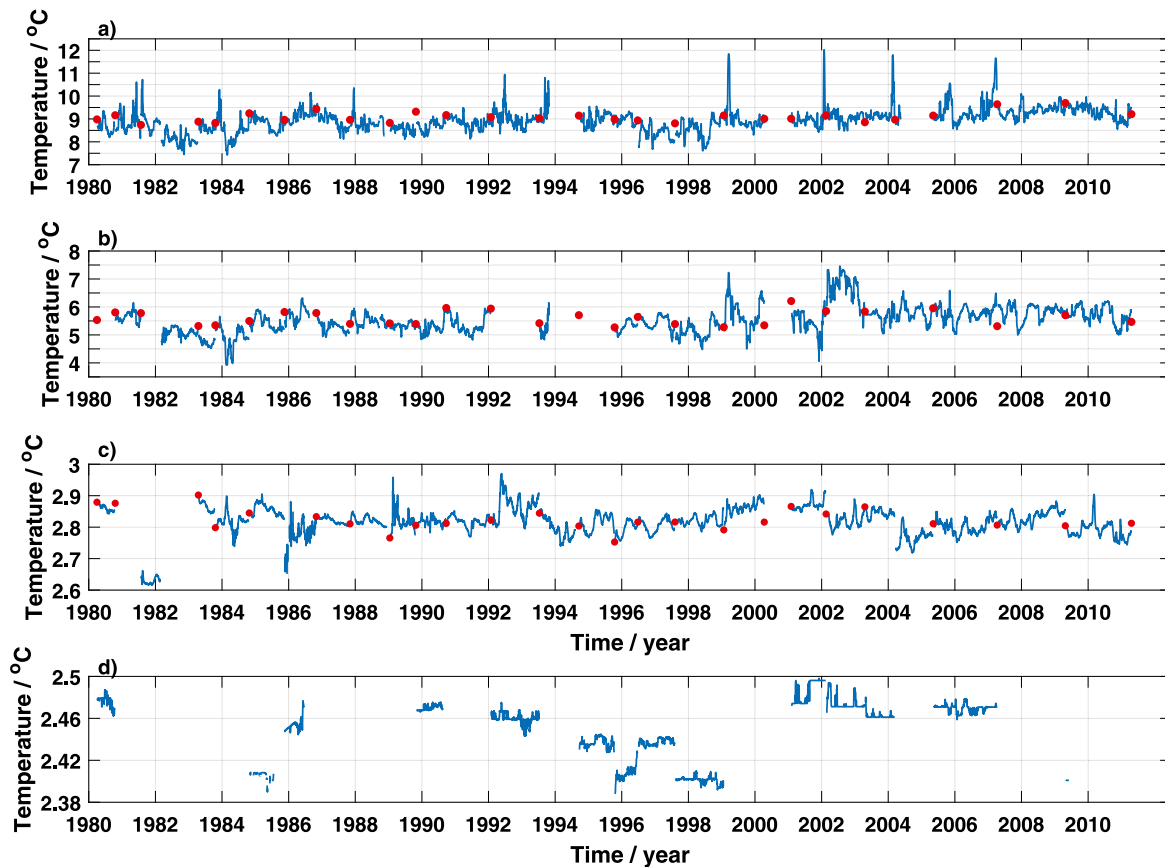


Fig. 3. Kiel 276 daily averaged temperature. Depth corrected daily values of temperature measured at the Kiel 276 mooring together with the CTD recorded temperature (red circles) at the depths levels (a) 1000 m, (b) 1600 m, (c) 3000 m and (d) 5000 m until the last mooring used (1980–2011). In 1981, the 3034 m temperature record of the deployment V276020 is not adapted to 3000 m due to the shorter CTD cast (Müller and Waniek, 2013). The temperature at 5000 m is not depth corrected due to the too scarce records. Please note the different temperature scales at each depth level.

used in the first moorings turned out to be not reliable, the temperature is the only remaining (passive) parameter to identify MEDDIES. However, it can be assumed that an increase in temperature requires an increase in salinity (and vice-versa) to keep a MEDDY (or a low temperature/low salinity lens) floating at its background density level. The temperature anomalies associated with the passage of MEDDIES were calculated subtracting the median over the 30-year records from the daily averages. To discuss long-term changes (in Section 3.2), the MEDDIES-signal was removed from the daily averages (Table 2).

3. Results & discussion

3.1. Mesoscale variability

The integral time scales for the velocity components and temperature indicate time-scales of the duration of the dominant processes in the time-series. At this site, Müller and Waniek (2013) calculated the ITS for the individual deployments (Fig. 2). In general, the ITS increase with the record length (Fig. 2). However, for records' length of up to two years, the maximum ITS does not exceed 50 days for temperature and both velocity components. Also, from record lengths of approximately 400 days on, the ITS flatten, i.e. they do not further increase. From the ITS' flattening, we conclude that after approximately two years of continuous measurements, the ITS reached its final level of 30 to 40 days, a hint that mesoscale variability dominates each record at the Kiel 276 site.

The daily temperature and current averages over the entire observation period are shown in Figs. 3 and 4, respectively. The mean currents are predominantly south/southwestward at all four levels, and

are of the order of a few cm s^{-1} or almost not distinguishable from zero (Fig. 4, Table 2). The mean current variability (expressed as the standard deviation) is of the same order or higher than the mean values (Müller and Waniek, 2013). The daily temperature averages show higher variability at 1000 m and 1600 m depth levels, and less variability at 3000 m (Fig. 3). Both, currents and temperature records are marked by strong year-to-year variability, consistent with previous observations at this site using shorter time-series (e.g. Schmitz et al., 1988; Siedler et al., 2005; Waniek et al., 2005).

The 30-year records of velocity are marked by irregular strong current events that occupy the entire water column below the main thermocline (Fig. 4). The mesoscale signals are irregular, and have time scales of one up to three months at all levels, suggesting a low modal structure already put forward by shorter records at this site (Müller and Siedler, 1992; Waniek et al., 2005). They are often unidirectional with depth, confirming the presence of the barotropic component in the water column (Müller and Siedler, 1992). As there is no apparent difference between the timescales in the upper two levels (1000 m and 1600 m) and the deeper levels (3000 m and 5000 m), this is an indication of the prevalence of mesoscale events in the entire water column (Fig. 2). Our integral time scales at the deeper levels are longer than those reported by Saunders (1983), in the Madeira Abyssal Plain, close to the Kiel 276 position. This author reported ITS of the order of 5.5 ± 2 days for record lengths up to 225 days, which were interpreted as the occurrence of turbulent short-term processes of mesoscale activity near the bottom (at 10 m and 600 m above the sea bed). In our study, comparable short ITS result mostly for shorter records, often of less than 60 days (Fig. 2).

At 1000 m, events showing an increase of temperature associated with an increase and change in currents direction were identified

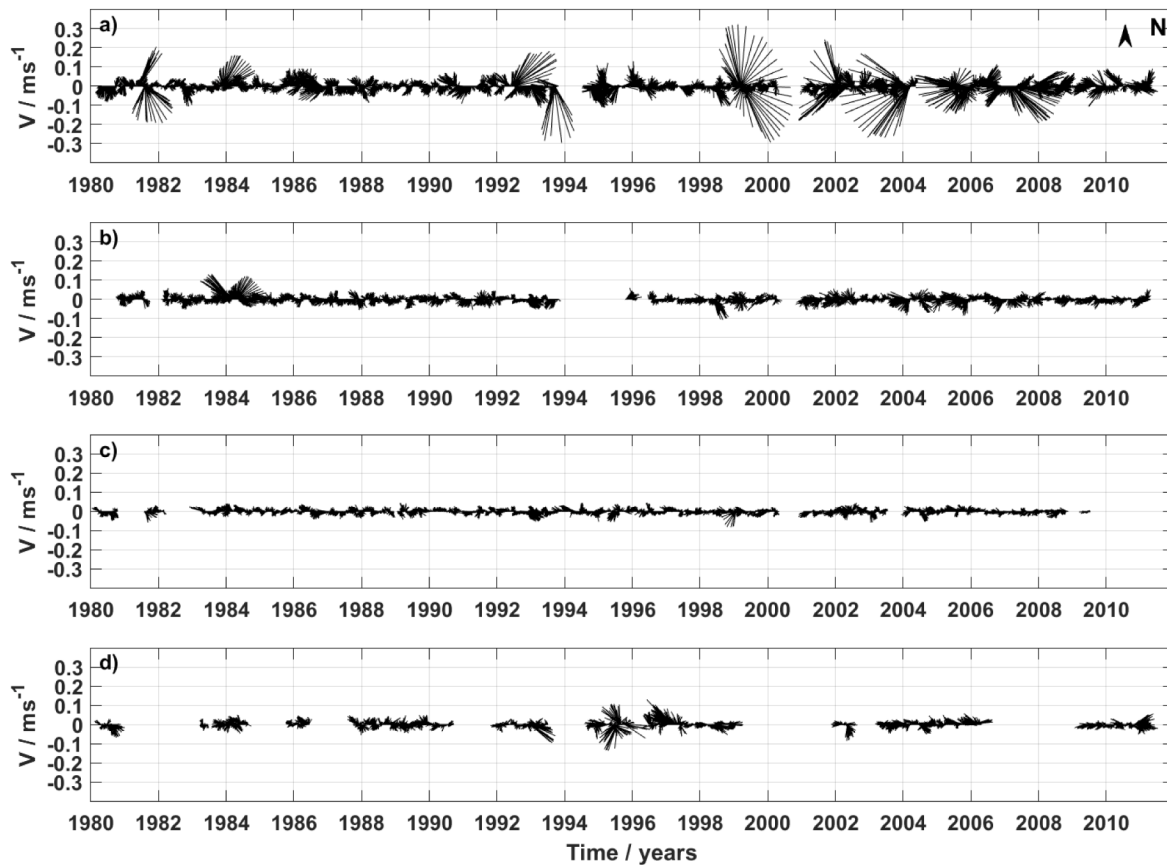


Fig. 4. Kiel 276 daily averaged currents. Daily mean velocity (m s^{-1}) at (a) 1000 m, (b) 1600 m, (c) 3000 m, and (d) 5000 m depth measured by all moorings used (1980–2011, Table 1). Upward velocity vectors indicate flow to the North.

by Siedler et al. (2005) as Mediterranean Water lenses (MEDDIES) for the period 1980–2000. These authors identified 7 MEDDIES in the 1980s and 3 MEDDIES in the 1990s. In addition, we identified 6 more MEDDIES between 2001–2009. The extreme temperature increases associated with MEDDIES exceeded $\Delta T > 1.28$ °C, up to ΔT of 3 °C. The events occurred in the last decade presented the highest temperature and current speed anomalies recorded over the 30-years compared with the background fields (Figs. 3, 4). They occurred at the end of the winter (in March and April 2005 and March 2006) and during summer months (July 2001, August 2003 and July 2006), occupying the water column for 4–18 days and 16–45 days, respectively. Siedler et al. (2005) described that the probability of detecting a MEDDY at this site depends on the position of the Azores Front relative to the mooring position. Thus, a more northward (southward) location of the front increases (decreases) the probability of a MEDDY crossing the mooring position. The mean position of the Azores Front moved northward since the 1980s, from 33.2°N in the 1980s, to 33.7°N in the 1990s, and to 34.1°N in the 2000s, at a rate of 0.06 ° year^{-1} since the 1960s (Fründt and Waniek, 2012). Although the Azores Front has been moving northward since the 1960s, the number of MEDDIES crossing the Kiel 276 site during the 1990s decreased drastically (50%) compared with the 1980s and 2000s. However, we are not able to explain why the number of MEDDIES is so uneven distributed since the 1980s, as already noticed by Siedler et al. (2005).

We calculated the kinetic energy profile below the main thermocline to distinguish which processes contribute to the energy field: if the mainly persistent currents (MKE) or the signals with different dynamic backgrounds, like eddies, Rossby Waves, or front displacements (FKE) (Fig. 5). MKE and FKE are maximum at 1000 m, decreasing their values to a minimum at 3000 m, and slightly increasing towards the seafloor (Fig. 5). While MKE is of the same order at all four levels, the FKE

values are almost twice as high as MKE in each deployment, indicating the dominance of short-scale events over the long-term current variability (Robinson, 1983; Müller and Siedler, 1992).

Both, MKE and FKE at all four depth levels (cyan plus sign in Fig. 5) are low compared to the values given by Krauss and Käse (1984) but agree with the values put forward by Dickson (1983) for depths greater than 1500 m (red stars and purple squares in Fig. 5). However, FKE values reported at NOAMP site are slightly higher, not only due to an increase of the FKE northward (Dickson, 1983) but also because they are influenced by the local topography at the Mid-Atlantic Ridge. All MKE and FKE reported in this study for Kiel 276 site are at the lower end of the estimates and fall into the low energy band in the Northeastern Atlantic (Dickson, 1983; Garçon et al., 2001).

3.2. Annual, decadal and long-term variability

The annual cycles of temperature and both velocity components are presented in Fig. 6 (solid black lines) at 1000 m, 1600 m, and 3000 m and in Supp. Fig. S.1 for all depth levels, respectively. For those, no significant changes on an annual scale, i.e. no seasonality was observed over the 30-year records below 1000 m. The monthly means of temperature and velocity are not significantly different from each other, and the differences throughout the year are indistinguishable.

At 1000 m, the temperature ranged between 8.80 °C and 9.03 °C, with higher variability in winter months (up to 0.71 °C in March), reducing to 0.41 °C throughout the year (Fig. 6b). At 1600 m, the monthly temperatures varied between 5.47 °C and 5.61 °C (Fig. 6d), and at 3000 m, the annual cycle shows temperature below 2.83 °C with reduced variability (up to 0.04 °C, Fig. 6f).

The monthly mean velocities are small at all depth levels (up to 2 cm s^{-1} for both components), with variability of several cm s^{-1} (Supp.

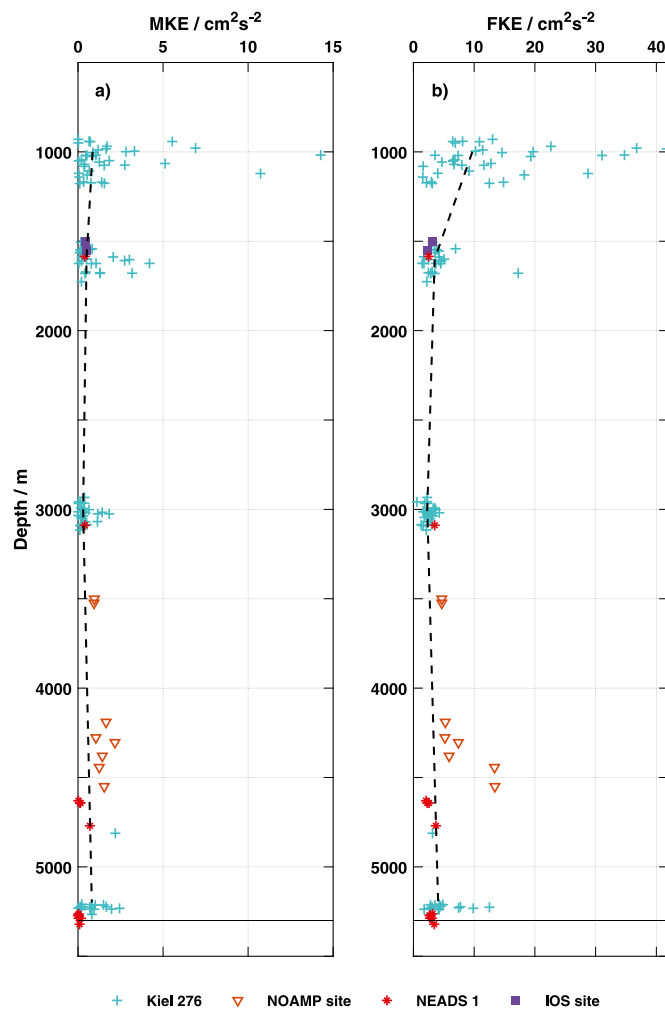


Fig. 5. Mean and fluctuating part of kinetic energy. Vertical profile of (a) MKE and (b) FKE for each deployment of the Kiel 276 mooring (33°N, 22°W Müller and Waniek, 2013, cyan plus sign), NEADS 1 site (operated in 1977 at the same site as Kiel 276; Dickson, 1983, red stars), South West of Azores site (32°N–33°N, 31°N30′W; Dickson, 1983, purple squares) and NOAMP site (centred at 47°20′N, 19°30′W; Klein and Mittelstaedt, 1992, orange triangles). The dashed black line connects the median values at each depth for the Kiel 276 data.

Fig. S.1). The mean zonal flow was predominantly westward, whereas the meridional flow was southward at the upper levels (at 1000 m and 1600 m), and northward during the winter months reversing to southward at the deeper levels (3000 m and 5000 m).

The annual cycles of kinetic energy are shown in Supp. Figs. S.2–S.5. MKE is higher during the winter months, with a maximum in February at 1000 m, 1600 m and 5000 m, and in December at 3000 m. FKE shows also a maximum in winter but its maximum shifts with depth. At 1000 m, FKE is highest in March, lagging to February at 1600 m, and to January at the deeper levels. The upper circulation in the eastern part of the subtropical gyre shows a significant seasonal signal, intensified during the summer and autumn, and weakened the rest of the year (Stramma and Siedler, 1988). The propagation of this seasonal signal into greater depths might explain why the maxima in kinetic energy occurred during winter, as already shown by Dickson et al. (1982) for the Rockall Through, although the oceanographic conditions are different compared to our region.

The mean temperature at 1000 m and 1600 m increased over the decades (Fig. 6b,d, Fig. 7a,b and Table 2). The warming was moderate over time, but it was not significant, neither from the 1980s to the 1990s nor from the 1990s to the 2000s (with a few exceptions in

May, July and August at 1000 m; Fig. 6b). However, the warming observed is significant ($p \ll 0.05$) comparing the 1980s to the 2000s at both depths, except in December at 1000 m and winter months at 1600 m. The warming is still seen after removing the MEDDIES-signals from the time-series at 1000 m (Table 2; Potter and Lozier, 2004; Fusco et al., 2008). At 3000 m, no changes on decadal scale were observed (Table 2), also reflected in the overlapping of the annual cycles calculated for each decade (Fig. 6f).

Our results show that the warming of the water column at Kiel 276 site is not confined to the main thermocline (Fründt et al., 2013) but reached 1600 m. As in the main thermocline, the increase of temperature was moderate from the 1980s to the 1990s, and remarkable warming was seen during the last decade, starting after 1998 (Fig. 7a,b). Over the 30-year records, the annual mean temperature increased by 0.03 ± 0.01 °C year⁻¹ at 1000 m and 0.02 ± 0.02 °C year⁻¹ at 1600 m, compared with the 1.4 °C and 1 °C at 240 m and 500 m at the same site, respectively (Fründt et al., 2013). The increase of temperature at 1000 m exceeded the warming reported by Potter and Lozier (2004) at the MOW core in the Northeast Atlantic (0.101 ± 0.024 °C decade⁻¹) and by Levitus et al. (2000) for the North Atlantic. Our estimates also agree with the tendency reported by Desbruyères et al. (2014) for the subtropical Northeast Atlantic after the 1990s, associated with both heave of neutral surfaces and also changes in the water mass properties (Millot et al., 2006; Leadbetter et al., 2007).

Like temperature, also current speed (and therefore kinetic energy) increased over the decades (Fig. 8, Table 2). Contrary to the temperature, an intensification of the currents is observed in the entire water column, and as a direct consequence, the mean energy field intensified decade by decade (Table 2). Our results show that the increase of MKE was not only observed at the main thermocline (Fründt et al., 2013) but extends through the entire water column. Fründt et al. (2013) related the variations in the energy field in the main thermocline to a northward displacement of the subtropical gyre. In fact, Fründt and Waniek (2012) calculated a mean northward displacement of the northeastern boundary of the gyre by -0.01 ° year⁻¹ in the 1980s, 0.15 ° year⁻¹ in the 1990s and 0.035 ° year⁻¹ in the 2000s. Recently, Yang et al. (2020) showed evidence of a northward displacement of the main surface currents of the ocean gyres, most likely as a response to global warming in the last four decades.

The FKE increased on an inter-decadal scale only at 1000 m, with the changes below 1600 m indistinguishable within the decades (Table 2). The increase of FKE might be caused by an overall increase of the MEDDIES strength that crossed the mooring site since 1999. Nevertheless, our study together with the results of Fründt et al. (2013) shows an increase of the fluctuating part of the kinetic energy in the upper 1000 m of the water column. These results are in line with the recently reported increase of eddy kinetic energy in the global ocean for the upper 2000 m after the 1990s, in response to a global intensification of the surface winds (Hu et al., 2020).

4. Conclusions

Thirty years (1980–2009) of current and temperature records below the main thermocline (1000 m, 1600 m, 3000 m and 5000 m) obtained at the Kiel 276 mooring site is one of the most extensive datasets available in the Northeast Atlantic.

The integral time scales between 1000 m and 5000 m depth are of the order of one to a maximum of two months, and they do not differ significantly with depth, indicating that the water column is influenced by processes occurring at the same time scale, namely associated with mesoscale events.

Over the three decades from 1980 to 2011, the temperature at 1000 m and at 1600 m increased moderately by 0.03 ± 0.01 °C year⁻¹ and 0.02 ± 0.02 °C year⁻¹, respectively, similar to the observed trend

Table 2

Decadal means together with the standard deviation for selected parameters calculated for all four depth levels. Extreme values for temperature (°C) and current velocities (cm s^{-1}) were calculated using daily resolution data. Given is also the long-term mean (LTM, 1980–2009) and respective standard deviation. Statistics for T at 1000 m are also given removing the influence of the Mediterranean Water lenses (T without MEDDIES). T — temperature; u, v — zonal and meridional components of the velocity; V — absolute velocity (cm s^{-1}); Dir — mean direction of the flow (°); MKE — Mean Kinetic Energy ($\text{cm}^2 \text{s}^{-2}$); FKE — Fluctuating Kinetic Energy ($\text{cm}^2 \text{s}^{-2}$).

Parameter/Depth	1980–1989	1990–1999	2000–2009	LTM (1980–2009)
1000 m				
\bar{T} (without MEDDIES)	8.69 ± 0.38	8.80 ± 0.33	9.20 ± 0.27	8.88 ± 0.40
\bar{T}	8.70 ± 0.40	8.83 ± 0.40	9.26 ± 0.38	8.91 ± 0.46
T_{min}	7.42	7.61	8.43	
T_{max}	10.72	11.84	12.02	
\bar{u}	-0.33 ± 2.23	-0.02 ± 3.01	-0.96 ± 4.68	-0.42 ± 3.41
u_{min}	-12.41	-12.57	-33.91	
u_{max}	14.66	24.71	25.82	
\bar{v}	-0.13 ± 2.93	-0.75 ± 3.77	-0.69 ± 3.47	-0.51 ± 3.25
v_{min}	-19.32	-29.51	-26.87	
v_{max}	20.55	32.31	24.35	
\bar{V}	0.35	0.75	1.18	0.66
V_{min}	0.08	0.03	0.01	
V_{max}	22.09	32.48	33.92	
\overline{Dir}	244	181	237	220
\overline{MKE}	0.06	0.28	0.70	0.22
\overline{FKE}	6.78	11.64	16.97	11.10
1600 m				
\bar{T}	5.30 ± 0.35	5.36 ± 0.35	5.86 ± 0.43	5.53 ± 0.46
T_{min}	3.92	4.48	4.06	
T_{max}	6.31	7.23	7.46	
\bar{u}	-0.79 ± 1.87	-0.79 ± 1.73	-1.11 ± 1.96	-0.90 ± 1.87
u_{min}	-14.61	-8.65	-12.89	
u_{max}	14.39	6.74	7.67	
\bar{v}	0.00 ± 1.89	-0.44 ± 1.56	-0.43 ± 1.34	-0.29 ± 1.62
v_{min}	-5.53	-10.76	-8.50	
v_{max}	13.16	5.91	6.03	
\bar{V}	0.79	0.90	1.19	0.95
V_{min}	0.08	0.07	0.02	
V_{max}	17.41	11.76	13.01	
\overline{Dir}	269	238	250	252
\overline{MKE}	0.31	0.41	0.71	0.45
\overline{FKE}	3.53	2.71	2.82	3.06
3000 m				
\bar{T}	2.83 ± 0.03	2.82 ± 0.03	2.82 ± 0.04	2.82 ± 0.03
T_{min}	2.65	2.74	2.72	
T_{max}	3.23	2.97	2.92	
\bar{u}	-0.50 ± 1.47	-0.58 ± 1.55	-0.82 ± 1.53	-0.63 ± 1.52
u_{min}	-6.58	-8.25	-8.36	
u_{max}	5.69	6.71	4.46	
\bar{v}	-0.24 ± 1.32	-0.16 ± 1.26	-0.20 ± 1.08	-0.20 ± 1.23
v_{min}	-5.73	-8.20	-5.73	
v_{max}	4.48	4.58	4.42	
\bar{V}	0.55	0.60	0.84	0.66
V_{min}	0.02	0.00	0.03	
V_{max}	7.01	9.14	8.44	
\overline{Dir}	245	254	257	253
\overline{MKE}	0.15	0.18	0.36	0.22
\overline{FKE}	1.95	2.00	1.75	2.33
5000 m				
\bar{T}	2.44 ± 0.04	2.43 ± 0.03	2.47 ± 0.01	2.45 ± 0.03
T_{min}	2.39	2.39	2.40	
T_{max}	2.49	2.48	2.50	
\bar{u}	-0.43 ± 1.71	-0.68 ± 2.51	-0.83 ± 1.97	-0.64 ± 2.14
u_{min}	-7.18	-12.16	-7.93	
u_{max}	6.77	12.12	9.79	
\bar{v}	0.25 ± 1.57	-0.06 ± 1.91	-0.13 ± 1.47	0.02 ± 1.70
v_{min}	-6.77	-13.63	-8.54	
v_{max}	5.03	13.06	5.72	
\bar{V}	0.50	0.68	0.84	0.64
V_{min}	0.03	0.00	0.04	
V_{max}	8.30	17.38	9.88	
\overline{Dir}	293	262	264	269
\overline{MKE}	0.12	0.23	0.35	0.21
\overline{FKE}	2.69	4.97	3.02	3.73

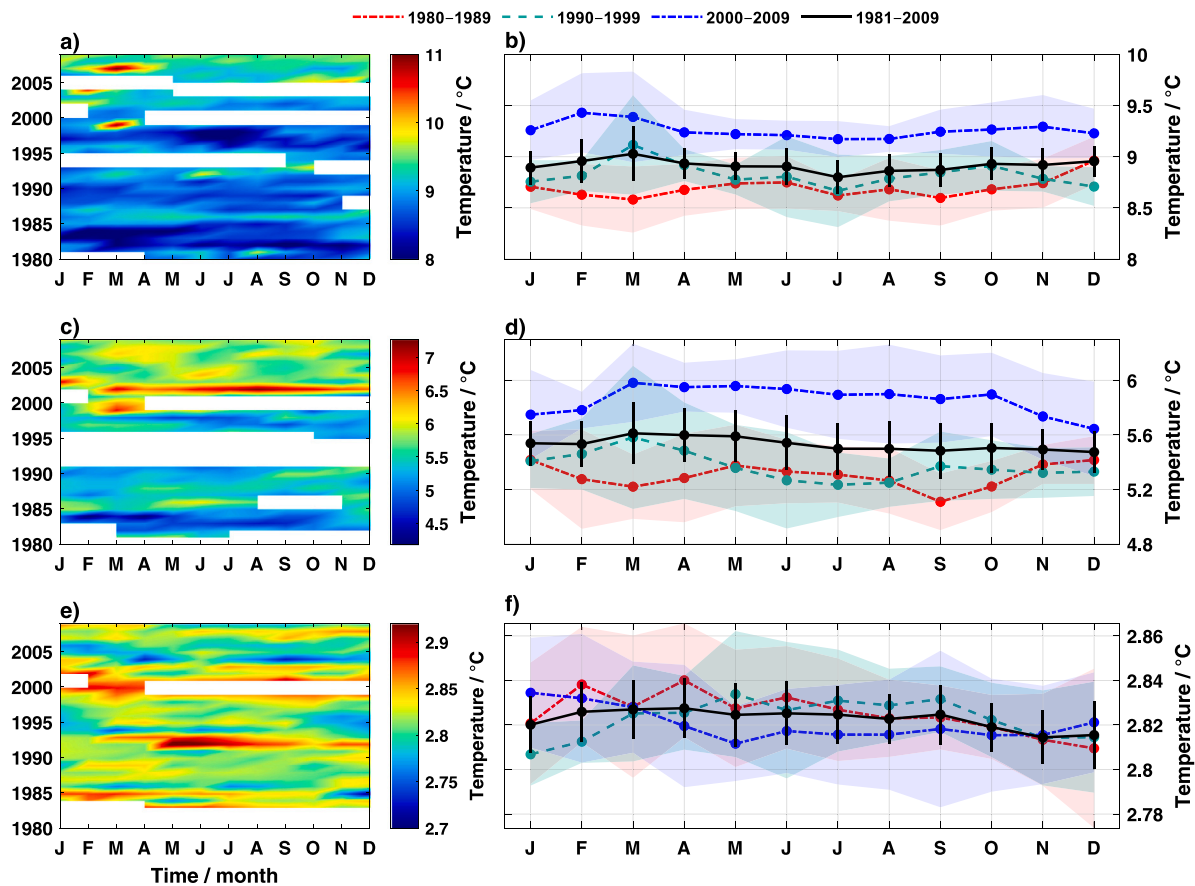


Fig. 6. Annual cycles of temperature. Hovmöller diagrams with monthly mean temperatures at (a) 1000 m, (c) 1600 m and (e) 3000 m. Annual mean cycle of temperature (solid black line) and the 95% confidence interval (black bars), together with the decadal mean annual cycles for the periods 1980–1989 (dashed red line), 1990–1999 (dashed cyan line) and 2000–2009 (dashed blue line) at (b) 1000 m, (d) 1600 m and (f) 3000 m. The annual cycles were calculated using monthly mean temperatures of each year. Note that the vertical lines and the shadowed areas indicate the 95% confidence intervals calculated for the decadal periods with a t-student test.

in the upper thermocline (Fründt et al., 2013). At 3000 m depth, no increase was observed at all.

The mean currents intensified at all depth levels since 1980, and as a consequence, the mean kinetic energy also increased within the decades. The fluctuating part of the kinetic energy only increased at 1000 m, possibly as a consequence of the increase in the strength of MEDDIES crossing the Kiel 276 site. Between 1980 and 2009, 16 MEDDIES crossed the Kiel 276 mooring, with 10 MEDDIES during the first two decades, and 6 MEDDIES after 2000. After 1999, the overall strength of MEDDIES increased in terms of temperature and currents anomalies compared to the background field.

Our results show that the previously reported changes in the main thermocline between 1980–2009 are also observed at deeper levels. The warming extends until 1600 m, while the mean currents (and also the mean kinetic energy) intensified in the entire water column on a decadal scale. Also, the increase of the fluctuating kinetic energy reached 1000 m depth. These changes in the water column, even at deeper levels, are in line with the most recent studies reporting warming of the upper 2000 m and increase of the eddy kinetic energy in the upper 1000 m both for the Northeast Atlantic and on a global scale.

CRedit authorship contribution statement

H.C. Frazão: Ran all the analyses, Prepared the graphs and the draft. **R.D. Prien:** Analyses, Revised the manuscript. **T.J. Müller:** Supervised the mooring work, Led the cruises assigned to the deployment, Recovery of Kiel 276 mooring, Revised the manuscript. **D.E. Schulz-Bull:** Revised the manuscript. **J.J. Waniek:** Supervised the mooring work, Led the cruises assigned to the deployment, Recovery of Kiel 276 mooring, Secured the funding, Revised the manuscript.

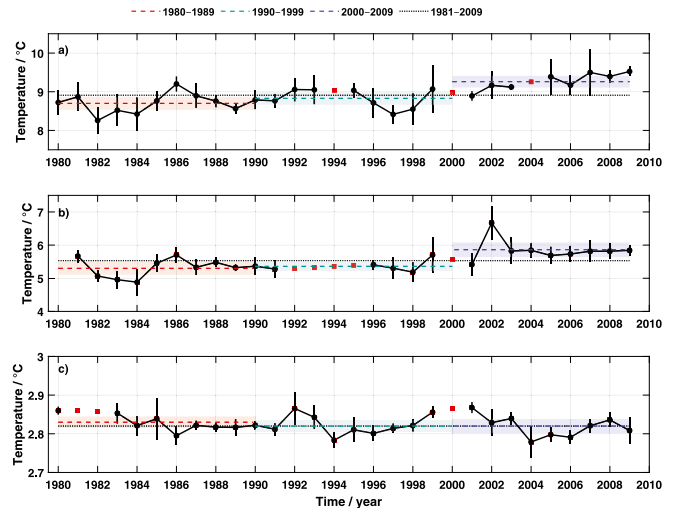


Fig. 7. Long-term changes in temperature. Annual mean values of temperature at (a) 1000 m, (b) 1600 m and (c) 3000 m over the 30-years record. Red squares are interpolated values using a shape-preserving piecewise cubic interpolation. Decadal means are also presented: 1980–1989 (dashed red line), 1990–1999 (dashed cyan line) and 2000–2009 (dashed blue line). The error bars are the standard deviation for each annual mean. The shadowed areas indicate the 95% confidence intervals for each decadal mean. The black dotted line is the long-term mean.

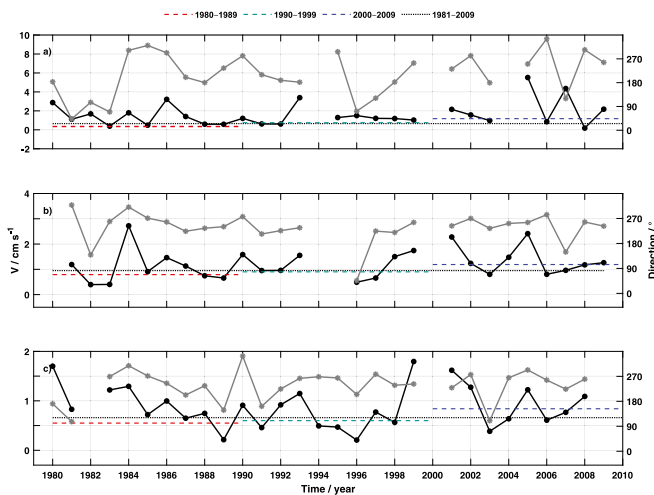


Fig. 8. Long-term changes in the absolute velocity. Annual mean absolute velocity (solid black line) and current direction (solid grey line) at (a) 1000 m, (b) 1600 m and (c) 3000 m over the 30-years record. Decadal means of the absolute velocity are also presented: 1980–1989 (dashed red line), 1990–1999 (dashed cyan line) and 2000–2009 (dashed blue line). The dotted line is the long-term mean of the absolute velocity. Please note the different velocity scales.

Data availability statement

The records of each deployment are freely available at the:

• World Data Center Pangaea:

<https://doi.pangaea.de/10.1594/PANGAEA.836686>.

• Ocean Time Series site:

<http://tds0.ifremer.fr/thredds/catalog/CORISOLIS-OCEANSITES-GDAC-OBS/DATA/K276/catalog.htm>.

Acknowledgements

We gratefully acknowledge the financial support by Deutsche Forschungsgemeinschaft (DFG) over many years in a variety of grants to different German institutions and individuals involved in the work at the site Kiel 276. We also thank the masters, crews, technicians and scientists who supported the work during numerous sampling campaigns aboard a number of German research vessels. Our special thanks are directed to the masters and crews of RV POSEIDON as most of the recent cruises were carried out on board of this ship. J.W. acknowledges the financial support from DFG, Germany (No. WA2175/1-1 to WA2175/1-5) and Leibniz Institute for Baltic Sea Research Warnemünde, Germany. We also thank the anonymous reviewers for valuable suggestions to improve our study.

Appendix A. Supplementary data

Supplementary material related to this article can be found online at <https://doi.org/10.1016/j.jmarsys.2021.103517>.

References

AANDERAA Instruments, 1978. Operating manual for the recording current meter model 4. In: Tech. Descr. No. 119, Bergen.

AANDERAA Instruments, 1987. Operating manual, recording current meter, models 7 & 8. In: Tech. Descr. No. 159.

Armi, L., Zenk, W., 1984. Large lenses of highly saline Mediterranean Water. *J. Phys. Oceanogr.* 14, 1560–1576. [http://dx.doi.org/10.1175/1520-0485\(1984\)014<1560:LLOHSM>2.0.CO;2](http://dx.doi.org/10.1175/1520-0485(1984)014<1560:LLOHSM>2.0.CO;2).

Cheng, L., Abraham, J., Hausfather, Z., Trenberth, K.E., 2019. How fast are the oceans warming? *Science* 363 (6423), 128–129. <http://dx.doi.org/10.1126/science.aav7619>.

Church, J.A., White, N.J., Konikow, L.F., Domingues, C.M., Cogley, J.G., Rignot, E., Gregory, J.M., van den Broeke, M.R., Monaghan, A.J., Velicogna, I., 2011. Revisiting the Earth's sea-level and energy budgets from 1961 to 2008. *Geophys. Res. Lett.* 38 (18), L18601. <http://dx.doi.org/10.1029/2011GL048794>.

Desbruyères, D.G., McDonagh, E.L., King, B.A., Garry, F.K., Blaker, A.T., Moat, B.I., Mercier, H., 2014. Full-depth temperature trends in the northeastern Atlantic through the early 21st century. *Geophys. Res. Lett.* 41, 7971–7979. <http://dx.doi.org/10.1002/2014GL061844>.

Desbruyères, D.G., Purkey, S.G., McDonagh, E.L., Johnson, G.C., King, B.A., 2016. Deep and abyssal ocean warming from 35 years of repeat hydrography. *Geophys. Res. Lett.* 43, 10,356–10,365. <http://dx.doi.org/10.1002/2016GL070413>.

Dickson, R., 1983. Global summaries and intercomparisons: Flow statistics from long-term current meter moorings. In: Robinson, A.R. (Ed.), *Eddies in Marine Science. Topics in Atmospheric and Oceanographic Sciences*. Springer, Berlin, Heidelberg, http://dx.doi.org/10.1007/978-3-642-69003-7_15.

Dickson, R.R., Gould, W.J., Gurbutt, P.A., Killworth, P.D., 1982. A seasonal signal in ocean currents to abyssal depths. *Nature* 295, 193–198. <http://dx.doi.org/10.1038/295193a0>.

Dickson, R.R., Gould, W.J., Müller, T.J., Maillard, C., 1985. Estimates of the mean circulation in the deep (>2,000 m) layer of the Eastern North Atlantic. *Prog. Oceanogr.* 14, 103–127. [http://dx.doi.org/10.1016/0079-6611\(85\)90008-4](http://dx.doi.org/10.1016/0079-6611(85)90008-4).

Emery, W., Meincke, J., 1986. Global water masses: summary and review. *Oceanol. Acta* 9 (4), 383–391.

Fründt, B., Müller, T.J., Schulz-Bull, D.E., Waniek, J.J., 2013. Long-term changes in the thermocline of the subtropical Northeast Atlantic (33°N, 22°W). *Prog. Oceanogr.* 116, 246–260. <http://dx.doi.org/10.1016/j.pcean.2013.07.004>.

Fründt, B., Waniek, J., 2012. Impact of the azores front propagation on deep ocean particle flux. *Cent. Eur. J. Geosci.* 4 (4), 531–544. <http://dx.doi.org/10.2478/s13533-012-0102-2>.

Fusco, G., Artale, V., Cotroneo, Y., Sannino, G., 2008. Thermohaline variability of Mediterranean Water in the Gulf of Cadiz, 1948–1999. *Deep-Sea Res.* 55 (12), 1624–1638. <http://dx.doi.org/10.1016/j.dsr.2008.07.009>.

Garçon, V.C., Oschlies, A., Doney, S.C., McGillicuddy, D., Waniek, J., 2001. The role of mesoscale variability on plankton dynamics in the North Atlantic. *Deep-Sea Res.* 48 (10), 2199–2226. [http://dx.doi.org/10.1016/S0967-0645\(00\)00183-1](http://dx.doi.org/10.1016/S0967-0645(00)00183-1).

Gould, W., 1985. Physical oceanography of the Azores front. *Prog. Oceanogr.* 14, 167–190. [http://dx.doi.org/10.1016/0079-6611\(85\)90010-2](http://dx.doi.org/10.1016/0079-6611(85)90010-2).

Hu, S., Sprintall, J., Guan, C., McPhaden, M.J., Wang, F., Hu, D., Cai, W., 2020. Deep-reaching acceleration of global mean ocean circulation over the past two decades. *Sci. Adv.* 6 (6), eaax7727. <http://dx.doi.org/10.1126/sciadv.aax7727>.

IPCC, 2014a. Observations: Atmosphere and surface. In: *Climate Change 2013 – the Physical Science Basis: Working Group I Contribution to the Fifth Assessment Report of the Intergovernmental Panel on Climate Change*. Cambridge: Cambridge University Press, pp. 159–254. <http://dx.doi.org/10.1017/CBO9781107415324.008>.

IPCC, 2014b. Observations: Ocean pages. In: *Climate Change 2013 – the Physical Science Basis: Working Group I Contribution to the Fifth Assessment Report of the Intergovernmental Panel on Climate Change*. Cambridge: Cambridge University Press, pp. 255–316. <http://dx.doi.org/10.1017/CBO9781107415324.010>.

Jones, P.D., New, M., Parker, D.E., Martin, S., Rigor, I.G., 1999. Surface air temperature and its changes over the past 150 years. *Rev. Geophys.* 37 (2), 173–199. <http://dx.doi.org/10.1029/1999RG900002>.

Jones, P.D., Wigley, T.M.L., Wright, P.B., 1986. Global temperature variations between 1861 and 1984. *Nature* 322, 430–434. <http://dx.doi.org/10.1038/322430a0>.

Karl, D.M., Bates, N.R., Emerson, S., Harrison, P.J., Jeandel, C., Llinás, O., Liu, K.-K., Marty, J.-C., Michaels, A.F., Miquel, J.C., Neuer, S., Nojiri, Y., Wong, C.S., 2003. Temporal studies of biogeochemical processes determined from ocean time-series observations during the JGOFS era. In: Fasham, M.J.R. (Ed.), *Ocean Biogeochemistry. Global Change – the IGBP Series (Closed)*. Springer, Berlin, Heidelberg, http://dx.doi.org/10.1007/978-3-642-55844-3_11.

Käse, R.H., Siedler, G., 1982. Meandering of the subtropical front south-east of the Azores. *Nature* 300 (5889), 245–246. <http://dx.doi.org/10.1038/300245a0>.

Klein, H., Mittelstaedt, E., 1992. Currents and dispersion in the abyssal Northeast Atlantic. Results from the NOAMP field program. *Deep-Sea Res.* 39 (10), 1727–1745. [http://dx.doi.org/10.1016/0198-0149\(92\)90026-P](http://dx.doi.org/10.1016/0198-0149(92)90026-P).

Krauss, W., Käse, R.H., 1984. Mean circulation and eddy kinetic energy in the eastern North Atlantic. *J. Geophys. Res.* 89 (C3), 3407–3415. <http://dx.doi.org/10.1029/JC089iC03p03407>.

Leadbetter, S.J., Williams, R.G., McDonagh, E.L., King, B.A., 2007. A twenty year reversal in water mass trends in the subtropical North Atlantic. *Geophys. Res. Lett.* 34, L12608. <http://dx.doi.org/10.1029/2007GL029957>.

Levitus, S., Antonov, J.I., Boyer, T.P., Baranova, O.K., Garcia, H.E., Locarnini, R.A., Mishonov, A.V., Reagan, J.R., Seidov, D., Yarosh, E.S., Zweng, M.M., 2012. World ocean heat content and thermocline sea level change (0–2000 m), 1955–2010. *Geophys. Res. Lett.* 39, L10603. <http://dx.doi.org/10.1029/2012GL051106>.

- Levitus, S., Antonov, J.I., Boyer, T.P., Locarnini, R.A., Garcia, H.E., Mishonov, A.V., 2009. Global ocean heat content 1955–2008 in light of recently revealed instrumentation problems. *Geophys. Res. Lett.* 36, L07608. <http://dx.doi.org/10.1029/2008GL037155>.
- Levitus, S., Antonov, J.I., Boyer, T.P., Stephens, C., 2000. Warming of the world ocean. *Science* 287 (5461), 2225–2229. <http://dx.doi.org/10.1126/science.287.5461.2225>.
- Millot, C., Candela, J., Fuda, J.L., Tber, Y., 2006. Large warming and salinification of the Mediterranean outflow due to changes in its composition. *Deep-Sea Res. I* 53 (4), 656–666. <http://dx.doi.org/10.1016/j.dsr.2005.12.017>.
- Müller, T.J., Siedler, G., 1992. Multi-year current time series in the eastern North Atlantic Ocean. *J. Marine Res.* 50 (1), 63–98. <http://dx.doi.org/10.1357/002224092784797755>.
- Müller, T.J., Waniek, J.J., 2013. KIEL276 Time Series Data from Moored Current Meters 33° N, 22° W, 5285 M Water Depth. March 1980 - April 2011. Background Information and Data Compilation. GEOMAR Report Nr. 13. http://dx.doi.org/10.3289/GEOMAR_REP_NS_13_2013.
- Potter, R.A., Lozier, M.S., 2004. On the warming and salinification of the Mediterranean outflow waters in the North Atlantic. *Geophys. Res. Lett.* 31, L01202. <http://dx.doi.org/10.1029/2003GL018161>.
- Reynolds, O., 1895. IV. On the dynamical theory of incompressible viscous fluids and the determination of the criterion. *Phil. Trans. R. Soc. A* 186 (1895), 123–164. <http://dx.doi.org/10.1098/rsta.1895.0004>.
- Robinson, A.R., 1983. *Eddies in Marine Science*. Springer Verlag, Berlin, Heidelberg, p. 609.
- Saunders, P.M., 1983. Benthic observations on the madeira abyssal plain: Currents and dispersion. *J. Phys. Oceanogr.* 13 (8), 1416–1429. [http://dx.doi.org/10.1175/1520-0485\(1983\)013<1416:BOOTMA>2.0.CO;2](http://dx.doi.org/10.1175/1520-0485(1983)013<1416:BOOTMA>2.0.CO;2).
- Saunders, P.M., 1987. Flow through discovery gap. *J. Phys. Oceanogr.* 17 (5), 631–643. [http://dx.doi.org/10.1175/1520-0485\(1987\)017<0631:FTDG>2.0.CO;2](http://dx.doi.org/10.1175/1520-0485(1987)017<0631:FTDG>2.0.CO;2).
- Schmitz, J., William, J., Price, J.F., Richardson, P.L., 1988. Recent moored current meter and SOFAR float observations in the eastern Atlantic near 32N. *J. Marine Res.* 46 (2), 301–319. <http://dx.doi.org/10.1357/002224088785113658>.
- Siedler, G., Armi, L., Müller, T.J., 2005. Meddies and decadal changes at the Azores Front from 1980 to 2000. *Deep-Sea Res. II* 52 (3–4), 583–604. <http://dx.doi.org/10.1016/j.dsr2.2004.12.010>.
- Siedler, G., Zenk, W., Emery, W.J., 1985. Strong current events related to a subtropical front in the Northeast Atlantic. *J. Phys. Oceanogr.* 15 (7), 885–897. [http://dx.doi.org/10.1175/1520-0485\(1985\)015<0885:SCERTA>2.0.CO;2](http://dx.doi.org/10.1175/1520-0485(1985)015<0885:SCERTA>2.0.CO;2).
- Stocker, T.F., 2013. The ocean's role in the climate system. In: Siedler, G., Church, J., Gould, J. (Eds.), *Ocean Circulation & Climate, a 21st Century Perspective*. pp. 3–25, volume 193 of *International Geophysics*.
- Stramma, L., Siedler, G., 1988. Seasonal changes in the North Atlantic subtropical gyre. *J. Geophys. Res.* 93, 8111–8118. <http://dx.doi.org/10.1029/JC093iC07p08111>.
- Tomczak, M., Godfrey, J.S., 1994. *Regional Oceanography: An Introduction*. p. 422.
- Voelker, A.H., Colman, A., Olack, G., Waniek, J.J., Hodell, D., 2015. Oxygen and hydrogen isotope signatures of Northeast Atlantic water masses. *Deep-Sea Res. II* 116, 89–106. <http://dx.doi.org/10.1016/j.dsr2.2014.11.006>.
- Waniek, J.J., Schulz-Bull, D.E., Blanz, T., Prien, R.D., Oschlies, A., Müller, T.J., 2005. Interannual variability of deep water particle flux in relation to production and lateral sources in the northeast Atlantic. *Deep-Sea Res. I* 52 (1), 33–50. <http://dx.doi.org/10.1016/j.dsr.2004.08.008>.
- Yang, H., Lohmann, G., Krebs-Kanzow, U., Ionita, M., Shi, X., Sidorenko, D., Gong, X., Chen, X., Gowan, E.J., 2020. Poleward shift of the major ocean gyres detected in a warming climate. *Geophys. Res. Lett.* 47, e2019GL085868. <http://dx.doi.org/10.1029/2019GL085868>.
- Zanna, L., Khatiwala, S., Gregory, J.M., Ison, J., Heimbach, P., 2019. Global reconstruction of historical ocean heat storage and transport. *Proc. Natl. Acad. Sci. USA* 116 (4), 1126–1131. <http://dx.doi.org/10.1073/pnas.1808838115>.
- Zenk, W., Armi, L., 1990. The complex spreading pattern of Mediterranean Water off the Portuguese continental slope. *Deep-Sea Res. A* 37 (12), 1805–1823. [http://dx.doi.org/10.1016/0198-0149\(90\)90079-B](http://dx.doi.org/10.1016/0198-0149(90)90079-B).

30 years temporal variability of temperature and
currents below the main thermocline between 1980–2009
in the subtropical Northeast Atlantic (Kiel 276, 33°N,
22°W)

Frazão, H. C.^{a,*}, Prien, R. D.^a, Müller, T. J.^b, Schulz-Bull D. E.^a, Waniek
J. J.^a

^a*Leibniz Institute for Baltic Sea Research Warnemünde, Seestraße 15, 18119 Rostock,
Germany*

^b*GEOMAR Helmholtz Centre for Ocean Research Kiel, Düsternbrokerweg 20, 24105
Kiel, Germany*



*Frazão, H. C.

Email address: `helena.frazao@io-warnemuende.de` (Frazão, H. C.)

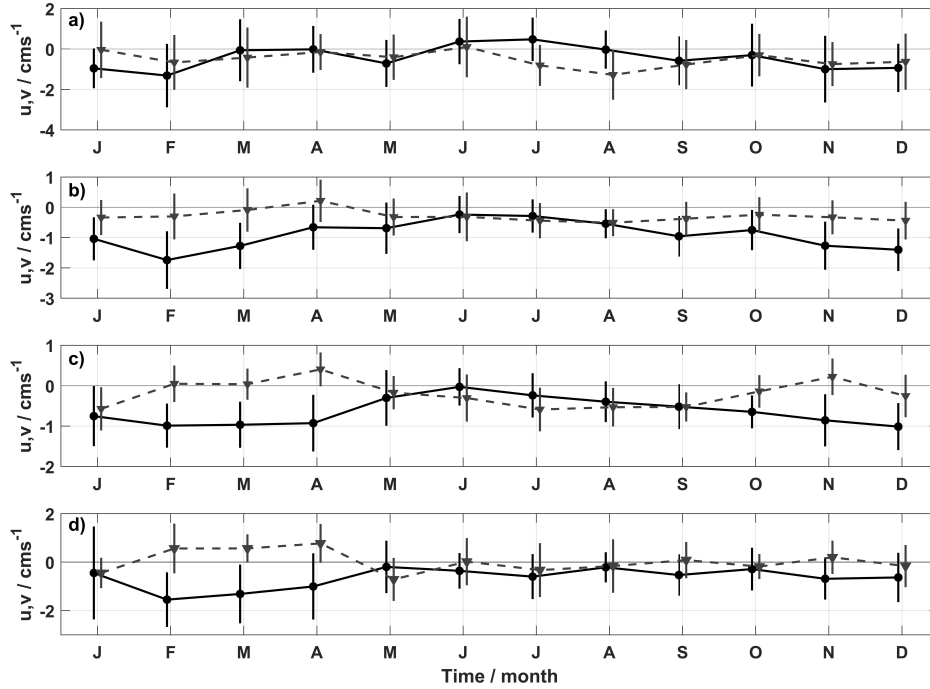


Figure S.1: **Annual cycles of velocity components** (u – black solid line; v – dashed grey line; in cm s^{-1}) at (a) 1000 m, (b) 1600 m, (c) 3000 m, and (d) 5000 m. Positive values of u are directed towards east and positive values for v are directed northward. The vertical lines represent the 95% confidence intervals. For graphical reasons the monthly means of each component are lagged (shifted) by 3 days.

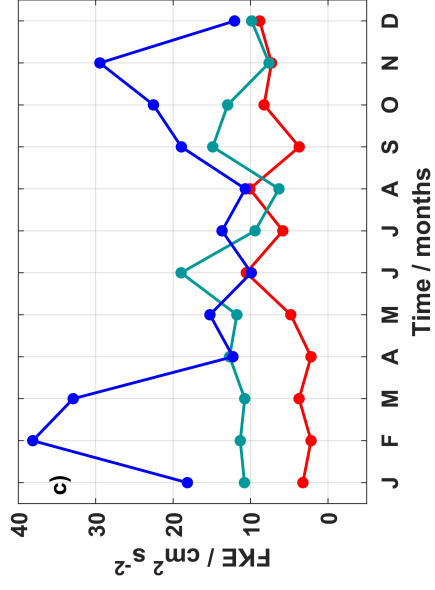
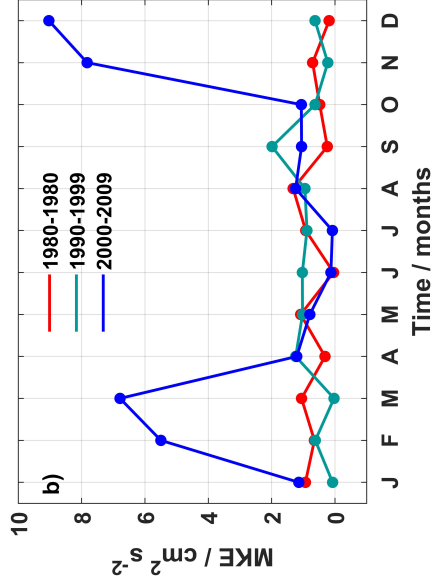
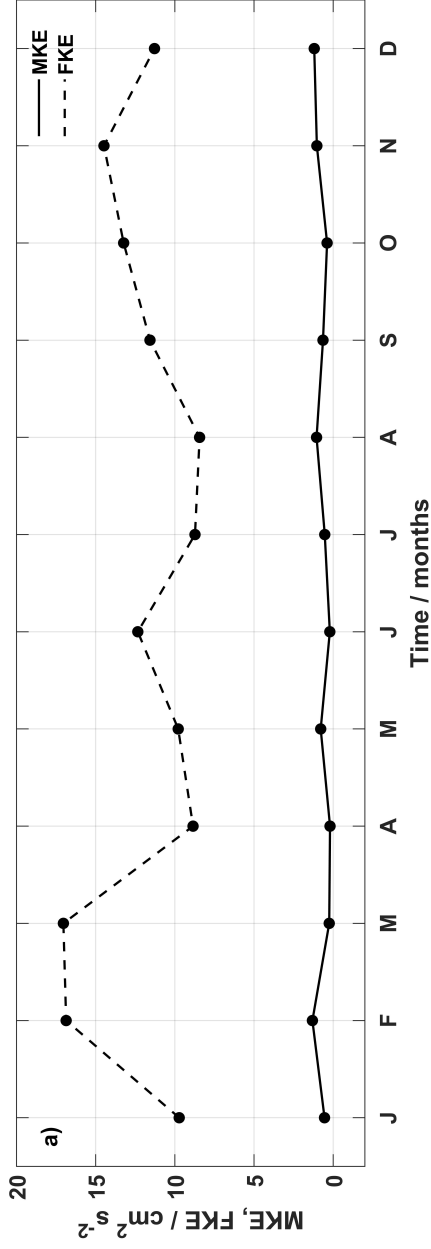


Figure S.2: Monthly mean and fluctuating kinetic energy at 1000 m. (a) Annual cycle of Mean Kinetic Energy (MKE, solid black line) and Fluctuating Kinetic Energy (FKE, dashed black line) in $\text{cm}^2 \text{s}^{-2}$. (b) MKE and (c) FKE annual cycles for the periods 1980–1989 (solid red line), 1990–1999 (solid cyan line) and 2000–2009 (solid blue line). The annual cycles were calculated using the monthly mean and monthly mean fluctuations of the velocity components according to equations 1 and 2 in Data & Methods, respectively.

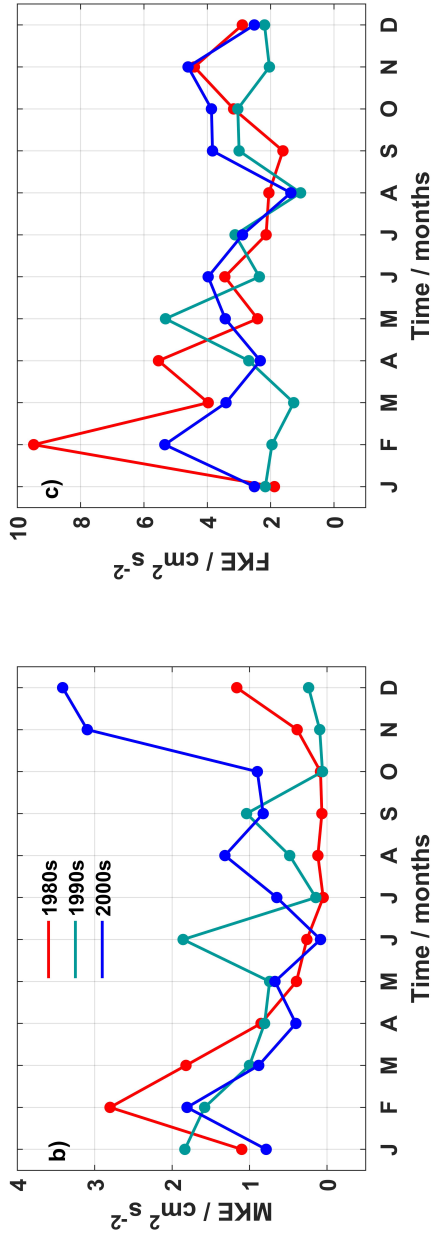
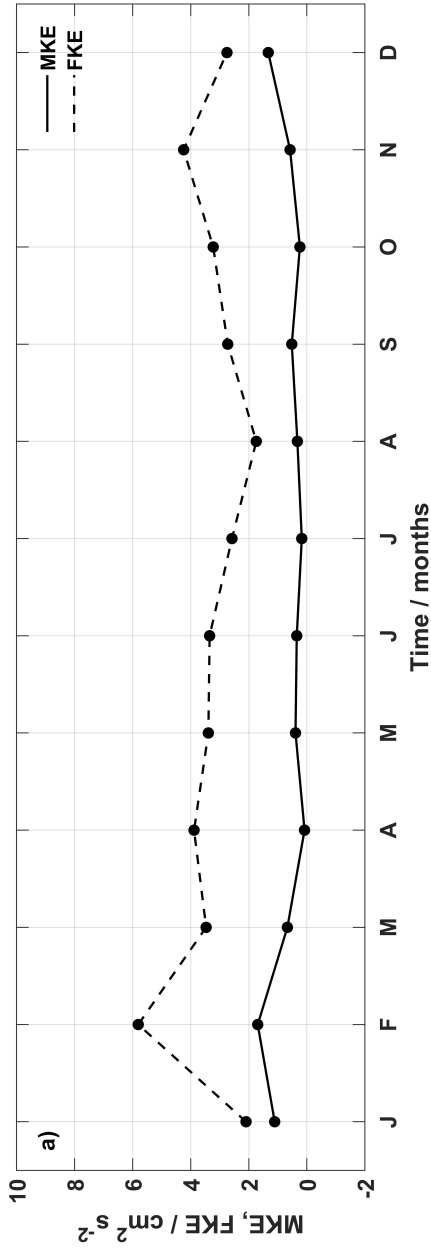


Figure S.3: Monthly mean and fluctuating kinetic energy at 1600 m. (a) Annual cycle of Mean Kinetic Energy (MKE, solid black line) and Fluctuating Kinetic Energy (FKE, dashed black line) in $\text{cm}^2 \text{s}^{-2}$. (b) MKE and (c) FKE annual cycles for the periods 1980–1989 (solid red line), 1990–1999 (solid cyan line) and 2000–2009 (solid blue line). The annual cycles were calculated using the monthly mean and monthly mean fluctuations of the velocity components according to equations 1 and 2 in Data & Methods, respectively.

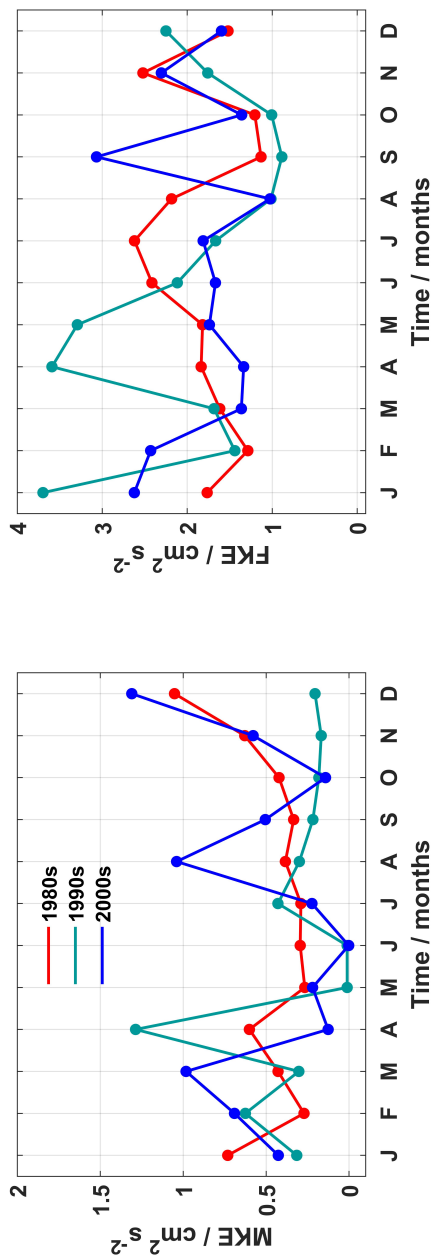
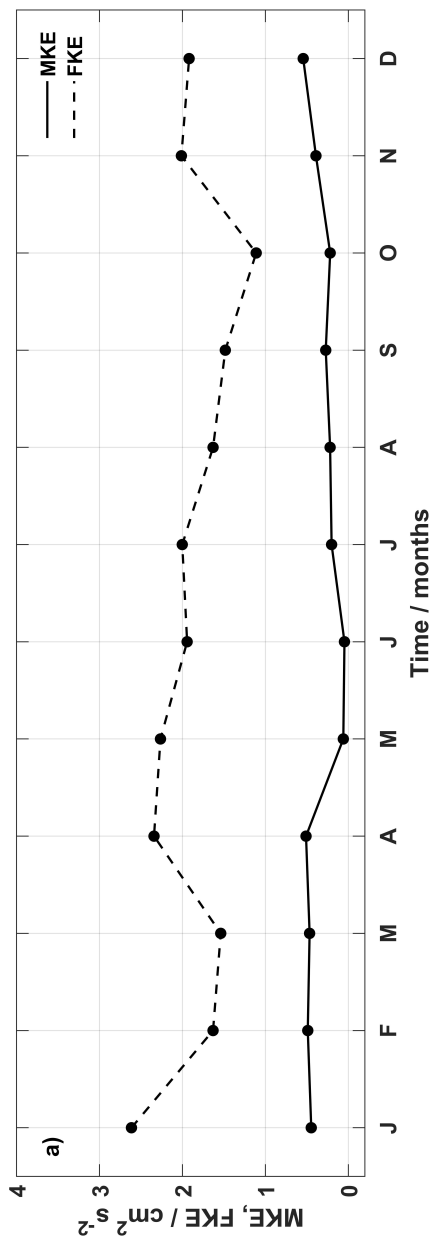


Figure S.4: Monthly mean and fluctuating kinetic energy at 3000 m. (a) Annual cycle of Mean Kinetic Energy (MKE, solid black line) and Fluctuating Kinetic Energy (FKE, dashed black line) in $\text{cm}^2 \text{s}^{-2}$. (b) MKE and (c) FKE annual cycles for the periods 1980–1989 (solid line), 1990–1999 (solid cyan line) and 2000–2009 (solid blue line). The annual cycles were calculated using the monthly mean and monthly mean fluctuations of the velocity components according to equations 1 and 2 in Data & Methods, respectively.

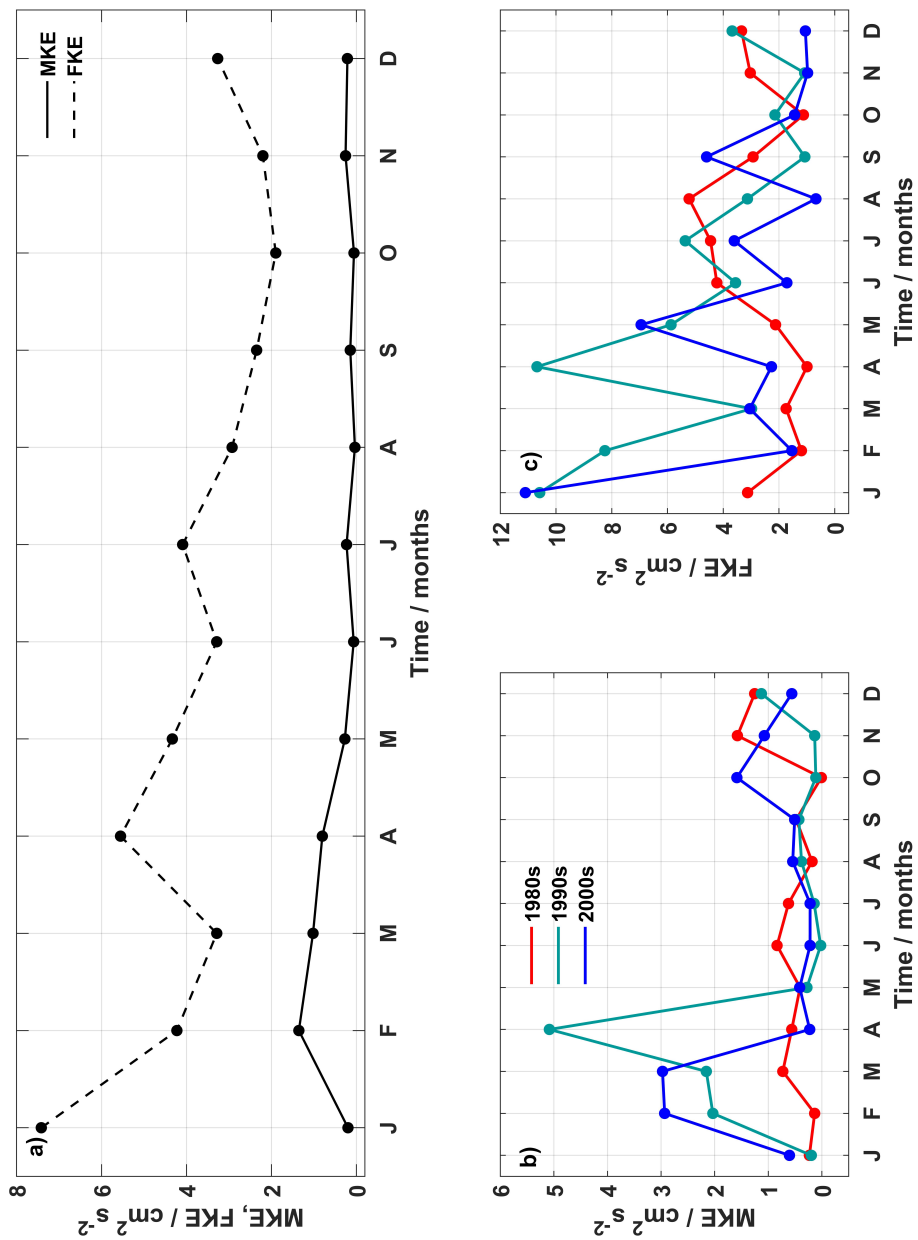


Figure S.5: Monthly mean and fluctuating kinetic energy at 5000 m. (a) Annual cycle of Mean Kinetic Energy (MKE, solid black line) and Fluctuating Kinetic Energy (FKE, dashed black line) in $\text{cm}^2 \text{s}^{-2}$. (b) MKE and (c) FKE annual cycles for the periods 1980–1989 (solid red line), 1990–1999 (solid cyan line) and 2000–2009 (solid blue line). The annual cycles were calculated using the monthly mean and monthly mean fluctuations of the velocity components according to equations 1 and 2 in Data & Methods, respectively.

List of Figures

- Figure 1.1.** Global mean surface Chl *a* concentrations (indicated by the colorbar) from MODIS-Aqua (average for 2020, 4 km resolution) together with a schematic representation of the main currents at the surface of the North Atlantic Subtropical Gyre: Gulf Stream (GS), North Atlantic Current (NAC), Azores Current (AzC), Canary Current (CC), North Atlantic Equatorial Current (NAEC), North Atlantic Equatorial Countercurrent (NECC), Antilles Current (AnC), and Caribbean Current (CaC) (solid black lines; adapted from Daniault et al., 2016; Voelker et al., 2015). Superimposed is the long-term mean wind stress curl over the North Atlantic basin (small black arrows) calculated from the (SODA-POP v2.2.4 product; Carton & Giese, 2008; Giese & Ray, 2011). The Chl *a* data is available at <https://oceancolor.gsfc.nasa.gov/13/>. 4
- Figure 3.1.** **Working Areas** used in the three publications: black (Frazão et al., 2022; Azores region between 30°N–40°N, 36°–20°W; Gulf Stream region between 30°–45°N, 75°–45°W), light blue (Frazão & Waniek, 2021; 30°–40°N, 29°–15°W), and star (Frazão et al., 2021; Kiel 276 mooring nominal position at 33°N, 22°W). Additionally, the main surface circulation of the North Atlantic Subtropical Gyre is also represented in yellow: Gulf Stream (GS), Azores Current (AzC), Canary Current (CC), North Atlantic Equatorial Current (NAEC), North Atlantic Equatorial Countercurrent (NECC), Antilles Current (AnC), Caribbean Current (CaC), and North Atlantic Current (NAC) (adapted from Daniault et al., 2016; Voelker et al., 2015). Orange arrays are a schematic representation of the main MOW pathways after exiting the Strait of Gibraltar (adapted from Carracedo et al., 2014; Daniault et al., 2016; de Pascual-Collar et al., 2019). 12
- Figure 3.2.** Comparison between the reconstructed vertical distributions (isolines in background) and the in situ measurements (colored circles) of nitrate (a) and Chl *a* (b) at the closest point of the BATS station (31.25°N, 64.25°W). (c) Validation of the calculated Chl *a* concentration at the surface (solid blue line) with the surface Chl *a* concentration measured remotely (solid orange line). In situ surface Chl *a* concentration measured during the surveys around the BATS station are also represented by a yellow cross. 18

Figure 4.1.	(a) Monthly vertical average absolute velocity (upper 1000 m) along the Azores Current core (between 32°N and 36°N, 36°W and 20°W). (b) Monthly vertical average absolute velocity (upper 1000 m) along the Gulf Stream core for each sub-region (western: 75°–65°W, solid blue line; central: 65°–55°W, solid yellow line; eastern: 55°–45°W, solid green line). All time-series are smoothed using a 60-months moving mean between 1871 and 2010 (adapted from Frazão et al., 2022).	20
Figure 4.2.	Monthly integrated Ocean Heat Content (OHC) in the NEA for the upper 400 m of the water column (solid green line), and the monthly AF position averaged between 30° and 20°W (solid blue line). Both time-series are 60-months smoothed (from Frazão et al., 2022).	22
Figure 4.3.	Salinity distribution averaged over the MOW’s core (1000–1100 m) from the WOA18 (Zweng et al., 2018) (a) between 1965–1974, and (b) 1985–1994. (c) Salinity difference between (a) and (b). The black star represents the location of the Kiel 276 mooring (adapted from Frazão & Waniek, 2021).	27
Figure 4.4.	Deep-ocean observing platforms in the North Atlantic (adapted from the interactive map available online at https://deepoceanobserving.org/deep-ocean-observations/).	29
Figure 4.5.	Integral Time Scale (τ , in days) based on individual deployments of the Kiel 276 mooring as a function of the record length for the (a) τ_u – zonal velocity component, (b) τ_v – meridional velocity component, and (c) τ_T – temperature. The depths of the instruments are color coded. Adapted from Müller & Waniek (2013) and Frazão et al. (2021)	30
Figure 4.6.	Averaged monthly temperature (solid gray line) and integrated nitrate concentration (dashed green line) in the upper 300 m at BATS (a) and Kiel 276 site (b). Monthly integrated Chl <i>a</i> and equivalent carbon uptake in the upper 300 m at BATS (c) and Kiel 276 site (d). The averaged monthly mean temperature was calculated using the SODA-POP v2.2.4 dataset at Kiel 276 and BATS positions (Carton & Giese, 2008; Giese & Ray, 2011). Carbon uptake was estimated at each site using a C/Chl <i>a</i> ratio of 50 (Fründt et al., 2015a). The time-series are smoothed with a 60-month moving mean filter.	33

-
- Figure 4.7. North Atlantic subtropical basin** (a) annual mean solar radiation flux, (b) average water temperature, (c) integrated nitrate concentration and (d) integrated Chl *a* concentration (solid black line) and equivalent Carbon uptake concentration (solid red line) in the upper 300 m of the water column averaged over the entire North Atlantic subtropical basin between 10°–40°N and 80°–10°W. The grey solid lines in (b) and (c) are the monthly time-series. The time-series are smoothed with a 60-month moving filter. (e) Linear trend of the integrated Chl *a* concentration in the upper 300 m (dotted regions are statistically significant at $p < 0.001$). (f) Integrated Chl *a* difference between 2010 and 1871, and correspondent carbon uptake in the NASTG. 35

List of Abbreviations

AAIW Antarctic Intermediate Water.	MAR Mid-Atlantic Ridge.
AF Azores Front.	MEDDY Mediterranean Water lense.
AMO Atlantic Multidecadal Oscillation.	MKE Mean Kinetic Energy.
AMOC Atlantic Meridional Overturning Circulation.	MLD Mixed Layer Depth.
AMT Atlantic Meridional Transect.	MOC Meridional Overturning Circulation.
AzC Azores Current.	MOW Mediterranean Water Outflow.
AzCC Azores Countercurrent.	
	NA North Atlantic.
BATS Bermuda Atlantic Time series Study.	NAC North Atlantic Current.
BGC-Argo Biogeochemical Argo.	NADW North Atlantic Deep Water.
	NAEC North Atlantic Equatorial Current.
CC Canary Current.	NAO North Atlantic Oscillation.
Chl <i>a</i> Chlorophyll <i>a</i> .	NAST North Atlantic Subtropical Gyral Province.
	NAST-E Eastern North Atlantic Subtropical Gyral Province.
DCM Depth of Chlorophyll Maximum.	NASTG North Atlantic Subtropical Gyre.
EKE Eddy Kinetic Energy.	NEA Northeast Atlantic.
ESTOC European Station for Time-series in the Ocean, Canary Islands.	NEADS North East Atlantic Dynamics Study.
	OHC Ocean Heat Content.
FKE Fluctuating Kinetic Energy.	POP Parallel Ocean Programming.
GO-SHIP Global Ocean-Based Hydrographic Investigations Program.	PP Primary Production.
GS Gulf Stream.	
GSNW Gulf Stream North Wall.	RCM Recording Current Meters.
	SODA-POP Simple Ocean Data Assimilation.
ITS Integral Time Scale.	SST Sea Surface Temperature.
	WMDW Western Mediterranean Deep Water.
JGOFS Joint Global Ocean Flux Study.	WOA18 World Ocean Atlas 2018.
LIW Levantine Intermediate Water.	WOCE World Ocean Circulation Experiment.
LSW Labrador Sea Water.	WOD18 World Ocean Database 2018.

Curriculum Vitae

PERSONAL INFORMATION

Name: Helena Cristina Vieira Frazão
Birthdate: 13.12.1992
Nationality: Portuguese

PROFESSIONAL EXPERIENCE

2018–2022 **PhD Student**
Leibniz Institute for Baltic Sea Research Warnemünde
Group of Bio-physical Interactions in Marine Chemistry Department
Supervision: Prof. Dr. Joanna J. Waniek

2016–2018 **Scholarship Researcher**
MARE – Marine and Environmental Sciences Centre, Lisbon, Portugal
Project: Development of UAV Technology for dual and conjunct scope
use
Supervision: Dr. Fatima M. Sousa

EDUCATION

2017–2018 **Post-graduation in Data Science** (Grade: 15/20)
Faculty of Sciences, University of Lisbon, Portugal

2014–2016 **MSc in Marine Science** (Grade: 18/20)
Faculty of Sciences, University of Lisbon, Portugal

2012–2014 **BSc in Meteorology, Oceanography and Geophysics** (Grade: 13/20)
Faculty of Sciences, University of Lisbon, Portugal

2010–2012 **BSc in Geological and Mining Engineering** (4 Semesters)
Instituto Superior Técnico, Lisbon, Portugal

PEER REVIEWED PUBLICATION

- 2022** **Frazão, H. C.**, Prien, R. D., Schulz-Bull, D. E., Seidov, D., Waniek, J. J. (2022): The forgotten Azores Current: a long-term perspective. *Accepted in Frontiers in Marine Science*. doi: 10.3389/fmars.2022.842251
- 2021** Kuss, J., **Frazão, H. C.**, Zhong, Y., Gao, Y., Waniek, J. J. (2021): The impact of Typhoon “Mangkhut” on Surface Water Nutrient and Chlorophyll Inventories of the South China Sea in September 2018. *Journal of Geophysical Research: Biogeosciences*, 126, e2021JG006546. doi: 10.1029/2021JG006546
- Osterholz, H., Burmeister, C., Busch, S., Dierken, M., **Frazão, H. C.**, Hansen, R., Jeschek, J., Kremp, A., Kreuzer, L., Sadkowiak, B., Waniek, J. J., Schulz-Bull, D. E. (2021): Nearshore dissolved and particulate organic matter dynamics in the southwestern Baltic Sea: environmental drivers and time series analysis (2010—2020). *Frontiers in Marine Science* 8, 795028. doi: 10.3389/fmars.2021.795028
- Frazão, H. C.** & Waniek, J. J. (2021): Mediterranean Water properties at the eastern limit of the North Atlantic Subtropical Gyre since 1981. *Oceans* 2(1), 266—280. doi: 10.3390/oceans2010016
- Frazão, H. C.**, Prien, R. D., Müller, T. J., Schulz-Bull, D. E., Waniek, J. J. (2021): 30 years of temporal variability of temperature and currents below the main thermocline between 1980-2009 in the subtropical Northeast Atlantic (Kiel 276, 33°N, 22°W). *Journal of Marine Systems*, 217, 103517. doi: 10.1016/j.jmarsys.2021.103517
- Deich, C., **Frazão, H. C.**, Appelt, J.-S., Li, W., Pohlmann, T., Waniek, J. J. (2021): Occurrence and distribution of estrogenic substances in the northern South China Sea. *Science of Total Environment*, 770, 145239. doi: 10.1016/j.scitotenv.2021.145239

THESES

- MSc:** Hydrological features of Submarine Groundwater Discharges along Algarve coast. <http://hdl.handle.net/10451/25642> (in Portuguese)
- BSc:** Application of an autonomous tool, FUZZYUPWELL, on satellite images from the West coast of Portugal (in the summer of 1996, 1997, 2003-2006). (in Portuguese)

ORAL PRESENTATIONS

C. Deich, M. Kanwischer, **H.C. Frazão**, J.-S. Appelt, R. Zhang, W. Li, T. Pohlmann, J.J. Waniek (2021): Estrogenic compounds in the Pearl River Estuary and coastal South China Sea. In: Waniek, J. J., Schulz-Bull, D. E., Gaye, B., Ebinghaus, R., Kunz, F., Pohlmann, T. and Emeis, K.-C. (eds), 2021: Megacity's fingerprint in Chinese marginal seas. Rostock: Leibniz Institute for Baltic Sea Research Warnemünde. Meereswissenschaftliche Berichte, 116, pp.31–32.

F. Sousa, **H. Frazão**, G. Carrara, J. Fernandes, D. Boutov, F. Leitão, P. Range (2018). Hydrological Characteristics of the Submarine Groundwater Discharges at Olhos de Água, Algarve. FREEZE Project. Atlas of IX Symposium of the Iberian Atlantic Margin – MIA 2018, p. 37-38 (eds. P. P. Cunha, J. Dias, H. Veríssimo, L. V. Duarte, P. Dinis, F. C. Lopes, A. F. Bessa and J. A. Carmo).

H. Frazão, F. M. Sousa, FREEZE project team (2016). Submarine Groundwater Discharges in Olhos de Água (Algarve) – CTD survey results. p. 28 of Overview book of Oceanography Meeting APOCEAN, S. Pedro Moel, Portugal.

RESEARCH CRUISES

R/V Sonne SO269, Singapore – Hong Kong, South China Sea. Chief Scientist: Prof. Dr. Joanna Waniek (August 2019).

R/V Poseidon POS521, Las Palmas, Canary Islands – Malaga, Spain. Chief Scientist: Prof. Dr. Joanna Waniek (March 2018).

R/V Poseidon POS501, Malaga, Spain – San Miguel, Azores. Chief Scientist: Prof. Dr. Joanna Waniek (June 2016).

ADDITIONAL TRAINING

1st International Winter School on “Analysis of Climate Variability”, March 2019, Leibniz Institute for Baltic Sea Research Warnemünde, Germany.

5th ESA Advancing Training on Ocean Remote Sensing and Synergy, September 2017, Porto, Portugal.

Remote Sensing – Sea Temperature and Ocean Colour course; SOPHIA project, January 2016, Lisbon, Portugal (40 hours training).

Remote Sensing – Synthetic Aperture Radar Applications course; SOPHIA project, January 2016, Lisbon, Portugal (20 hours training).

Acknowledgments

Almost six years ago, a younger me had the chance to participate on a research cruise in the Madeira Basin, my first one (POS501), where Prof. Dr. Joanna J. Waniek was the Chief Scientist. Back then, I wouldn't imagine what was coming and how much my life was about to change in two years. This cruise was the starting point of all this pretty exciting adventure that implied moving to Germany and doing my PhD under the supervision of Prof. Joanna J. Waniek.

First and foremost, my deepest and warmest thanks go to Prof. Joanna J. Waniek for giving me the opportunity of doing a PhD under her supervision. She offered me countless advice, never stopped challenging me (which I'm most grateful for), and always had her door open for endless questions. I'm grateful for all opportunities you offered me during this process, including the cruise in the South China Sea. There is more that I could say, but right now, I feel fortunate to have you as a supervisor, and I think we had fun doing science together. Vielen vielen Dank!

I cannot let pass the opportunity to thank Dr. Ralf Prien. You were the first person I met in Germany (it was already a good sign), and your friendly welcome made my life so much easier. All the endless conversations we had during my PhD, always with a nice cup of coffee (and sweets), made me learn so much more about science and German. I'm very grateful for all your help and friendship since I first arrived. To Prof. Dr. Detlef Schulz-Bull, the head of the Chemistry Department at IOW, I would like to thank him for all his support and care doing my PhD. To the members of my thesis committee, Dr. Thomas Neumann and Dr. Anja Eggert, thank you for your helpful comments and support throughout my PhD. Finally, I want to thank Dr. Thomas J. Müller and Dr. Dan Seidov, co-authors in the publications, for the patience and helpful comments to improve our manuscripts.

Some people I came across in Germany greatly contributed to my PhD and life in Germany, and I want to thank them all. Mein Dank gilt zunächst Helga und Achim, die mich immer mit offenen Armen und einem Lächeln im Gesicht empfangen haben. Mit ihnen hatte ich mein erstes langes Gespräch auf Deutsch (zumindest habe ich es versucht). Also, a big thank you goes to Charlotte, Arne and Line for being my closest friends in Germany and always by my side. To my colleagues in the Chemistry Department and my office, thank you a lot for lightening the mood and turning my days in the office into such a pleasant time.

To my friends in Portugal, that one way or another were there for me, despite the distance. Dear Isabel, I have no words to describe all your support and all the times you pushed for me. To Susana, Sérgio and Bela, your honesty and friendship have always comforted me. To the IST friends, and former colleagues from MARE and FCUL, thank you all for the phone calls in the last years. It is nice to have you all around.

Por último, quero agradecer aos meus pais e família por todo o apoio e carinho ao longo destes ano. Sem eles e todos os seus sacrifícios, não estaria ou seria aquilo que sou hoje. Obrigada!